Department of Spatial Sciences

Fractals and Fuzzy Sets for Modelling the Heterogeneity and Spatial Complexity of Urban Landscapes using Multiscale Remote Sensing Data

Zahurul Islam

This thesis is presented as part of the requirements for the award of the Degree of Doctor of Philosophy

of the

Curtin University of Technology

October 2004

Declaration

This thesis contains no material which has been accepted for the award of any other degree or diploma in any university.

To the best of my knowledge and belief this thesis contains no material previously published by any other person except where due acknowledgment has been made.

Signature: ... .

Date: .....05/10/2004.....

ABSTRACT

This research presents models for the analysis of textural and contextual information content of multiscale remote sensing to select an appropriate scale for the correct interpretation and mapping of heterogeneous urban land cover types. Spatial complexity measures such as the fractal model and the Moran's *I* index of spatial autocorrelation were applied for addressing the issue of scale, while fuzzy set theory was applied for mapping heterogeneous urban land cover types. Three local government areas (e.g. the City of Perth, the City of Melville and the City of Armadale) of the Perth metropolitan area were selected, as the dominant land covers of these areas are representative to the whole metropolitan area, for the analysis of spatial complexity and the mapping of complex land covers.

Characterisation of spatial complexity of the study areas computed from SPOT, Landsat-7 ETM+, and Landsat MSS was used for assessing the appropriateness of a scale for urban analysis. Associated with this outcome, the effect of spectral resolution and land cover heterogeneity on spatial complexity, the performance of fractal measurement algorithms and the relationship between the fractal dimension and Moran's *I* were identified. A fuzzy supervised approach of the fuzzy *c*-means algorithm was used to generate fuzzy memberships of the selected bands of a Landsat-7 ETM+ scene based on the highest spectral separability among different urban land covers (e.g. forest, grassland, urban and dense urban) as determined by a transformed divergence analysis. Fuzzy land cover maps resulting from the application of fuzzy operators (e.g. maximum, minimum, algebraic sum, algebraic product and gamma operators) were evaluated against fuzzy memberships derived from the virtual field reference database (VFRDB). The performance of fuzzy operators in generating fuzzy categorical maps along with the effect of land cover heterogeneity on fuzzy accuracy measures and sources of classification error were assessed.

The analysis of spatial complexity computed from remote sensing images using a fractal model indicated that the various urban land cover types of the Perth metropolitan area are best represented at a resolution of 20 m (SPOT) as the fractal dimension (*D*) was found higher, as compared to the 25 m and 50 m resolutions of

the Landsat-7 ETM+ and Landsat MSS, respectively. Likewise, the results demonstrated the ability of the fractal model in distinguishing variations in the composition of built-up areas in the green and red bands of the satellite data, while forested areas typical of the urban fringe appear better characterised in the NIR band. Moran's *I* of spatial autocorrelation was found useful in describing the spatial pattern of urban land cover types. A comparison between the *D* and Moran's *I* of the study areas revealed a negative correlation, indicating that the higher the Moran's *I*, the lesser the fractal dimension indicating a lower spatial complexity.

The accuracy of the fuzzy categorical maps associated with multiple spectral bands of a Landsat-7 ETM+ scene using various fuzzy operators reveals that the fuzzy gamma operator ($\gamma = 0.90$) outperformed the categorical accuracy measures obtained by applying the fuzzy algebraic sum and other fuzzy operators for the City of Perth, while the accuracy measures of γ value of 0.95 were found highest for the City of Melville and the City of Armadale. A comparison of the accuracy measures of the fuzzy land cover maps of the study areas indicated that the overall accuracy of the City of Perth was up to 13% higher than the overall accuracy of the City of Melville and the City of Armadale which was found 69% and 71%, respectively. The lower accuracy measures of the City of Melville and the City of Armadale was attributed to highly mixed land cover classes resulting in mixed pixels in Landsat-7 ETM+ scene. In addition, the spectral similarity among the class forest and grassland, urban and dense urban were identified as sources of classification errors.

The analysis of spatial complexity using multiscale and multisource remote sensing data and the application of fuzzy set theory provided a viable methodology for assessing the appropriateness of scale selection for an urban analysis and generating fuzzy urban land cover maps from a multispectral image. It also illustrated the longstanding issue of carrying out the accuracy of the fuzzy land cover map considering the fuzzy memberships of the classified data and the reference data using a fuzzy error matrix.

ACKNOWLEDGMENTS

I am deeply indebted to my supervisor, Associate Professor Graciela Metternicht for her constant support and valuable guidance throughout this research. This thesis is an outcome of her constructive comments, unsparing criticism and painstaking editing. Without her help, this work would not be possible. I would also like to thank Dr Julie Delaney for her guidance in formulating the earlier version of this research proposal.

I would like to express my gratitude to Curtin University of Technology for offering the Australian Postgraduate Award (APA), which helped to complete the study. The initial stipend (Christopher Worth Memorial Scholarship) offered by the Department of Spatial Sciences along with research assistantship from Strategic Partnerships with Industry – Research and Training (SPIRT) project grant of the Australian Research Council, Agriculture Western Australia and SpecTerra Services Pty Ltd are gratefully acknowledged.

I would like to record my appreciation to a number of organisations, who provided the most valuable support through sharing of data, without them it was not possible to complete the thesis. Especially, I am thankful to Dr Richard Smith and Mr Peter Sanders of the Satellite Remote Sensing Services (SRSS), Leeuwin Centre for Earth Sensing Technologies, Perth, Western Australia for the provision of the satellite data set used in this research. I would also like to extend my thanks to SpecTerra Services Pty Ltd for the provision of air-borne data, the City of Armadale for land zoning map and Mr John Patterson of the Department of Planning and Infrastructure (DPI), Western Australia for the provision of updated city boundaries.

The help of Dr Dale A. Quattrochi, NASA and Dr. Charles W. (Jay) Emerson, Western Michigan University, USA for providing Image Characterisation and Modelling System (ICAMS) software is gratefully acknowledged. I must also mention the useful help from the academics, administrative staff and my fellow colleagues at the Department of Spatial Sciences who helped me greatly in various ways. Of particular, I express my heartfelt thanks to Mr. Tony Parrelli for his cooperation and support in setting the GPS equipment for field data collection, as

well as Ms Georgina Warren and Ms Deavi Purnomo for constructive problem solving discussions.

I would also like to thank Mr Quamrul Islam Siddique who inspired me to choose this area of study, which is increasingly emerging as the most potential area for natural resource management. Editorial support that I received from my friend Dr Shane Greive, Mrs Lori Patterson of the Department of the Spatial Sciences and Dr Maureen Massam of Student Support Unit deserve special mention. My close interaction with Dr Greive and involvement in a number of studies during my candidature at the University of Western Australia gave me an opportunity understanding the application of GIS at a wider level, which helped in strengthening my knowledge.

Finally, I want to thank my parents for their wholehearted support during the whole period of research. It is especially worthwhile to mention the encouragement I received from my mother that gave me fortitude for many late-night hours required to complete this research. Last but not the least, I would like to thank the continuous inspiration and encouragement from Dr Rita Afsar and her children for their support during the whole research.

TABLE OF CONTENTS

LIST OF FIGURES

LIST OF PLATES

LIST OF TABLES

LIST OF ACRONYMS

ABS	Australian Bureau of Statistics
AML	Arc Macro Language
ASCII	American Standard Code for Information Interchange
AVHRR	Atmospheric Very High Resolution Radiometric
BIL	Band Interleaved by Line
CAMS	Calibrated Airborne Multispectral Scanner
CV	Coefficient of Variation
D	Fractal Dimension
DN	Digital Number
ESRI	Environmental System Research Institute
ETM+	Enhanced Thematic Mapper
FMV	Fuzzy Membership Value
GERIS	Geophysical Environmental Research Imaging Spectrometer
GIS	Geographical Information Systems
GPS	Global Positioning System
ICAMS	Image Characterisation and Modelling System
LGA	Local Government Area
MSS	Multispectral Scanner
NASA	National Aeronautics and Space Administration
NDVI	Normalised Difference Vegetation Index
NIR	Near Infrared
OA	Overall Accuracy
PA	Producer's Accuracy
PDOP	Position Dilution of Precision
MIR	Middle Infrared
PMA	Perth Metropolitan Area
TM	Thematic Mapper
RAAF	Royal Australian Air Force
SPOT	*System Pour l'Observation de la Terre*
TIFF	Tag Image File Format
TPSA	Triangular Prism Surface Area

UA	User's Accuracy
UTM	Universal Transverse Mercator
VFRDB	Virtual Field Reference Database
WGS	World Geodetic System

Chapter 1

INTRODUCTION

This chapter outlines the research problem and background information for selecting an appropriate scale of remote sensing data for the correct interpretation and mapping of spatially complex urban land covers. Subsequently, the research objectives are defined, as are the expected outcomes and the benefits of the research. Lastly, the research methods are formulated and the thesis structure is outlined.

1. 1 Problem Formulation

Urban landscapes tend to be spatially complex as a result of heterogeneous land covers. They are characterised by the complex mixture and erratic spatial arrangement of artificial and natural land cover types. At landscape level, the complexity results from natural and human-induced activities, which modify processes and regulate the landscape structure (Quattrochi *et al.*, 1997), indicating a relationship between complexity and natural and human-induced activities.

With rapid transformations that are taking place in urban areas due to natural and human-induced processes, the change in urban landscapes is pronounced. Take for instance, the case of the Perth metropolitan area (PMA), which registered a sharp increase of population growth during the 1970s and 1980s, and experienced a substantial increase of urban population during the last four decades when urban population increased more than four times and reached around 1.40 million in 2001 (ABS, 2001). Existing estimates suggest that the annual population growth rate of the PMA has risen by far more than any other Australian capital city for at least 25 years with the exception of Brisbane between 1981 and 1986 (Birrell and Tonkin, 1992). Based on 'medium' projections, PMA is expected to have a population of two million by the year 2021 which translates into a requirement of over 0.4 million additional dwellings for the anticipated growth in household numbers (Department of Planning and Urban Development, 1991). In addition, the increase in demographic phenomenon has manifested increasing economic activities and services, transportation development and traffic flows.

The expansion of urbanisation decreases areas of remnant native vegetation, open space/grassland and water bodies. According to the Western Australian Planning Commission (1998), only 28 percent of the native vegetation remains on the major landforms of the PMA. Clearly, the problems related to the rapid transformations that are taking place within the PMA in terms of land cover and land use changes are pronounced. As a result, the availability of detailed, timely information on urban areas is of considerable importance both to the management of current activities and to forward planning. To this end, it is believed that satellite remote sensing has the potential to provide information regarding the spatial complexity and heterogeneity of land covers and their changes over time.

It is widely recognised that satellite remote sensing has the potential to provide up-to-date information related to the land covers and land uses of the earth surfaces. Accordingly, the application of remote sensing has grown rapidly in the last decades due to the increasing availability of commercial satellite remote sensing data which are acquired in a wide range of wavelengths varying from visible to microwave, with spatial resolutions varying from sub-metre to a kilometre. With such variety of data, the question of an appropriate scale and resolution for the interpretation of heterogeneous urban land covers often arises. In remote sensing, scale is related to spatial resolution (Woodcock and Strahler, 1987) which refers to the smallest distinguishable part of an object (Tobler, 1988), and it often determines the capability of a sensor for mapping and monitoring tasks.

A number of difficulties associated with the complexity of the urban landscapes arise due to the extreme heterogeneity of surface materials (land cover) at both the inter-pixel and intra-pixel scales. Using finer resolution satellite data (e.g. IKONOS), the inter-pixel variability of the digital numbers is high, as compared to the low intra-pixel variability. On the other hand, the inter-pixel variability of a coarser resolution satellite data (e.g. Landsat MSS) is low compared to a high intra-pixel variability (Jupp *et al.*, 1988). Depending upon the scale of observation, processes that appear homogeneous at a small scale may become heterogeneous at a larger scale (Lam and Quattrochi, 1992). Turner *et al.* (1989) showed that landscape pattern has a significant influence on the response of measurements related to changes in spatial scale. The underlying axiom of the spatial scale is the spatial complexity, which

changes with variations in scale (Meentemeyer and Box, 1987). This indicates that spatial processes are scale dependent and their interpretation varies from one scale to another (Stone, 1972). Accordingly, results are scale specific and the conclusions drawn from studies performed at one scale and applied to another may be incorrect (Foody and Curran, 1994). Thus, for a meaningful interpretation of heterogeneous land covers of an urban area, analysis of spatial complexity using multisource and multiscale remote sensing data with various spatial and spectral resolution needs to be investigated for selecting an appropriate sensor for such data analysis.

This requires the analysis of textural and contextual information content of multiscale remote sensing to select an appropriate scale for the correct interpretation and mapping of heterogeneous urban land covers.

1. 2 Background

1.2.1 Characterisation of Urban Spatial Complexity using Remote Sensing Data

Fractal analysis has been found effective for characterising the spatial pattern of land cover types identified from satellite- and air-borne imagery (De Cola, 1989; de Jong and Burrough, 1995). The key parameter in fractals is the fractal dimension, D, which is used to describe the spatial complexity of point patterns, lines and surfaces. The higher the fractal dimensions the more complex is the form (Quattrochi *et al.*, 1997; Read and Lam, 2002). Digital remotely sensed data are considered to be one form of spatial surfaces and the spatial complexity of these spatial surfaces can be measured by fractals. In addition to characterising the spatial pattern of land cover types, fractals and fractal analysis have been suggested for identifying the effects of scale changes on the properties of satellite and air-borne imagery (Lam and Quattrochi, 1992; de Jong and Burrough, 1995; Emerson *et al.*, 1999). Emerson *et al.* (1999) investigated the changes in fractal dimensions with changing spatial resolution (pixel size) and suggested selecting a finer resolution satellite data (high resolution) for analysing heterogeneous land uses (e.g. urban). In their study, it was indicated that the spatial resolution at which the greatest difference in spatial complexity occurs is optimal for distinguishing the land covers. Thus, fractal dimension of remote sensing data of an urban landscape acquired at different spatial,

temporal and spectral resolutions can be compared, and the effect of scale and spectral resolutions for characterising spatial complexity can be assessed.

Research has indicated that the *D* can help formulating hypotheses in relation to the spatial scale of process-pattern interactions. For example, Krummel *et al.* (1987) showed that a fractal model could be applied for analysing remotely sensed data, as the measured *D* provides an indication of the scale at which processes are occurring (i.e. operational scale). Changes in *D* computed from remote sensing data, therefore, have primary implications for changes in land uses and environmental conditions over extensive areas of the earth. O'Neill *et al.* (1988) demonstrated that the fractal dimension has a highly significant correlation with the degree of human manipulation of the landscape. Landscapes dominated by agriculture tend to have simple polygons and low fractal dimensions (negative correlation between the *D* and landscape of agriculture) and landscapes dominated by forest tend to have complex shapes and high fractal dimensions (positive correlation between the *D* and landscape of forest). Likewise, Read and Lam (2002) could explain the transition from a high degree to a lower degree of human disturbance by using *D*; from a low *D* for agriculture to a higher *D* for forest using Landsat-TM bands and NDVI. Thus, the application of fractals allows not only describing spatial patterns, but also help generating hypotheses about the cause of the patterns.

Operating on the assumption that the scale at which the highest *D* is measured may be the scale at which most of the processes operate (Goodchild and Mark, 1987; Lam and Quattrochi, 1992), one could apply the fractal model for analysing the spatial complexity of urban landscapes using multisource and multiscale remote sensing to determine the appropriateness of the scale (i.e. spatial resolution) for classifying heterogeneous urban land covers.

1.2.2 Mapping Urban Landscapes using Remote Sensing Data

Thematic mapping of urban landscapes using remote sensing images is challenging due to the heterogeneity of the land covers types. Often, the individual pixels of remote sensing image associated with urban land covers are the result of the interaction of more than one surface material (e.g. soil, grass, shrubs, concrete, asphalt) present within the area covered by a pixel (Forster, 1985). This results in the

occurrence of mixed pixels, especially when working with remotely sensed images of coarse spatial and/or spectral resolution. Conventional remote sensing classifiers (e.g. parallelepiped, maximum likelihood, minimum distance from the mean) that rely on the assumption that a training area is composed of unique, internally homogenous classes work poorly for urban land cover mapping (Zhang and Foody, 1998; Small, 2003). This is a limitation of the traditional parametric methods for deriving urban land covers (Zhang and Foody, 1998). Therefore the performance of classifiers that use morphological and contextual information or fuzzy classifiers based on fuzzy set theory for mapping heterogeneous urban land cover types has begun to be investigated.

In a fuzzy classification, a pixel is assigned a value representing its grade to each possible individual (e.g. land cover class) in the universe of discourse (e.g. urban areas). This grade corresponds to the degree to which that pixel belongs to its associated land cover class and it is termed 'fuzzy membership value' (FMV) (Lowell, 1994). To some extent, the FMVs reflect the land cover composition of a mixed pixel which enables a more accurate and realistic representation of land covers, overcoming some of the assumptions of the conventional classifications (Fisher and Pathirana, 1990; Foody and Cox, 1994). For example, Wang (1990a) demonstrated that FMVs provide more information about land cover compositions, which can be used for identifying mixed pixels by analysing the combination of fuzzy membership grades. Likewise, Pathirana (1999) utilised the FMVs, derived from the Thematic Mapper and SPOT multispectral data for determining the spatial distribution of mixed pixels, indicating its effect on the amount of errors in the classified data. Working with IKONOS multispectral bands (4 m resolution) and panchromatic band (1 m resolution) for urban land cover mapping, Shackelford and Davis (2003) reported an improvement of the classification accuracy, using a hierarchical fuzzy classification technique, as compared to the maximum likelihood classification. The hierarchical fuzzy classification utilised both spectral and spatial information to classify data which was found effective for discriminating spectrally similar classes such as buildings and roads, reducing the misclassification produced by the maximum likelihood classifier.

From previous work, it is apparent that fuzzy classification is conceptually superior to crisp classification techniques. Furthermore, fuzzy classification is advantageous due to its information richness with respect to class continua, which can be usefully explored to address the uncertainties of the classified data (Zhang and Foody, 1998). Several authors have suggested that fuzzy boundaries could be derived quantitatively using different criteria on fuzzy classified data, which provide theoretically sound and data-driven solutions to assess the uncertainties. For example, Burrough (1996) employed the concept of the confusion index to generate fuzzy boundaries evaluated as one minus the difference between the fuzzy membership values of location x belonging to the first maximum fuzzy membership and the second maximum fuzzy membership. The assumption underlying such an index is that the greater the confusion index, the smaller the difference in fuzzy membership values between the first most likely and the second most likely classes, and thus the more uncertain is the classification of location x. Similarly, Zhang and Kirby (1999) used the maximum fuzzy membership values of individual locations while Foody (1995) employed the concept of entropy to decide the class label to be assigned to a pixel with multiple FMVs. In this way, fuzzy classification can be implemented not only to generate FMVs of heterogeneous urban land cover types but also uncertainties of the classified data.

For multi-spectral satellite images, FMVs associated to predetermined informational classes can be generated for each band. According to An *et al.* (1991), the integration of FMVs of more than one layer of information sometime compensate each other in the final result. However, the question often arises as to how to select the most suitable combination of bands, which are to be fuzzified and integrated in the classification process. Assuming a Landsat-7 ETM+ data set is used for classifying four land cover types, without undertaking a band selection it would end up creating a total of 28 information layers (7 bands * 4 land cover types). This would result in a cumbersome number of layers to be integrated for obtaining fuzzy urban land cover maps, which in addition may contain redundant information. To this end, feature selection techniques such as the transformed divergence analysis can be employed for selecting the most appropriate sensor's band, or set of bands, to be fuzzified as part of the procedure for deriving urban land cover maps using fuzzy supervised classification (Metternicht, 1996; Metternicht and Zinck, 1997 and 1998).

Fuzzy operators based on fuzzy set theory (Zadeh, 1965) can be used to integrate the fuzzy memberships of selected bands, as these operators allow manipulating and processing incomplete and/or imprecise information to obtain the most reasonable output. Mohan *et al.* (2000) applied fuzzy operators to integrate the fuzzy memberships of different land uses as derived from multitemporal images, reporting a significant increase in classification accuracy. Though research has been carried out applying a variety of fuzzy operators for integrating fuzzy membership of geophysical and geological data sets (An *et el.*, 1991; Moon *et el.*, 1991), not many applications have focussed on the use of fuzzy operators for integrating fuzzy memberships of urban land cover, as computed on various bands of multispectral satellite image.

1.2.3 Accuracy Assessment of Interpreted Data

Accuracy assessment determines the quality of the output classification results derived from remotely sensed data. In a typical accuracy assessment analysis, the derivation of accuracy measures such as overall classification accuracy and the *Kappa* coefficient of agreement (Janssen and van der Wel, 1994) are associated with only one class in the classification and its corresponding class in the reference or ground data. Such accuracy measures are only appropriate for 'crisp' classification (e.g. where a pixel is classified as only one class). In fuzzy classification, the output can be hardened and pure pixels of the classified data can be compared with the reference or ground data and accordingly, accuracy measures can be determined (Foody and Trodd, 1993; Zhang and Foody, 1998). Although this provides a basis for evaluating the accuracy measures of fuzzy classification, the accuracy may remain dubious due to the difficulty in establishing a "truth" ground reference data set (Lunetta *et al.*, 2001). This may lead to a serious source of confusion in the derived map (Joria and Jorgenson, 1996). It can be noted that in an accuracy assessment, a pixel is used as a spatial unit and it is necessary to bring the ground data to the same spatial unit of the remotely sensed data for a meaningful comparison (Fisher, 1997). Therefore, knowledge of fuzzy ground data is needed for accuracy assessment in a fuzzy classification.

A number of ways can be applied to generate fuzzy ground data. For example, Gopal and Woodcock (1994) derived fuzzy ground data using a linguistic scale based

on quality of map labels which were converted into a numerical scale ranging from one to five indicating the degree of belonging to a particular class. Zhang and Foody (1998) used sub-pixel land cover proportions and indicator *kriging*, while Foody (1995) suggested a probabilistic approach using the proportion of different classes within a polygon or other mapping unit, such as pixel's equivalent area on the ground to generate the fuzzy ground data. Measures of closeness and fuzzy similarity can be employed to ascertain the accuracy between the land cover composition in the fuzzy classification and the composition measured by fuzzy ground data (Kent and Mardia, 1988; Jager and Benz, 2000). However, this approach may suffer from heuristic solution and lack of information concerning the sampling design (Foody, 1996a).

Zhang and Foody (1998) applied the 'maximisation' process in determining the accuracy measures using fuzzy classification and fuzzy ground data. This enabled them to label a pixel of fuzzy classification and fuzzy ground data as belonging to the individual class having the maximum fuzzy membership value and accordingly, conventional classification accuracy measures can be employed. The value of maximum fuzzy membership with reference to a pre-determined threshold can also be used to harden the output of a fuzzy classification and fuzzy ground data for enabling the use of conventional accuracy measures as done by Shackelford and Davis (2003). Others utilised the correlation between the proportions of corresponding memberships of reference and classified data by means of a coefficient of determination (r^2) in assessing the accuracy measures of the fuzzy classified data (e.g. Foody and Arora 1996).

The above discussion suggests that accuracy assessment of fuzzy classification requires fuzzy ground data. The idea of using hardened fuzzily classified data and fuzzy ground data in a traditional error matrix suffers loss of information and accordingly, the derived accuracy measures do not necessarily reflect how correctly the class memberships of the fuzzy classification match with the fuzzy ground data. Similarly, the measure of closeness and fuzzy similarity between the fuzzy membership of classified and reference data suffer from lack of appropriate sampling design. More importantly, these measures go beyond the traditional error matrix and do not provide site specific accuracy (Congalton, 1991). In a non-site specific accuracy assessment, locational accuracy is completely ignored. A fuzzy error

matrix, which is a generalisation of the traditional error matrix, designed to accommodate the fuzzy memberships of classified and reference data together with a fuzzy confusion index can be implemented to assess site specific accuracy of fuzzy classifications (Binaghi *et al.*, 1999).

1. 3 Research Objectives

1.3.1 Research Objectives

Scale is one of the most essential considerations for characterising the spatial complexity and heterogeneity of urban landscapes as the spectral and spatial resolution of remote sensing data varies from one sensor to another. Accordingly, a proper combination of digital image interpretation techniques need to be developed to: (i) analyse the spatial complexity and heterogeneity of urban landscapes using multiscale and multisource remote sensing data; and (ii) assess the appropriateness of these data for the interpretation of heterogeneous urban land covers. To this end, this research proposes using fractal theory for characterising the spatial complexity of urban land cover types and fuzzy set theory for characterising and modelling the heterogeneity of land cover compositions. Fractal theory is applied to:

(a) Determine the fractal dimensions (D) of land covers typical of urban landscapes, such as dense urban, urban residential and urban fringe using different types of remotely sensed data;
(b) Assess the effect of spectral and spatial resolutions of various sensor data on the fractal dimension of urban landscapes;
(c) Evaluate the correlation between fractal dimension (seen as an index of spatial complexity) and spatial statistical measures of variability (e.g. spatial autocorrelation);
(d) Test the performance of different fractal measurement algorithms on the determination of the fractal dimension of selected urban land cover types.

A fuzzy classification approach is used to map land covers that characterise highly complex and heterogeneous urban landscapes from multispectral satellite images. This requires:

(a) Selection of the best set of multispectral bands that provide the highest separability among the land cover classes;
(b) Derivation of fuzzy memberships of the selected bands;
(c) Testing the performance of different fuzzy operators for integration of fuzzy memberships from the selected bands;
(d) Fuzzy accuracy assessment of the land cover maps generated by applying various fuzzy operators;
(e) Selection of an optimal fuzzy operator for generating fuzzy land cover maps.

The fulfilment of these research objectives will enable answering the following research problems identified for the Perth metropolitan area:

(a) Can a viable methodology be developed for generating urban land cover maps using fuzzy sets?
(b) How can the accuracy assessment of the fuzzified land cover maps be carried out?
(c) Is there any relationship between the heterogeneity of urban land covers and the accuracy of the classified data?

Likewise, the use of fractal theory and measures of spatial autocorrelation will facilitate answering:

(a) How does the sensor's spatial and spectral resolution affect the spatial complexity measured by fractal geometry and spatial autocorrelation measures?
(b) How can spatial statistical measures be used to identify various land covers (e.g., dense urban, urban residential and urban fringe).

1.3.2 Expected Outcomes

Based on the research objectives and their proposed application in the study area, three expected outcomes are foreseen:

(a) The appropriateness of fractal measurement algorithms to analyse the spatial complexity of urban areas using multiscale and multisource remote sensing images;
(b) The appropriateness of the sensor data (e.g. spatial and spectral characteristics) for the analysis of heterogeneous urban land covers;

(c) A viable methodology to interpret heterogeneous urban land covers from remote sensing images using fuzzy modelling.

1. 4 Benefits of the Research

Remotely sensed data offer the opportunity to characterise, map and model spatial complexity and heterogeneity of urban landscapes. Accordingly, the study presents a method that includes analysis of spatial complexity of urban landscapes using multisource and multiscale remote sensing images followed by interpretation of heterogeneous urban land covers. Specifically, this study will contribute the following:

(a) A comprehensive approach for the analysis of spatial complexity using multiscale and multisource remote sensing data. This will demonstrate the effect of spatial and spectral resolution on the spatial complexity of urban landscapes and the appropriateness of specific sensor's data for interpretation of urban land covers;
(b) A better understanding of the performance of fractal measurement algorithms and other spatial methods (e.g. spatial autocorrelation measure) in determining the spatial complexity of urban landscapes;
(c) A viable methodology to interpret urban land covers from multispectral remotely sensed data using fuzzy classification, integrating multi-band fuzzy memberships by means of fuzzy operators and finally, accuracy assessment analysis using a fuzzy approach;
(d) The results of this case study can be adopted for use in other environments with similar conditions.

1. 5 Research Methods

There are two major aspects of this research. Firstly, the analysis of spatial complexity of urban landscapes using multiscale and multisource remote sensing data and secondly, interpretation of major land covers using fuzzy classification of remotely sensed data.

Available literature suggests that spectral location and bandwidth of remote sensing images affect the estimation of D. Therefore, when analysing the effect of different spatial resolutions, it is important to use a multi-sensor data set presenting

correspondence of spectral band location and width, to avoid the introduction of "noise". In doing so, three hypotheses were formulated to characterise the urban landscapes using multiscale and multisource remote sensing data. These are as follows:

(a) Any variation of D for the same land cover type and wavelength is due to changes in spatial resolution;
(b) Variations of D for the same land cover type and spatial resolution will be due to the effect of spectral band location;
(c) Variations of D for the same spatial and spectral resolution will be due to the different land cover types.

In order to test these hypotheses, fractal measurement algorithms such as the isarithm and the Triangular Prism Surface Area (TPSA) methods were applied in three study areas representing dense, medium and urban fringe areas to determine D using multisource Landsat ETM+, SPOT and Landsat MSS data. In addition, spatial autocorrelation measures were applied to examine whether there is a relationship between measures of spatial complexity (D) and measures of spatial autocorrelation.

Urban land cover types are characterised by high spectral variability of surface materials, which include a wide range of roofs, roads, sidewalks and parking lots along with bare soil, vegetation, and trees. The diversity of urban land cover types and their spectral response particularly in a moderate resolution imagery (30 m) results in mixed pixels representing an area on the ground which comprises more than one discrete land cover type and accordingly, display composite spectral response (Small, 2003). The allocation of the mixed pixels is problematic for statistical classification methods as most of the algorithms are based on the assumption of spectral homogeneity within a particular type of land cover and often results in relatively high rates of misclassification in an urban environment (Small, 2003). Thus it was hypothesised that the heterogeneity of land cover compositions can be better characterised and modelled using fuzzy set theory.

In order to test the above hypothesis, the fuzzy supervised approach of fuzzy c-means algorithm was applied in three study areas to generate FMVs of four major urban land cover classes in pre-selected Landsat-7 ETM+ bands. Fuzzy operators

(e.g. maximum, minimum, algebraic sum, algebraic product and gamma operators with γ values ranging from 0.1 to 0.95) were applied to integrate the FMVs determined for each urban land cover on the multi-spectral data set. The performance of the land cover maps generated by various fuzzy operators was assessed using a fuzzy error matrix.

1. 6 Thesis Structure

This thesis is comprised of eight chapters. Chapter 1 outlines the research problem and background information for selecting an appropriate scale of remote sensing data for the correct interpretation and mapping of spatially complex urban land covers. Subsequently, the research objectives have been defined, as well as the expected outcomes and the benefits of the research. Lastly, the research methods have been formulated.

Chapter 2 reviews the principles of aspatial and spatial methods for measurement of spatial complexity and fuzzy set theory for the interpretation and accuracy assessment analysis of urban land covers using multispectral remote sensing data. Previous research regarding measurement of spatial complexity and the application of fuzzy set theory for mapping urban land covers is also discussed. The methods and techniques available and the various criteria to be considered are described.

Chapter 3 describes the research approach applied to measure the spatial complexity and mapping of heterogeneity of urban land cover types using remotely sensed data. Spatial autocorrelation measures and fractal techniques were used for the analysis of spatial complexity and accordingly, the principles of these approaches are described. The transformed divergence analysis was implemented for selecting the most appropriate combination of bands of a multispectral satellite image, which were used to derive the fuzzy memberships of the major land covers. Fuzzification was undertaken using a supervised approach of the fuzzy *c*-means algorithm. The conceptual overview and the general methodology of the fuzzy *c*-means algorithm and the principles of fuzzy operators, which were used to integrate the fuzzy memberships of the selected bands, are described. Then, the methods for generating fuzzy ground data, used to carry out the accuracy of fuzzily classified data are discussed.

The location and the characteristics of the major land cover types of the study areas are illustrated in Chapter 4. The multiscale remote sensing images such as SPOT, Landsat-7 ETM+ and Landsat MSS, which were used in the analysis of spatial complexity and interpretation of urban land covers, are discussed. In addition to remote sensing images, secondary source data such as aerial photographs, land use and land zoning maps used in this study are also discussed. An overview of the major software that were used in the analysis is outlined.

Chapter 5 illustrates the implementation of a spatial autocorrelation measure, Moran's *I* and the fractal measurement algorithms such as the isarithm and the TPSA to determine the spatial complexity of the three study areas characterising the urban landscapes of the Perth metropolitan area as described in Chapter 4. Then the supervised approach of the fuzzy *c*-means algorithm, which was written in Arc Macro Language (AML) of Arc/Info is implemented for deriving the fuzzy memberships of urban land cover types from the selected bands of a Landsat-7 ETM+. The final section of the chapter discusses the implementation of the fuzzy operators, which were used to integrate the fuzzy memberships of the selected bands, the defuzzification and fuzzy accuracy assessment.

The analysis of spatial complexity of the study areas computed from SPOT, Landsat-7 ETM+, and Landsat MSS using fractal measurement algorithms and a spatial autocorrelation measure (Moran's *I*) is presented in Chapter 6. Based on the hypotheses, the analyses on (i) how the spectral and spatial resolution affect the analysis of spatial complexity of urban landscapes; and (ii) how the spatial complexity varies in changing the land cover compositions of the study areas are presented. The parameters and the performance of different fractal measurement algorithms in measuring the spatial complexity are discussed. Finally, the selection of an appropriate sensor data for the interpretation of land cover classes based on fractal analysis is discussed.

Chapter 7 presents the accuracy measures determined from the fuzzy error matrix of the fuzzy categorical maps generated by different fuzzy operators as discussed in Chapter 5. In addition to accuracy measures, uncertainty maps were used for assessing the performance of the fuzzy operators for generating fuzzy land cover maps. Furthermore, this chapter discusses the sources of classification error of

individual land cover classes of the fuzzy categorical maps derived from the best fuzzy operator. Finally, the fuzzy categorical maps derived from the best fuzzy operator of the study areas are used to assess the effect of land cover heterogeneity on the accuracy measures.

The main conclusions based on the findings of this research and recommendations for further research are presented in Chapter 8. The first expected outcome was to select the scale (spatial resolution) in which the processes of urban landscapes occurred based on fractal dimension computed from SPOT, Landsat-7 ETM+ and Landsat MSS. Associated with this outcome, the effect of spectral resolution and land cover heterogeneity on spatial complexity and the performance of fractal measurement algorithms in computing fractal dimension are discussed. The second outcome is related to the performance of fuzzy classifiers, including the use of fuzzy operators in generating fuzzy categorical maps along with determining the effect of land cover heterogeneity on fuzzy accuracy measures and identification of sources of classification errors. Finally, recommendations for future research are presented.

Chapter 2

SPATIAL COMPLEXITY AND INTERPRETATION OF URBAN LANDSCAPES USING REMOTE SENSING DATA

Chapter 2 reviews the principles of spatial methods for the measurement of spatial complexity and fuzzy set theory for the interpretation and accuracy assessment analysis of urban land covers using multispectral remote sensing data. Previous research regarding the measurement of spatial complexity and the application of fuzzy set theory for mapping urban land covers and accuracy assessment analysis is also discussed. The methods and techniques available and the various criteria to be considered are described.

2. 1 Measurement of Spatial Complexity of Urban Landscapes

Spatial complexity of urban landscapes can be measured using the spatial arrangement of differences in pixel values (either brightness values or transformed values) relative to one another, which characterise a scene of a remote sensing image. Various spatial statistical methods (semivariogram, spatial autocorrelation measures, and fractal geometry) can be applied to characterise the spatial complexity of urban landscapes. The principles associated with the measurement of spatial complexity using these methods with particular focus on the fractal theory and its application for characterising multiscale and multisource remote sensing data, are described in the following sections.

The coefficient of variation (CV) is the local variability of remotely sensed data which measures the total relative variation of pixel values in an area (de Jong and Burrough, 1995). However, it does not provide any information about spatial patterns and irregularities. Similarly, other neighbourhood operations such as diversity or variation filters can be employed but they also do not provide information on spatial complexity (Burrough, 1993a; Klinkenberg, 1992; Snow and Meyer, 1992; Unwin, 1989).

2.1.1 Semivariogram

The semivariogram is based on the concept that the statistical variation of data is a function of distance. For a pair of pixels, the semivariance is half of the differences of the variances of digital numbers embedded with the pixels. Measurement of dissimilarity between spatially separate pixels is useful, as it provides a concise and unbiased description of the scale and pattern of spatial variability of remotely sensed data (Curran, 1988).

In a semivariogram, experimentally derived semivariances are commonly used to fit with a mathematical model (e.g. linear, spherical, exponential) which interpolates and optimises the sampling networks. For details, see Curran (1988) and Woodcock *et al.* (1988a, 1988b). Typically, a semivariogram, fitted in a model, contains a range, a nugget, and a sill. These parameters along with mathematical modelling are used to assess spatial patterns present in remotely sensed data (Curran, 1988; Woodcock *et al.*, 1988b; de Jong and Burrough, 1995). In general, the nugget provides information on variability between adjacent pixels, the sill indicates the total variability and the range presents information on spatial dependence of reflectance (Webster and Oliver, 1992; Ten Berge *et al.*, 1983; McBratney and Webster, 1981). However, these parameters along with the shape of the variogram change with change of the spatial resolution of remote sensing images. Woodcock *et al.* (1988a, 1988b) examined the effect of spatial resolution on the shape of the variograms, making the following observations:

(a) The height of the sill (or the variance of the variable) decreases as the spatial resolution decreases. This indicates that the variability of data decreases with decreasing the spatial resolution. Conversely, the variability increases with increasing the spatial resolution;

(b) The range of influence or the distance to sill increases with decreasing the spatial resolution. It signifies the level of spatially uncorrelated variation in the data increases with decreasing the spatial resolution; and

(c) The height of the variogram at the first measured interval of h increases in relation to the sill.

Available literature suggests that the semivariogram is a robust tool to measure the spatial variability of remotely sensed data but yet the method suffers from a number

of disadvantages. Firstly, the estimated variogram for the same landscape units may differ using different samples i.e. sets of observations (Webster and Oliver, 1992; Isaaks and Srivastava, 1989). Secondly, the variogram of a transect is a global estimator and does not give information on local variation. Thus, a local estimator is needed to analyse the image to distinguish different land cover patterns (de Jong and Burrough, 1995). Thirdly, it is difficult to define a 'best model criteria' for estimating variogram parameters in an automatic procedure (de Jong and Burrough, 1995).

2.1.2 Spatial Autocorrelation Measures

Spatial autocorrelation measures attempt to deal simultaneously with similarities in the location of spatial objects and their attributes (Longley *et al.*, 2001). It is a scale-dependent statistic used as an indicator of the degree of clustering, randomness or fragmentation of a pattern (Read and Lam, 2002). Accordingly, the attributes of a given variable are said to be spatially correlated if there exists a systematic spatial variation. This variation can exist in two forms, positive or negative spatial autocorrelation. In the positive case, the value of a variable at a given location tends to be similar to the values of that variable in nearby locations. Conversely, negative spatial autocorrelation is characterized by dissimilar variate values in nearby locations. For example, a low variate value may be surrounded by high values in nearby locations when negative spatial autocorrelation exists. Moran's I and Geary's C (Cliff and Ord, 1973) are two most commonly used indices of spatial autocorrelation measures.

In an analysis using remote sensing images, spatial autocorrelation measures consider the digital number (DN) values of the pixels. In general, adjacent pixels would be more likely to display similar values than pixels that are spatially separated (Woodcock *et al.*, 1988a). According to Jupp *et al.* (1988), spatial autocorrelation in an image can be affected by object size, spacing and shape. In addition, a sensor's spatial resolution will have an effect on the overall spatial autocorrelation present in a remotely sensed image. Thus, spatial autocorrelation measures can be employed to measure the spatial complexity of urban landscapes using multiscale remote sensing images.

2.1.3 Fractal Geometry: An Overview

Most spatial patterns of nature including curves and surfaces are irregular and fragmented. These features do not exhibit a deterministic pattern or an Euclidean shape. For example, the coastline of an island is neither straight nor circular. It is difficult to describe the forms of such feature in classical geometry (e.g. Euclidean geometry). Fractal analysis provides a mathematical framework for describing complicated, irregular features of variation (Burrough, 1993b). In fractal geometry, the dimension of a coastline can be any value between 1 and 2, depending on the curve's degree of complexity. The higher the fractal dimensions the more complex is the form. Similarly, a plane may have a dimension whose values lie between 2 and 3 (Lam, 1990). The concept of fractal dimension was first formulated by mathematicians Hausdorff-Besicovitch; it being Mandelbrot (1977) who labelled "fractal dimension" and defining fractals as "a set for which the Hausdorff-Besicovitch dimension strictly exceeds the topological dimension" (cited in Lam, 1990).

The key notion of fractal analysis is the use of 'self- similarity' property (Falconer, 1990). Many curves and surfaces are self-similar either strictly or statistically indicating the fact that each portion of the curve or surface can be portrayed as a reduced scale of the whole curve or surface. This can be explained by the example of the Koch curve (Figure 2.1). In Figure 2.1, a straight line is divided into three equal segments and replaces the middle segment by the two sides of an equilateral triangle of the same lengths. Then, each of the four segments is divided into three equal parts and replaces the middle segments by two sides of an equilateral triangle. Infinite recursion of this process can yield a curve which is non-differentiable and of infinite length. Clearly, it demonstrates that each part of the curve is indistinguishable and a copy of itself and thus self-similar. The fractal dimension, D of a Koch curve can be derived using the following equation:

$$D = \log N / \log (1/G) \tag{2.1}$$

where G is the step size and N number of steps required to traverse the curve. The above equation can be simplified as it follows if a linear regression is performed between the length of the curve and the step size.

$$\log L = C + B \log G \tag{2.2}$$

$$D = 1 - B \tag{2.3}$$

where L is the length of the curve, B is the slope of the regression line and C is a constant.

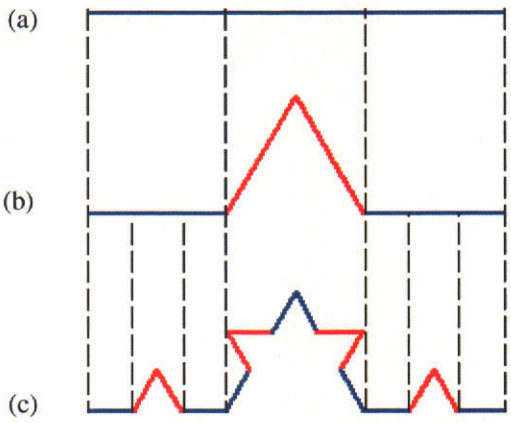

Figure 2.1 Self-similarity property of Koch curve

Considering the 'self-similarity' property, fractal models assume that the form or pattern of the spatial phenomenon remains unchanged throughout all scales. Empirical studies showed that most of the real world phenomena such as coastlines and surfaces are seldom pure fractals and self similarity rarely exists at all scales (Goodchild, 1980; Mark and Aronson, 1984; Klinkenberg and Goodchild, 1992). In such cases, specific fractal dimensions are defined only for specific scale ranges at which the regression behaves linearly (Quattrochi *et al.*, 2001). Research in spatial science indicated that the complicatedness of spatial phenomena is a direct consequence of the operation of many different spatial processes at a wide range of scales (De Cola, 1989). Accordingly, the spatial phenomenon may have different forms at different scales of measurement. Thus, D can be used to assess the changes of a spatial phenomenon in changing the scale or in other words, D can provide an indication of spatial complexity at different scales (Lam, 1990). Various fractal measurement algorithms such as the variogram, the isarithm and the triangular prism surface area (TPSA) can be applied to determine the fractal dimension of multiscale and multisource using remote sensing images. These methods are described in detail in Chapter 3 and a brief overview of their performance is described hereafter.

2.1.4 Fractal Models in Remote Sensing

Fractal analysis is a relatively new technique for characterising remote sensing images to identify the effects of scale changes on the properties of images (De Cola, 1989, 1993; Lam and Quattrochi, 1992; de Jong and Burrough, 1995; Quattrochi *et al.*, 1997; Emerson *et al.*, 1999). The idea of using fractals in image analysis is to determine the textural heterogeneity, which is locally estimated in areas around pixels and a fractal map is produced as a result. Table 2.1 lists the fractal measurement algorithms commonly used for estimating the fractal dimension of land cover types using remotely sensed data.

Digital remotely sensed data can be considered to be one form of spatial surfaces and the complexity of these spatial surfaces can be measured by fractals (Lam, 1990). This can be demonstrated by considering a single band image as a virtual topographic surface where the rows and columns represent the cell coordinates while the digital numbers of each cell are an imaginary elevation. For an image comprising the same cell value, the resulting virtual topographic surface would be flat which corresponds to a fractal dimension of 2.0 whereas, an infinitely complex image having highly uncorrelated cell value results in a fractal dimension of 3.0 (Turcotte, 1992). Available literature shows the use of fractal models in a variety of remotely sensed data such as ground-based photography (Carr, 1990), aeromagnetic data (Gregotsky *et al.*, 1991), Landsat TM (De Cola, 1989; Lam, 1990; de Jong and Burrough, 1995; Quattrochi *et al.*, 1997; Ricotta *et al.*, 1998; Emerson *et al.*, 1999; Read and Lam, 2002), Landsat-7 ETM and IKONOS data (Read, 2003), thermal infrared multispectral data (Jaggi *et al.*, 1993), airborne imaging spectrometer data (de Jong and Burrough, 1995), AVHRR data (Ricotta and Avena, 1998), airborne laser altimetry data (Pachepsky *et al.*, 1997) and hyperspectral data (Qiu *et al.*, 1999) for estimating D in various applications, as shown in Table 2.1.

Several studies have applied the fractal technique for dealing with reflectance patterns of land cover types (Lam, 1990; De Cola, 1993; de Jong and Burrough, 1995; Ricotta and Avena, 1998); spatial patterns of land cover types (De Cola, 1989); landscape diversity (Milne, 1991; Lagro, 1991; Olsen, *et al.*, 1993; Ricotta *et al.*, 1998); and characterisation of surface shapes derived from images (Pentland, 1984; Kube and Pentland, 1988; Rees, 1992).

Table 2.1 Most commonly used algorithms for estimating the fractal dimension from remotely sensed data

Algorithm	Reference	Type of Land Cover Type	Sensor/ Satellite	Spatial Resolution (m)
Area-Perimeter Method	Read and Lam (2002)	Forest, Scrub, Pasture, Agriculture, Urban and Barren	Landsat TM	25
	Ricotta *et al.* (1998)	Mediterranean Vegetation	Landsat TM	30
	Olsen *et al.* (1993)	Six Landscape Patches	Landsat TM	30
	De Cola (1989)	Hardwoods, Hayland, Softwoods, Water, Brush, Wetland, Grassland, Bare, Corn and Urban	Landsat TM	30
Triangular Prism Surface Area Method	Read (2003)	Logged Forest, Old-Growth Forest, Logged Forest excluding Major Roads	Landsat-7 ETM+ and IKONOS	30, 15, 4 and 1
	Read and Lam (2002)	Forest, Scrub, Pasture, Agriculture, Urban and Barren	Landsat TM	25
	Qiu *et al.* (1999)	Urban and Rural	Hyperspectral	17
	De Jong and Burrough (1995)	Badlands, Rangelands, Open and Closed Garrigue, Maquis and Agriculture	Landsat TM and Air-borne Image	30 and 10
	Jaggi *et al.* (1993)	Forest, Agriculture and Water	Air-borne	30
Isarithm Method	Read and Lam (2002)	Forest, Scrub, Pasture, Agricultural, Urban and Barren	Landsat TM	25
	Quattrochi *et al.* (2001)	Urban and Desert	Landsat TM	25
	Qiu *et al.* (1999)	Urban and Rural	Hyperspectral	17
	Emerson *et al.* (1999)	Agriculture, Forest and Urban	Air-borne and Landsat TM	10 and 30
	Jaggi *et al.* (1993)	Forest, Agriculture and Water	Air-borne	30
	Lam (1990)	Urban, Rural and Coastal	Landsat TM	25
Variogram Method	Ricotta and Avena (1998)	Grassland, Shrubs, Forest and Livestock Grazing Area	AVHRR	1000
	De Jong and Burrough (1995)	Badlands, Rangelands, Open and Closed Garrigue, Maquis and Agriculture	Landsat TM and Air-borne	30 and 10
	Jaggi *et al.* (1993)	Forest, Agriculture and Water	Air-borne	30
	Rees (1992)	Ice-Sheet	Landsat TM	25

De Cola (1989) demonstrated the application of the fractal model to describe the spatial complexity of different land cover types (see Table 2.1) which was found to be useful for improving the classification accuracy. In this approach, the classified Landsat TM image was segmented into class-induced regions and fractal analysis was carried out using the perimeter and area of these regions. The results suggested that urban areas exhibited complicated forms as compared to intensive agriculture, hardwood forests, and water, spanning the range of extreme D values. Apart from estimating D, this method generated grid-based GIS data structure based on regions, which is useful for detailed examination and identification of features including

statistics for diagnosis of misclassification. Olsen *et al.* (1993) applied fractals as a measure of distribution of landscape diversity. In their study, six 10- by 10 cell (300- by 300 m) sub-landscapes which are subsets of 5- by 5 km classified Landsat TM were used to examine the landscape diversity. The results indicated that the use of sub-landscapes was a better measure to evaluate diversity in the context of a large landscape. It is important to note that the methodologies of these studies focused on the post-classification of remotely sensed data and considered the area and the perimeter of various landscape patches for describing the spatial pattern.

On the other hand, Lam (1990) used the reflectance properties of all seven (visible, near, mid-infrared and thermal) bands of a Landsat TM image to characterise the spatial complexity of various land covers by measuring their fractal dimension. In her study, subsets of 201- by 201 cell of Landsat TM image with 25- by 25 m spatial resolution data were used for three different land cover types (e.g. urban, rural and coastal area). The results revealed that the land cover types exhibited different fractal dimension and the urban area was found to be the most spatially complex with high fractal dimension (D) values in bands two and three. For example, in an urban area, D was found 2.73 in band three while band two resulted a D of 2.72. The results demonstrated a number of avenues for future study. For example, multi-sensor data sets for the same study area acquired at about the same time could be used to examine the effects of various spectral and spatial resolutions from the resultant fractal dimension. This was further emphasised by Jaggi *et al.* (1993) in their study of implementation of fractal measurement algorithms for analysis of NASA's Calibrated Airborne Multispectral Scanner (CAMS) of 30 m resolution data. Although the results varied according to the type of algorithm used, the quantification of the spatial complexity and the information content of satellite images at multiple spatial resolutions (e.g. 10, 20, 30 m) over the same area is emphasised to understand the effect of scale.

de Jong and Burrough (1995) introduced a fractal model for improving the classification of satellite imagery when individual, but neighbouring pixels have different spectral signatures characterising a given land cover type. The results indicated that fractal modelling can be used as additional information in spectral classification procedures to improve the classification results. In addition, it also

demonstrated the effect of spatial resolution on the measurement of *D* using Landsat TM with a pixel size of 30- by 30 m and Geophysical Environmental Research Imaging Spectrometer (GERIS) with a nominal pixel size of 10- by 10 m. In their study, six different Mediterranean vegetation types were selected and the fractal dimension was calculated using the variogram and the triangular prism surface area (TPSA) methods. Reflectance values measured randomly by hand-held radiometer with a field of view of 1 m^2 along various transects were used in the variogram method whereas the TPSA was applied on the multi-spectral images with different spatial resolution. The results of the two methods were useful for classifying the land cover types, although there were instances where the results varied. An in-depth analysis of the results showed that the ability of *D* to separate the land-cover types depends on the spatial resolution of the imagery used, indicating the effect of scale on the heterogeneity of land cover types. Thus, they concluded that fractal modelling could be used to analyse multiscale remote sensing data for choosing an appropriate spatial scale and the type of remote sensing data to be used in specific landscape analyses.

Emerson *et al.* (1999) investigated the application of the fractal model to examine the effect of spatial and temporal resolution on spatial complexity, using the Normalised Difference Vegetation Index (NDVI) derived from an airborne high-resolution scanner, and Landsat TM images. In their study, the airborne scanner acquired over a medium sized city with a spatial resolution of 10 m was re-scaled to coarser resolutions of 20, 30 and 40 m while Landsat TM acquired four months apart over a mountainous areas separated by broad valleys with a spatial resolution of 30 m was re-scaled to 60, 120, 240, 480 and 960 m. The fractal dimensions computed from the air-borne scanner of the selected land covers revealed that the spatial complexity of an agricultural image increases as pixel size increases, while the forested area showed a general decline of *D* and areas of the images corresponding to urban land cover remained roughly self-similar over the range of pixel sizes tested (10 to 80 m). A similar analysis of multi-temporal Landsat TM imagery indicated a more complex relation between spatial resolution and fractal dimension. This was attributed to the absence of snow cover in the summer image.

Read and Lam (2002) examined the potential of spatial methods such as the fractal model and Moran's *I* of spatial autocorrelation, and selected landscape pattern metrics such as Shannon's diversity index (McGarigal and Marks, 1995) and the contagion index (Li and Reynolds, 1993) for characterising unclassified remotely sensed data for land-cover discrimination and change detection. The results revealed that the fractal dimension and Moran's *I* were useful for distinguishing differing degrees of spatial complexity represented by land-cover types. Specifically, the ability of fractal signatures to distinguish forest and non-forest cover types in the study area was demonstrated. Similarly, Read (2003) investigated the potential of spatial methods such as the fractal model and Moran's *I* for characterising recent (less than one year old) logging activities using Landsat-7 ETM+ and IKONOS data. The results showed that fractal dimension and Moran's *I* index of spatial autocorrelation were effective for distinguishing canopy disturbances resulting from logging activities.

With the inherent ability of the fractal technique for addressing the multiple scale phenomena as evidenced from previous research, remote-sensing data acquired from various sensors at different spatial and spectral resolution can be compared and evaluated. For example, fractal dimension of Landsat TM data can be used to measure the spatial complexity and can be compared with other types of remotely sensed data such as Landsat MSS, SPOT, IKONOS, and Quickbird. This can provide a basis to select appropriate remote sensing data for the interpretation of heterogeneous urban land covers on the assumption that the scale at which the highest fractal dimension is measured may be the scale at which most of the processes of the urban landscape analysed operate.

2.1.5 Performance of Fractal Measurement Algorithms

As discussed in the previous section, fractal modelling is useful for analysing the spatial complexity of different land cover types using remotely sensed data. However, conflicting results on the performance of the fractal measurement algorithms have been reported. For examples, Jaggi *et al.* (1993) tested the performance of the isarithm, the triangular prism surface area (TPSA) and the variogram methods in measuring the *D* using NASA's Calibrated Airborne Multispectral Scanner (CAMS) data acquired at a spatial resolution of 30 m. The

results showed that the TPSA method slightly underestimated the spatial complexity of images, as compared to the isarithm method. However, the variogram method exhibited higher D compared to the values provided by the other methods. Klinkenberg and Goodchild (1992) found similar inconsistencies on the results from different methods in their study for characterising the fractal properties of topography using a digital elevation model. They hypothesised that the variability of the D is not a reflection of any theoretical inadequacy of the self-similar fractal model, but rather a function of the methods applied.

Working with satellite and airborne data with a spatial resolution of 30 m and 10 m respectively, de Jong and Burrough (1995) found discrepancies in the fractal dimension (D) of different land cover types of the Mediterranean vegetation (see Table 2.1) from the variogram and the TPSA techniques. The following observations were made to the variations of the results:

(a) The differences of the techniques (the variogram and the TPSA) and the spatial resolution (which varied from one meter along transects to 30 m for Landsat TM image) were attributed as the source of discrepancies on the results. However, the same resolution data were used for estimating D by both techniques, yet the results differed. The inconsistencies of the results indicated that the computation technique influences the measurement of D, as also reported by Klinkenberg and Goodchild (1992).

(b) The variations of the results for the same technique were attributed to a noise factor and the varying spatial resolution of the images used in the analysis.

Likewise, Quattrochi *et al.* (1997) applied the variogram and the isarithm method to a Landsat TM scene of 201 x 201 pixels to measure the D. The results revealed variations in the D as a result of changes in the parameters of the methods. For example, the variogram method was found very sensitive to the breakpoints included in the regression. They randomly selected 1007 points from TM band 1 with breakpoints from 1 to 30 and constructed the variogram. From the slope of the regression, the D was found to be 2.97 with a regression coefficient equal to 0.54. This value (i.e. 2.97) was likely to change if a different range of points was used to determine the regression slope. Thus, the regression coefficient is important in measuring the slope, and a number of researchers concluded that in order to estimate

the *D* it is better to select a range of points yielding higher r^2 (Mark and Aronson, 1984; Jaggi *et al.*, 1993; Lam and De Cola, 1993). For the isarithm method, the average *D* was found to be 2.69, considering all the isarithms. The results were consistent with those yielded from a previous study carried out in the same area by Lam (1990). However, the *D* was found to be much higher (2.90) if only isarithms, which yield a $r^2 \geq 0.9$ were included in the averaging process. There are other issues which influence the measurement of the *D* in the isarithm method (for details see Section 3.3.2.1). Likewise, Lam *et al.* (1997) found that the isarithm method performed well in returning *D* values close to those of true surface dimensions.

Kolibal and Monde (1998) examined the accuracy and noise susceptibility of fractal measurement algorithms using an image of known fractal plane. In terms of accuracy, the results indicated that the TPSA method produced consistently accurate results whereas the variogram method showed the poorest performance since it overestimated the fractal dimension compared to other methods. However, the variogram results were found least influenced by noise since this technique averages the pixel values across the entire image, thus tending to minimise its effect in the image. The TPSA method also appeared resistant to the influence of noise. They concluded that algorithmically, the TPSA method is the easiest to implement. Likewise, working with simulated surfaces of known fractal dimension, Lam *et al.* (2002) reported that the TPSA method estimates the most accurate fractal dimension of surfaces having higher spatial complexity.

The TPSA method is easy to implement given that it requires only one user input parameter (i.e. number of measuring steps) (see details in Section 3.3.2.2), but it tends to underestimate the fractal dimension computed from the remotely sensed data (Jaggi *et al.* 1993; Lam *et al.*, 1997). A slight modification of the TPSA method which uses the number of measuring grids (e.g. 1, 2, 4, 8, 16), instead of the square of the measuring grids (e.g. 1, 4, 16, 64, 256) exhibited more accurate results (Qiu *et al.*, 1999). Lam *et al.* (1997) found the variogram method to be unsuitable for use with remote sensed imagery, which has a tendency to display higher dimensionality than topographic surfaces. Accordingly, the isarithm and the TPSA techniques were selected for characterising the spatial complexity of remotely sensed data acquired over an urban area.

2. 2 Fuzzy Classification for Urban Land Cover Types using Remote Sensing

In fuzzy classification using satellite- or air-borne remotely sensed data, urban land covers can be defined as fuzzy sets, and pixels as set elements. Accordingly, each pixel is attached with a group of membership grades to indicate the extent to which the pixel belongs to predetermined land covers. The membership grades are termed fuzzy membership values (FMVs). The notion of fuzzy classification is to generate FMVs based on the fuzzy set theory introduced by Zadeh (1965). Thus, derivation of FMVs is the single most important consideration in fuzzy classification.

2.2.1 Derivation of Fuzzy Membership Values (FMVs)

2.2.1.1 Defining Fuzzy Sets

Zadeh (1965) proposed the concept of fuzzy set, which introduces vagueness by eliminating the sharp boundary dividing members from non-members of a class. Specifically, it assigns a membership value, as a function of its similarity to the individual class, and typically varies between 0 and 1. A membership close to 1 denotes strong relations to a particular class, whereas a membership close to 0 represents weaker relationships.

A fuzzy set can be defined mathematically. Let X denote a universal set (e.g. urban area) with a generic element of X denoted by x, thus $X = \{x\}$.

$$A = \{x, \mu_A(x)\}; x \in X \tag{2.4}$$

A fuzzy set A (land cover class) in X is characterised by a membership function $\mu_A(x)$ which associates with each point in X a real number in the interval [0,1]. The value of $\mu_A(x)$ represents the grade of membership of x in A (Zadeh, 1965).

2.2.1.2 Defining Fuzzy Membership Values

The membership function of a fuzzy set, usually expressed as $\mu_A(x)$, defines how the grade of membership of x in A is determined. There are two possible ways of deriving these membership functions. The first approach is the Semantic Import (SI) approach. It uses an *a priori* membership function with which individuals can be assigned a membership grade. This is useful in situations where users have a very

good, qualitative idea of how to group data, but for various reasons have difficulties with the exactness associated with the standard Boolean model (Burrough and McDonnell, 1998). The SI approach relies on expert knowledge where boundary values are chosen by custom, law or external taxonomy to generate the fuzzy memberships (Burrough, 1986). The selection of class boundaries and class intervals can be an objective or subjective process, depending on the way scientists agree to define classes (Burrough and McDonnell, 1998). However, it does not mean that selecting class intervals is an arbitrary process, as often careful consideration is devoted to the selection of sensible boundaries between classes (Metternicht, 1998). According to Burrough and McDonnell (1998), the membership function should ensure that the grade of membership is 1.0 at the centre of the set that it falls off in an appropriate way through the boundaries to the region outside the set where it takes the value of 0. The location where the fuzzy membership equals 0.5 is called the 'crossover point'. These conditions need to be considered in defining fuzzy membership function. There are several suitable functions, which can be adapted to define membership grades. For example, Metternicht (1998 and 1999) adopted a bell-shaped model as described by Dombi (1990) to generate fuzzy membership.

The second approach, named by Robinson (1988) as the similarity Relation Model, resembles cluster analysis and numerical taxonomy is that the value of the membership function is a function of the classifier used. A common version of this model is the fuzzy *c*-means, also known as fuzzy *k*-means model based on cluster analysis. The cluster analysis refers to the identification of distinguished clusters whose subsets contain points, which have high intracluster resemblance and simultaneously, low intercluster similarity. Fuzzy clustering was introduced by Ruspini (1969) and was later developed into fuzzy *c*-means clustering by Dunn (1974) and generalised by Bezdek (1975). In fuzzy *c*-clustering, the idea is to represent the similarity a point shares with each cluster using a membership function which varies between 1 and 0 (Zadeh, 1965). This indicates that points do not belong to only one particular cluster, rather they are assigned membership values for each individual cluster being constructed. Thus, each sample will have a membership to every cluster and membership values close to 1 signify a high degree of similarity between the sample and the cluster, while membership values close to 0 imply little similarity between the sample and that cluster. The net effect of such a

function for clustering is to produce fuzzy c-clusters for a given data set along with the membership grades of each location.

The most commonly used algorithm of fuzzy c-clustering is the fuzzy c-means, which has been applied in numerous remote sensing studies to define memberships of the c-clusters (McBratney and Moore, 1985; Cannon *et al.*, 1986a; Trivedi and Bezdek, 1986; Key *et al.*, 1989; Fisher and Pathirana, 1990; Foody, 1992; Foody and Trodd, 1993; Foody, 1996a; Zhang and Foody, 1998; Pathirana, 1999; Mohan *et al.*, 2000). It can be used in a supervised or unsupervised classification fashion. In unsupervised classification, it works by an iterative procedure with an initial random allocation of the objects to be classified to c or k clusters while in supervised classification prior knowledge about c-clusters needs to be provided. Apart from the fuzzy c-means algorithm, a range of classifiers namely, maximum likelihood classifier (Foody *et al.*, 1992), fuzzy supervised classification (Wang, 1990a and 1990b), linear mixture modelling (Settle and Drake, 1993), artificial neural networks (Foody, 1996a) and supervised nonparametric classifier (Skidmore and Turner, 1988) can be applied to derive partial membership within a pixel. Recently, possibilistic-c means clustering (Foody 2000) and support vector machines (Brown *et al.*, 2000) have also been applied to unmix the class proportion within a pixel.

2.2.2 Fuzzy Classification in Land Cover Mapping

As already mentioned, fuzzy classification allows a gradual transition between land cover classes as the fuzzy membership of any location (pixel) lies in the interval [0.1]. The conceptual superiority of fuzzy classification has been demonstrated in many studies as it avoids problems associated with crisp classification technique (e.g. maximum likelihood classifier) and has become a popular alternative method for land cover mapping. For example, Wang (1990a, 1990b) showed that the proportions of land covers in mixed pixels can be identified using fuzzy memberships of the major land cover classes. In this study, the membership functions are defined based on the maximum likelihood classification algorithm with fuzzy mean and fuzzy covariance matrix instead of the conventional mean and covariance matrix. Accordingly, fuzzy memberships of predetermined land covers were generated using Landsat MSS data. In order to compare the accuracy, the fuzzy training data were hardened and accordingly, the conventional maximum likelihood

classification was performed on the same data set. The accuracy was assessed on the hardened classification generated from the fuzzy partition matrix, which showed an improvement (5.11 percent) in overall classification accuracy as compared to the output of conventional classification. Likewise, Fisher and Pathirana (1990) investigated the application of fuzzy classification in determining the land cover compositions of pixels in a suburban environment using Landsat MSS data. The results showed that the fuzzy classifier enabled extraction of information about individual pixels and subpixel phenomena, which were not addressed by other classifiers (e.g. parallelepiped, maximum likelihood, minimum distance from the mean). In their study, the fuzzy membership functions were defined using unsupervised approach of fuzzy *c*-means algorithm and accordingly, fuzzy memberships of the predetermined clusters were generated. The results of these studies showed how the fuzziness of mixed land cover classes occurring within a pixel was addressed.

Foody and Trodd (1993) examined two alternative approaches to model the continuous representation of heathland vegetation using measures of the strength of membership to discrete classes, namely probabilities of class membership from a maximum likelihood classification and fuzzy membership function from the fuzzy *c*-means algorithm. The measures of the strength of class membership generated from both approaches were found to be significantly correlated to the variations in heathland composition along a transect, which graded from dry heath to wet heath. Likewise, Foody (1992) and Foody *et al.* (1992) showed that the fuzzy membership can be used to discriminate accurately between the end points of a set of continua and the strength of class memberships are related to the canopy compositions.

Foody (1996a) investigated the accuracy of the derived fuzzy membership using a discriminant analysis, an artificial neural network and the fuzzy *c*-means algorithm. The results showed that the fuzzy representations were more accurate than the conventional crisp classification. In addition, the outputs of the derived fuzzy memberships from the artificial neural network and the fuzzy *c*-means algorithm in particular were strongly related to the land cover on the ground and provided the most accurate land cover representations.

In an attempt of sub-urban land cover mapping from multispectral satellite image, Zhang and Foody (1998) investigated the accuracy of crisp and fuzzy classification using crisp and fuzzy evaluation techniques. In their study, bands 1, 2, and 3 of SPOT HRV and bands 3, 4, and 5 of Landsat TM were used to generate the FMVs using the supervised approach of fuzzy *c*-means algorithm. Two methods were employed to generate the fuzzy ground data. Firstly, sub-pixel land cover proportions, as relevant to SPOT HRV data (10 m) and Landsat TM (10 m), were derived from the aerial photographs. Secondly, indicator kriging was used to spatially interpolate class membership. The results showed that the Kappa coefficients were more than doubled when applying the fuzzy evaluation technique as opposed to crisp evaluation technique.

Pathirana (1999) investigated the spatial distribution of misclassified pixels and the amount of these pixels associated with each cover types using the fuzzy memberships of the land cover classes. Thematic Mapper (TM) and SPOT multispectral data sets were used and the fuzzy *c*-means algorithm was run to generate the FMVs of the land cover classes. The results showed that the spatial distribution of erroneously classified pixels was not random and varied depending on the nature of land cover types. The proportions of such pixels were higher in spectrally less clearly defined land cover types such as grassland.

Shackelford and Davis (2003) demonstrated the usefulness of fuzzy classification in discriminating the spectrally similar classes in order to improve classification accuracy from a high resolution multispectral imagery of an urban area. Panchromatic and multispectral IKONOS data sets were classified using the maximum likelihood classifier which produced significant amounts of misclassification errors between spectrally similar classes such as road and building and grass and tree. A hierarchical fuzzy classification which incorporates both spectral and spatial information discriminated the spectrally similar classes and accordingly, resulted a higher classification accuracy (up to 10 percent) as compared to maximum likelihood classifier.

Zhang and Kirby (1999) presented the methods of deriving the fuzzy boundaries of land covers from the output of the fuzzy classified data. In their study, SPOT HRV data and Landsat TM were used and the fuzzy memberships of selected land cover

classes were generated using the supervised approach of the fuzzy *c*-means algorithm. Three criteria, namely, maximum fuzzy membership values (Zhang, 1996), confusion index (Burrough, 1986), and a measure of entropy (Foody, 1995) were applied to generate the fuzzy boundaries using the output of fuzzy classified data. The results demonstrated a theoretically sound and data-driven solution to estimate the errors in attributes and identifying the uncertain zones of the classified data.

It is apparent that fuzzy classification holds advantages over conventional classification in:

(a) Expressing the vagueness of spatially distributed categories e.g. land covers derived from remote sensing images;
(b) Offering information on continua of land cover classes; and
(c) Generating fuzzy boundaries e.g. uncertain zones among the land cover classes.

Thus, fuzzy classification seems to an obvious choice for mapping urban land covers due to the heterogeneity of land covers, which results in the occurrence of mixed pixels in remote sensing data. However, the arbitrariness of defining the fuzzy membership is a major constraint in generating final fuzzy land cover maps and subsequent accuracy assessment analysis. Zadeh (1968) proposed the idea of presenting fuzzy memberships above a suitable threshold as unions of defuzzified areal classes and fuzzy boundaries. The concept of a defuzzification technique based on the maximum membership values obtained for individual locations can be applied to generate fuzzy land cover map using the outputs of fuzzy classification (Zhang and Goodchild, 2002).

2. 3 Accuracy Assessment of Fuzzy Classification

2.3.1 Background Information

In a typical accuracy assessment analysis, pixels of land cover classification are compared with corresponding locations of the sample data to ascertain whether the land cover classification assigned to the pixel matches the true classification of the sample data. The conventional accuracy measures are only appropriate for hard classifications, which indicates that the derivation of accuracy measures are

associated with only one class in the classification and its corresponding class in the reference or ground data (Foody, 1995). It, however, fails to examine closely the source and magnitude of errors (e.g., mismatches between classification and reference map) in classifications (Gopal and Woodcock, 1994). Furthermore, it cannot provide any accuracy measures below the individual class level (Zhang and Foody, 1998). Clearly, it fails to accommodate the accuracy measures of the mixed pixels. This is a major limitation for evaluating the accuracy of the fuzzy classification, and the lack of such methods in the conventional accuracy assessment is a barrier to adoption of fuzzy classification (Goodchild, 1994).

Gopal and Woodcock (1994) demonstrated the suitability of fuzzy set theory in the accuracy assessment of thematic maps in order to analyse the nature, frequency, source, and magnitude of errors using fuzzy ground data. They argued that the situation of a sample in the field of a particular category being exactly right and all other categories being equally and exactly wrong often does not exist. This leads to the possibility of uncertainty in assigning the map label in the traditional map evaluation process, as the map label can be either correct (agreement) or incorrect (disagreement). However, the uncertainty of map labelling can be improved introducing a membership based on the land cover compositions of the ground sample sites. Gopal and Woodcock (1994) used a linguistic scale based on quality of map labels and accordingly, each site was assigned the most suitable linguistic value. The linguistic values were converted into a numerical scale ranging from one to five indicating the membership functions. Various functions (e.g. max, right, difference and membership), based on fuzzy set theory were used to assess the magnitude, source, and nature of errors of the classified data (see Gopal and Woodcock, 1994, Woodcock and Gopal, 2000, Laba *et al.*, 2002 for details). The results of the empirical data analysis demonstrated the usefulness of fuzzy sets in accuracy assessment.

The generation of membership of field data based on a linguistic scale was implemented in a large project to carry out the accuracy assessment. For example, Laba *et al.* (2002) used the methodology proposed by Gopal and Woodcock (1994) and compared the output map accuracy using conventional and fuzzy accuracy assessment. From their results, they concluded that conventional accuracy

assessment serve as a basis of primary source of information on the quality of land cover maps. However, in the case of uncertainty on quality and ambiguity associated with a given classification, the fuzzy accuracy assessment method was recommended. Muller *et al.* (1998) slightly modified the methodology and carried out the accuracy assessment in a land-cover map of the Kuparuk river basin in Alaska. In their methodology, the arithmetic mean of the *difference* was calculated individually for matches and mismatches categories. The study concluded that the use of fuzzy methods provided a more realistic field observation, which contributed to a fairly accurate image classification. The combination of fuzzy sets with the error matrix provided a more precise analysis of the nature and source of classification errors.

It is apparent that Gopal and Woodcock (1994) considered the fuzziness of reference data to measure a range of indicators such as nature, frequency, magnitude and distribution of errors of classification performance. The additional accuracy indicators clearly demonstrate the advantages of this method over the traditional method. However, it shares the disadvantage that the methods are only appropriate for the situation in which there is ambiguity in the ground data but not the classification data (i.e. the ground data are fuzzy and the classified data are 'hard').

Entropy which is a measure of uncertainty was suggested by a number of researchers to assess the accuracy of fuzzy classification (e.g. Finn, 1993; Maselli *et al.*, 1994; Foody, 1995). Foody (1996a) argued that entropy is inappropriate for the evaluation of fuzzy classification as the fuzziness of the land cover on the ground is overlooked, and emphasised the need of accommodating the fuzziness of classification output and ground data for a meaningful accuracy assessment. One such approach is the measure of closeness between the fuzzy memberships derived from remote sensing image and the fuzzy memberships of ground data derived from various methods such as sub-pixel land cover compositions (Zhang and Foody, 1998), indicator kriging (Zhang and Foody, 1998) and probabilistic approach (Foody, 1995). However, this approach may suffer from heuristic solution and lack of information concerning the sampling design (Foody, 1996).

Zhang and Foody (1998) demonstrated the accuracy measures of fuzzy classification using the maximisation operation which enables to label a pixel of fuzzy

classification and fuzzy ground data as belonging to a particular class having the maximum fuzzy value and accordingly, conventional classification accuracy measures can be derived. The value of the maximum fuzzy membership with reference to a pre-determined threshold can also be used to harden the output of the fuzzy classification and fuzzy ground data for enabling the use of conventional accuracy measures. This process is termed as slicing process (Zhang and Foody, 1998). Many authors utilised the correlation between the proportions of corresponding memberships of reference and classification data by means of a coefficient of determination (r^2) or correlation coefficient (e.g. Foody and Arora 1996) to assess the accuracy. However, the measures of determination or correlation lack a spatial component, and therefore they do not necessarily reflect the reality of specific locations (Binaghi *et al.*, 1999).

Jager and Benz (2000) presented a mathematical framework based on fuzzy similarity to evaluate fuzzy classification and fuzzy ground truth data. The outputs are numbers ranging from zero to one indicating increasing similarity between the fuzzy classified data and the reference data. Using empirical data, Jager and Benz (2000) compared the accuracy measures obtained from the confusion matrices and the fuzzy similarity measures. In the confusion matrices, defuzzified classification and defuzzified ground truth data were used while fuzzy classification and fuzzy ground truth data were utilised in the fuzzy similarity measures. The accuracy measures from the confusion matrices varied substantially, as compared to those of fuzzy similarity measures. The study concluded that accuracy measures based on fuzzy classification and fuzzy ground truth data are more reliable and the accuracy values give the correct interpretation. However, obtaining reliable fuzzy ground truth data is a concern which is decisive in carrying out accuracy assessment analysis.

Seemingly the methods discussed above generated encouraging results and have something to offer in assessing the accuracy of fuzzy classification but none of them are universally applicable. More importantly, a major limitation of most of the approaches described above is that they go beyond the error matrix and do not provide 'location preserving' accuracy. According to Congalton (1991), in a 'non-location preserving' accuracy assessment, locational accuracy is completely ignored.

This indicates that total amounts of a category are considered without regard for the location. In such a situation, ceasing out of errors might lead to a higher accuracy but misleading.

Binaghi *et al.* (1999) proposed a new method based on fuzzy set theory to extend the applicability of the traditional error matrix to the evaluation of fuzzy classification. Typically, the error matrix associated with the new method is termed as 'fuzzy error matrix'. In this approach, the derived descriptive techniques are reformulated in the context of the theoretical framework of fuzzy set. Accordingly, the grades of membership representing the classes of classification and/or reference data can be used and the fuzzy error matrix performs precisely as the corresponding traditional matrix in producing the accuracy measures. It is important to note that fuzzy error matrix preserves the property of error 'localisation' consisting in 'the capability of identifying the contribution of each category relative to the actual category verified in the reference data' (Binaghi *et al.*, 1999).

2.3.2 Derivation of Fuzzy Ground Data

The discussions of the previous section indicate that accuracy assessment of a fuzzy classification requires fuzzy ground-truth data. A number of approaches can be implemented to generate fuzzy ground-truth data. One such method is the sub-pixel land cover proportions, which can be derived from a higher resolution satellite- and air-borne data as compared to the remote sensing data used in deriving the fuzzy memberships. Zhang and Foody (1998) demonstrated the derivation of sub-pixel land cover proportions using aerial photographs, as relevant to SPOT HRV data (10 m) and Landsat TM data (30 m). They used the technique of photogrammetric digitisation of land cover classes from aerial photographs using a reconstituted stereo model on an analytical plotter. This process resulted in land cover ground data polygons, which were rasterised to grids with a cell size of 1 m. The finer grid data were then aggregated in accordance with the SPOT HRV and Landsat TM pixel sizes independently. Data for the proportions of sub-pixel components of the land covers were calculated on a pixel-by-pixel basis with respect to the land cover classes considered.

Indicator kriging which estimates the conditional probability distribution without making assumptions about the form of the prior distribution functions can be used to generate fuzzy ground data. In this approach described by Zhang and Foody (1998), a set of classified samples was identified from screen-displayed photogrammetric data so that each point represents full membership (1.0) of the named class with zero membership values to the other classes. They were transformed to a grid with a cell size equal to 2.5 m and the semi-variograms were calculated. Then, kriging was undertaken with the output grid cell sizes equal to the pixel sizes of SPOT HRV and Landsat TM data respectively. This resulted in probability vectors at individual locations and accordingly, the sub-pixel land cover proportions could be computed.

Another way of deriving fuzzy ground data as suggested by Foody (1995) was to generate probabilities from the proportion of different classes present within a polygon or other mapping unit, such as a pixel's equivalent area on the ground. Then interpolation methods may be applied to map the gradual variations along the boundaries (Zhang and Foody, 1998). In this method, the changing pattern of the class probabilities depends on a function, which is based on distance between the points of the candidate class. Lowell (1994) proposed an approach of map 'skeletonisation' which attempts to delineate the defined boundaries of different classes and then convert the boundaries into fuzzier classes using a distance function. However, the distance based interpolation may not be appropriate for a discrete class such as lake whose probability will vary abruptly rather continuously. Importantly, even for a continuous class, the probability of the candidate points may not be a simple function of the distances from the points of known probabilities (Zhang and Foody, 1998). Gopal and Woodcock (1994) demonstrated the suitability of using a linguistic scale to derive fuzzy memberships of the ground-truth data based on the proportions of the land cover types of the sample sites. The advantage of this approach is that a statistically sound sampling strategy can be employed in order to overcome bias.

2.3.3 Derivation of a Fuzzy Error Matrix

An error matrix is a square array of numbers set out in rows and columns. Traditionally, the results of remotely sensed data classifications are tabulated in the error matrix whose columns represent the sample data (e.g. reference) and rows

indicate the classified data (Card, 1982) and form the basis for a series of descriptive and analytical statistical techniques (Congalton, 1991; Rosenfield and Fitzpatrick-Lins, 1986). A typical error matrix in Table 2.2 shows the accuracy measures of N number of pixels classified into c categories. The main diagonal of the matrix indicates correctly allocated pixels whilst the off-diagonal elements represent incorrect allocation (Story and Congalton, 1986). From an error matrix, using the correct and incorrect allocation of the pixels, a number of accuracy measures such as user's accuracy, producer's accuracy, error of commission, error of omission and overall accuracy can be derived (Story and Congalton, 1986).

Table 2.2 A typical error matrix showing commonly used accuracy measures

Classified Data, C_m	Reference Data, R_n 1	2	.....	C	User's Accuracy (UA) (%)
1	N_{11}	N_{12}	.....	N_{1c}	$N_{11}/\Sigma N_{1i}$
2	N_{21}	N_{22}	.....	N_{2c}	$N_{22}/\Sigma N_{2i}$
.....	.....	.....	.....	.....	.....
C	N_{c1}	N_{c2}	.....	N_{cc}	$N_{cc}/\Sigma N_{ci}$
Producer's Accuracy (PA) (%)	$N_{11}/\Sigma N_{i1}$	$N_{22}/\Sigma N_{i2}$	.....	$N_{cc}/\Sigma N_{ic}$	

Similar to an error matrix, fuzzy error matrix is a square matrix whose columns represent the actual categories (reference data) while the rows indicate the classified data. It is a generalisation of the traditional error matrix, which is based on the concept of fuzzy set theory introduced by Zadeh (1965). The advantage of the fuzzy error matrix is that it accommodates the fuzzy memberships of the reference and classification data in deriving the accuracy measures. The derivation of a fuzzy error matrix from the traditional error matrix can be explained using the classical set theory and derived set operations. Let X denote a universal set, R_n be the set of ground truth data assigned to class n and C_m be the set of classified data assigned to class m, with $1 \le n \le c, 1 \le m \le c$ and c as the number of classes.

In conventional accuracy assessment, ground truth and classified data are considered as crisp. Thus, each individual observation of the ground truth and classified data can be represented into two groups (e.g. members and nonmembers). This indicates that a sharp, unambiguous distinction exists between members and nonmembers of

the ground truth and classified data and they are separated by a hard boundary. The process by which individuals from a given sample data set X are determined to be either member or nonmembers of the classes n and m is defined by the following characteristic or discrimination function of the sets R_n and C_m (Binaghi *et al.*, 1999).

$$\mu_{R_n} : X \rightarrow \{0,1\} \tag{2.5}$$

$$\mu_{C_n} : X \rightarrow \{0,1\} \tag{2.6}$$

For the above given sets, the membership values (e.g. member or nonmember) assigned to the functions $\mu_{R_n}(x)$ and $\mu_{C_n}(x)$ respectively, to every $x \in X$ in the following manner

$$\mu_{R_n}(x) = \begin{cases} 1 \text{ if } x \in R_n \\ 0 \text{ Otherwise} \end{cases} \tag{2.7}$$

$$\mu_{C_n}(x) = \begin{cases} 1 \text{ if } x \in C_m \\ 0 \text{ Otherwise} \end{cases} \tag{2.8}$$

The elements of the conventional error matrix M in row and column of Table 2.1 represent the cardinality of their intersection set $C_m \cap R_n$ which can be expressed by the following equation.

$$M(m,n) = |C_m \cap R_n| = \sum_{x \in X} \mu_{C_m \cap R_n}(x) \tag{2.9}$$

with the following characteristic function:

$$\mu_{C_m \cap R_n}(x) = \begin{cases} 1 \text{ if } x \in C_m \wedge x \in R_n \\ 0 \qquad \text{Otherwise} \end{cases} \tag{2.10}$$

In the context of soft classification, the crisp set of R_n and C_m are represented in fuzzy set proposed by Zadeh (1965) and lets denote them as $\tilde{R}_n$ and $\tilde{C}_n$. Accordingly, the membership function of the fuzzy sets $\tilde{R}_n$ and $\tilde{C}_n$ can be expressed by the following functions.

$$\mu_{\tilde{R}_n} : X \rightarrow [0,1] \tag{2.11}$$

$$\mu_{\underset{C_m}{\sim}} : X \rightarrow [0,1] \tag{2.12}$$

where $[0,1]$ denotes the interval of real numbers between 0 to 1.

The fuzzy memberships of the two fuzzy partitions of $\{\tilde{R}_n\}$ and $\{\tilde{C}_m\}$ of the sample data set X are used in the derivation of fuzzy error matrix $\tilde{M}$. Similar to conventional error matrix, the assignment to the element of fuzzy error matrix $\tilde{M}(m,n)$ involves the computation of the degree of fuzzy memberships in the fuzzy intersection set $\tilde{C}_m \cap \tilde{R}_n$. For the intersection operation, several different classes of functions have been proposed in the literature (Dubois and Prade, 1985). However, the standard operation fuzzy AND (minimum) as model of intersection of the fuzzy set theory still possess particular significance (Klir and Folger, 1988). Another argument of using Fuzzy AND is its simplicity as compared to the variety of fuzzy set operators.

Accordingly, fuzzy AND, a logical intersection that combines the fuzzy memberships of two or more bands using the minimum operator introduced in the original formulation of the theory of fuzzy sets (Zadeh, 1977) can be used to determine the generic element of the fuzzy error matrix. This can be expressed mathematically by the following (Binaghi *et al.*, 1999):

$$\tilde{M}(m,n) = \left| \tilde{C}_m \cap \tilde{R}_n \right| = \sum_{x \in X} \mu_{\underset{C_m}{\sim}} \cap_{\underset{R_n}{\sim}} (x) = \sum \min\left(\mu_{\underset{C_m}{\sim}}(x), \mu_{\underset{R_n}{\sim}}(x) \right) \tag{2.13}$$

The above expression clearly demonstrates that the assignment of the generic element of the error matrix $\tilde{M}(m,n)$ is an extension of the conventional error matrix (see Equation 2.10). The theoretical aspects and the various accuracy ameasures of a an error matrix and fuzzy error matrix are further described in Chapter 3.

2.3.4 Sampling Strategy for Generation of Fuzzy Ground Data

It is cumbersome to consider every image pixel in generating a representative error matrix and hence, various sampling schemes have been proposed to select pixels to carry out the accuracy assessment. Therefore, an appropriate sampling strategy is required to select sample data that are logistically feasible, spatially accurate, and statistically relevant. The factors associated with sampling strategy such as sampling unit (e.g. pixels or polygons), sample size and sampling technique (e.g. random sampling) are discussed below.

2.3.4.1 Sampling Unit

A sample data set consists of a number of sampling units. The first step in devising a sampling strategy in any accuracy assessment is to choose the sampling unit. There are four possibilities: a single pixel, a cluster of pixels (often a 3×3 pixel square), a polygon, and a cluster of polygons as a sampling unit for area based accuracy assessment (Congalton and Green, 1999). In a land cover map derived from satellite data, area is often used to evaluate the accuracy and the ideal sampling unit is the individual pixel if a per-pixel classification is required (Janssen and van der Wel, 1994). However, the choice of single pixel may be misleading. This is because, its representation as an arbitrary square shaped landscape unit may not relate to the actual delineation of the land cover (Congalton, 1991). Moreover, the accuracy of a GPS receiver combined with the potential accuracy of the map itself could add a high level of uncertainty in locating individual pixels on the ground (Muller *et al.*, 1998). Thus, a cluster of pixels, typically a 3×3 block, is commonly used as a sample unit to collect sample data (Muller *et al.*, 1998; Congalton and Green, 1999). The choice of a cluster of pixels allows to account for GPS receiver imprecision while comparing ground reference data with map data, and also minimises image registration problems since it is larger than one pixel and therefore easier to locate on the reference data (Muller *et al.*, 1998; Congalton and Green, 1999).

2.3.4.2 Sample Size

One important task of an accuracy assessment analysis is to select the appropriate sample size. Collection of samples is expensive. Thus, the sample size should be kept to a minimum with an adequate representation from each category, so that the

accuracy assessment analysis is statistically valid. However, selection of the majority of samples from the most accurate category and few from the confused categories appears to give better accuracy (Congalton and Green, 1999).

There are a number of ways in which a sample size can be determined. For example an equation based on the binomial distribution or the normal approximation to the binomial distribution has been used to compute the sample size (Rosenfield *et al.*, 1982; Curran and Williamson, 1986; Congalton, 1988). The equations are based on the proportion of correctly classified samples (pixels, clusters or polygons) with some allowable errors. These techniques are statistically sound for ascertaining the sample size, but the conceptual issues associated with these techniques limit use in the error matrix. It is important to note that an error matrix does not simply consider the amount of correct or incorrect samples but it accounts for confusion amongst categories (Hay, 1979; Fitzpatrick-Lins, 1981). Therefore, the use of these techniques for determining the sample size appears inappropriate.

Remote sensing analysis generally deals with large numbers of pixels and the more traditional sampling scheme (e.g. random) is often practical. Thus, there is a need to balance between a statistically sound sample and a practical sample. A general guideline suggested the collection of a minimum of 50 samples for each land cover category present in the error matrix (Hay, 1979; Congalton, 1991; Muller, *et al.*, 1998; Congalton and Green, 1999). The guidelines further state that if the area is especially large or the classification has a large number of land cover categories (i.e., more than 12 categories), the minimum number of samples should be increased to 75 or 100 per category. Alternatively, the appropriate sample size can be computed using a multinomial distribution, which demonstrates a good balance between statistical validity and practicality (Congalton and Green, 1999).

2.3.4.3 Sampling Technique

Apart from sample unit and sample size, the distribution of samples plays an important role in accuracy analysis. In order to reach a valid conclusion about a map's accuracy, there is a need to ensure that the selection of the sample is made without bias. This confirms which sampling technique gives the smallest variance and highest precision for a given cost (Cochran, 1977). Failure to meet the above

criteria might lead the resulting error matrix to over or underestimate the true accuracy. Therefore, the selection of a proper sampling technique is critical in generating an error matrix, which represents the entire map.

There are five common sampling techniques: simple random sampling, stratified random sampling, systematic sampling, stratified systematic unaligned sampling, and cluster sampling (Congalton and Green, 1999). In a simple random sampling, a random number generator is used to choose random x, y coordinates to select samples. In almost any statistical analysis, the benefit of randomness is that each member of the sample data has an equal and independent chance of being selected and thus, ensures that the sample will be selected without bias. Stratified random sampling is similar to simple random sampling, however, some prior knowledge about the study area is used to divide the area into groups or strata. In the case of accuracy assessment of remotely sensed data, the classified image has been stratified into land cover types. The major advantage of a stratified random sampling is that all strata (i.e., land cover types), no matter how small, will be included in the sample.

Systematic sampling is a method in which the samples are selected at some interval over the study area. In most cases, the first sample is randomly selected and each successive sample is taken at some specified interval. The major advantage of systematic sampling is in choosing samples uniformly over the entire study area. Stratified systematic unaligned sampling attempts to combine the advantages of randomness and stratification with the ease of a systematic sample without falling into the pitfalls of periodicity common to systematic sampling. In addition to the sampling techniques already discussed, cluster sampling has been frequently used in assessing the accuracy of remotely sensed data, especially to collect information on many samples quickly.

In an accuracy assessment analysis, the statistically ideal design is either a simple random sampling or stratified random sampling (Hord and Brooner, 1976; Hay, 1979). Zonneveld (1974) suggested a stratified random sampling is preferable and Van Genderen *et al.* (1978) agreed that a stratified random sampling is the 'most appropriate method of sampling in natural resource studies using remotely sensed data'. This has been further substantiated in the study by Janssen and van der Wel (1994). According to Janssen and van der Wel (1994), 'preferably, stratified random

sampling should be used and should be based on distinguished classes'. Congalton (1988) compared the sampling techniques using different number of samples over remotely sensed images of forest, rangeland and grassland and concluded that the performance of random sampling is suitable for selecting samples from less spatially complex classes, whereas systematic and stratified systematic unaligned sampling greatly overestimate the parameters. He further stated that stratified random sampling worked well for the case of small, but important areas, which need to be included in the sample. Congalton's concern with the bias of systematic and stratified systematic unaligned sampling seems contradictory to Fitzpatrick-Lins's (1981) and Campbell's (1987) interpretation. Campbell (1987) stated, "if the analyst knows enough about the region to make a good choice of grid size, the stratified systematic nonaligned samples is likely to be among the most effective".

2. 4 Summary

This chapter reviews the principles of analysing spatial complexity of urban landscapes using multiscale remote sensing data, which provides a basis for selecting an appropriate sensor for the mapping and accuracy assessment of major urban land cover types. The investigation of spatial complexity using multiscale remote sensing data includes spatial statistical methods like the semivariogram, spatial autocorrelation measures and fractal theory, while the mapping of urban land covers and accuracy assessment are based on fuzzy set theory.

The semivariogram is a robust method, based on the idea that the statistical variation of data is a function of distance. The variogram parameters such as the nugget provide information on variability between adjacent pixels, the sill gives information on the total variability of the area considered and the range presents information on spatial dependence. It is apparent that the variogram parameters are useful for describing the spatial patterns of remotely sensed data and could be used in the analysis of multiscale remote sensing image. However, one of the major limitations of this method is in defining 'best model criteria' for estimating variogram parameters in an automatic procedure (de Jong and Burrough, 1995).

Spatial autocorrelation measures are effective for examining the spatial variation of the attributes (digital numbers of pixels) of a given variable (remote sensing image).

When there is systematic spatial variation in the values (digital numbers) of the pixel of an image, spatial autocorrelation exists. This variation can exist in two forms called positive or negative spatial autocorrelation. Moran's *I* and Geary's *C* (Cliff and Ord, 1973) are two most commonly used indices of spatial autocorrelation measures which can be employed to measure the spatial complexity of urban landscapes using multiscale remote sensing images, and therefore they will be tested in this study.

Fractal theory provides a mathematical framework to describe complicated and irregular variations of lines and surfaces. Digital remotely sensed data are considered to be one form of spatial surfaces and the spatial complexity of these spatial surfaces can be measured by fractals. The key concept of fractal is the self-similarity property. In other words, the shape of a fractal object or surface is independent of the scale at which it is measured. Thus, the spatial complexity of remote sensing data acquired at different spatial, temporal and spectral resolutions can be measured and the effect of spatial and spectral resolutions can be assessed. The analysis of spatial complexity of multiscale remote sensing images indicates that an optimal spatial resolution for distinguishing the various land covers is one at which the greatest difference in complexity occurs (Emerson *et al.*, 1999). Thus, the multiscale analysis of remote sensing images using a fractal model is thought to provide information for selecting an appropriate sensor for mapping urban land cover types. Accordingly, fractal model using fractal measurement algorithms such as the isarithm and the TPSA will be applied to multiscale remote sensing images for selecting an appropriate sensor for urban land covers using the analysis of spatial complexity.

Fuzzy set theory provides useful concepts and tools for dealing with the uncertainty of derived urban land cover maps from remotely sensed data. The key to the derivation of fuzzy land cover maps relies on defining appropriate fuzzy membership functions (Klir and Yuan, 1995). Two broad approaches, namely the semantic import (SI) model and the similarity relation model, which resembles cluster analysis can be employed to define the fuzzy memberships. For remote sensing images, a typical method of defining fuzzy memberships is the fuzzy *c*-means algorithm (Bezdek *et al.*, 1984). In this algorithm, fuzzy membership values for each pixel

belonging to all candidate classes are generated either in an iterative way (unsupervised approach) or supervised mode using the signatures of training data. The supervised approach of the fuzzy *c*-means algorithm will be applied to generate fuzzy memberships of selected bands of multispectral remote sensing image that provided the highest spectral separability among predetermined urban land covers.

The accuracy assessment of fuzzy classification requires fuzzy ground truth data. A number of ways such as assigning membership using linguistic values based on land cover compositions, sub-pixel land cover compositions, indicator kriging and probabilistic approaches, can be applied to generate fuzzy ground truth data. Using the fuzzy memberships of the classified and ground data, various approaches such as measure of closeness, fuzzy similarity, entropy, and correlation measures can be applied to assess the accuracy of fuzzy classified data. Another approach consists of slicing the fuzzy memberships of classified and ground data using a particular threshold so that conventional accuracy measures can be determined afterwards. These approaches offer some encouraging results in assessing the accuracy of fuzzy classifications but none of them are universally applicable. A major limitation of these approaches is that they suffer from an appropriate sampling strategy and do not provide 'location preserving' accuracy which might mislead the mapping accuracy.

A fuzzy error matrix based on fuzzy set theory will be applied to assess the accuracy of a fuzzy classification. This matrix is a generalisation of the conventional error matrix which preserves the property of error "localisation" consisting on "the capability of identifying the contribution of each category relative to the actual category as verified in the reference data" (Congalton, 1991). The fuzzy error matrix requires fuzzy memberships of the classified and ground truth data. In generating fuzzy ground data, selection of sample data should be logistically feasible, spatially accurate, and statistically relevant. Accordingly, factors associated with sampling strategy such as sampling unit (e.g. pixels or polygons), sample size and sampling technique (e.g. random sampling) need to be considered.

The method selected for measuring the spatial complexity of urban land cover types in the Perth metropolitan area, as well as the research approach adopted for characterising and modelling the heterogeneity of the urban landscape, as mapped from remotely sensed data are discussed in the following chapter.

Chapter 3

METHODS AND TECHNIQUES

This chapter describes the research approach applied to measure the spatial complexity and mapping of the heterogeneity of urban land cover types using remotely sensed data. Spatial autocorrelation measures and fractal techniques were used for the analysis of spatial complexity and the principles of these approaches are described. The transformed divergence analysis was implemented for selecting the most appropriate combination of bands of a multispectral satellite image, which were used to derive the fuzzy memberships of the major land covers. Fuzzification was undertaken using a supervised approach of the fuzzy *c*-means algorithm. The conceptual overview and the general methodology of the fuzzy *c*-means algorithm and the principles of fuzzy operators, which were used to integrate the fuzzy memberships of the selected bands, are described. Then, the methods for generating fuzzy ground data, used to carry out the accuracy of fuzzily classified data are discussed.

3. 1 Methodological Approach

The methodological approach adopted in this research is composed of four major steps:

(a) Study area selection;
(b) Characterisation of the spatial complexity of urban landscapes using multiscale and multisource remote sensing data;
(c) Derivation of fuzzy membership values (FMVs) of selected urban land cover types using multispectral image;
(d) Creation of virtual field reference database (VFRDB) and accuracy assessment of the fuzzily classified data.

The methods and techniques associated with the above methodological approaches are described in the following sections.

3. 2 Study Area Selection

The Perth metropolitan area (PMA) consisted of 29 local government areas (LGAs) which are characterised by commercial, industrial, residential, grassland, parks, irrigated pasture, grazing areas and forested areas. Among the LGAs, the City of Perth, the City of Melville and the City of Armadale were selected (Figure 3.1) as the dominant land cover types of the three LGAs were considered to be representative of the range of land covers and their spatial variability over the PMA. An examination of the secondary source data (e.g. land zoning map, metropolitan region schemes) and random field visits indicated that the land cover types of the City of Perth are characterised by commercial and industrial areas while the land cover types of the City of Melville is dominated by residential and grassland. The major land cover types of the City of Armadale include residential area, irrigated pastures, grazing area and forested areas, being a typical 'urban fringe' area of the PMA. A detailed description of the study areas is provided in Chapter 4.

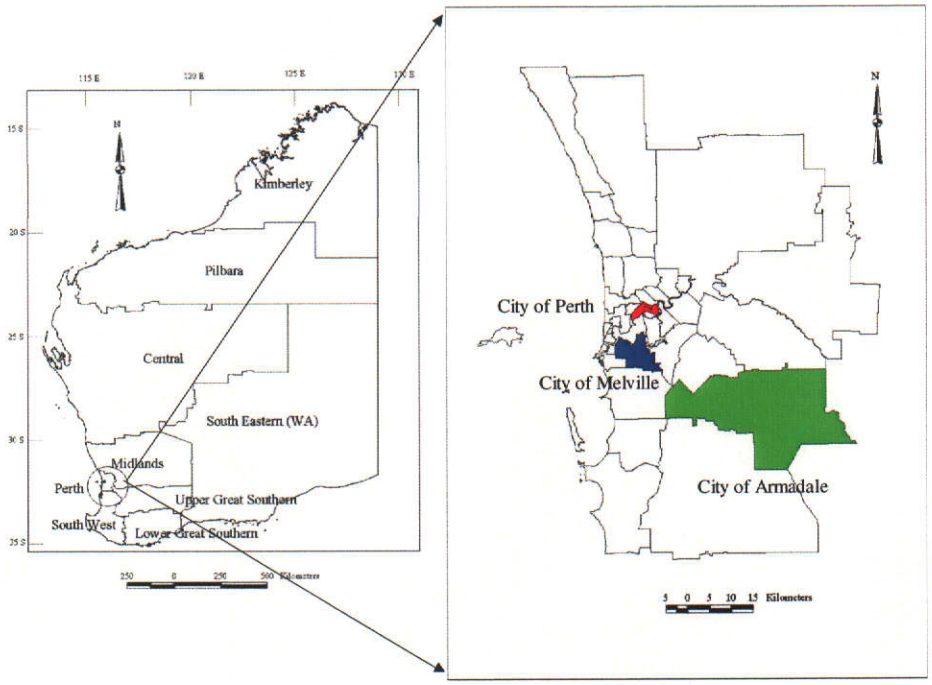

Figure 3.1 Location map of the Perth metropolitan area in Western Australia

3. 3 Characterisation of the Spatial Complexity of Urban Landscapes

The spatial complexity of urban landscapes described by spatial statistics such as spatial autocorrelation measures and fractal measurement algorithms, applied on

multiscale and multisource remote sensing data. These methods are described hereafter.

3.3.1 Spatial Autocorrelation Measures

Moran's I and Geary's C (Cliff and Ord, 1973) are two indices of spatial autocorrelation which can be applied to characterise the spatial complexity of urban landscapes. These measures are computed from the following formulas:

$$I(d) = \frac{n \sum_{i}^{n} \sum_{j}^{n} w_{ij} z_i z_j}{W \sum_{i}^{n} z_i^2} \tag{3.1}$$

$$C(d) = \frac{(n-1) \sum_{i}^{n} \sum_{j}^{n} w_{ij} (y_i - y_j)^2}{2W \sum_{i}^{n} z_i^2} \tag{3.2}$$

Where w_{ij} is the weight at distance d so that $w_{ij} = 1$ if point j is within distance d from point i ; otherwise, $w_{ij} = 0$; z's are deviations (i.e. $z_j = y_i - y_{mean}$ for variable y), and W is the sum of all the weights where $i \neq j$. Moran's I varies from +1.0 for a perfect positive correlation (a clumped pattern) to -1.0 for a perfect negative correlation (a checkerboard pattern) whereas Geary's C normally ranges from 0.0 to 3.0, with 0.0 indicating positive correlation, 1.0 indicating no correlation, and values greater than 1.0 indicating negative correlation. It is interesting to note that Moran's I and Geary's C do not explicitly consider the shapes and sizes of objects once the weights W_{ij} in Equations 3.1 and 3.2 are determined. Among these measures, Moran's I was found to be useful for characterising the spatial complexity of various land cover types (e.g. forest, scrub, pasture, agriculture and urban) which is inversely correlated with the fractal dimension (Read and Lam, 2002). Accordingly, Moran's I index of spatial autocorrelation was used in this research as shown in Chapter 5.

3.3.2 Fractal Measurement Algorithms

The application of fractal models can be categorised into two major types. The first set of applications uses fractal as a model to simulate the real world for analytical and display purposes, while the second set of applications utilises the fractal

dimension as an index for describing the spatial complexity of curves and surfaces. As mentioned by Lam (1990) and Lam and Quattrochi (1992), a number of approaches such as the shear displacement method (Goodchild, 1980; Lam, 1990), the modified Markov method (Dutton, 1981), the inverse Fourier transformation technique (Fournier *et al.*, 1982), and the recursive subdivision (Goodchild, 1980; Mark and Aronson, 1984) can be used for generating fractal curves and surfaces as mentioned by Lam (1990) and Lam and Quattrochi (1992). Likewise, there are several techniques to determine the fractal dimension (D) of remotely sensed data, when aiming to use D as an index for describing the spatial complexity of lines, curves and surfaces. Among the techniques, the isarithm, the variogram, and the triangular prism surface area (TPSA) have attracted most attention from researchers (Clarke, 1986, Jaggi *et al.*, 1993, Lam and De Cola, 1993).

Previous work shows high variability in the computation of D when different algorithms are used (Klinkenberg and Goodchild, 1992; Jaggi *et al.*, 1993; Lam and De Cola, 1993; de Jong and Burrough, 1995; Quattrochi *et al.*, 1997; Kolibal and Monde, 1998). Available literature suggests that many of the algorithms have not been tested on a wide range of data sets and comparative studies have been relatively few. Moreover, the theoretical and practical limitations of these techniques have not been adequately researched and deserve further investigation.

3.3.2.1 The Isarithm Technique

This technique measures the fractal dimension of the isarithmic lines (e.g. contours, digital numbers of a satellite imagery). It is an extrapolation of a one-dimensional technique termed the line-divider method (Shelberg *et al.*, 1982; Shelberg *et al.*, 1983). The principle of this approach is to characterise the different 'step sizes' representing the segments that are necessary to traverse a curve (See Section 2.1.3). Thus, a smaller 'step size' is required to traverse a highly irregular curve, whereas a larger 'step size' is required to traverse less irregular curves. Using the number of steps and 'step size', the fractal dimension (D) can be computed using Equation 2.3 in Chapter 2. For an irregular curve, at larger step sizes the detail of the line is lost, and the total line length diminishes. This results in a negative slope of the regression line. Thus, the fractal dimension of a curve always lies between 1 and 2. For remotely sensed data, this method considers lines of equal digital values, or contours

of the image, as the objects for estimation of the fractal dimension and is calculated by the following equation.

$$D = 2 - B \tag{3.3}$$

The above algorithm was reported by Shelberg *et al.* (1983) and subsequently modified for determining the fractal dimension of remotely sensed data. The basic steps associated with the modified algorithm are as follows (Lam and De Cola, 1993; Jaggi *et al.*, 1993):

(a) Generate contours or the isarithms of the image by dividing the pixel values into equally spaced intervals;
(b) Divide the pixels into two regions using the threshold value of the current isarithm value. Typically, pixels with values below the isarithm value are set to 'off' while pixels greater or equal to the isarithm value are set 'on'. This transforms the image into a simple binary set of 1s and 0s forming a matrix of rows and columns representing the image for that particular isarithm value;
(c) Compare each neighbouring cell along the rows or column, or row-column (both), for boundary cells and calculate the length of the each isarithm line represented by the number of boundary cells encountered using various step sizes;
(d) Determine the fractal dimension from the regressed slope of the plot drawn between the logarithm of the number of edges and the logarithm of the step sizes; and
(e) Calculate the fractal dimension of the entire image by averaging the fractal dimension for each isarithm.

The number of step sizes can be set up to the maximum number of pixels of the image being used and accordingly, the algorithm generates the different walk sizes following a geometric series which are defined in units of grids (i.e. 1, 2, 4, 8, 16, 32, etc.) (Lam and De Cola, 1993; Jaggi *et al.*, 1993). Similarly, the isarithim interval is pre-determined by the user, using the following equation.

$$\text{Number of isarithm lines} = (\text{maximum pixel value} - \text{minimum pixel value})/\text{isarithm interval} \tag{3.4}$$

The above discussion indicates that few parameters such as isarithmic interval, the number of isarithm lines, step size (or the number of cells) and the direction of computing fractals control the estimation of fractal dimension. For a remote sensing image, Clarke (1986) recommended choosing values that represent the 'step size', or number of cells which are increased as a power of two so that the observations on the independent variable for the regression are spaced equally in the log transformed plot. Lam (1990) used an isarithmic interval of two and a maximum step size of six to calculate the fractal dimension of three study areas from all bands of a Landsat TM, using the row and the column method. The results indicated discrepancies in the resultant D values computed from the row and column method, particularly for urban areas. This was attributed to the directional bias, as roads and highways were found aligned with the rows and columns of the image analysed. Similar discrepancies were found by Jaggi *et al.* (1993). Lam and De Cola (1993) described three fundamental factors that affect the computation of fractal dimension from remotely sensed data. These are as follows:

(a) The orientation patterns have an effect on the resultant D, when only the row or column methods are used. Thus, for an image which has distinct directional pattern, the row-column method is recommended;

(b) Zero values of the cells near the edges of the boundary for each 'step size' need to be excluded;

(c) The maximum 'step size' has more likelihood of encountering zero boundary cells. Moreover, use of excessively large step sizes tends to create points that fluctuate at the right end of the regression plot, resulting in low r^2 values.

3.3.2.2 The Triangular Prism Surface Area (TPSA) Technique

The triangular prism area surface area (TPSA) technique was proposed by Clarke (1986). This is a three-dimensional geometric equivalent of the "walking dividers" approach, by which the fractal dimension of an image is computed from the surface areas of four imaginary triangular prisms (with base h x h) generated by the pixel values of four corner pixels (i.e., the center of a pixel). Typically, the average of the pixel values located at the four corners of the triangular prism defines the average height of the apex of the prism. This is placed in a node common to all four pixels

and accordingly, it defines four triangular surfaces comprising the triangular prisms (Figure 3.2).

For a specific square size (i.e. step size), a series of triangular prisms are created from the entire image, and using Heron's formula (Clarke, 1986), their surface areas are computed. The calculation is repeated for different square sizes and the relationship between the surface areas of the imaginary triangular prisms and the square sizes provides the fractal dimension. Similarly, the total area of the triangular prism decreases with increasing in the size of the squares. This demonstrates a negative slope of the regression line of the plot between the logarithm of the total area and the logarithm of the step size. Using the regressed value, the fractal dimension can be calculated by using Equation 3.3.

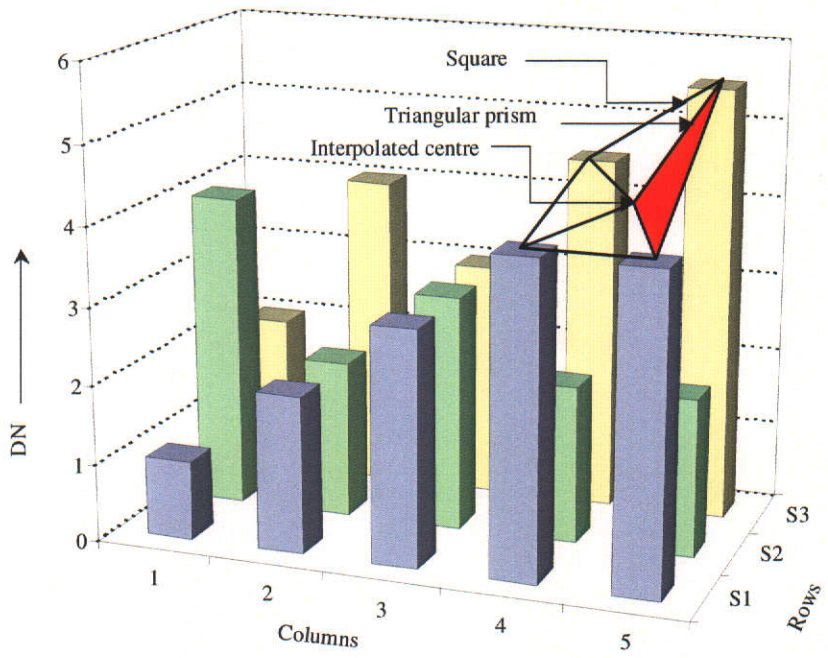

Figure 3.2 Typical example of imaginary triangular prisms generated from adjacent pixels (adapted from de Jong and Burrough, 1995)

In the TPSA method, the number of steps or square grids depend on the size of the images. Typically, the largest square is computed from 2^n, where n is an integer which would give the value of 2^n as close as that of the shortest side of the square. Thus, the side of the maximum square of an image comprised of 128 x 128 pixels is 64 (less than 128) and the maximum step size equals 6 (2^6). However, for a certain

size of image (128 x 128 pixels), one cell larger than the image (129 x 129) can be employed. The advantage of squares of sides increasing by powers of two, is that it provides a uniform spread of observations on the independent variable during the log-log regression (Clarke, 1986).

3. 4 Derivation of Fuzzy Urban Land Cover Maps

The conceptual model devised for deriving the fuzzy membership of urban land covers using multispectral satellite image is composed of three major steps, as shown in Figure 3.3 (using an example of Landsat-7 ETM+ and four urban land cover classes):

(a) Selection of the best set of bands of multispectral image using transformed divergence analysis;
(b) Computation of fuzzy membership values for each land cover type of the selected bands; and
(c) Integration of fuzzy membership values for land cover types A, B, C, ...n of the selected bands 1, 2, ...n using different fuzzy operators.

The theoretical basis of the model is presented hereafter.

3.4.1 Optimal Band Selection

Several statistical separability measures such as divergence, transformed divergence, canonical analysis, can be used to evaluate class separability of pre-determined feature classes within the spectral bands of multispectral image (Richards and Jia, 1999). The advantage of transformed divergence analysis is that it provides a prior probability of correct classification based on statistical separability measures which can be computed on any combination of bands, enabling to exclude the bands, or combinations thereof, that as a function of spectral class separation may not yield or correct classification result. Accordingly, transformed divergence $\left(TD_{ij}\right)$ analysis was used in this research to select the best set of bands from the multispectral images. This measure is a modification of the divergence measure $\left(D_{ij}\right)$ which provides a prior probability of correct classification using the statistical separability

based on the degree of overlap of the probability distributions between a pair of spectral classes (Richards and Jia, 1999).

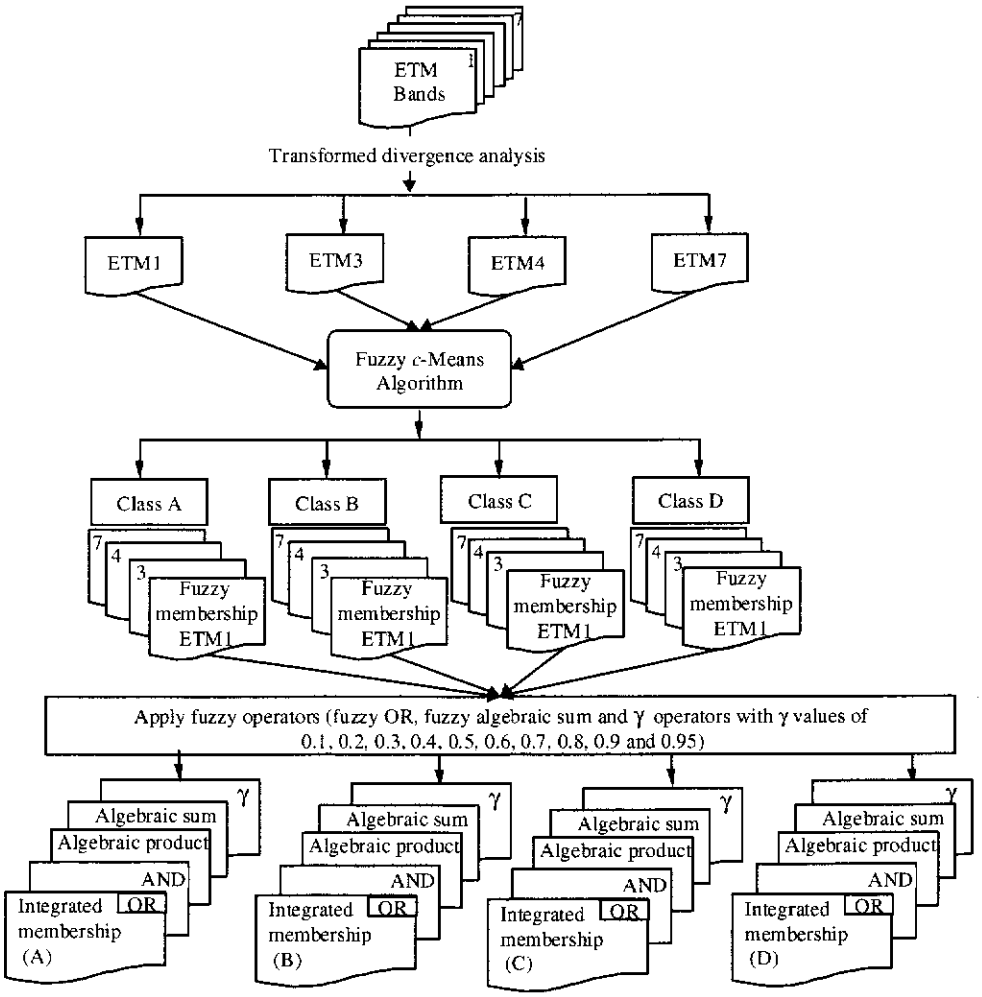

Figure 3.3 The conceptual model for deriving fuzzy land cover maps

Thus, the larger the transformed divergence, the greater the statistical distance between the training signatures, and the higher the probability of correct classification. It can be computed from the following formula (Swain and Davis, 1978):

$$D_{ij} = \frac{1}{2} tr\left[\left(V_i - V_j\right)\left(V_i^{-1} - V_j^{-1}\right)\right] + \frac{1}{2} tr\left[\left(V_i^{-1} - V_j^{-1}\right)\left(M_i - M_j\right)\left(M_i - M_j\right)^T\right] \tag{3.5}$$

$$TD_{ij} = 2000\left(1 - \exp\left(\frac{-D_{ij}}{8}\right)\right) \tag{3.6}$$

where:

i and j = the two signatures (classes) being compared

V_i = the covariance matrix of signature I

M_i = the mean vector of signature i

tr = the trace function (matrix algebra)

T = the transposition function

Thus, transformed divergence analysis firstly requires:

(a) Determining the urban land cover types to be mapped; and

(b) Creating a training set of the classes so that statistical parameters needed for the computation of transformed divergence can be obtained.

Equation 3.6 indicates that transformed divergence increases as the distance between the classes increases, usually varying between 0 and 2000. According to Jensen (1996), a transformed divergence value of 2000 suggests an excellent class separation, 1900 provides a good separation while values below 1700 represent a poor separability between classes. This technique has been applied in several studies to evaluate the separability of informational classes and select the best band combination to be used in the subsequent image classification (Metternicht, 1996; Metternicht and Zinck, 1997 and 1998).

3.4.2 Derivation of Fuzzy Membership Value (FMV)

Chapter 2, Section 2.2.1 discussed different approaches for deriving FMVs. As the fuzzy *c*-means algorithm has been adopted for deriving FMVs of major urban land cover types of the Perth metropolitan area, a conceptual overview is presented hereafter.

3.4.2.1 The Fuzzy *c*-Means Clustering Algorithm

3.4.2.1.1 Conceptual Overview

The fuzzy *c*-means clustering algorithm is developed based on the fuzzy *c*-clustering principle. It assigns a membership function to each data sample for every class on the basis of its similarity to the class mean. However, membership calculation is an

iterative process. In each iteration, all pixels begin and end with memberships in each of the specified number of clusters and each iteration adjusts these membership function values to minimise an error function. In the fuzzy *c*-means clustering algorithm generalised by Bezdek (1981), the least squared error function is used.

There are two aspects of the fuzzy *c*-means clustering algorithm that deserve further discussions. Firstly, an assumption that governs deriving FMVs from the classifiers is the frequency distribution of the classes. With the exception of the fuzzy *c*-means algorithm, the classifiers are based on either non-parametric or gaussian normal distributions of the classes. It is therefore, essential to consider the frequency distribution of different classes of the input image for a reliable output. For example, probabilistic measures of maximum likelihood classification may become unreliable if a gaussian normal distribution cannot be assumed for each class (Wilkinson, 1991). In a situation where the frequency distribution does not follow gaussian normal distribution, fuzzy *c*-means clustering can be more appropriate (Foody and Trodd, 1993). The advantage of fuzzy *c*-means algorithm is that it does not consider the frequency distribution of the classes and can be used for either unsupervised (e.g., Cannon *et al.*, 1986b) or supervised classification (e.g., Key *et al.*, 1989). Fuzzy *c*-means algorithm is particularly advantageous as the degree of fuzziness is controlled by the analyst. Secondly, the iteration and clustering technique is different from either a 'lumper' approach which operates by combining small clusters into larger clusters, or a 'splitter' which begins with all pixels belonging to the same class and then subdividing them. Instead, in the fuzzy *c*-means clustering algorithm, the fuzzy memberships are adjusted in each iteration to the specified number of clusters and accordingly each iteration adjusts these memberships to minimise the error function. The method has received growing interest for its particular value and applied in many studies addressing the imprecision in interpreting land cover types from remotely sensed data (Fisher and Pathirana, 1990; Foody and Trodd, 1993; Foody, 1996(b); Zhang and Foody, 1998; Pathirana, 1999; Mohan *et al.*, 2000).

From the above discussion, it is evident that the fuzzy *c*-means clustering algorithm calculates optimal membership through a generalised squared error function. Thus, it

is necessary to explain the mathematics of the generalised least squared error function and its associated parameters that control the membership functions.

According to Bezdek (1981), the generalised least-squared errors function which is used in the fuzzy *c*-means clustering algorithm can be determined by the following equation:

$$J_m(U,v)=\sum_{k=1}^{N}\sum_{i=1}^{c}(u_{ik})^m\|y_k - v_i\|_A^2 \tag{3.7}$$

The above equation contains a number of variables. These are as follows:

$Y=\{y_1, y_2, ...y_n\}\subset R^n$ = the data,

c = number of clusters in Y; $2\le c<n$,

m = weighting exponent; $1\le m<\infty$

U = fuzzy c-partition of Y; $U\in M_{fc}$

$(u_{ik})^m$ = the mth power of y_ks membership in cluster i

$v_i=(v_{i1}, v_{i2}, v_{i3}, ...v_{in})$= center of cluster i;

$\|\ \|_A$ = induced A-norm on R^n

A = positive definite $(n\times n)$ weight matrix

The squared distance between y_k and v_i shown in the above equation is computed in the A-norm as

$$d_{ik}^2=\|y_k - v_i\|_A^2=(y_k - v_i)^T A(y_k - v_i) \tag{3.8}$$

where,

d_{ik}^2 = squared A-distance from point y_k to center of mass v_i

Bezdek (1981) showed mathematically that the least squared error, *Jm* minimises only optimal values of the fuzzy membership and the mean value, (U, v), and it achieves the optimal fuzzy c-clusterings of Y. Thus, in order to get the least squared error, it is necessary to achieve the optimal values of the fuzzy membership and

mean values (U, v). For m > 1, if $y_k \neq \hat{v}_j$ for all j and k, $\left(\hat{U}, \hat{v}\right)$ may be locally optimal for J_m only if

$$\hat{v}_{il} = \sum_{k=1}^{N}\left(\hat{u}_{ik}\right)^m y_{kl} \Big/ \sum_{k=1}^{N}\left(\hat{u}_{ik}\right)^m ; 1 \le i \le c; \quad l = 1, 2, \ldots\ldots p \tag{3.9}$$

$$\hat{u}_{ik} = \left(\sum_{j=1}^{c}\left(\frac{\hat{d}_{ik}}{\hat{d}_{jk}} \right)^{2(m-1)} \right)^{-1} ; \; 1 \le k \le N; 1 \le i \le c \tag{3.10}$$

Where d_{ik}^2 can be measured using Equation 3.8. Thus, it is clear that in order to achieve a least squared error for given clusters, it is necessary to calculate the pairs $\left(\hat{U}, \hat{v}\right)$ through an iteration process. According to Bezdek (1981), the following steps are needed to produce the pairs $\left(\hat{U}, \hat{v}\right)$.

(a) Select the number of clusters, c, 2 < c < n-1; m (weighting exponent of fuzzy c-means), 1 < m < ∝; A, the positive-definite $(n \times n)$ weight matrix of Rp, where p is the number of features; U^0, the initial fuzzy c-partition of Y, where $U^0 \in M_{fc}$, fuzzy c-partition space and ε, the value for the stopping criterion (ε = 0.01 gives a reasonable convergence).

The next stage includes re-iterating steps b to d until convergence is reached.

(a) Calculate the c fuzzy group centroids, v_i, using the Equation 3.9,

(b) Update U^{l+1} using Equation 3.10,

(c) Finally, compare U^{l+1} to U^l in any convenient matrix norm. If the difference between all corresponding elements is less than or equal to ε, then stop. Otherwise set $U^l = U^{l+1}$ and return to (b).

It is important to note that the results are largely influenced by parameters, such as, the weighting exponent, m, the initial fuzzy matrix, U_0 and A-norm which are used in

Equations 3.7-3.10. The effects of these parameters are discussed in the following section.

3.4.2.1.2 Parameters of the Fuzzy *c*-Means Clustering Algorithm

(I) Weighting Exponent (*m*)

The weighting exponent *m* controls the relative weights placed on each of the squared errors d_{ik}^2 in Equation 3.8 and it is used to determine the membership function. As $m \rightarrow 1$, partitions that minimize *Jm* approaches to be increasingly crisp and become completely crisp at *m* = 1, usually called *k*-means clustering (McBratney and Moore, 1985). Consequently, increasing *m* tends to degrade membership towards the fuzziest state and each entry of optimal $\hat{U}_S$ for *Jm* approaches (1/*c*) as $m \rightarrow \infty$. Thus, the weighting exponent *m* controls the extent of membership sharing between fuzzy clusters in *X*.

McBratney and Moore (1985), tested a range of values for *m* and found that *m* = 100, yielded fuzzy membership almost constant at 0.5 for each two classes, indicating that clustering was so fuzzy that no clusters would be distinguished. They, however, found that an *m* of approximately 2 is optimal, though when using a large number of groups, *m* should have a smaller value, as compared to the *m* values of a relatively small number of groups. In this regard, it is important to note that there is no theoretical basis for choosing *m*, but typically $1.1 \leq m \leq 5$ is reported as the most useful range for drawing the values (Cannon *et al.*, 1986a). Key *et al.* (1989) reported that the range of useful values of *m* varies from 1 to 30, while for most data, $1.5 \leq m \leq 3.0$ exhibits good results.

(II) Initial Matrix

The initial U^0 matrix which is used in Equations 3.7 and 3.9 can be generated in the algorithm either from randomly fuzzy values, randomly non-fuzzy values or uniform fuzzy values. Bezdek *et al.* (1984) randomly chose the U^0 matrix where each member is given a membership value between 0 and 1 while McBratney and Moore (1985) opted for almost uniform fuzzy values. For uniform values, a membership function is assigned to a member by 1/*c* plus or minus a small random component.

In a non-fuzzy state, the membership is assigned 1 to a randomly selected class and 0 to the remaining set.

(III) *A*- Norm

There are many *A*-norms available for use in Equation 3.8 but the fuzzy *c*-means clustering algorithm allows only three different norms (e.g. *Euclidean*, *Diagonal* and *Mahalanobis*) each induced by a specific weight matrix (Bezdek, 1981). The norms can be explained by the following example. Let, c_y and C_y be the sample mean and sample covariance matrix of data set *Y*. Typically, they can be represented by the following equations.

$$c_y = \sum_{k=1}^{N} y_k \Big| N \tag{3.11}$$

$$C_y = \sum_{k=1}^{N} (y_k - c_y)(y_k - c_y)^t \tag{3.12}$$

Let $\{a_i\}$ denote the eigenvalues of C_y ; let D_y be the diagonal matrix with diagonal elements $(d_y)_{ii} = a_i$; and finally, let *I* be the identity matrix. With these conditions, Bezdek (1981) proposes the norms being simplified by the following expressions.

$$A = I \sim \textit{Euclidean Norm} \tag{3.13}$$

$$A = D_y^{-1} \sim \textit{Diagonal Norm} \tag{3.14}$$

$$A = C_y^{-1} \sim \textit{Mahalanobis Norm} \tag{3.15}$$

The geometric and statistical implications of the data clusters depends on the choice of *A*-norms. For example, the *Euclidean* norm is the best for statistically independent, equally variable features, for hyperspherical clusters. Available literature suggests that the *Euclidean* norm has been extensively used for clustering of geological and remote sensing data. For example, Pal *et al.* (2000), Cannon *et al.* (1986b) and Trivedi and Bezdek (1986) have used the *Euclidean* norm for segmenting different remote sensing images (e.g. IRS and SPOT, Landsat Thematic Mapper and aerial photographs) while Pathirana (1999) used the *Euclidean* norm for clustering the dominant land cover class to develop membership functions for each pixel. For other norms, particularly *Mahalanobis,* the clusters are hyperellipsoidal

and have been used in generating fuzzy memberships of land cover types using remote sensing data (Foody, 1996(a); Foody and Trodd, 1993).

3.4.2.1.3 Validity Functions of the Fuzzy *c*-Means Clustering Algorithm

Numerical convergence of the fuzzy *c*-means clustering algorithm is generally carried out through iterations. However, sometimes, the convergence through iterations for given clusters, which produce a least squared error, may be inappropriate. In order to overcome this problem, two validity functions are used to evaluate the effect of varying the number of clusters. These are the partition coefficient, F, and the entropy, H, which are derived using the following equations.

$$F = \sum_{i=1}^{c} \sum_{k=1}^{n} (u_{ik})^2 / n \tag{3.16}$$

$$H = - \sum_{i=1}^{c} \sum_{k=1}^{n} (u_{ik} \log_{\alpha} u_{ik}) / n \tag{3.17}$$

The logarithm base, α, is commonly used as e or 10 (Key, *et al.*, 1989). From the above equation it is clear that the value of F varies between 1/c and 1, while H varies between 0 and $\log_{\alpha} c$. Thus the clustering is crisp when F is 1 or H is 0.

3.4.2.2 Supervised Approach of the Fuzzy *c*-Means Clustering Algorithm

According to the earlier discussion, it is evident that the fuzzy *c*-means algorithm requires the user specifying a number of clusters, c, weighting exponent m, termination criteria, ε. With a given number of clusters and termination criteria, the algorithm iterates and determines optimum membership grades and cluster centers $\left(\hat{U}, \hat{v}\right)$ of each data sample which in turn minimises the generalised least square error, J_m. However, for very large data sets such as satellite imagery, the number of computations are enormous as the data set contains a huge number of data items (pixels), features and clusters. For example, in Equation 3.10, for each value of i and l, there are n exponentiations in the denominator and n exponentiations and products in the numerator. A simple interpretation of the algorithm is that it requires $c \times p \times n$ uses of the exponentiation operators and $c \times p$ divisions. Since the algorithm is iterative, the mean values are calculated repeatedly and subsequently these are used

to calculate the fuzzy membership using Equation 3.10. In order to speed up the fuzzification of large data sets, the algorithm can be modified into a supervised approach and the computations can be carried out 30 to 40 times faster than the unsupervised approach as it requires only one pass through the entire data sample (Key *et al.*, 1989). As such, it has been applied in the interpretation of a wide range of satellite data (e.g. AVHRR and Airborne Thematic Mapper) and has resulted in unique and accurate class memberships (Key *et al.*, 1989; Foody and Trodd, 1993; Zhang and Foody, 1998).

In the fuzzy *c*-means supervised approach, the class means are provided in the algorithm in a manner analogous to the training sites of supervised classification and the algorithm assigns strength of membership as a function of the weighted distance between the class mean and the individual data sample. Thus, it is evident that the class means play a very important role in generating fuzzy membership, and thus the selection of class mean values, particularly for classes spectrally similar, deserves special emphasis. For example, Key *et al.* (1989) found that classes with similar brightness values did not generate uniquely defined fuzzy sets, rather they were clustered together. In such situations, using the adjusted class mean in the algorithm for a realistic solution is suggested. However, a better solution would be to add a weighting function, *m*, to the algorithm so that it influences the calculation of the membership grade of the features which better define a particular class (Key *et al.*, 1989).

From the above discussion, it is apparent that unlike the unsupervised approach, the algorithm does not iterate to calculate the mean value, it rather generates the fuzzy membership corresponding to the given mean value of a class. However, in this approach several sets of membership grades can be generated by changing the weighting exponent, *m* and the optimum fuzziness can be ascertained from the measurement of a *'partition coefficient'* and *'entropy'*. A detailed discussion on *'partition coefficient'* and *'entropy'* has been presented in earlier sections.

3.4.3 Fuzzy Operators for Integration of Fuzzy Membership

The use of multispectral imagery in the process of a fuzzy supervised classification of urban land cover types, as proposed in this research, requires finding an optimal

fuzzy operator for integrating the FMVs derived from *'n'* spectral bands for each land cover considered (Figure 3.3). Among the fuzzy operators, the fuzzy AND, fuzzy OR, fuzzy algebraic product, fuzzy algebraic sum and the fuzzy gamma operator are the most frequently applied to integrate the fuzzy memberships of various data sets or information layers (An *et al.*, 1991, Bonham-Carter, 1994). Accordingly, the performance of these operators was assessed for integrating fuzzy memberships derived for each predetermined land cover types from the selected bands of multispectral image. Accuracy assessment of the outputs of each fuzzy operator was undertaken using a fuzzy error matrix. The principles of these operators are described below.

3.4.3.1 Fuzzy AND

Fuzzy AND is a logical intersection which combines the fuzzy memberships of two or more layers (e.g. Landsat-7 ETM+ bands) using a fuzzy minimum operator. It can be defined as

$$\mu_{\text{land cover A}} = MIN\left(\mu_{A1}, \mu_{A2}, \mu_{A3}, \ldots \mu_{An}\right) \tag{3.18}$$

where μ_{A1}, μ_{A2}, μ_{A3} .. μ_{An} represent the membership values of land cover A in the Landsat-7 ETM+ bands 1, 2, 3,...*n* respectively, at a particular location. This indicates that the operator generates a map displaying minimum membership values for each location. Thus, the resultant image is a conservative estimation of a set of memberships, which tends to produce small values (Bonham-Carter, 1994).

3.4.3.2 Fuzzy OR

Fuzzy OR combines the fuzzy memberships of land cover A from two or more layers (e.g. Landsat-7 ETM+ bands) using a fuzzy maximum operator. The output membership values are controlled by the maximum membership values of the input bands for any particular location. This can be defined as

$$\mu_{\text{land cover A}} = MAX\left(\mu_{A1}, \mu_{A2}, \mu_{A3}, \ldots \mu_{An}\right) \tag{3.19}$$

3.4.3.3 Fuzzy Algebraic Product

The fuzzy algebraic product is a modified intersection which combines remote sensing data by multiplying the membership of land cover A on each selected band, as defined by the following equation,

$$\mu_{\text{land cover A}} = \prod_{i=1}^{n} \mu_{\text{Ai}} \tag{3.20}$$

where μ_{Ai}, is the fuzzy membership in land cover A for the *i-th* band, and i = 1,2,3, ...*n* bands to be combined. With this operator, the combined fuzzy membership values tend to be very small due to the effect of multiplying several numbers lower than one. The output is always smaller than, or equal to, the smallest contributing membership value, and it is therefore "decreasive". Although the fuzzy algebraic product gives an output that is decreasive in nature, it does utilise every membership value to produce the result, unlike the fuzzy minimum (e.g. AND) or maximum (OR) operators (Bonham-Carter, 1994).

3.4.3.4 Fuzzy Algebraic Sum

The fuzzy algebraic sum is a modified fuzzy union, which is expressed as a probabilistic sum (Zimmermann, 1991). For a fuzzy membership, μ_{Ai}, in land cover A, where *i-th* bands are to be combined, the probabilistic sum can be simplified by the following equation

$$\mu_{\text{land cover A}} = 1 - \prod_{i=1}^{n} (1 - \mu_{\text{Ai}}) \tag{3.21}$$

The combined fuzzy membership value of land cover A is always larger or equal to the largest contributing fuzzy membership value. Thus, the effect is increasive. If two or more pieces of evidence favour a hypothesis (e.g. the possibility of a pixel being classified as land cover A, as expressed by fuzzy membership values in the Landsat-7 ETM+ bands 1 to *n*), it reinforces one another, and the combined evidence is more supportive than either pieces individually (Bonham-Carter, 1994).

3.4.3.5 Fuzzy Gamma Operation

The gamma (γ) operator is defined in terms of the fuzzy algebraic product and the fuzzy algebraic sum by the following equation.

$$\mu_{\text{land cover A}} = (\text{Fuzzy algebraic sum})^{\gamma} * (\text{Fuzzy algebraic product})^{1-\gamma} \quad (3.22)$$

where γ is a parameter chosen in the range (0, 1) (Zimmermann, 1985). Equation 3.22 indicates that when γ equals 1, the combined fuzzy membership of land cover *A* is the same as the fuzzy algebraic sum whereas the combination equals the fuzzy algebraic product when γ equals 0. Clearly, the choice of γ compromises between the "increasive" tendencies of the fuzzy algebraic sum and the "decreasive" effect of the fuzzy algebraic product.

3.4.4 Accuracy Assessment of a Fuzzy Classification

The accuracy assessment of the fuzzy classification, as adopted in this research, is composed of five major steps. These are as follows:

(a) Creation of a virtual field reference database (VFRDB) and derivation of fuzzy memberships of this ground data;
(b) Defuzzification of the fuzzy memberships of the classified data;
(c) Derivation of fuzzy error matrix;
(d) Determination of the accuracy measures; and
(e) Generation of uncertainty maps.

3.4.4.1 Creation of a Virtual Field Reference Database and Derivation of Fuzzy Memberships

A "Virtual Field Reference Database (VFRDB)" was developed to store field observations and digital imagery acquired with a digital camera from selected sites of the study areas. The VFRDB was designed to assign the fuzzy memberships of the visited sites for assessing the fuzzy categorical maps derived from a Landsat-7 ETM+ scene using a fuzzy supervised classification (see Section 3.4 for details). The conceptual idea for the design and implementation of this database was adopted from previous work by Lunetta *et al.* (2001). They state that such a database is

useful for characterising representative urban land cover types with known variability of land cover compositions in each sample site throughout the study areas. In their study a high classification accuracy was achieved due to the application of a VFRDB, comprised of field-based measurement and digital image (camera) data which guided accurate class labeling of the reference data. The basic approach for assigning the fuzzy membership of the field reference data required using the classification scheme adopted in this study (see Section 5.3.1). This required field data collection, which included sampling design, field visits and field data documentation. These are described in the following sections.

3.4.4.1.1 Sampling Design

Selection of samples requires a sampling technique, sample size and sampling unit. Accordingly, a simple random sampling strategy, which is statistically ideal for accuracy assessment analysis was employed in selecting sample sites from the study areas (Hord and Brooner, 1976; Hay, 1979). Following the rule of thumb of choosing a minimum 50 samples for each land cover class (Hay, 1979; Congalton, 1991; Muller, *et al.*, 1998; Congalton and Green, 1999) considered in the classification scheme (see Section 5.3.1), a total of 200 sample points were selected from each of the study areas.

3.4.4.1.2 Field Visits and Field Data Documentation

Field visits were undertaken during April through June of 2002 and 2003. According to location and distribution of the sample points, daily routes were designed and each of the sample points was visited and spatial and aspatial attributes recorded using a hand held Global Positioning System (GPS) receiver (Ensign, Trimble Navigation) and a digital camera. The GPS receiver was configured using Universal Transverse Mercator (UTM) coordinates system with WGS 84 datum and three-dimensional (3D) mode of operation. In 3D operational mode, Ensign GPS triangulates a position when four or more satellites are connected. Positional accuracy was checked using the position dilution of precision (PDOP). It provides the possible errors related to the geometry of the satellites that are used to triangulate a position on Earth. Good accuracy is obtained when the PDOP ranges between 1 to 4, implying field error locations between 5 and 15 m (Kennedy, 2002). An accuracy less than ±10 m was found for the Ensign GPS in an accuracy assessment between the measured easting

and northing of six positions representing the corners of Mt Eliza Reservoir of the Kings Park and Botanic Garden of the City of Perth and their corresponding location in the image. Average PDOP values ranging between 2 and 4 were obtained, which were considered to be acceptable. A field data collection form was designed which included site identification number, calendar date, *X*, *Y* coordinates, percent of total area occupied by land cover classes and observation level. A detailed description of the parameters included in the field data collection form is presented in Appendix 1. A high resolution (896 by 592 pixels) natural colour imagery was acquired using the digital camera for each site in addition to documentation of the visual identification of the land cover composition using the field data collection form.

3.4.4.1.3 Assigning Fuzzy Memberships

A linguistic scale ranging from one to ten was adopted for assigning fuzzy membership to each field reference data. Such scale is a modification of the one to five scale proposed by Gopal and Woodcock (1994). As the classification accuracy of this study considered fuzzy membership of the classified and field reference data, it is assumed that the modified linguistic scale varying from one to ten would be more realistic as compared to the one to five, for determining the accuracy measures. A description of the linguistic values and the corresponding fuzzy membership values is presented in Table 3.1.

Table 3.1 Modified linguistic scale or 'fuzzy values' used in assigning fuzzy membership at each sample site

Value	Fuzzy Value	Description
1	0.0	Absolutely Wrong: Totally unacceptable
2	0.2	Bad Match: Not acceptable, way beyond right match
3	0.3	Mostly Wrong: Quite wrong, not close at all
4	0.4	Moderately Wrong: Unhappy to accept, not close
5	0.5	Understandably Right: Merely acceptable, just close to match
6	0.6	Reasonably Right: Mostly acceptable, quite close to match
7	0.7	Moderately Right: Pretty close to match, acceptable
8	0.8	Almost Right: Mostly right, very close to match
9	0.9	Good Answer: Happy to find this answer on the map
10	1.0	Absolutely Right (Perfect): No doubt about the match

The advantage of this approach is that an appropriate sampling strategy can be employed to select the sites for generating the fuzzy membership. Importantly, the

sampling strategy is an integrated part of deriving the accuracy measures from conventional and fuzzy error matrix. The advantage of an error matrix and fuzzy matrix is that they preserve the property of error ``localization'' which can identify the contribution of each category relative to the actual category as verified in the reference data'' (Congalton, 1991). Accordingly, the approach of assigning fuzzy memberships based on linguistic scale was adopted to generate the fuzzy ground data using 50 randomly selected samples from each category of land cover classes.

3.4.4.2 Defuzzification of the Fuzzy Classification

Defuzzification provides a basis for carrying out the accuracy assessment of fuzzily classified data. It is a technique that determines the most appropriate single value from the fuzzy memberships representing the land cover classes considered in deriving the fuzzy memberships. Thus, it is an inverse step of fuzzification, which transforms the fuzzy membership of multi-dimensional representation to a one-dimensional representation.

Zadeh (1968) indicated that defuzzified maps can be generated by converting fuzzy maps as unions of defuzzified areal classes and fuzzy boundaries, using subsets exceeding or falling below a suitably chosen quantitative α-cut level. In a typical defuzzification, the pixels are assigned to the classes to which they have maximum belonging, measured by specific class membership functions (Rondeau *et al.*, 1997; Zhang and Goodchild, 2002). This can be shown mathematically by the following expression.

$$u(x_s) = U_k \text{ if } \mu_A(x_s) = \mu_{\max}(x_s) = \max(\mu_1(x_s), \ldots\ldots\ldots \mu_c(x_s)) \qquad (3.23)$$

where U_k is the classified layer for a particular location, x_s, k is the range of the land cover classes which varies between 1 and c, and s is the range of the pixels (locations) of a classified data varying from 1 to n. In this approach, the maximum membership value determined by Equation 3.23 for a location x_s is always higher than the pre-determined threshold α. Thus, defuzzification provides a basis to produce single value map (either crisp or fuzzy) using the outputs of fuzzy classification and fuzzy ground data. The conceptual model adopted for generating

fuzzy land cover maps using the defuzzification technique mentioned above is shown in Figure 3.4.

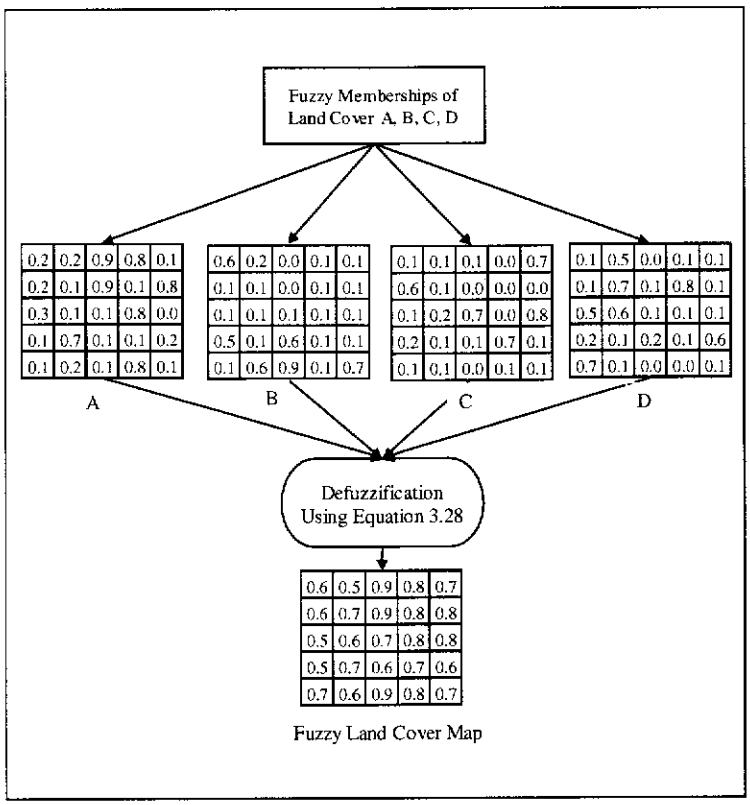

Figure 3.4 Conceptual model for generating fuzzy land cover maps using defuzzification

3.4.4.3 Derivation of a Fuzzy Error Matrix

The defuzzified memberships derived from remotely sensed data and ground truth data are used in the process of evaluating classification accuracy. This can be explained by the following vectors F and G:

$$F(x) = (f_1(x), \ldots\ldots\ldots\ldots f_c(x)) \tag{3.24}$$

$$G(x) = (g_1(x), \ldots\ldots\ldots\ldots g_c(x)) \tag{3.25}$$

where $f_i(x)$ and $g_i(x)$ (i = 1, ... c) are pixel x's fuzzy membership values derived from remotely sensed data and its corresponding ground data. The concept of defuzzification using the maximum memberships for each location is used in this research to generate fuzzy land cover map comprised of a single fuzzy membership and accordingly, fuzzy error matrix was derived. A conceptual model of the accuracy assessment is shown in Figure 3.5. In this model, the elements of the fuzzy

error matrix (11 to 44) as shown in Figure 3.5 were generated using the concept of intersection between the fuzzy membership of the classified and field reference data as explained in Section 2.3.3.

3.4.4.4 Accuracy Measures of the Fuzzy Error Matrix

Similar to an error matrix, the elements of a fuzzy error matrix are used to determine the accuracy measures such as overall accuracy, producer's and user's accuracy. In the conventional error matrix, the total number of samples coincides with the total number of reference data and thus, the accuracy measures are derived. However, in a fuzzy error matrix, assuming the orthogonal hypotheses, three cases such as coincidence, underestimation and overestimation of the memberships of reference data and sample data might arise (Binaghi *et al.*, 1999). For all cases, the overall accuracy (OA), which is a measure of total match between reference and classification data, is computed by dividing the sum of the membership grades of the

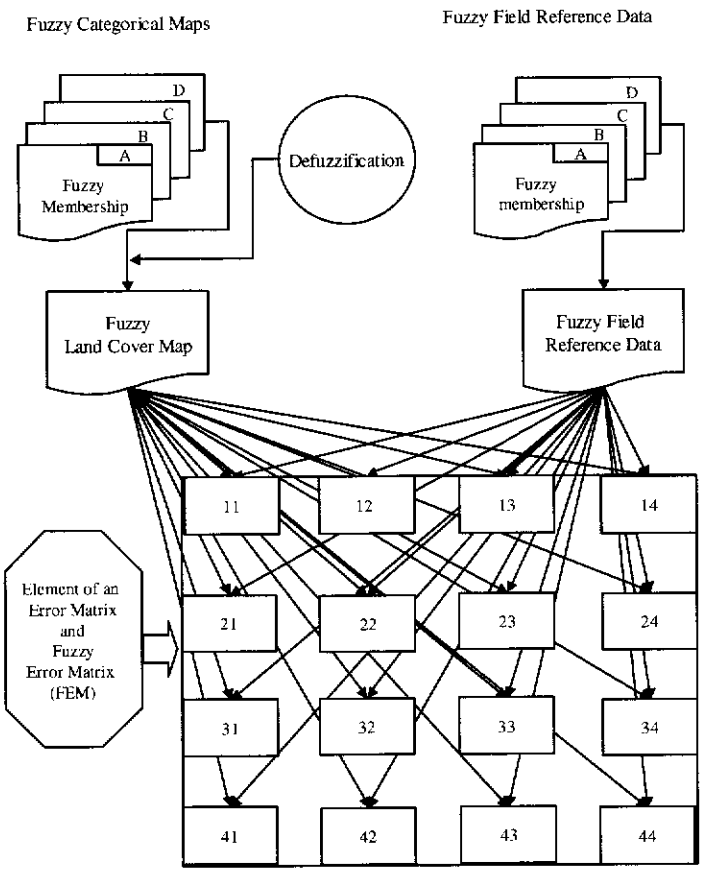

Figure 3.5 The conceptual model of deriving fuzzy error matrix

major diagonal by the sum of the membership grades found in reference data (see Table 3.2). The producer's accuracy (PA) and user's accuracy (UA) are the same for the case of coincidence as the fuzzy memberships of sample data exactly matches with the reference data. As can be seen in Table 3.2, the user's accuracy is calculated by dividing the membership grades of correctly classified samples by the sum of the membership grades of the column, while the producer's accuracy is calculated by dividing the membership grades of correctly classified samples by the column total.

Table 3.2 An example of computing accuracy measures of fuzzy error matrices for the cases of (a) coincidence, (b) underestimation and (c) overestimation (after Binaghi, *et al.*, 1999)

	Reference data			Total Grades	Accuracy measures	
Classified data	$\tilde{R}_1$	$\tilde{R}_2$	$\tilde{R}_3$		Producer's Accuracy	User's Accuracy
(a) Coincidence (OA =1)						
$\mu_{\tilde{R}1}(x)=0.4,\ \mu_{\tilde{R}2}(x)=0.4,\ \mu_{\tilde{R}3}(x)=0.4$						
$\mu_{\tilde{C}1}(x)=0.4,\ \mu_{\tilde{C}2}(x)=0.4,\ \mu_{\tilde{C}3}(x)=0.4$						
	0.4	0.4	0.4	0.4	$PA_1 = 1$	$UA_1 = 1$
	0.4	0.4	0.4	0.4	$PA_2 = 1$	$UA_2 = 1$
	0.4	0.4	0.4	0.4	$PA_3 = 1$	$UA_3 = 1$
Total Grades	0.4	0.4	0.4			
(b) Underestimation (OA = 0.833)						
$\mu_{\tilde{R}1}(x)=0.4,\ \mu_{\tilde{R}2}(x)=0.4,\ \mu_{\tilde{R}3}(x)=0.4$						
$\mu_{\tilde{C}1}(x)=0.2,\ \mu_{\tilde{C}2}(x)=0.4,\ \mu_{\tilde{C}3}(x)=0.4$						
	0.2	0.2	0.2	0.2	$PA_1 = 0.50$	$UA_1 = 1$
	0.4	0.4	0.4	0.4	$PA_2 = 1$	$UA_2 = 1$
	0.4	0.4	0.4	0.4	$PA_3 = 1$	$UA_3 = 1$
Total Grades	0.4	0.4	0.4			
(C) Overestimation (OA =0.9)						
$\mu_{\tilde{R}1}(x)=0.4,\ \mu_{\tilde{R}2}(x)=0.4,\ \mu_{\tilde{R}3}(x)=0.4$						
$\mu_{\tilde{C}1}(x)=0.6,\ \mu_{\tilde{C}2}(x)=0.4,\ \mu_{\tilde{C}3}(x)=0.4$						
	0.4	0.4	0.4	0.6	$PA_1 = 1$	$UA_1 = 1$
	0.4	0.4	0.4	0.4	$PA_2 = 1$	$UA_3 = .67$
	0.4	0.4	0.4	0.4	$PA_3 = 1$	$UA_3 = 1$
Total Grades	0.4	0.4	0.4			

The result of estimating the user's accuracy can be interpreted as the probability of a sample data or reference location labeled as category *C*, belonging to category *C*. For example, a user's accuracy of 90 percent of a particular class signifies 90 percent of the pixels classified to the respective class can be found in reality (e.g. in the ground). Likewise, the producer's accuracy indicates the probability of a sample data or reference location of category *C* is accurately classified as category *C*.

The interpretation of these accuracy measures is sometimes deceiving and simplified accuracy measures are expressed in terms of 'error of omission' and 'error of commission' (Janssen and van der Wel, 1994). Errors of omission refer to the samples of a certain category of the reference data that are incorrectly classified to another category. The samples are omitted from the correct class. Likewise, errors of commission refer to the samples of a certain category of the classified data that are wrongly classified (i.e. committed to an incorrect class). These accuracy measures can be derived by the following equations using the user's and producer's accuracy.

$$\text{Commision}\,(\%) = 1 - \text{user's accuracy}\,(\%) \tag{3.26}$$

$$\text{Omission}\,(\%) = 1 - \text{producer's accuracy}\,(\%) \tag{3.27}$$

Three cases such as coincidence, underestimation and overestimation might arise between the fuzzy memberships of the reference and classified data as reported by Binaghi *et al.* (1999). In case, the fuzzy memberships of the reference data coincide with the fuzzy memberships of the classified data, the OA, PA and UA are equal to one for all classes (Table 3.2). In case of underestimation of the fuzzy memberships of the classified data as compared to the reference data, the PA is less than the UA as the PA corresponds to the underestimated class. On the other hand, the UA is less than the PA for the case of overestimation of the fuzzy memberships of the classified data, as the UA corresponds to overestimated class (Table 3.2).

3.4.4.5 Generation of Uncertainty Maps

A measure for uncertainty or ambiguity can be determined using the confusion index, which is computed as 1.0 minus the difference between the fuzzy membership values of the most likely and the next most likely classes (Burrough, 1996). The underlying assumption of the confusion index is that the greater the confusion index, the smaller

the difference in fuzzy membership values between the most likely and the next most likely classes, and thus the more likely that the location is prone to misclassification. Therefore, the confusion index could be used to examine the spatial patterns of misclassification of a fuzzy classification. Accordingly, the confusion index maps of the study areas were generated by the following expression for each location using the fuzzy categorical maps produced by various fuzzy operators:

$$CI = 1 - (mf_{\max 1} - mf_{\max 2}) \tag{3.28}$$

where CI is the confusion index, $mf_{\max 1}$ and $mf_{\max 2}$ are the first maximum and the second maximum membership of the classes for a particular location x, respectively.

3. 5 Summary

The methodological approach adopted in this research consisted of four major steps: (i) study area selection; (ii) characterisation of the spatial complexity of urban landscapes using multiscale and multisource remote sensing data; (iii) derivation of fuzzy membership values (FMVs) of selected urban land cover types using multispectral image; and (iv) creation of virtual field reference database (VFRDB) and accuracy assessment of the fuzzily classified data.

Methods and techniques associated with the research approach included characterisation of spatial complexity using spatial autocorrelation measures and fractals, transformed divergence analysis for selecting the best band combinations of multispectral image, derivation of fuzzy memberships from remotely sensed data and ground data, defuzzification of the fuzzy memberships of remote sensing image and ground data, computation of accuracy measures using fuzzy error matrix, and generation of uncertainty maps.

The analysis of spatial complexity using the multiscale and multisource remote sensing images is done using fractal models. The isarithm and the TPSA techniques are tested for their ability in deriving D of major land cover types. The D values enable determination of the scale at which most of the processes related to the urban landscape in the Perth metropolitan area occur. Transformed divergence analysis was applied in selecting the best set of bands of a multispectral image to be used in the fuzzy supervised classification of the Perth metropolitan area. The derivation of

fuzzy memberships is the key of fuzzy classification and accordingly, the supervised approach of the fuzzy *c*-means algorithm is used to generate the fuzzy memberships of the land cover classes using the selected bands of multispectral image. Then, the fuzzy operators (e.g. maximum, minimum, algebraic sum, algebraic product and gamma operators) are applied to integrate the fuzzy memberships of urban land cover types. The fuzzy memberships of the ground data are derived using a modification of the fuzzy linguistic scale proposed by Gopal and Woodcock (1994). Details about the study area, data sets and software used in this research are presented in the following chapter.

Chapter 4

STUDY AREA AND DATA SETS

Chapter 4 describes the location and characteristics of major land cover types of the study areas. The multiscale and multisource remote sensing images such as SPOT, Landsat-7 ETM+ and Landsat MSS, which were used in the analysis of the spatial complexity and interpretation of urban landscapes, are described. In addition to remote sensing images, aerial photographs, land use and land zoning maps, which were used in this analysis, are also discussed. An overview of the major software that were used in the analysis is provided.

4. 1 Geography of the Study Area

The Perth Metropolitan Area (PMA) is situated in the south-west of Western Australia and covers an area approximately 122,401 km^2. It is geographically located between 31° 27′ 36″ south to 32° 27′ 36″ south and 115° 33′ 36″ east to 116° 24′ 36″ east (Figure 3.1). It comprises 29 local government councils. The major land cover types of the local government councils are native vegetation, open spaces, residential, commercial and industrial uses.

4.1.1 Major Landforms

The Perth metropolitan area (PMA) is divided into two distinct geological landforms. These are the Swan Coastal Plain and the Darling Scarp and Plateau which is also known as the Darling Range (Figure 4.1). The Swan coastal plain is composed of sedimentary deposits, being located in the western part of the PMA while the Darling Range is located in the eastern part of the PMA and consists of granitic rock which is some 2,500 million years old (Western Australian Planning Commission, 1998). Within the Swan Coastal Plain, there are six major landforms, running from north to south of the PMA and between the Darling Range and the coast. From east to west of the Swan Coastal Plain, the major landforms are the Dandaragan Plateau, the ancient beach, dune and colluvial deposits of the foothills, the river and stream deposited clays and sands of the Pinjarra Plain, and three sets of dune sands, the

Bassendean, Spearwood and Quindalup, the last being the present day coastal plains (Western Australian Planning Commission, 1998).

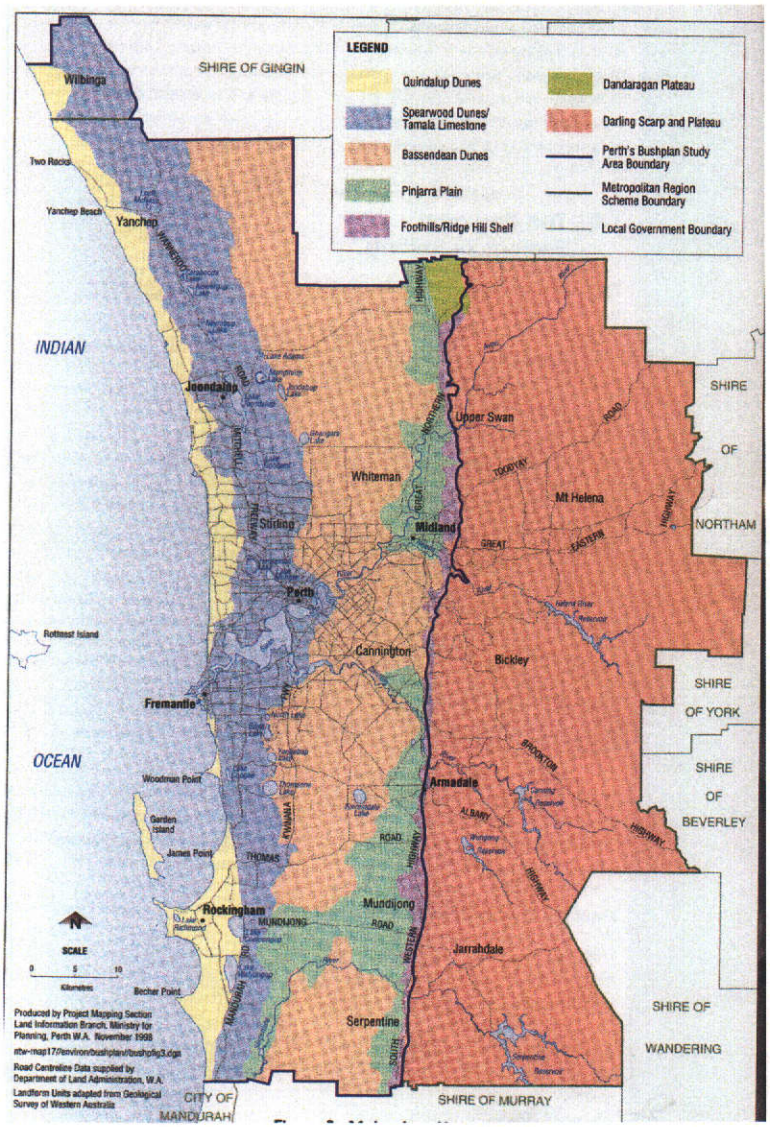

Figure 4.1 Major landform units of the Perth metropolitan area (from Western Australian Planning Commission, 1998)

4.1.2 Climate

The climate of the PMA can be described as Mediterranean type with long dry summers and mild rainy winters. There are four seasons: summer, autumn, winter and spring that characterise the climate of the PMA. The average monthly rainfall, temperature and the relative humidity of summer vary substantially as compared to winter, whereas similar conditions can be found in autumn and spring (Table 4.1). The warmest months of the year are January and February, when temperatures can

reach the mid to high 30°C. The mild winter begins in June and finishes in September, coinciding with the rainy season and the average day temperature falls between 16 to 18°C. There are occasional storms, characterised by thunder, lightning and heavy downpours of rain in winter. Among the climatic data recording stations, Perth Airport, Mount Lawley, Gosnells City, Jandakot Airport, Pearce RAAF, Swanbourne and Rottnest Island are the most relevant describing the climatic conditions of the study areas (Figure 4.2).

Table 4.1 Average rainfall, temperature and relative humidity of the PMA

Season	Rainfall (mm)	Temperature (°c)	Relative Humidity (%)
Summer (December to February)	3.49	28.83	54.10
Autumn (March to May)	41.47	25.72	61.48
Winter (June to August)	125.62	18.94	77.71
Spring (September to November)	51.06	22.66	61.38

Source: Compiled from Bureau of Meteorology (2001)

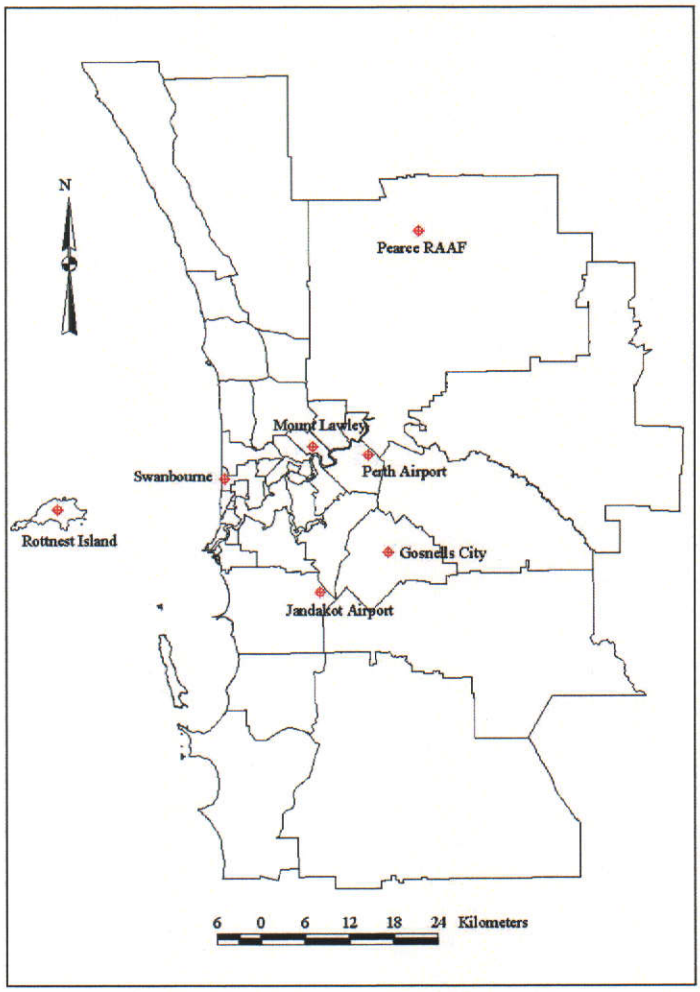

Figure 4.2 Map showing the location of climatic data recording stations within the Perth metropolitan area

4.1.2.1 Rainfall

The average monthly rainfall of the PMA is presented in Figure 4.4 which shows that the lowest rainfall occurs in the months of January, while July tends to record the highest rainfall at all recording stations. It is important to note the spatial variability in the amount of rain falling in the PMA. For instance, Figure 4.3 shows that Swanbourne, close to the coast as can be seen in Figure 4.2, registered the highest annual and the average monthly rainfall, which is nearly 30 percent more than the lowest rainfall registered in Pearce RAFF, located in the eastern part of the PMA. Furthermore, nearly 90 percent of the rainfall occur during May to September, indicating the dry period in the remaining months of the year.

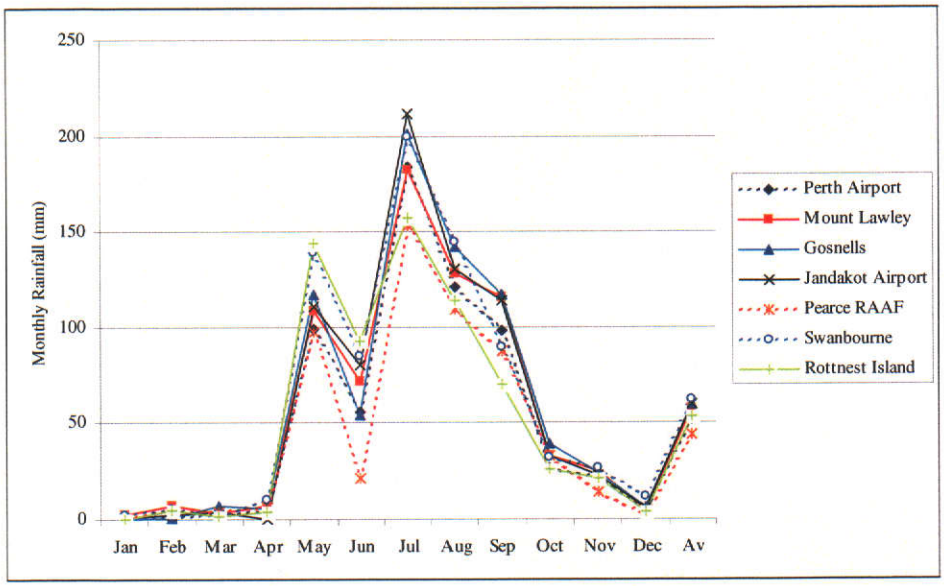

Figure 4.3 Monthly rainfall (mm) of Perth metropolitan area (adapted from Bureau of Meteorology, 2001)

4.1.2.2 Temperature

The average monthly temperature of the PMA varies between 17.5°C and 32.4°C (Figure 4.4). Figure 4.4 shows that the highest average monthly temperature occurs in most of the recording stations in January, while the lowest temperature tends to occur in August. Clearly, January, February and March are the warmest months as the average monthly temperatures of all the recording stations are higher as compared to the other months. On the other hand, the coolest month of the year is August, reaching an average temperature of around 18°C in all the recording stations.

The highest average monthly temperature is recorded in Pearce RAAF while the lowest average temperature is found to be on Rottnest Island (Figure 4.4).

4.1.2.3 Relative Humidity

The relative humidity obtained from all the recording stations is shown in Figure 4.5. As can be seen in Figure 4.5 that the lowest and the highest monthly average relative humidity are recorded in March and June respectively, in all recording stations.

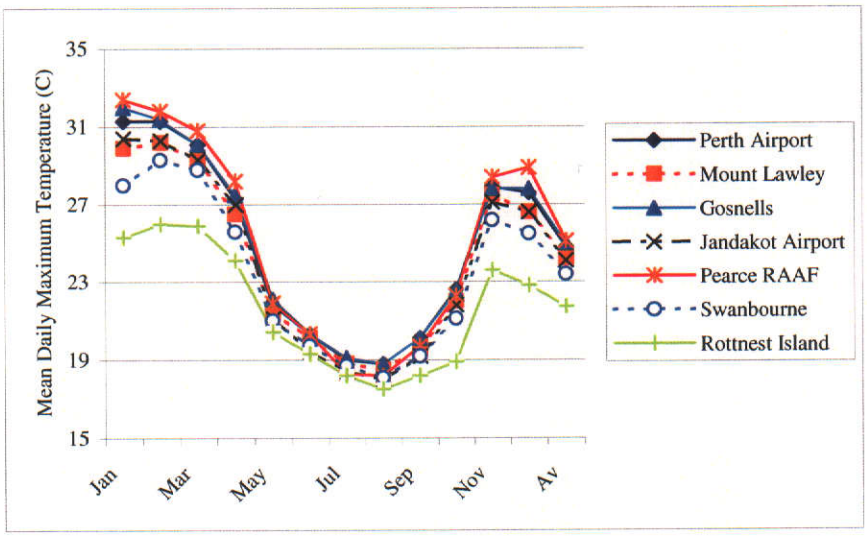

Figure 4.4 Mean daily maximum temperature of Perth metropolitan area (adapted from Bureau of Meteorology, 2001)

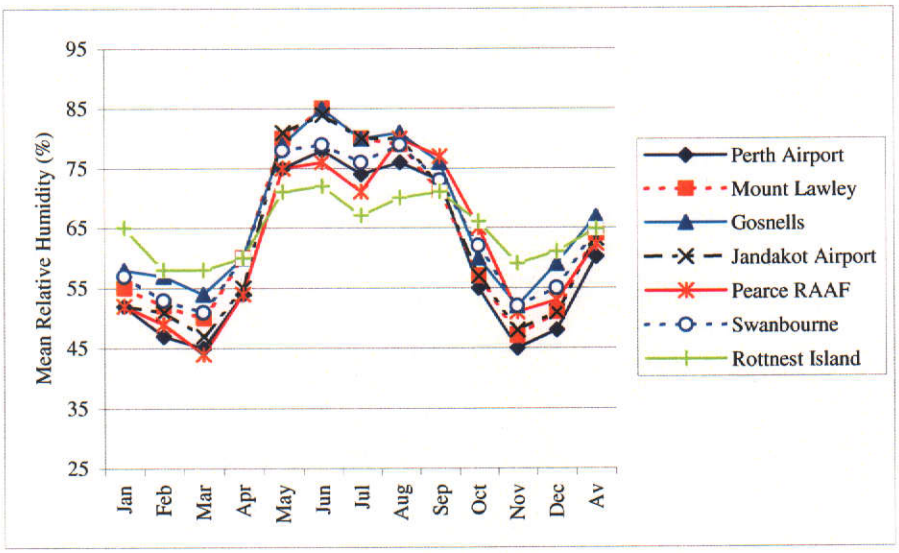

Figure 4.5 Mean relative humidity (at 9.00 AM) of Perth metropolitan area (adapted from Bureau of Meteorology, 2001)

It is important to note that the average monthly relative humidity recorded from May to September is 41 percent higher compared to the October-April period. This is consistent with the rainfall data, registering 90 percent of total precipitation in the same period, indicating the intensity of wetness.

4. 2 Characterisation of the Study Areas

As explained in Chapter 3, three local councils namely the City of Perth, the City of Melville and the City of Armadale, were selected for the analysis due to their dominant land cover types which are representative of the whole metropolitan area (Figure 4.6). According to the geological landforms, the City of Perth and the City of Melville fall in the Spearwood Dunes of the Swan Coastal Plain while the majority of the City of Armadale falls in the Darling Range (see Figure 4.1). The land cover types, particularly the native vegetation of the Spearwood Dunes, are extensively cleared and are replaced by urban land uses. However, pine plantations, grazing and horticulture, significant conservation reserves also exist in this landform. The Darling Range retains the bushland, which is dominated by native forest. In addition to bushland and water catchment reserves, some cleared corridors of private land associated with the Albany Highway and Brookton Highway exist in this landform.

In addition to analysing the secondary source data (land zoning maps, metropolitan region schemes) random field visits were made to the local councils of the PMA to characterise the dominant land covers. Accordingly, the City of Perth, the City of Melville and the City of Armadale representing dense urban, medium urban and urban fringe areas respectively, were selected for the analysis of spatial complexity and the mapping of the major land cover types using multisource and multiscale remote sensing images. As shown in Figure 4.6 the dominant land cover types of the City of Perth are characterised by dense built-up areas, which include large buildings, major and minor road networks. On the other hand, the land uses of the City of Melville are characterised as residential which varies from buildings with tile roofs surrounded by asphalt/concrete road (Figure 4.6, b-1) to houses surrounded with trees and vegetation (Figure 4.6, b-2). The land uses of the City of Armadale as shown in Figure 4.6(c) are dominated by natural vegetation and forested areas. A

summary of the major land cover types of the study areas is presented in Table 4.2, and discussed in detail in the following sections.

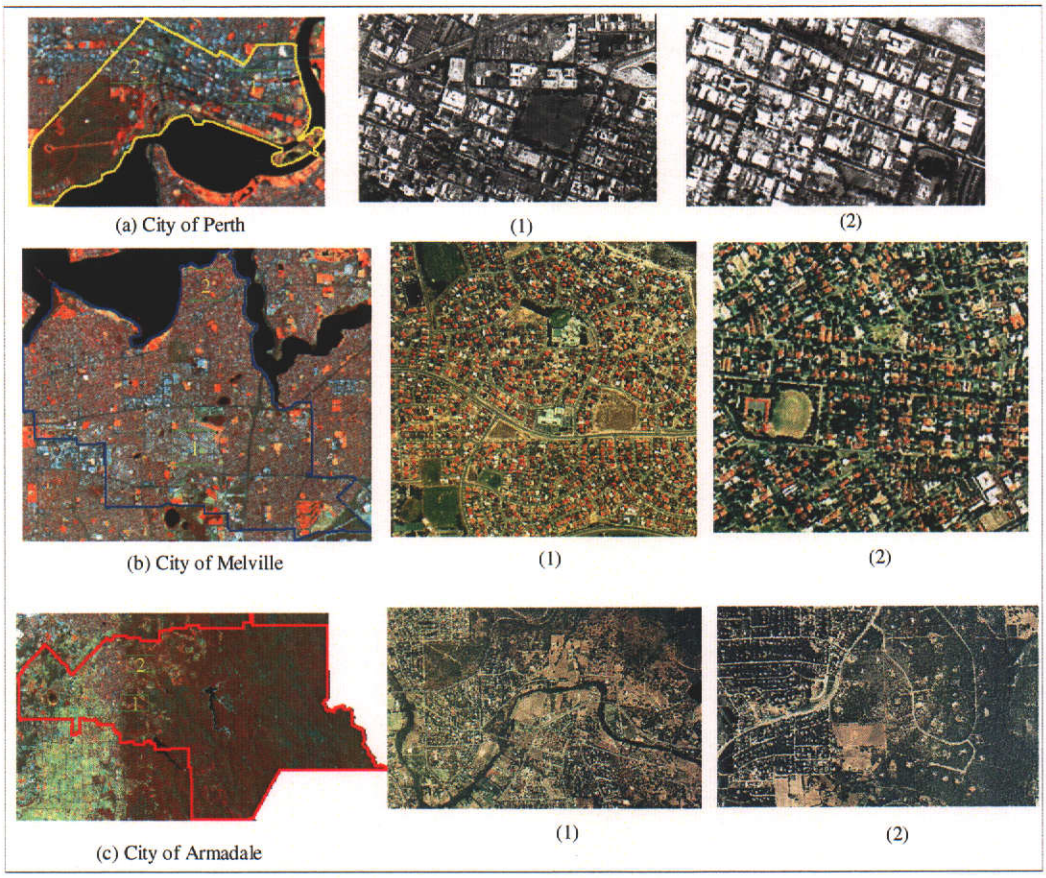

Figure 4.6 Characterisation of the dominant land cover types of the study areas: a-1) Large buildings with major and minor roads, a-2) Large buildings with minor roads, b-1) Residential buildings with tile roofs, b-2) Residential buildings surrounded by trees, c-1) Sparse vegetation, c-2) Forested area

Table 4.2 Major land cover types of the study areas

Study Area	Major Land Cover Types	Description
City of Perth	Dense Urban	Commercial buildings, shopping complexes
	Urban	Large open roofs, major and minor roads
	Forest	Variety of native plants
	Grassland	Recreational areas characterised by grasses, shrubs and occasional native plants
City of Melville	Dense Urban	Shopping complexes, administrative centres
	Urban	Residential area, minor and internal roads
	Forest	Variety of native plants
	Grassland	Open space, playgrounds and recreational areas
City of Armadale	Dense Urban	Industrial and shopping areas
	Urban	Residential area, minor and internal roads
	Forest	Native plants dominated by open forest
	Grassland	Open space, playgrounds, grazing and recreational areas

4. 3 Major Land Covers in the Study Areas

4.3.1 The City of Perth

The study area is within the council boundary of the City of Perth (ABS, 1996), which is the capital of Western Australia and located in the centre of the PMA (Figure 3.1). It covers an area of 13 km^2, which includes the Perth City area, mainly commercial and the Kings Park and Botanic Garden. In addition to data from secondary sources such as land use maps, aerial photographs with a resolution of 2.5 m, ground truth data were collected to build the virtual field reference database as explained in Section 3.4.4.1. The Kings Park and Botanic Garden comprise forested areas while heavily built-up areas dominate the western, central and eastern part of the Perth City area. Other land cover types are recreational areas (grassland), which exist in several locations within the study area. These land covers were identified in field visits and correlated with their characteristic spatial patterns in the aerial photographs and the land use maps to assist with image interpretation and for reference data compilation. A brief description of the land covers is presented in the following sections.

4.3.1.1 Forest

Forested areas in the City of Perth are associated with open forest to woodland, characterised by a wide variety of native plants, either individually or in various combinations of *Eucalyptus gomphocephala*, *Eucalyptus calophylla*, and *Eucalyptus marginata*. Most of the forested areas are found in the Kings Park and Botanic Garden, which cover approximately 400 ha including 267 ha of significant remnant bushland.

The bushland of the Kings Park and Botanic Garden contains two readily distinguished plant communities that reflect the soils and landforms on which they are found. These are mixed closed heath on the shallow calcareous soils with exposed limestone on the escarpment; and woodland to open forests characterised by *Eucalyptus/Allocasuarina/Banksia* on the deep calcareous sands. Plate 4.1, Figures 1 to 3 show examples of the open forest, woodland and mixed closed heath. There are 290 (indigenous) species of native flowering plants growing in the area, which represents about 19 percent of the native flora of the Perth region. There are also

quite a variety of large fungi found in the bushland. The mixed closed heaths of the escarpment contain a diverse and unique assemblage of shrubs, herbs, sedges and grasses normally associated with limestone heaths of nearer coastal areas. The mixed closed heaths at Kings Park and Botanic Garden are one of the most inland occurrences of these estuarine cliff communities and are contiguous with adjacent bushland areas (Meney, 1999).

4.3.1.2 Urban

The class urban in the City of Perth represents approximately 50 to 80 percent construction materials with large open roofs as well as large open transportation facilities, e.g. parking lots, and multi-lane freeway with a certain amount of vegetation cover (20 percent), internal roads and rail lines. An example of multi-lane freeways and open roof with vegetation is shown in Plate 4.1, Figures 4 to 5.

4.3.1.3 Dense Urban

The class dense urban is characterised by 80 to 100 percent construction materials. Typically, large structures, shopping complexes, the commercial and business centres and residential apartments of the eastern, central and western part of the Perth City area represent the class dense urban. Plate 4.1, Figure 6 shows a shopping complex representing the class dense urban.

4.3.1.4 Grassland

Grassland areas are dominated by high percentage of grasses, shrubs, herbs and occasional native plants, which characterise recreational areas such as playgrounds, recreational and amusement parks. Plate 4.2 shows the land cover composition of the Wellington Square, which is utilised as a playground. It is managed intensively and comprises a high percentage of grasses. Plate 4.2 also shows the children's park in the Kings Park and Botanic Garden, which is characterised by high percentage of grasses, shrubs and occasional native plants. Similar land cover compositions can be found in Langley Park, located along the riverside edge of the City.

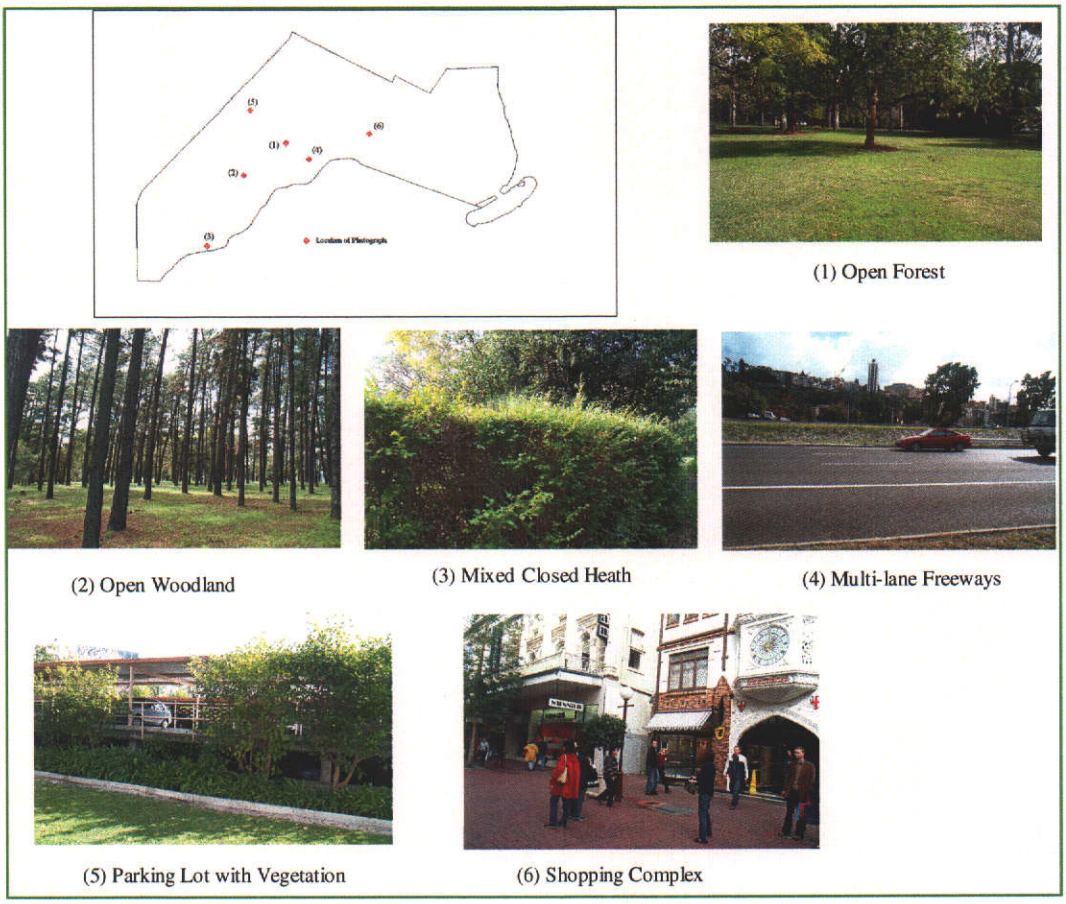

Plate 4.1 Photographs of the classes forest, urban and dense urban of the City of Perth

Plate 4.2 Photographs of the class grassland of the City of Perth

4.3.2 The City of Melville

The City of Melville, selected as an expression of "medium urban areas" that is, areas mostly residential as can be seen in Figure 4.6 is located approximately 8 km from the Perth Central area (Figure 3.1). It accommodates 18 suburbs covering an area of nearly 53 km^2 and is surrounded by the City of East Fremantle, the City of Fremantle, the City of Canning, the City of Cockburn, the Swan and Canning River. According to the land cover zoning, the study area is comprised of residential areas (living area), bushland reserves, open space typically grassland, industrial and commercial areas. These are described below.

4.3.2.1 Residential

Residential developments of the City of Melville vary from one suburb to another. For example the houses of Kardinya, Bicton, Winthrop and Bullcreek are typically comprised of detached building constructed on allotments varying in area from 500 to 800 m^2 and internal roads. Most structures have a roof area of approximately 150 to 250 m^2, predominantly of clay or concrete tile construction, but less frequently made of fibre cement or street materials (see Plate 4.3, Figure 1). This differs from the houses in Applecross and Leeming where the buildings are surrounded by trees, shrubs and grassland (Plate 4.3, Figure 2). Variations in vegetation type and canopy cover between the two photographs are particularly worth noting.

4.3.2.2 Dense Urban

Plate 4.3, Figure 3 shows an area typical of the commercial class in the study area, which is characterised by large roof areas and surrounded by extensive areas of open space, generally paved with either asphalt or concrete. Roofing materials are mostly fibre cement or metal, and compared to residential areas, most commercial sites are almost totally devoid of vegetation. Factory or warehouse sites have very similar land cover characteristics to retail sites, and are typical of the example in Plate 4.3, Figure 4.

4.3.2.3 Native Forest/Bushland

The forested area of the City of Melville is comprised of regionally significant bushland and other native vegetation. According to the Western Australian Planning Commission (1998), the forested area comprises woodland, low woodland, open heath to shrubland. Plate 4.3, Figure 5 shows an area of woodland with *Eucalyptus calophylla* trees providing the canopy and a combination of low flowering shrubs forming the understorey. The density of vegetation varies from woodland to open woodland and open heath due to the types of the trees and the percentage of canopy cover. This can be seen in Plate 4.3, Figure 6 which shows an area of low woodland comprised with *Bankasia attenuata and Bankasia menziesii* trees while Plate 4.3, Figure 7 shows an open heath comprised of shrubs.

4.3.2.2 Grassland

The class grassland in the City of Melville occurs largely as a transitional land cover, bare ground that follows the clearing of bushland for residential development, and recreational areas such as golf clubs, amusement parks and playing grounds. Clearly, the class grassland contains a diverse range of large areas of open grassland. This differs from the class grassland of the City of Perth, which only represents intensively managed recreational areas.

4.3.3 The City of Armadale

The City of Armadale typically represents an urban fringe, which stretches from the plains of the metropolitan area to the large dams, lakes, parks, grazing areas and forest. It is located approximately 29 km from Perth Central Area (Figure 3.1) and it accommodates seven suburbs comprising an area of nearly 545 km^2. According to the geological landform, the city includes a portion of the eastern side of the Swan Coastal Plain and the Darling Range. A large portion of the City's area is reserved as native forest and water catchment, occupying nearly 80 percent of the total area. According to the land cover zoning, the study area is comprised of forest, residential, rural, agricultural protection area, public purposes, water ways/lakes, and industrial areas to a lesser extent. These are described below.

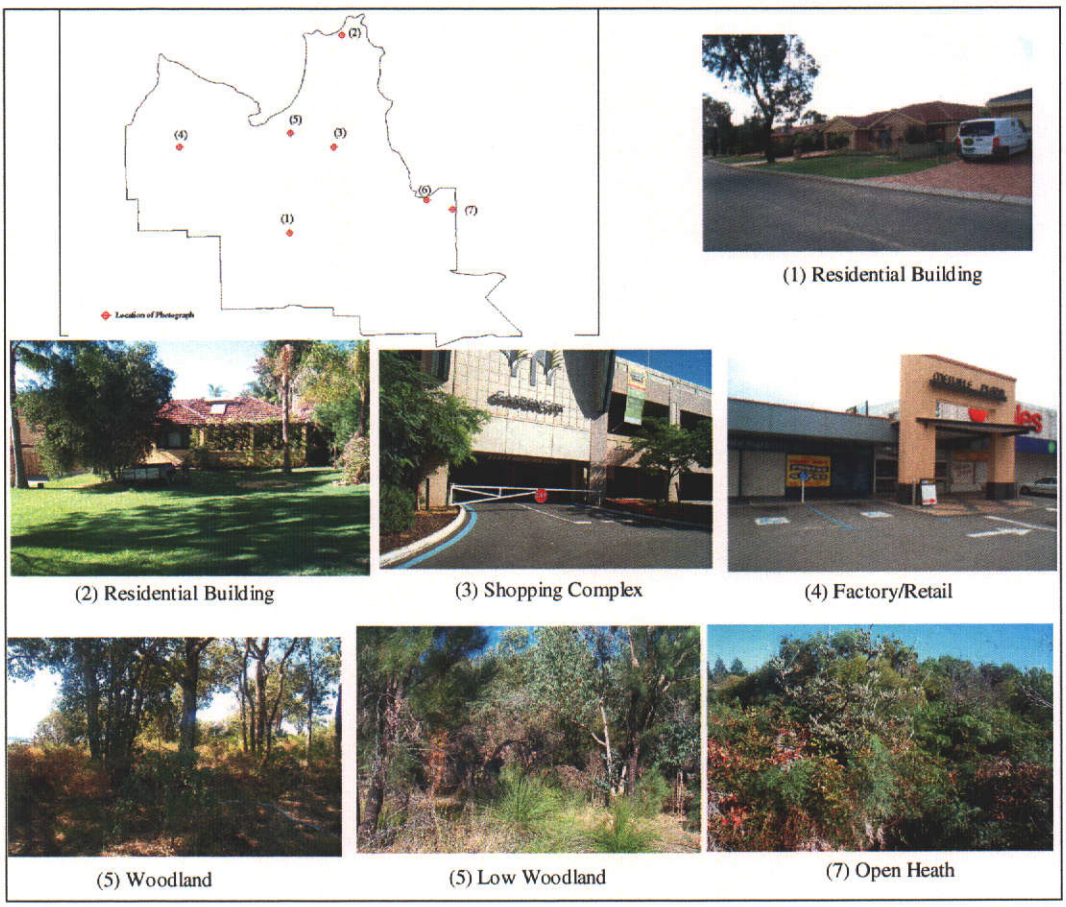

Plate 4.3 Photographs of the classes urban, dense urban and forest of the City of Melville

4.3.3.1 Forest

According to Heddle *et al.* (1980), the majority of the native vegetation in the Darling Range is reserved as State Forest, occupying most of the City's area. There is also remnant vegetation in the study area that occurs in the eastern side of the Swan Coastal Plain landform. The forested area is associated with open forest to woodlands characterised by a variety of trees such as *Eucalyptus calophylla*, *Eucalyptus wandoo, Banksia attennuata* over a very diverse understorey. Example of open forest and woodland in the Darling Range are shown in Plate 4.4, figures 1 to 2.

4.3.3.2 Residential

Armadale comprises a mix of old and new suburbs as well as rural, semi-rural and urban estates. The type of housing varies from one area to another. For example, the traditional detached housing can be seen in the suburban areas of Westfield,

Armadale and Kelmscott (Plate 4.4, Figures 3 to 4) while special housing is found in the hills of Araluen, Roleystone and Churchmans Brook. Similarly the housing of rural or lake side lots in Forrestdale and Brookdale or shop top housing in the City Centre is different.

4.3.3.3 Industrial/Commercial

The industrial/commercial areas include the city centre which is the home of major shopping complexes such as *Coles*, *Woolworths*, *K-Mart*, *Action*, *Harvey Norman* and the industrial and regional level health facilities in Kelmscott, comprising large structures. These areas are typically characterised by large roof areas and surrounded by extensive areas of open space, generally paved with either asphalt or concrete. Roofing materials are mostly fibre cement or metal, and compared to residential areas, most commercial sites are almost totally devoid of vegetation (Plate 4.4, Figure 5).

4.3.3.4 Grassland

Similarly to the City of Melville, the class grassland occurs in the bare ground following clearing for residential development, but prior to the commencement of housing construction, recreational areas such as golf clubs, amusement parks and playing grounds. In addition, it also occurs in the grazing area, which is abundant in the rural areas of the city. It is important to note that the parks and recreation and the grazing areas are also designated as rural.

4.3.3.5 Water Ways/ Lakes

The water bodies of the City of Armadale are characterised with dams, lakes, and seasonally inundated/waterlogged basins. Most of the water bodies particularly the dams such as the Canning, Churchman, and Wungong occur in the west of the current extent of urban development of the City of Armadale. These dams also serve as public water supply catchment areas of the Darling Range.

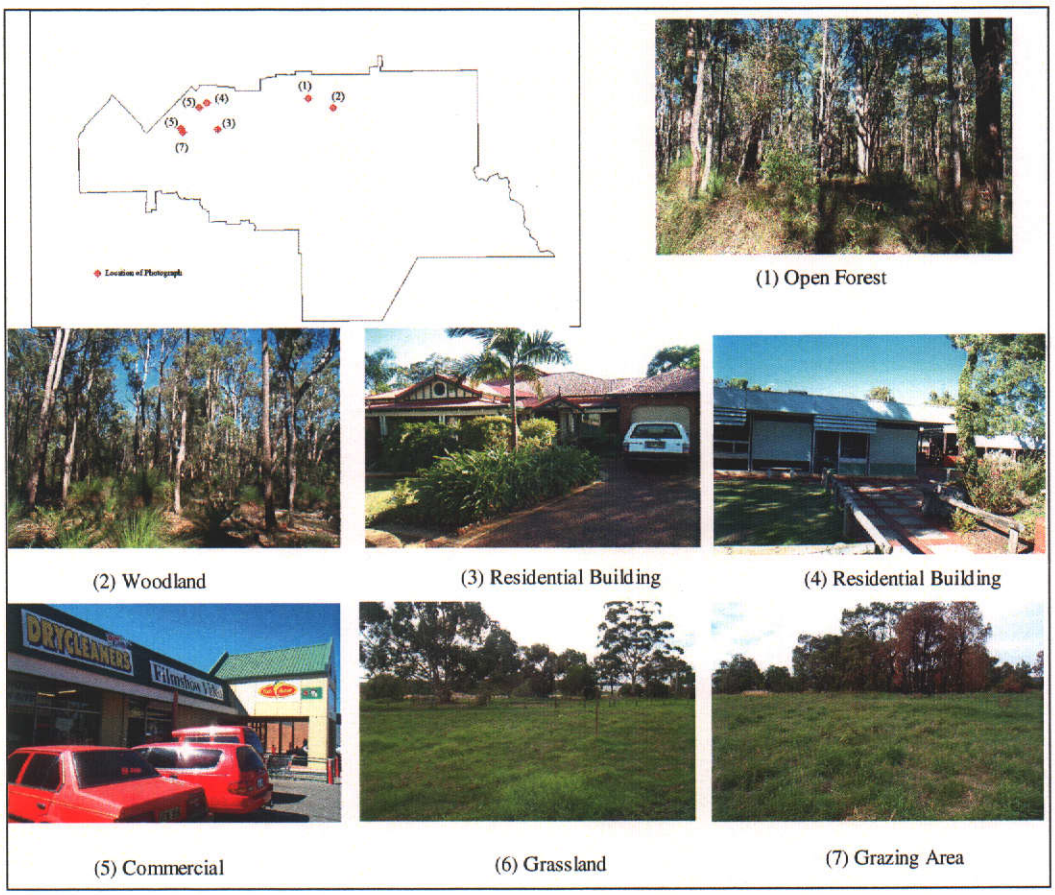

Plate 4.4 Photographs of the classes forest, urban, dense urban and grassland of the City of Armadale

4. 4 Satellite Data

This research examines the effect of various urban land cover types and scale (spectral and spatial resolution) on the spatial complexity computed from fractal measurement algorithms. Furthermore, the interpretation and mapping of the major land cover types utilising fuzzy classification and fuzzy accuracy assessment is carried out. Various sensor data such as SPOT, Landsat-7 ETM+, and Landsat MSS were used in the analysis of the spatial complexity while Landsat-7 ETM+ was used to interpret and map the major land cover types of the study areas described in the preceding section. The characteristics of these sensor data including background information are described in the following sections.

4.4.1 Sensor Characteristics

The spectral locations in the electromagnetic spectrum, the spatial resolution and the radiometric resolution of the multisource and multiscale data used in this research are

outlined in Table 4.3 and Figure 4.7. Table 4.3 shows that the spatial resolution varies from one sensor to another and ranges from 20 m for SPOT to 79 m for Landsat MSS. Similarly, the spectral bands also vary from one sensor to another. A brief description highlighting the characteristics of these sensors and their corresponding spectral bands is presented hereafter.

4.4.1.1 Landsat MSS

The Landsat remote sensing program was initiated by the National Aeronautical and Space Administration (NASA) and so far seven Landsat satellites have been launched. The Multispectral Scanner (MSS) was the first Landsat satellite, launched in 1972 and continued as the main sensor on Landsat 2 and Landsat 3 satellites. With the launch of Landsat 4 in 1982, the MSS sensor became subsidiary to the Thematic Mapper (TM) sensor, which was also the case for Landsat 5. There was no MSS sensor for Landsat 6 and 7 and hence, the availability of this data will cease since the MSS sensor was turned off on Landsat 5 in December 1997. The radiometric, spectral and spatial characteristics are summarised in Table 4.3.

4.4.1.2 Landsat-7 ETM+

Landsat 7 was launched on April 15, 1999. In Landsat 7, the TM sensor was replaced by the Enhanced Thematic Mapper Plus (ETM+) sensor, which replicates the capabilities of the TM sensor. The ETM+ also includes new features that make it more versatile and efficient for global change studies, land cover monitoring and assessment, and large area mapping. Similar to Landsat 5, ETM+ acquires data in seven spectral bands (Table 4.3). In addition to Landsat 5, the added features of Landsat-7 ETM+ are as follows:

(a) A panchromatic band (0.52-0.90 μm) with 15m spatial resolution,
(b) On board, full aperture, 5 percent absolute radiometric calibration,
(c) A thermal IR channel with 60 m spatial resolution.

4.4.1.3 SPOT

The SPOT (*System Pour L'Observation de la Terre*) was designed by the CNES (Centre National d'Etudes Spatiales) in France, and developed with the participation of Sweden and Belgium. SPOT 1 satellite was launched on 22 February 1986 and so

far five satellites have been launched. The SPOT satellite carries two identical High Resolution Visible (HRV) imaging instruments, which operate in multispectral or panchromatic mode. It acquires data in three multispectral bands with 20 m spatial resolution, while a single panchromatic band is acquired with 10 m spatial resolution (Table 4.3).

Table 4.3 Characteristics of SPOT, Landsat-7 ETM+ and Landsat MSS

Sensor	Spatial Resolution	Spectral Resolution	Radiometric Resolution	Swath (km)	Revisits Days	Altitude (km)	Sun Angle Inclination
SPOT Multispectral	20 m	3 Bands Blue, Green, NIR	8-bit	60	1-4	822	98 Degrees
SPOT Panchromatic	10 m	1 Band (0.51 – 0.73 microns)	8-bit	60	1-4	822	98 Degrees
Landsat-7 ETM+ Multispectral	30 m	7 Bands Blue, Green, Red, NIR, MIR	8-bit	18	16	705	98.2 Degrees
	60 m	Thermal					
Landsat-7 ETM+ Panchromatic	15 m	1 Band (0.52 – 0.90 microns)	8-bit	18	16	705	98.2 Degrees
Landsat MSS	79 m	4 Bands Green, Red, NIR, NIR	6-bit	185	18	917	99 Degrees

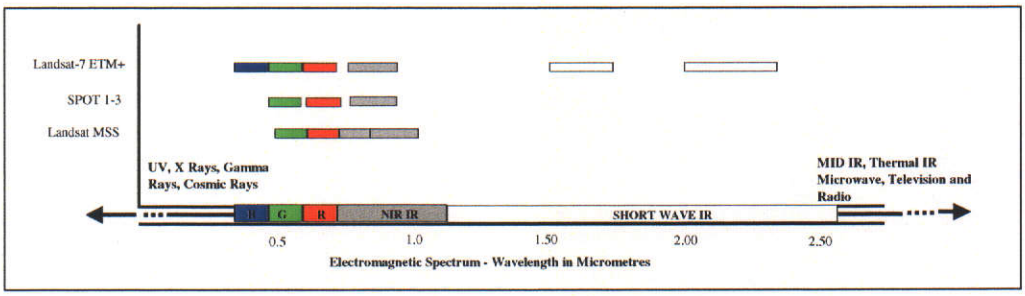

Figure 4.7 Location of spectral bands of multiscale remote sensing images

4.4.2 Digital Satellite Data

The characteristics of the sensors used in this research were discussed in the previous section. One scene from each satellite covering the whole metropolitan area was used to analyse the spatial complexity using a fractal model. Table 4.4 summarises the acquisition dates and the spatial and radiometric characteristics of the data acquired. It also specifies the use of the data within the investigation. The Landsat-7 ETM+ acquired in 2001 was used for the interpretation of major urban land cover types using fuzzy set theory.

Table 4.4 Summary of the acquisition date, spectral, spatial and radiometric resolution of the sensor used in this research

Sensor	Acquisition Date	Spatial Resolution	Spectral Resolution	Radiometric Resolution	Used For
SPOT Multispectral	4th December, 1991	20 m	3 Bands: Blue, Green, NIR	8-bit	Fractal Analysis
Landsat-7 ETM+ Multispectral	16th December, 2001	25 m	7 Bands: Blue, Green, Red, NIR, MIR, Thermal, MIR	8-bit	Fractal Analysis and Fuzzy Classification
Landsat MSS	3rd December, 1980	50 m	4 Bands: Green, Red, NIR, NIR	8-bit	Fractal Analysis

All scenes were geometrically rectified using a first-order polynomial interpolation with nearest neighbour resampling. The root mean square error for each scene was found to be less than a pixel. Landsat-7 ETM+ and Landsat MSS were resampled to a pixel size of 25 m and 50 m respectively to facilitate a comparison of the results among the study areas. In addition, the radiometric resolution of Landsat MSS was converted from 6 to 8 bit in order to have same radiometric resolution with those of Landsat-7 ETM+ and SPOT. A false colour composite (FCC) of the Landsat-7 ETM+ (bands 4, 5 and 7) for the Perth Metropolitan Area is shown in Figure 4.8.

The local council boundary (ABS, 1996) was used to clip the City of Perth, the City of Melville and the City of Armadale from each of the image scenes. For the analysis of the spatial complexity of urban land cover types using a fractal model, SPOT, Landsat-7 ETM+ and Landsat MSS were divided into several square or rectangular grids (subsets) of 324 ha along transects of the study areas (see details in Sections 6.1.1, 6.1.2 and 6.1.3). A detail explanation about the relevance of the square or rectangular grids to determine the spatial complexity using fractals has been described in Section 3.3.2.

According to the hypotheses enunciated in Section 1.5, the green and red bands of SPOT, Landsat-7 ETM+ and Landsat MSS were considered in the analysis of spatial complexity as they fall in the same spectral range of 0.5~0.6 μm and 0.6~0.7 μm respectively (see Figure 4.8). Likewise, the NIR band of Landsat-7 ETM+ and SPOT were considered. The NIR bands of Landsat MSS were excluded, as they do not fall in the same electromagnetic spectrum as compared to the NIR (0.76~0.9 μm) band of Landsat-7 ETM+ and SPOT (Figure 4.8).

4.4.3 Other Data Sources

In addition to remote sensing data, orthophotos, landuse maps and land zoning maps were used in the analysis to select the training sites from remote sensing image for generating descriptive statistics and carrying out the transformed divergence analysis. The orthophoto was acquired in 2002 and the spatial resolution is 2.5 x 2.5 m. The land use and land zoning maps show the major land covers of the respective local councils.

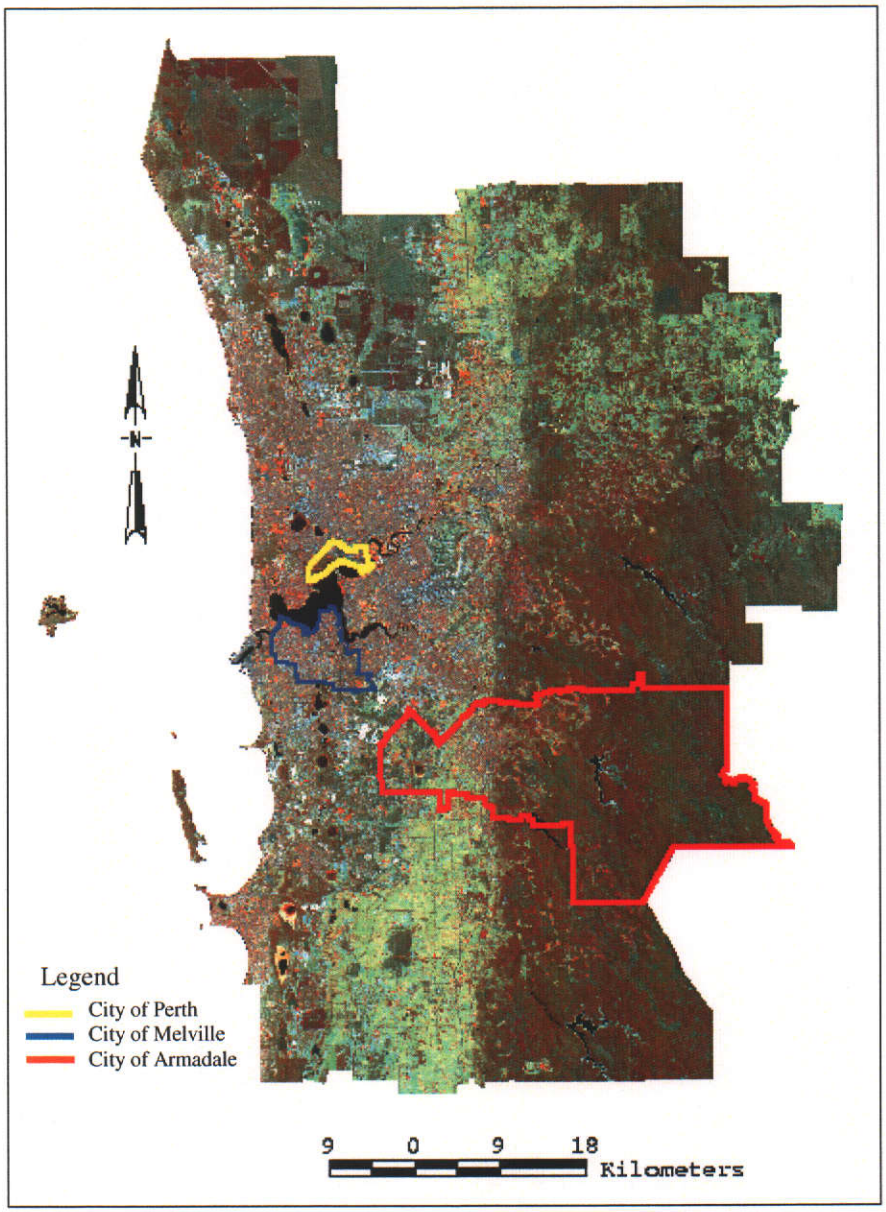

Figure 4.8 A false colour composite of Perth metropolitan area (Landsat-7 ETM+)

4. 5 Software Used

Various Geographical Information Systems (GIS) software such as Arc/Info and ArcView and image processing software such as ERDAS Imagine, ER Mapper, and Image Characterisation and Modelling System (ICAMS) were used in the analysis of spatial complexity and mapping of major urban land cover types.

The analytical capabilities of the grid cell-based model of Arc/Info through the map-algebra language allow performing various operations such as local, focal, zonal, global, surface, hydrologic, ground water and multivariate spatial functions (ESRI, 2000). Since GRID is integrated with Arc/Info, the functionality associated with the *Arc Macro Language (AML)* can be used in conjunction with GRID tools to develop complex models. Accordingly, several scripts were written using grid algebra and *AML* in various stages such as fuzzy classification, integration of fuzzy memberships and accuracy assessment analysis of the fuzzy categorical maps using fuzzy error matrix. The scripts are described in detail in Chapter 5.

ER Mapper is a user-friendly image processing software, equipped with built-in wizards for georeferencing and rectification. It provides seven different geocoding methods and allows rectifying the multiscale remote sensing images to fit into real world map coordinates (ER Mapper 6.2, 2000). The algorithm and vector annotation functionality provide a platform to overlay multiple images and vector data. This is useful delineating the training sites using vector data and aerial photographs together with satellite images for deriving descriptive class statistics.

ERDAS Imagine was used to carry out the transformed divergence analysis. The *Signature Editor* of ERDAS Imagine allows creating, managing, evaluating, editing, and classifying signatures. In evaluating signatures, the *Signature Separability* dialog enables computing of statistical distance between signatures using various measures (e.g. transformed divergence) to determine how distinct the signatures are from one another, which is used to determine the best subset of layers to use in the classification.

The ICAMS software developed by Louisiana State University in collaboration with National Aeronautics and Space Administration (NASA) was used to determine the spatial complexity of urban landscapes using multiscale remote sensing images. The

Image Characterisation Module contains spatial measures, which include fractal analysis, spatial autocorrelation statistics, and textural measures. In this sub-system, the input image is displayed in two-dimensional form and the analytical results and statistics are viewed as an output (Quattrochi, *et al.*, 1997). The details are described in Chapter 5. In addition, Microsoft Excel was used to carry out the statistical analysis.

4. 6 Summary

In this chapter, the land cover composition of the major land cover types of the study areas, brief characteristics of the various sensor data and the software that were used in the analysis have been discussed.

The major land cover classes as described in this chapter indicate that the land uses of each land cover particularly forest, urban and grassland vary from one study area to another. For example, the class forest is mostly characterised by open woodland, woodland and mixed closed heath in the City of Perth and City of Melville while the same class is represented by open forest to woodland in the City of Armadale. Similarly, the class urban is represented by residential area in the City of Melville and the City of Armadale whereas the major roads and parking represent the class urban in the City of Perth. The class grassland varies from one study area to another. In the City of Armadale, the recreational areas, bare ground and grazing area represent grassland. The class dense urban are represented by the same land uses. However, the extent of large structures, shopping complexes and commercial buildings is intense in the City of Perth compared to the City of Melville and the City of Armadale.

The spatial resolution of the various multispectral data used in the analysis varies from 20 m for SPOT to 50 m for Landsat MSS data. According to the hypotheses of this study, the selected green, red and the NIR bands were used to compute the fractal dimension for describing the complexity of the study areas. Then, the major land cover classes were mapped using the fuzzy set theory.

Several software programs which include ICAMS (Image Characterisation and Modelling System), Arc/Info, ERDAS Imagine, ER Mapper and ArcView were used

in the analysis of this study. ICAMS software was used to compute the fractal dimension using the isarithm and the TPSA method and Moran's *I* index of spatial autocorrelation of multiscale and multisource remote sensing images for characterising the spatial complexity of urban landscapes. ERDAS Imagine was used for transformed divergence analysis. The *Arc Macro Language* (*AML*) of Arc/Info was used to implement the fuzzy *c*-means algorithm for deriving the fuzzy memberships, various aspects of accuracy measures using the conventional and fuzzy error matrix and the uncertainty maps. The implementation models for computation of spatial complexity and mapping of urban land covers are discussed in the next chapter.

Chapter 5

IMPLEMENTING MODELS FOR COMPUTATION OF SPATIAL COMPLEXITY AND MAPPING URBAN LAND COVERS

Chapter 5 illustrates the implementation of the spatial autocorrelation measures and the fractal measurement algorithms to determine the spatial complexity of the three study areas characterising the urban landscapes of the PMA as described in Chapter 4. Then the supervised approach of the fuzzy *c*-means algorithm, which was written in *Arc Macro Language* (*AML*) of Arc/Info, is implemented for deriving the fuzzy memberships of urban land cover types from the selected bands of a Landsat-7 ETM+. The final section of the chapter discusses the fuzzy operators, which were used to integrate the fuzzy memberships of the selected bands for generating fuzzy categorical maps, the defuzzification of the fuzzy categorical maps and fuzzy accuracy assessment.

5. 1 Measurement of Spatial Complexity

Measures of spatial autocorrelation and the fractal dimension of three study areas of the Perth Metropolitan Area were determined from SPOT, Landsat-7 ETM+ and Landsat MSS imagery using Moran's *I*, and the isarithm and the TPSA algorithms described in the previous chapter. These methods are embedded in the Image Characterisation Module of the ICAMS, which was used in the analysis. A flowchart describing the implementation is shown in Figure 5.1.

5.1.1 Description and Operation of the Isarithm and the TPSA Algorithms

The isarithm algorithm embedded in ICAMS is analogous to the methods proposed by Goodchild (1980), Shelberg *et al.* (1983), and Lam and De Cola (1993). As discussed in Chapter 3, the algorithm requires square grids of differing sizes to compute fractal dimension. Based on the highest power of two of the side of the square grid, the maximum grid (step size) is calculated.

Figure 5.2 shows that the algorithm of the isarithm method determines the total number of isarithm lines based on the maximum and minimum pixel values (digital

numbers) of the image and user defined interval. Then, the isarithm value of each isarithm line was used to determine the fractal dimensions using the row, columns

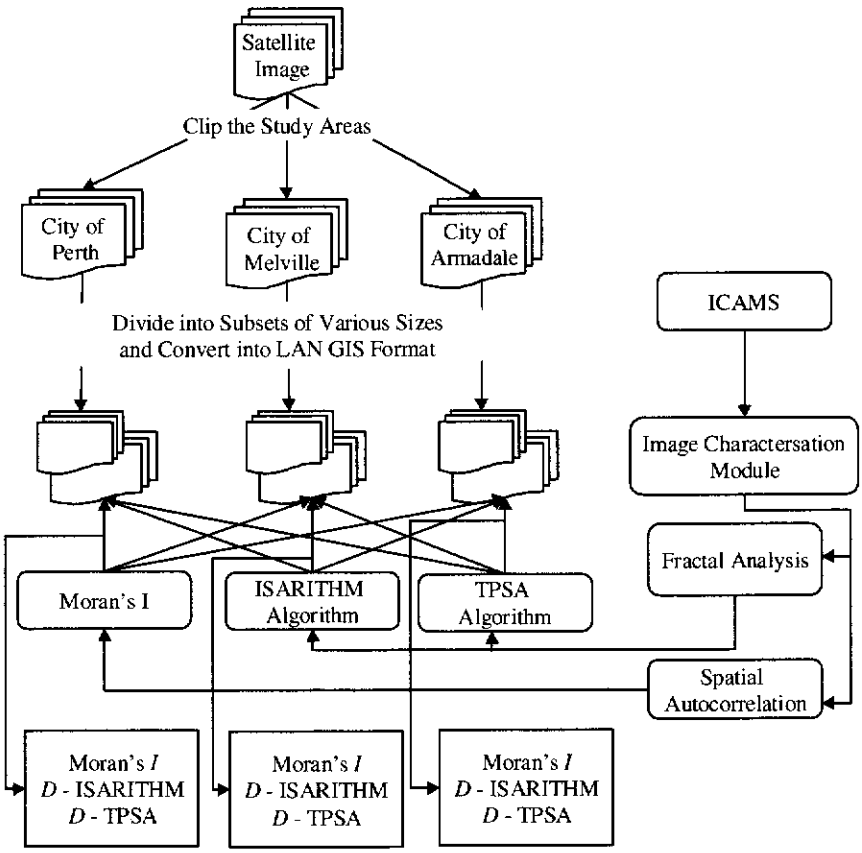

Figure 5.1 Flowchart for computing spatial complexity using the ICAMS software

or row-column method. The algorithm requires determining of the number of steps or walks, the isarithm interval, and the direction of interval and the method of operation (row, column or both). The TPSA method implemented in ICAMS is different from the original algorithm discussed in Clarke (1986) and Jaggi *et al.* (1993). Lam *et al.* (2002) showed that the regression between the prism surface areas with the logarithm of the step size instead of the logarithm of the squared step size provides the correct fractal dimension. Accordingly, the algorithm implemented by Jaggi *et al.* (1993) as shown in Figure 5.3 was modified, and embedded in ICAMS. This algorithm introduces an incremental variable initialised to unity as step size and accordingly, the square grids resulting from the step size and the corresponding surface area of the triangular prisms are calculated. Typically, the upper left corner of the image is selected as the origin for the grids and starting point for the first grid, and the area of the triangular prisms is cumulatively summed. The

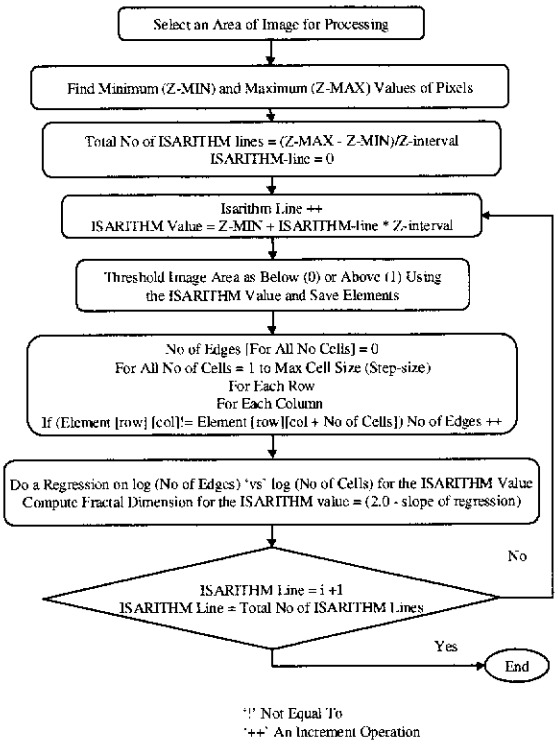

Figure 5.2 Flowchart of the isarithm algorithm using row-wise processing (after Jaggi *et al.*, 1993)

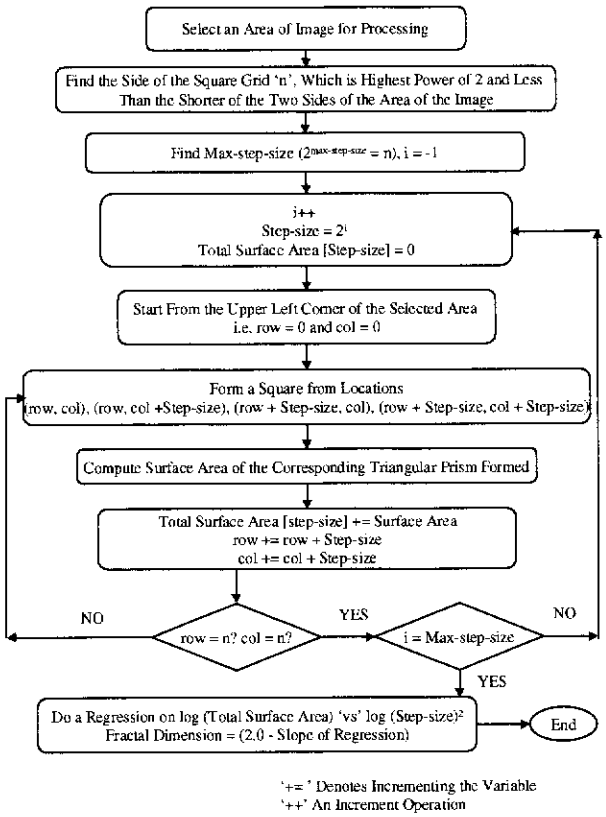

Figure 5.3 Flowchart of the TPSA algorithm (after Jaggi *et al.*, 1993)

computation is repeated for all step sizes, and the slope of the best-fitted line drawn from the plot of the logarithm of the total surface area and the logarithm of the step sizes (instead of squared step sizes) provides the fractal dimension. These algorithms require remote sensing data to be LAN GIS image format (e.g. ERDAS Imagine), tag image format (TIFF) or band interleaved by line (BIL) format. Additional to the maximum step size, the number of intervals and the method of counting the edges (e.g. row, column, row-column) as described in Section 3.3.2.1 are needed in the isarithm algorithm, while the processing method (e.g. exponential, arithmetic) is needed to determine fractal dimension using the TPSA algorithm.

5.1.2 Determination of the Fractal Dimension and Moran's *I*

The subsets comprising an area of 324 ha were selected along the transects of the study areas for the analysis of spatial complexity (see Sections 6.1.1, 6.1.2 and 6.1.3). Due to the varying spatial resolution of the sensors chosen, the number of pixels of the subsets of the study areas varied and consequently, the parameters particularly the step sizes adopted for SPOT, Landsat-7 ETM+ and Landsat MSS data varied as well. For example, the subsets that cover an area of 324 ha comprise 90 x 90 pixels of SPOT XS, 72 x 72 pixels of the Landsat-7 ETM+, and 35 x 35 pixels of the Landsat MSS data. Accordingly, a step size of six was chosen in the TPSA algorithm in order to compute the fractal dimension of SPOT XS and Landsat-7 ETM+ while step size of five was chosen for Landsat MSS data. It is important to note that the TPSA algorithm requires a minimum size of 2^6 x 2^6 pixels for calculating the fractal dimension based on step size six (Read and Lam, 2002). A summary of the subsets, corresponding pixels of various sensors and step sizes that were chosen to determine the fractal dimension is shown in Table 5.1.

Table 5.1 Summary of the subsets, their corresponding sensor's pixels and step sizes

Sensor	Subset of 324 Ha	
	Pixels	Step Size
SPOT	90 x 90	6
Landsat-7 ETM+	72 x 72	6
Landsat MSS	35 x 35	5

Following the hypotheses enunciated in Section 1.5, the spectral bands of SPOT, Landsat-7 ETM+, and Landsat MSS that fall in the same spectral location and width (Figure 4.8 in Chapter 4) were used to analyse the effect of spectral, spatial and land cover heterogeneity on the fractal dimension of the subsets using the isarithm algorithm ($D_{ISARITHM}$) and the TPSA (D_{TPSA}). A summary of the spectral bands of SPOT, Landsat-7 ETM+ and Landsat MSS that were used for the analysis of the spatial complexity of urban landscapes is presented in Table 5.2.

Table 5.2 Summary of the spectral bands of SPOT, Landsat-7 ETM+ and Landsat MSS used in the analysis

Sensor	Spectral Bands
SPOT	Green, red and NIR
Landsat-7 ETM+	Green, red and NIR
Landsat MSS	Green and red

Among the input parameters of the algorithm, the step sizes as shown in Table 5.1 were used. Other parameters such as the exponential method of the TPSA and an interval of two and the row, column and row-column methods were used in the isarithm algorithm. In addition to the fractal dimension of the subsets, Moran's *I* was also calculated using the spatial autocorrelation sub-module of the ICAMS. Moreover, the coefficient of variation was determined for each subset using the parameters of descriptive statistics such as mean and the standard deviation. An example of the fractal dimension, Moran's *I* and descriptive statistics which include mean, minimum, maximum, standard deviation (SD) and coefficient of variation (CV) of subset one of the City of Perth computed from Landsat-7 ETM+ is presented in Table 5.3.

Table 5.3 Fractal dimension, Moran's *I* of spatial autocorrelation and descriptive statistics of subset one of the City of Perth

Sensor	Band	Fractal Dimension		Moran's *I*	Descriptive Statistics				
		$D_{ISARITHM}$	D_{TPSA}		Min	Max	Mean	SD	CV
Landsat-7 ETM+ (25 m)	Green	2.88	2.94	0.7951	66	244	119.83	30.29	0.253
	RED	2.87	2.97	0.8081	58	255	132.81	36.75	0.277
	NIR	2.80	2.84	0.8344	35	164	76.63	17.82	0.233

The results of all subsets of the study areas are presented in Chapter 6, where they are analysed based on the objectives enunciated in Section 1.3.1; specially to

understand how spatial complexity can be useful in determining the appropriateness of a sensor data for determining the scale at which processes occur in the PMA using the *D*.

5. 2 Fuzzy Supervised Classification

The fuzzy supervised classification approach applied in this research comprised three major steps: (i) selection of the best set of bands of multispectral image to be fuzzified; (ii) derivation of the fuzzy memberships from the selected bands using a supervised approach of the fuzzy *c*-means algorithm; and (iii) integration of fuzzy memberships using fuzzy operators. These steps are summarised below.

5.2.1 Selection of the Best Set of Bands of Multispectral Image

5.2.1.1 Selection of Land Cover Classes of the Study Areas

The Anderson's level I classification scheme comprised water, forest land, cropland, bare cropland, barren land and urban or built-up areas which was designed mainly for land use/cover mapping by manual interpretation of remotely sensed data (Anderson *et al.*, 1976). However, for computer-assisted approach, Yang and Lo (2002) showed that a modified version of the Anderson scheme with hybrid levels I and II categories works well for mapping land use/cover from Landsat images with spatial resolution varying from 30 to 79m. In their study, a total of six land use/cover (e.g. high-density urban use, low-density urban use, cultivated/exposed land, grassland or cropland, forest and water) classes were considered for change detection using Landsat TM and MSS data. Likewise, Weng (2002) used a modified version of the Anderson scheme in the land use change analysis of the Zhujiang Delta of China. The land use categories were (i) urban or build-up land, (ii) barren land, (iii) cropland (rice), (iv) horticulture farms (primarily fruit trees), (v) dike-pond land, (vi) forest, and (vii) water. His study indicates that a modified version of the Anderson scheme with hybrid levels I and II categories works well. Accordingly, the major urban land cover classes of the study areas as presented in Table 4.2 were considered in classifying the Landsat-7 ETM+ data.

5.2.1.2 Transformed Divergence Analysis

This stage of the research comprised the selection of training areas representative of each of the land cover types, signature evaluation, and selection of the best band combination to be used in the fuzzy classification. During the training phase, representative samples of the predetermined classes (Table 4.2) of the study areas were selected from a Landsat-7 ETM+ scene based on reference (e.g. orthophoto, landuse database and land zoning) and field data. In creating the training sites for each class, adequate pixels were considered to conform with the general rule of extracting more than $10n$ pixels where n is the number band for each land cover class (Jensen, 1996; Richards and Jia, 1999). Accordingly, descriptive class statistics including mean, standard deviation, and covariance matrix were generated from the training samples of the three study areas as presented in Table 4.2 and summarised in Appendix 2. An example of the summary statistics of the class urban of the City of Perth is presented in Table 5.4.

Table 5.4 Summary statistics of the class urban generated from Landsat-7 ETM+ bands of the City of Perth

	Band 1	Band 2	Band 3	Band 4	Band 5	Band 7
Minimum	95	81	90	70	105	72
Maximum	127	117	138	93	174	160
Mean	113	99.83	109.67	81.58	127.08	97.42
Median	115	99	108	78	118	95
Std. Dev.	10.58	11.53	14.57	8.91	22.57	24.11

In addition, transformed divergence analysis was carried out to statistically evaluate the class signature separability and to select the best band combination for each of the study areas. Typically, the *Signature Editor* of the ERDAS IMAGINE (ERDAS, 2000) was used to create and evaluate signatures which enabled performing the transformed divergence analysis using the statistical separability between the training signatures. The best average spectral separability resulting from various band combinations of the study areas are presented in Table 5.5.

The transformed divergence analysis in Table 5.5 shows that bands 1, 3, 4 and 7 of Landsat-7 ETM+ of the City of Perth provided the highest separability among the predetermined land cover classes. Similarly, bands 1, 2, 3 and 7 of the City of Melville and bands 1, 3, 4, 5 and 7 of the City of Armadale exhibited the highest

spectral separability. Accordingly, these bands were selected to derive the fuzzy memberships of the urban land cover classes presented in Table 4.2 using the supervised approach of the fuzzy *c*-means algorithm.

Table 5.5 Transformed divergence analysis for selecting the best band combination of Landsat-7 ETM+ over the study areas

(a) City of Perth

No of Bands	Best Average Separability	Band Combination
6	1925	1 2 3 4 5 7
5	1967	1 3 4 5 7
4	1983	1 3 4 7
3	1980	2 4 5
2	1973	2 5
1	1864	3

(b) City of Melville

No of bands	Best average separability	Band combination
6	1929	1 2 3 4 5 7
5	1920	1 2 3 5 7
4	1937	1 2 3 7
3	1894	1 5 7
2	1851	4 5
1	1675	1

(c) City of Armadale

No of bands	Best average separability	Band combination
6	1781	1 2 3 4 5 7
5	1908	1 3 4 5 7
4	1877	3 4 5 7
3	1886	2 5 7
2	1700	5 7
1	18321	2

5.2.2 Derivation of the Fuzzy Memberships from the Selected Bands

This research implements a supervised approach of the fuzzy *c*-means algorithm as discussed in Section 3.4.2.1 using the *Arc Macro Language (AML)* of Arc/Info (ESRI, 2000). To this end, spectral values which contain several pixels of the study areas are considered as data vectors and, using the derived class means, a fuzzy membership matrix ($c \times n$, where c and n represent number of land cover classes and data vectors respectively) is generated. Thus, each data vector can be represented as a function of the fuzzy membership of land cover classes, and ideally the sum of the

membership grades of a data vector for a particular class is 1. It is important to reiterate that the fuzzy membership values vary between 0 and 1, and that a membership close to 1 represents a high degree of similarity between the class and the sample, where 0 signifies little similarity.

5.2.2.1 Description of the Algorithm

Let X describe the vector position of spectral values in N-dimensional feature space $(X_1, X_2, \ldots\ldots\ldots\ldots X_p)$, where X_p is the spectral value representing a land cover class in spectral band p. Thus, X can be represented as a $n \times p$ array where n represents the number of spectral values of selected land cover classes and p is the number of spectral layers in a multi-spectral satellite image. Let us consider c as the number of land cover classes, M_{fc} as the fuzzy c-partition space and U as a fuzzy c-partition of sample of n where each element of U, u_{ik}, represents the membership of a particular land cover class, x_k. According to Bezdek *et al.* (1984), the above partitioning can be given by the following expression.

$$M_{fc} = \left\{ U : u_{ik} \in [0,1] \; ; \; \sum_{k=1}^{n} u_{ik} > 0 \; .. i = 1 .. c \; ; \; \sum_{i=1}^{c} u_{ik} = 1 .. k = 1 ... n \right\} \tag{5.1}$$

The optimal fuzzy c-partition can be identified through the minimisation of the generalised least-squared error function as shown in Chapter 3 (Equation 3.12). The fuzzy memberships of the supervised approach of the fuzzy c-means algorithm are still a function of the weighted distance to the class means, but the algorithm no longer determines the class means through an iterative process. Thus, the supervised approach is a modification of the fuzzy c-means algorithm and the fuzzy memberships are generated using the following equation (Key *et al.*, 1989).

$$u_{ik} = \left[\left(1 / d_{ik}^{\,2} \right)^{1/(m-1)} \right] \left[1 / \sum_{j=1}^{c} \left(1 / d_{jk}^{\,2} \right)^{1/(m-1)} \right] \tag{5.2}$$

where d_{ik}^2, is the measure of dissimilarity, i.e. the squared distance between x_k and v_i, which can be calculated by Equation 3.13. From Equation 5.2, it can be seen that there are two distinct operations which need to be performed to derive the fuzzy

memberships. Firstly, the squared distance of x_k and v_i needs to be determined. For a single band case, Equation 3.13 takes the following simplified form using the Euclidean norm and a weighting exponent m equal to 2:

$$(d_{ik})^2 = (x_k - v_i)^2 \tag{5.3}$$

Finally, the fuzzy membership matrix can be generated using the Equation 5.2. Accordingly, the algorithm was written in *ARC Macro Language (AML)* in Arc/Info. The Euclidean norm and a weighting exponent (m) equal to 2 were used in the algorithm. A typical *AML* for deriving fuzzy memberships from a single band remote sensing data is shown in Appendix 3.

5.2.2.2 Implementation

The methodology for deriving the fuzzy memberships using the selected bands of Landsat-7 ETM+ of the City of Perth is shown in Figure 5.4. As shown in Figure 5.4, the selected bands of Landsat-7 ETM+ (see Table 5.2) were considered as data vectors, and the dissimilarity index, $(d_{ik})^2$, was calculated using Equation 5.3. In calculating the dissimilarity index for a particular class, all data vectors were considered, and the known mean value of the classes were used. This dissimilarity index was then used to calculate the vector, $\left(1/d_{ik}^{\,2}\right)^{1/(m-1)}$, which became the numerator of Equation 5.1 in determining the strength of membership. Similarly, all data vectors were again considered for the second, third, and following classes and the dissimilarity indexes were calculated in the same manner. Now, for a particular data vector, the expression, $\left(1/d_{ik}^{\,2}\right)^{1/(m-1)}$ for all classes considered was summed up and the newly created vector, $\sum_{j=1}^{c}\left(1/d_{jk}^{\,2}\right)^{1/(m-1)}$, (where c represents the number of classes) was stored as a separate record.

The process was repeated for all the remaining data vectors. For a particular class, the membership grade of a data vector was calculated by dividing the vector, generated by the expression $\left(1/d_{ik}^{\,2}\right)^{1/(m-1)}$, by the vector generated from the summation of the expression $\left(1/d_{ik}^{\,2}\right)^{1/(m-1)}$ i.e. $\sum_{j=1}^{c}\left(1/d_{jk}^{\,2}\right)^{1/(m-1)}$. A three decimal

place approximation of u_{ik} was chosen and accordingly, the membership grades were multiplied by 1000. The process was repeated for all the classes. Thus, each data vector (pixels of Landsat-7 ETM bands) was represented as a function of the fuzzy membership of land cover classes, and the sum of the fuzzy membership of each data vector for a location x was 1.

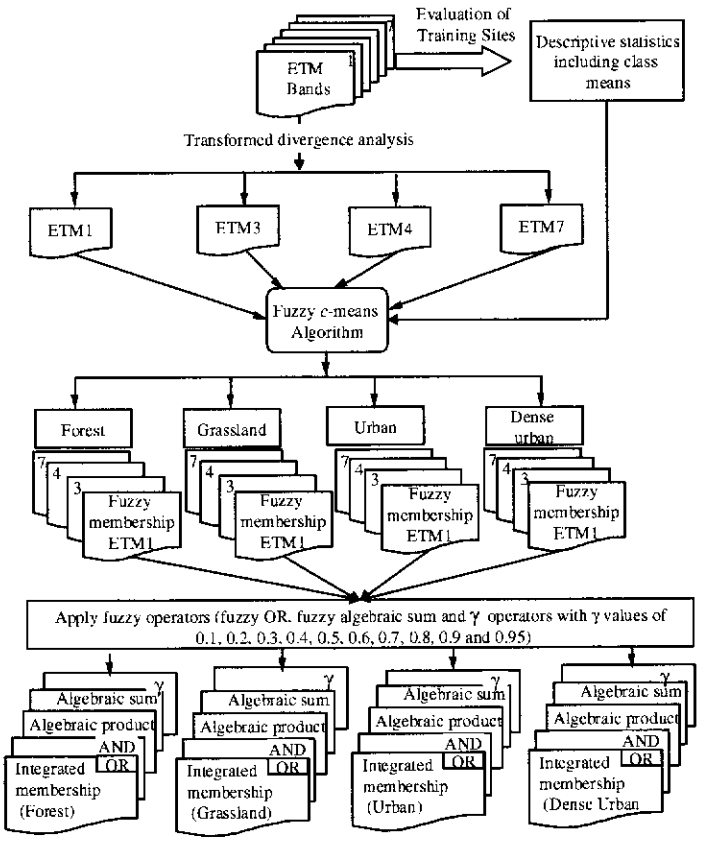

Figure 5.4 Flowchart for deriving fuzzy memberships using the selected bands of Landsat-7 ETM+ of the City of Perth

As a result, a total of 16 outputs were produced (e.g. a fuzzy layer for each of the four land cover classes in each of the four Landsat-7 ETM+ bands selected from the transformed divergence analysis) for all study areas. The fuzzy memberships of the class urban, dense urban, grassland and forest resulted from the selected bands (Table 5.3) of the City Perth, the City of Melville and the City of Armadale are shown in Appendix 4, Appendix 5 and Appendix 6, respectively. An example of the fuzzy memberships of the class urban generated using Landsat-7 ETM+ band three for each study area is shown in Figure 5.5.

5.2.3 Integration of the Fuzzy Memberships

The fuzzy memberships of the land cover classes on the selected bands of the three study areas were integrated using the fuzzy minimum, maximum, fuzzy algebraic product, fuzzy algebraic sum and fuzzy gamma operators as described in Section 3.4.3.

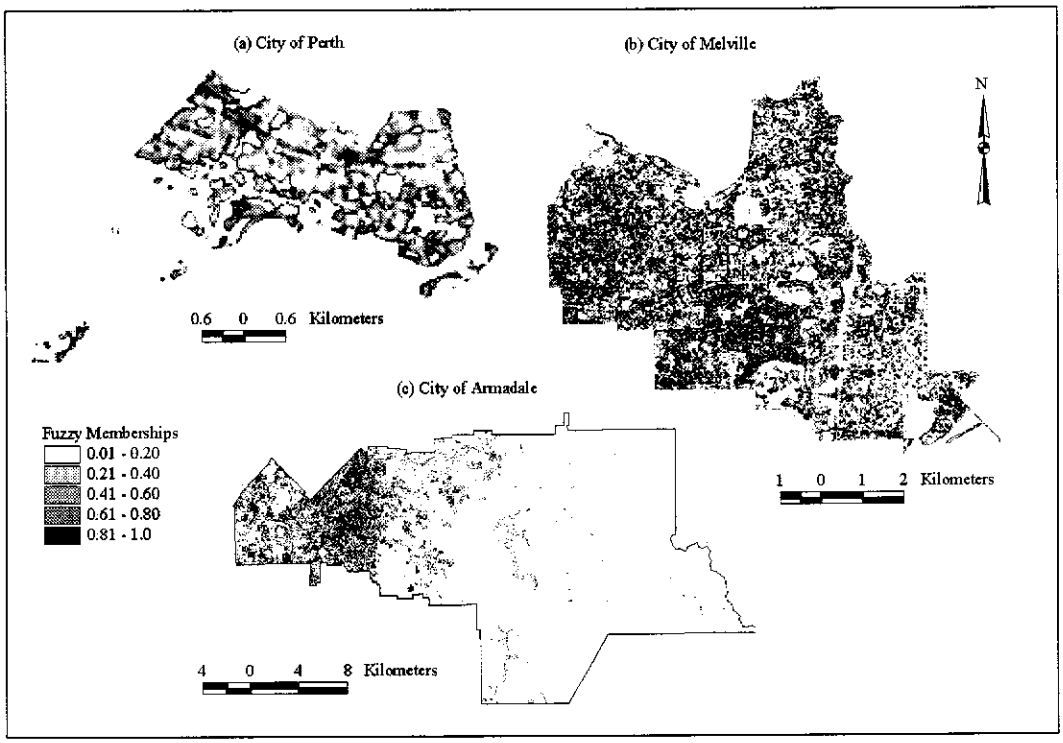

Figure 5.5 Fuzzy memberships of class urban, resulting from applying fuzzy *c*-means algorithm on Landsat-7 ETM+ band 3 over the study areas

Several γ values (0.1, 0.2, 0.3, 0.4, 0.5, 0.6, 0.7, 0.8, 0.9 and 0.95) were tested on the fuzzy gamma operator for all land cover classes considered. Various map algebra functions (e.g. *MAX*, *MIN*, *ADD*, *SUBSTRACT*, *MULTIPLY DIVIDE*, *POW*) available in GRID module of Arc/Info (ESRI, 2000) were used to implement Equations 3.23 to 3.27 (Chapter 3) for integrating the fuzzy memberships from the selected bands. To this end, the fuzzy memberships derived from the Landsat-7 ETM+ bands 1, 3, 4 and 7 for the City of Perth, bands 1, 2, 3, and 7 for the City of Melville, and bands 1, 3, 4, 5, and 7 for the City of Armadale were integrated. Accordingly, four fuzzy membership maps representing the four land cover classes were obtained for each fuzzy operator for all study areas. The integrated fuzzy memberships obtained for each land cover class using the fuzzy operators mentioned

above are shown in Appendix 7 for the City of Perth, Appendix 8 for the City of Melville and Appendix 9 for the City of Armadale. An example of the integrated fuzzy memberships produced using the fuzzy algebraic sum of the class urban over the study areas is shown in Figure 5.6.

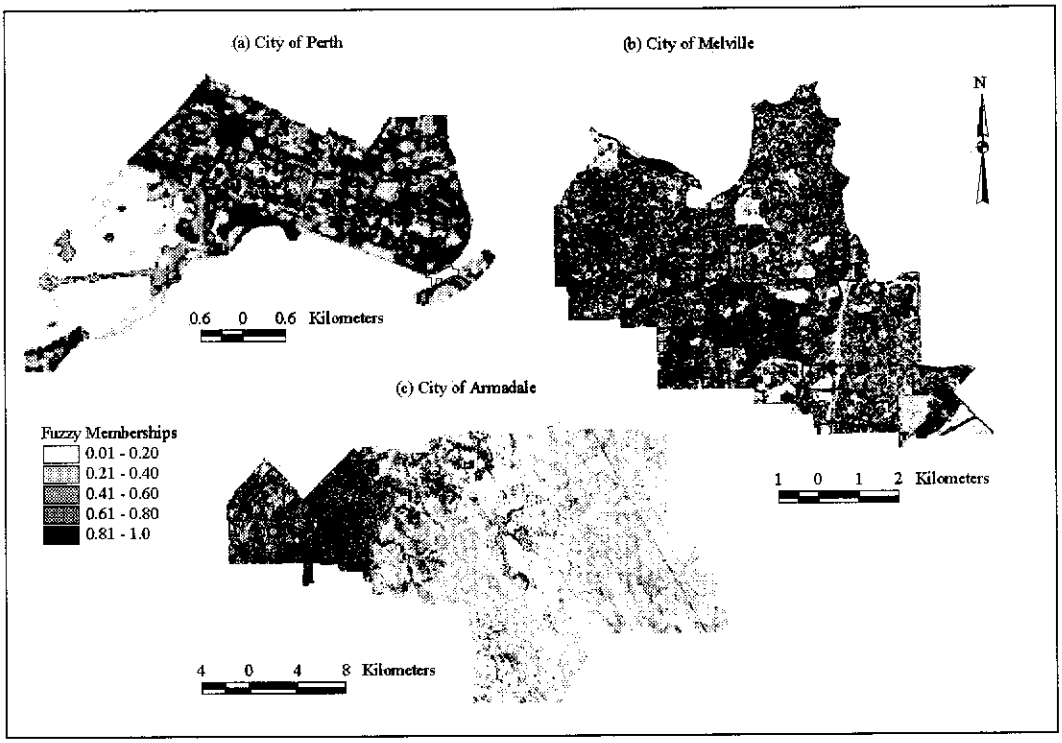

Figure 5.6 Integrated fuzzy memberships (e.g. fuzzy categorical map) for the class urban using fuzzy algebraic sum over the study areas

5. 3 Accuracy Assessment of Fuzzy Classification

The methodology of accuracy assessment of fuzzy classification comprised four major steps: (i) derivation of the fuzzy membership of the reference data; (ii) defuzzification of the fuzzy memberships of the classified data; (iii) construction and accuracy measures of the fuzzy error matrix; and (iv) generation of uncertainty maps.

5.3.1 Derivation of the Fuzzy Memberships of the Reference Data

In assigning membership of the reference data, a virtual field reference database (VFRDB) was developed as described in Section 3.4.4.1. The field data collection includes selection of samples followed by field visits and the assignment of membership values using the linguistic values presented in Table 3.1. In order to implement the sampling technique, the remote sensing data (e.g. Landsat-7 ETM+)

of the three study areas was converted into grids using the *IMAGEGRID* command of ARC module of Arc/Info (ESRI, 2000). Typically, *IMAGEGRID* converted Landsat-7 ETM+ bands into an equal number of grids. Then, using the grid, the easting and northing of each cell centre was generated. This was implemented using the *SAMPLE* command of GRID module of Arc/Info, which creates an ASCII file listing the northing and easting of all cell centres of the grid representing the study areas.

Using the ASCII file containing the northing and easting of all cell centres, a simple random sampling was carried out. Subsequently, the northing and easting of randomly selected points, Arc/Info point coverage was generated. The purpose of creating Arc/Info point coverage was twofold: firstly, to see the location and distribution of the sample points over the study area, secondly, to prepare optimal daily routes for maximising the number of sites to be visited in a day. The *GENERATE* command of the ARC module of Arc/Info was used to create Arc/Info coverages of easting and northing of the selected sample points. The location and distribution of the selected sample points over the three study areas, which were intended to visit, is shown in Figures 5.7. Locational based accuracy assessment was chosen and individual pixels were considered as the sampling unit (Janssen and van der Wel, 1994).

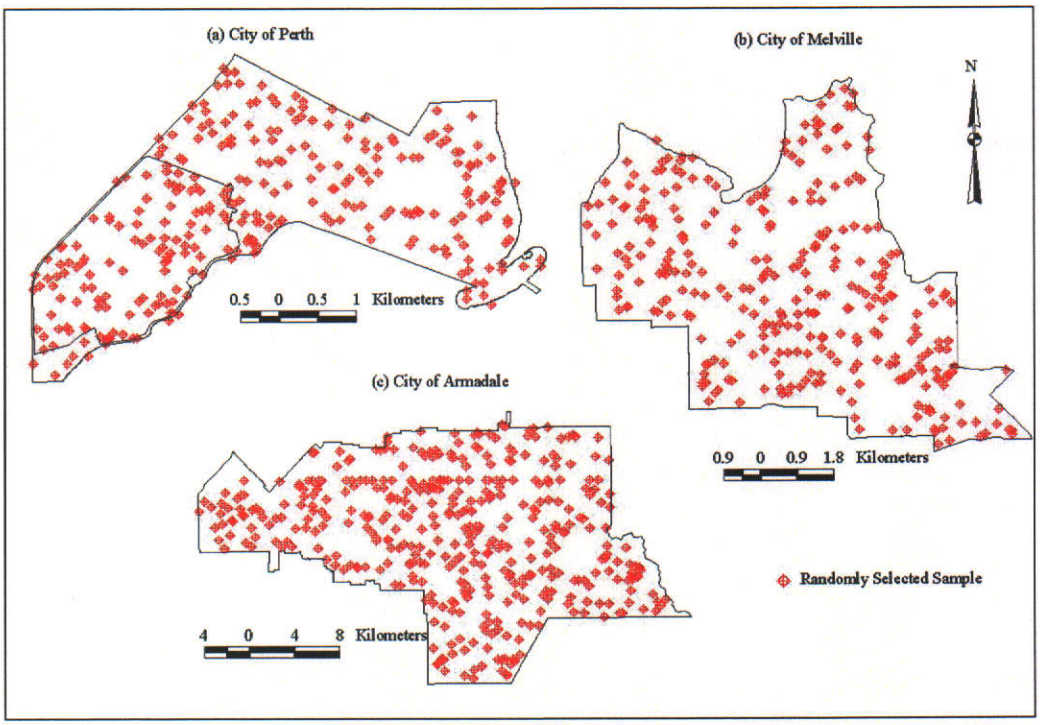

Figure 5.7 The distribution of the randomly selected samples over the study areas

The land cover compositions of each field sample of the virtual field reference database were evaluated using the 10 points linguistic scale ranging from 'absolutely right' (10) to 'totally unacceptable' (1) as described in Section 3.4.4.1.3. The field observations of each sample point were further analysed using the compositions of the land covers surrounding the pixel indicated in the digital photograph. Based on the linguistic scale and the land cover compositions indicated in the photograph, a fuzzy membership was assigned to each sample point. The fuzzy memberships of all sample points are presented in a matrix form (Appendix 10).

5.3.2 Defuzzification of the Fuzzy Categorical Maps

Defuzzification was applied to obtain a single value (fuzzy) by assigning a particular location to only one of the predefined classes. A typical defuzzification assigns pixels to the classes at which they have the maximum memberships (Zhang and Goodchild, 2002). As described in Section 3.4.4.2, the fuzzy categorical maps of each fuzzy operator for the three study areas were defuzzified to generate fuzzy land cover maps. This was done using the map-algebra functions (e.g. *MAX*, *ADD*, *SUBSTRACT*) of GRID module of Arc/Info (ESRI, 2000). Figure 5.8 shows the steps that were involved in defuzzification of the fuzzy categorical maps.

Following the methodology, fuzzy land cover maps were generated for each fuzzy operator over the three study areas, which are presented in Appendix 11 for the City of Perth, Appendix 12 for the City of Melville and Appendix 13 for the City of Armadale.

5.3.2.1 Converting Fuzzy Memberships of the Field Reference Data to Grids

The fuzzy memberships of the field reference data were categorised into their respective land cover classes. The easting and northing of the sample sites of each land cover class were used to generate Arc/Info point coverage. Then, the coverage of each land cover representing the field data was converted into a grid with a cell size of 25 x 25 m. This was done using the *POINTGRID* command of ARC module of Arc/Info. *POINTGRID* converts data associated with point features to a GRID cell format and each cell in the grid is assigned to a value according to the point(s) it overlays. Following the methodology, a grid coverage was generated for each land

cover type and these were used to determine the accuracy measures using the fuzzy error matrix. The main steps that are involved in generating the grid coverage using the field data are shown in Figure 5.9.

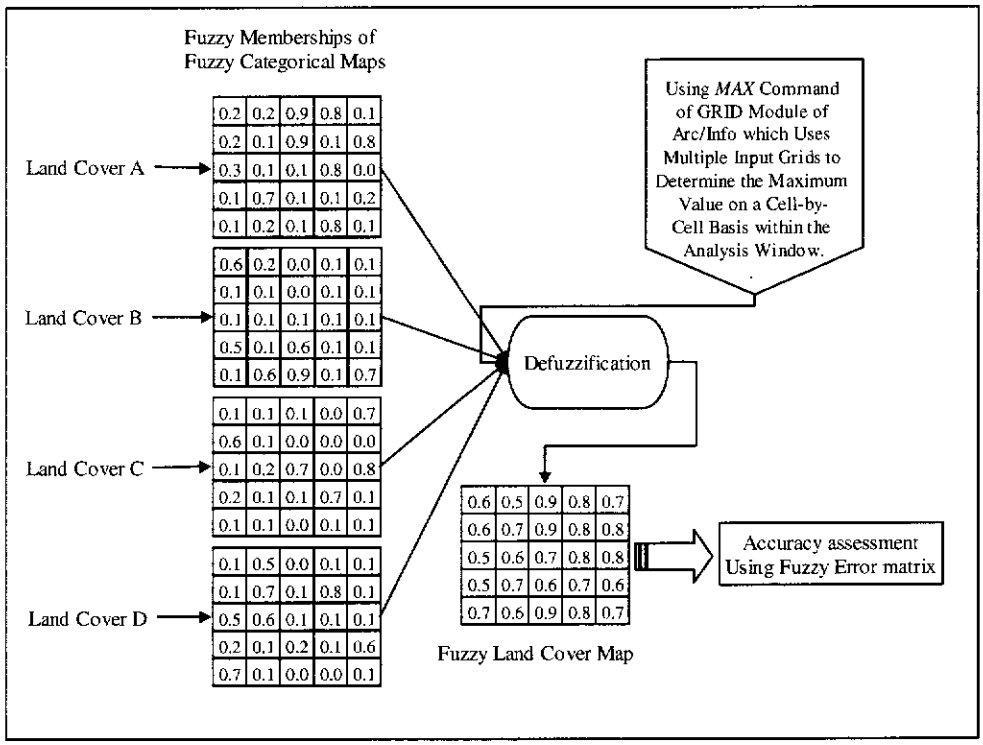

Figure 5.8 Defuzzification of the fuzzy memberships of a fuzzy categorical map for generating fuzzy land cover map

5.3.3 Accuracy Measures using the Fuzzy Error Matrix

The fuzzy land cover maps and the fuzzy field reference data were used to compute the elements of fuzzy error matrix. For each fuzzy operator, the fuzzy membership output represents the most likely land cover classes, which were cross tabulated with the fuzzy membership grids of the reference data. The *MINIMUM* operator (Zadeh, 1977) was used in cross tabulating the fuzzy land cover maps and the fuzzy reference data as described in Section 3.4.4.3. An *AML* (*Arc Macro Language*) was implemented for generating the elements of the fuzzy error matrix. Using the elements of error matrix, the fuzzy overall classification accuracy, fuzzy producer's accuracy and fuzzy user's accuracy were determined using the methodology described in Section 3.4.4.4. The accuracy measures for each fuzzy operator are presented in Appendix 14, Appendix 15, and Appendix 16 for the City of Perth, the City of Melville and the City of Armadale, respectively.

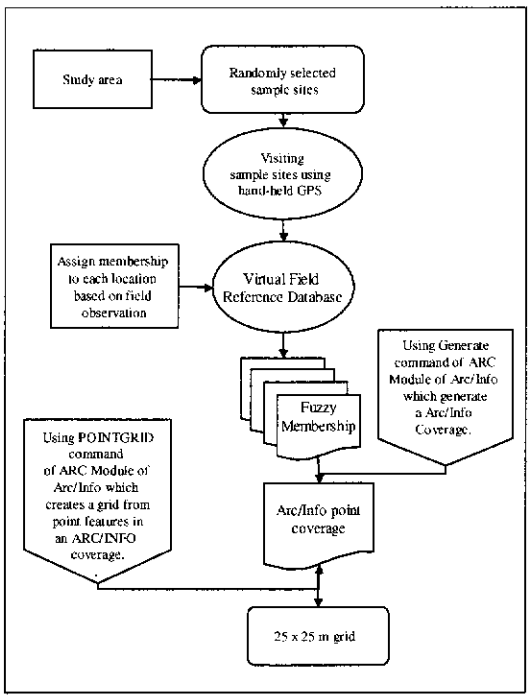

Figure 5.9 Generation of grids using the fuzzy membership of the field reference data

5.3.4 Uncertainty Maps

In order to visualise the spatial distribution of uncertainty, a fuzzy confusion index (see Section 3.4.4.5) was computed, and uncertainty maps were generated for each fuzzy operator using the fuzzy categorical maps. The *MAX* command available in GRID module of Arc/Info (ESRI, 2000) was used to generate the fuzzy land cover maps of the most likely class using the fuzzy categorical maps, as shown in Figure 5.10. Subsequently, the first maximum memberships were excluded from the fuzzy categorical maps. Thus, these outputs contain all the fuzzy memberships, except the maximum fuzzy memberships of the fuzzy categorical maps (Figure 5.10). Likewise, the *MAX* command was used to generate fuzzy land cover maps of the second most likely class for each location. The first and second fuzzy land cover maps containing the first maximum and the second maximum memberships respectively were used for generating the uncertainty map (confusion index map) for each fuzzy operator using Equation 3.33 (Chapter 3). The grid algebra function of Arc/Info was used to implement Equation 3.33. The uncertainty maps for each fuzzy operator of the study areas are shown in Appendix 17 for the City of Perth, Appendix 18 for the City of Melville and Appendix 19 for the City of Armadale. An example

of uncertainty maps generated using the fuzzy categorical maps produced by the fuzzy gamma operator ($\gamma = 0.95$) of the study areas is shown in Figure 5.11.

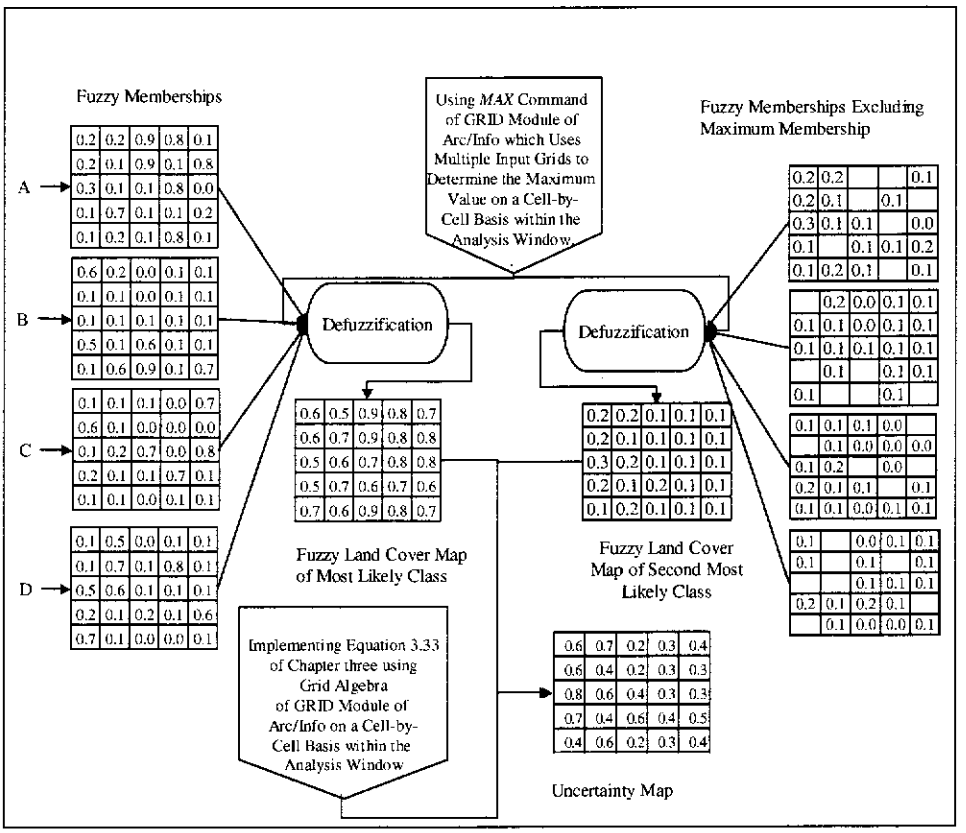

Figure 5.10 An example showing the generation of uncertainty maps

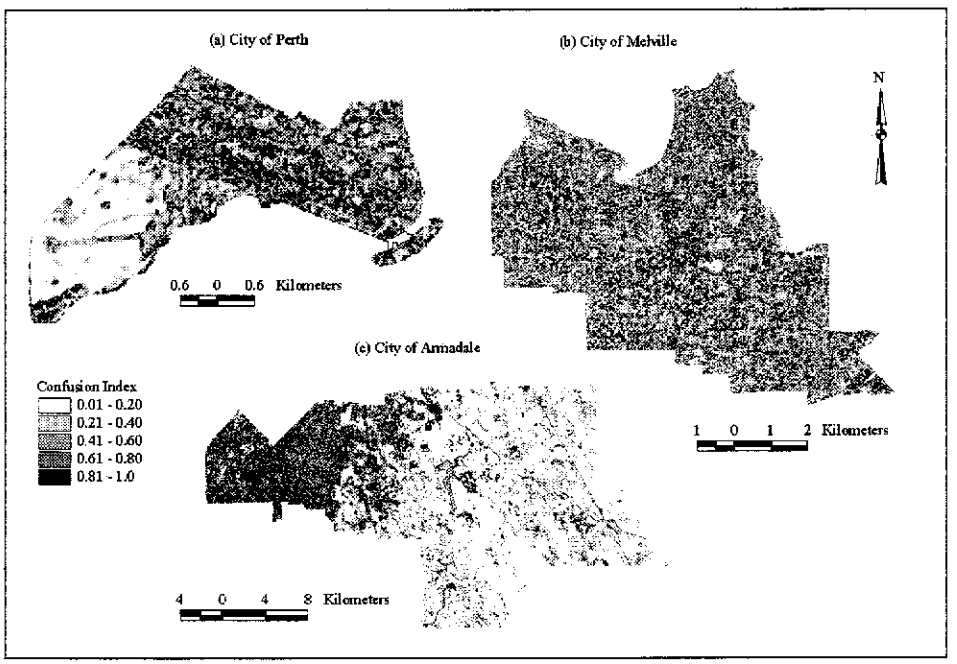

Figure 5.11 Uncertainty maps generated using the fuzzy categorical maps of the fuzzy gamma operator ($\gamma = 0.95$) over the study areas

5. 4 Summary

This chapter described the implementation of the method for determining the spatial complexity of three study areas representing dense urban, medium urban and urban fringe of the PMA using SPOT, Landsat-7 ETM+ and Landsat MSS data. The methods based on fuzzy set theory for deriving fuzzy categorical maps using Landsat-7 ETM+ and their accuracy assessment were then described.

The Image Characterisation Module of ICAMS was used to compute Moran's *I*, a measure of spatial autocorrelation. Various step sizes (e.g. five and six) were applied in the subsets of the study areas for determining the fractal dimension using the isarithm and the TPSA algorithms. In the isarithm algorithm, the row, column and row-column methods were used for computing the fractal dimension. Accordingly, Moran's *I* and the fractal dimension of the study areas using the selected bands of SPOT, Landsat-7 ETM+ and Landsat MSS were generated. The results were categorised to address: (i) how the spatial complexity varies with changes in the land cover compositions of the study areas; (ii) how the spectral and spatial resolution affect the spatial complexity of urban landscapes and (iii) the relationship between the *D*, an index of spatial complexity and Moran's *I*, a measure of autocorrelation. Furthermore, the performance of the fractal measurement algorithms such as the isarithm and the TPSA on the determination of the *D* of urban land cover types was addressed. The analyses of these enquiries including how spatial complexity can be useful in determining the appropriateness of a sensor data for determining the scale at which processes occur in the PMA using the *D* are discussed in Chapter 6.

The supervised approach of the fuzzy *c*-means algorithm was implemented to map the major land cover classes of the study areas using Landsat-7 ETM+. In implementing the fuzzy *c*-means algorithm, first, representative training sites of four representative land cover classes were analysed selecting the best band combinations of the Landsat-7 ETM+ based on spectral separability among the land cover classes. In addition, descriptive statistics of the land cover classes were generated which were used in the implementation of fuzzy *c*-means algorithm for deriving the fuzzy memberships from the selected Landsat-7 ETM+ bands. Various fuzzy operators (e.g. minimum, maximum, algebraic product, algebraic sum and fuzzy gamma) were used for integrating the fuzzy memberships of the four land cover classes computed

on each of the selected bands. Accordingly, each fuzzy operator produced an integrated fuzzy membership for each of the predetermined land cover classes. The performances of each of the fuzzy operators were assessed carrying out a fuzzy accuracy assessment analysis.

Randomly selected field samples were collected and stored in a VFRDB. The land cover composition of each field sample was assessed using a ten-point linguistic scale, and the fuzzy memberships of the reference data were derived as a result. The technique of defuzzification was applied to the fuzzy memberships of the fuzzy categorical maps and accordingly, the fuzzy land cover maps for each fuzzy operator were generated. These outputs were used in a fuzzy error matrix and the accuracy assessment was carried out. In addition, the uncertainty maps using the fuzzy memberships of the fuzzy categorical maps were generated to examine the distribution of misclassification over the study areas.

The accuracy analysis of the fuzzy categorical maps using the fuzzy error matrix resulted in (i) the accuracy of the fuzzy land cover maps generated from each of the fuzzy operators; (ii) the accuracy measures of the individual classes indicating the source of misclassification; and (iii) distribution of the misclassification associated with the fuzzy land cover maps over the study areas. These results provided the best fuzzy operator for generating the fuzzy categorical maps for each of the study areas. In addition, the effect of heterogeneity of land cover compositions of the major land cover classes was assessed using the accuracy measures of the fuzzy land cover maps. The analyses and the discussions are presented in Chapter 7.

Chapter 6

SPATIAL COMPLEXITY OF URBAN LANDSCAPES DERIVED FROM MULTISCALE AND MULTISOURCE REMOTE SENSING DATA

This chapter presents the analysis of spatial complexity of the study areas computed from SPOT, Landsat-7 ETM+, and Landsat MSS using fractal measurement algorithms and a spatial autocorrelation measure (Moran's *I*). Based on the hypotheses, the analyses of (i) how the spectral and spatial resolution affect the analysis of spatial complexity of urban landscapes; and (ii) how the spatial complexity varies in changing the land cover compositions of the study areas are presented. The parameters and the performance of different fractal measurement algorithms in measuring the spatial complexity are discussed. Finally, the selection of an appropriate sensor data for the interpretation of land cover classes based on fractal analysis is discussed.

6. 1 Characterisation of the Spatial Complexity

As mentioned in earlier chapters, the spatial complexity measured from multiscale remote sensing data can be used in selecting an appropriate scale at which the processes of urban landscapes are operating. Accordingly, fractal measurement algorithms such as the TPSA and the isarithm described in Section 3.3.2 were applied to SPOT, Landsat-7 ETM+, and Landsat MSS data to various subsets of three study areas comprised of different land cover compositions (see Chapter 4 for details). In the isarithm algorithm, three methods namely row, column and row-column methods were applied to determine the fractal dimension. As reported in the literature, the fractal dimension computed from the row and column methods suffer from directional bias (Lam, 1990; Lam and De Cola, 1993; Quattrochi *et al.*, 2001) and thus, only the results of the row-column method were used in the analysis. The analysis of spatial complexity for each study area comprised the following steps:

(a) Assess the effect of the spectral and spatial resolutions of various sensor data on the spatial complexity of urban landscapes. This includes analysing the

effect of spectral, spatial resolutions and land cover types on different fractal measurement algorithms;

(b) Assess the performance of the fractal measurement algorithms on the measurement of the spatial complexity;

(c) Evaluate the correlation between fractal dimension (seen as an index of spatial complexity) and spatial statistical measures of data variability (e.g. spatial autocorrelation) on the different urban land covers.

The land cover pattern of the City of Perth is spatially more complex than the land cover patterns of the City of Melville and the City of Armadale, which vary from spatially heterogeneous to a more homogeneous pattern. A synopsis of the analysis is shown in Figure 6.1, and the following sections provide a description of the analyses results obtained for three study areas.

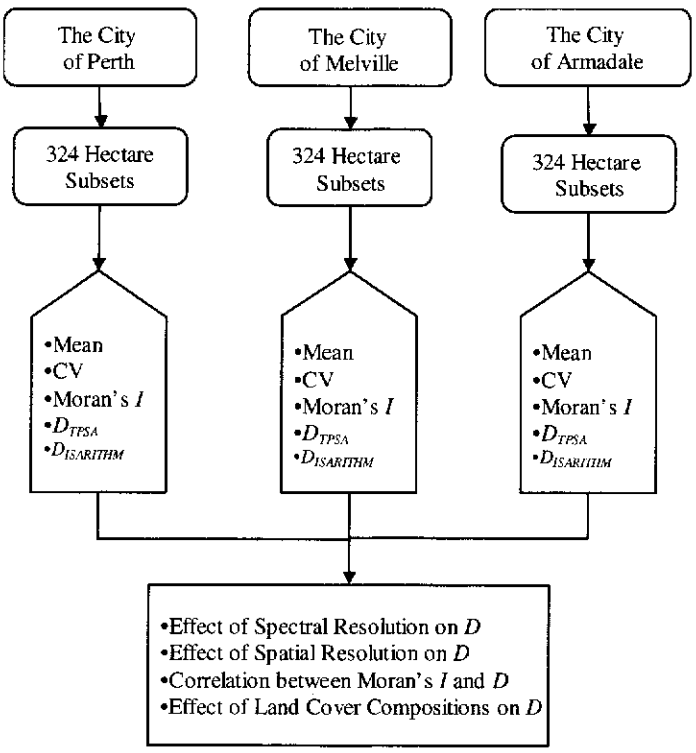

Figure 6.1 Summary of analyses performed in the subsets of the study areas

6.1.1 The City of Perth

As described in Chapter 4, subsets comprised of 324 hectares of SPOT, Landsat-7 ETM+ and Landsat MSS along the transects of the study areas were used in the analysis. The City of Perth contains the central business district and adjacent

commercial/residential areas. A field survey and an analysis of aerial photographs of the subsets of the City of Perth revealed the following land cover compositions.

(a) Subset one represents most of the commercial and business area of Perth central city. The land uses of this area are characterised by large commercial buildings, office buildings, shopping complexes, freeways, major roads and open parks (Figure 6.2b).

(b) A portion of the business area of the central city mostly occupied with office buildings along with freeways, major roads, grassland and residential area is included in subset two (Figure 6.2c).

(c) The land uses of subset three are dominated by residential areas parkland. In addition, the north-west portion of this subset comprises commercial and business area occupied by office buildings, shopping area and a railway station (Figure 6.2d).

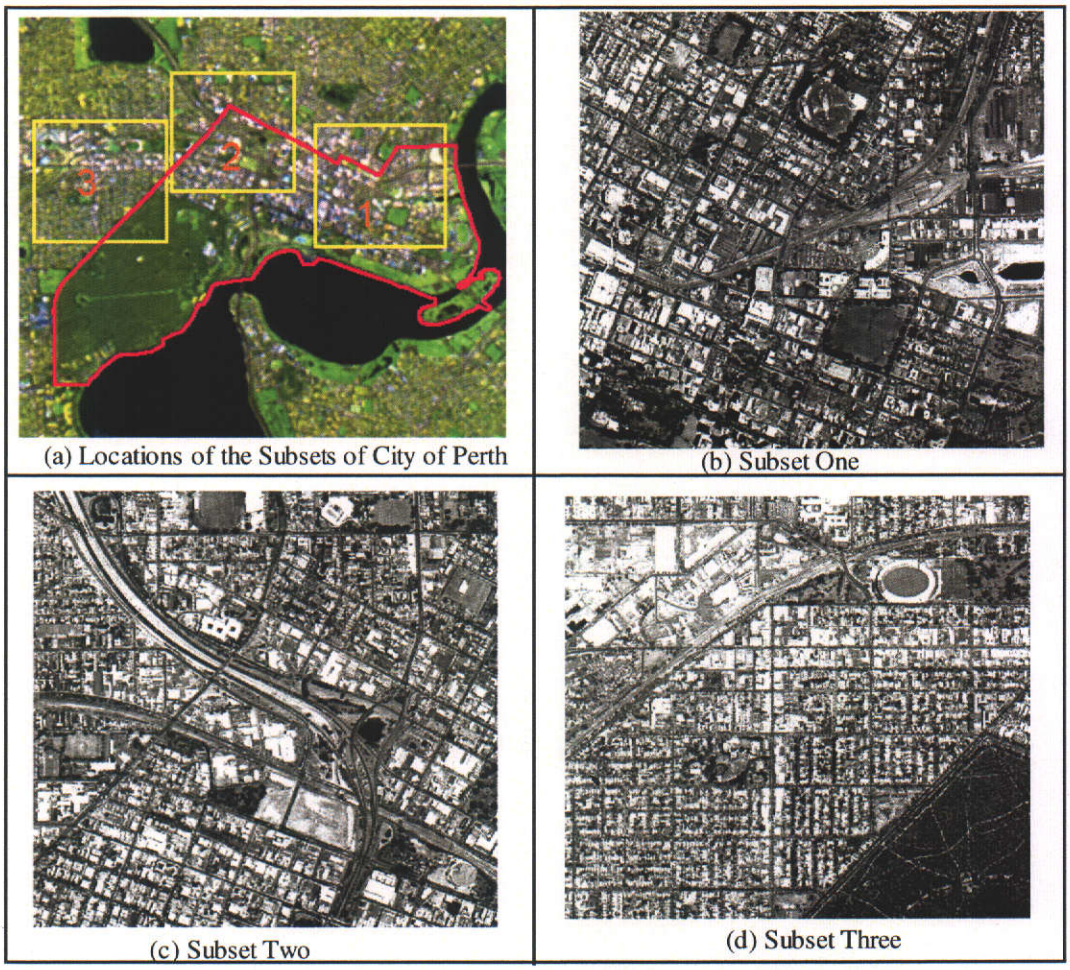

(a) Locations of the Subsets of City of Perth

(b) Subset One

(c) Subset Two

(d) Subset Three

Figure 6.2 Land cover compositions of the subsets of the City of Perth

The fractal dimension of SPOT, Landsat-7 ETM+, and Landsat MSS bands using the TPSA (D_{TPSA}) and the isarithm ($D_{ISARITHM}$) algorithms were computed on the three subsets of the City of Perth. According to the hypotheses described in Chapter 1, the fractal dimension of the selected bands (green, red and NIR) of SPOT, Landsat-7 ETM+ and Landsat MSS were selected for the analysis. In addition to fractal dimension, the Moran's *I* index of spatial autocorrelation, descriptive statistics of the subsets, which include minimum, maximum, mean, standard deviation and coefficient of variation of each subset were generated.

The results in Table 6.1 indicate that the D_{TPSA} and $D_{ISARITHM}$ are the highest in the ETM+ green, red and NIR bands of subset one, as compared to subsets two and three. As the *D* variation over the three subsets is consistent regardless of the spectral range, it is assumed that the changes in *D* are a result of the change in land cover compositions. According to the concept of the fractal theory, the higher the fractal dimension, the higher the spatial complexity. This implies that subset one of the City of Perth is spatially more complex than subsets two and three.

Table 6.1 Fractal dimension computed from the isarithm and the TPSA algorithm of the City of Perth

		Subset 1		Subset 2		Subset 3	
Sensor	Band	$D_{ISARITHM}$	D_{TPSA}	$D_{ISARITHM}$	D_{TPSA}	$D_{ISARITHM}$	D_{TPSA}
SPOT (20 m)	Green	2.98	2.89	2.91	2.93	2.96	2.92
	Red	2.94	2.88	2.89	2.88	2.93	2.88
	NIR	2.87	2.89	2.98	2.88	2.90	2.91
Landsat-7 ETM+ (25 m)	Green	2.88	2.94	2.85	2.81	2.79	2.84
	Red	2.87	2.97	2.87	2.81	2.82	2.86
	NIR	2.80	2.84	2.75	2.75	2.85	2.70
Landsat MSS (50 m)	Green	2.78	2.82	2.80	2.81	2.70	2.76
	Red	2.88	2.78	2.79	2.78	2.72	2.71

Statistical comparisons between the D_{TPSA} and the $D_{ISARITHM}$ of the subsets were carried out to determine whether these subsets are differentiable using the fractal dimension, an index of spatial complexity. Accordingly, a *t*-test with a 0.05 significance level and *p*-values were used to test the null (H_0: $\mu_1 = \mu_1$) and alternative (H_a: $\mu_1 \neq \mu_1$) hypotheses for examining whether the spatial complexity of the subsets is statistically different from each other.

Table 6.2 summarises the t and corresponding p-values resulting from the t-tests undertaken using the D_{TPSA} and the $D_{ISARITHM}$ of all Landsat-7 ETM+ bands between subsets one and two, subsets one and three and subsets two and three. The results of the paired t-test of subsets one and two and subsets one and three reveal a statistically significant difference between the D_{TPSA} values of these two subsets, whereas the spatial complexity of subset two and three was not found significantly different, as expressed by D (Table 6.2). These results are explained by the differences in the degree of homogeneity of land cover of the individual subsets, which in turn is a result of differences in the degree of fragmentation of the land cover composition types present in each subset. An examination of the land uses indicates that subset one is spatially more complex as the land uses are characterised by large commercial buildings, shopping complexes along with freeways, major roads, grassland and open parks compared to similar but relatively less heterogeneous land uses in subsets two and three. This can be seen in a graphic representation of the land uses extracted from aerial photos in Figure 6.2. The results of the paired t-test between the $D_{ISARITHM}$ values of the subsets one and three contradict with the results of the D_{TPSA} (Table 6.2) which could be attributed to the methodological approach as explained in Section 3.3.2. A further explanation of the effect of the D computed from the TPSA and the isarithm method is discussed in the following section.

Table 6.2 t-significance test among the subsets of the City of Perth using the D_{TPSA} and $D_{ISARITHM}$ of Landsat-7 ETM+ bands

	Subsets	1	2	3
D_{TPSA}	1		$t = 12.60, p=0.00006$*	$t = 7.23, p=0.0008$*
	2			$t = 1.51, p=0.19$
$D_{ISARITHM}$	1		$t = 4.2968, p=0.00774$*	$t = 0.52992, p=0.18659$
	2			$t = -0.557, p=0.60101$

* Statistically significant

Variations measured as standard deviations were used to describe the differences in degree of spectral homogeneity of the land covers of the individual subsets. The results showed that subset one has the highest absolute variation of pixel values centred on its mean in the green, red and NIR bands, whereas subsets two and three showed less variation (Table 6.3). The mean coefficient of variation (CV) which is a non-spatial index summarising the variations of the pixel values regardless of their locations showed relatively high in subsets one and there as compared to subset two.

The higher coefficient of variation indicates that the land covers of all subsets are spectrally heterogeneous.

Table 6.3 Summary statistics of Landsat-7 ETM+ of the subsets of the City of Perth

	Band	Minimum	Maximum	Mean	Standard Deviation	Coefficient of Variation
Subset One	Green	66	244	119.83	30.29	0.253
	Red	58	255	132.81	36.75	0.277
	NIR	35	164	76.63	17.82	0.233
Subset Two	Green	60	255	111.8	26.93	0.241
	Red	48	255	123.47	31.82	0.258
	NIR	32	186	75.91	16.01	0.211
Subset Three	Green	59	255	103.83	27.01	0.260
	Red	51	255	113.16	33.89	0.299
	NIR	45	179	80.18	14	0.175

The D_{TPSA} and the $D_{ISARITHM}$ computed from the SPOT image revealed a small variation of the D among the subsets (Table 6.1), indicating an insignificant variation of the spatial complexity. Using a significance level of 0.05, paired t-tests of the D_{TPSA} and the $D_{ISARITHM}$ among subsets one and two, subsets one and three and subsets two and three revealed that the spatial complexity among the subsets is not significantly different (Table 6.4). This can be attributed to variations in the land cover heterogeneity of subset one of the SPOT image. The land uses of subset one changed substantially over the years as the SPOT data was acquired in December 1991 when the proportion of vegetation was higher than built-up areas in subset one (Figure 6.3), compared to the acquisition of the Landsat-7 ETM+ scene in 2001, characterised by a higher percentage of built up areas (residential and commercial). Subset one became more heterogeneous over time, which contributed to a higher D_{TPSA} in the ETM+ bands, and thus an increased differentiation amongst the D values of subset one and subsets two and three (Table 6.2). The higher $D_{ISARITHM}$ of the subset one despite spatially less heterogeneous land covers could be attributed to the methodological approach of the isarithm method.

The standard deviations of the subsets of SPOT image in Table 6.5 shows that subset one has the least absolute variation of pixel values as compared to subsets two and

three. Likewise, the coefficient of variation of subset one appears to be low as compared to subsets two and three (Table 6.5). This indicates that the land cover of subset one is portrayed as spectrally less heterogeneous in the SPOT imagery. The lower coefficient of variation and the relatively lower fractal dimension of subset one compared to subsets two and three appears to indicate that the land covers are spatially less heterogeneous.

Table 6.4 *t*-significance test among the subsets of the City of Perth using the D_{TPSA} and $D_{ISARITHM}$ of SPOT bands

	Subsets 1	2	3
D_{TPSA}	1	t = -0.778, p=0.5178	t = -2.413, p=0.137
	2		t = -0.4629, p=0.6888
$D_{ISARITHM}$	1	t = 0.01694, p=0.988	t = 0.07478, p=0.94719
	2		t = 0.00233, p=0.99875

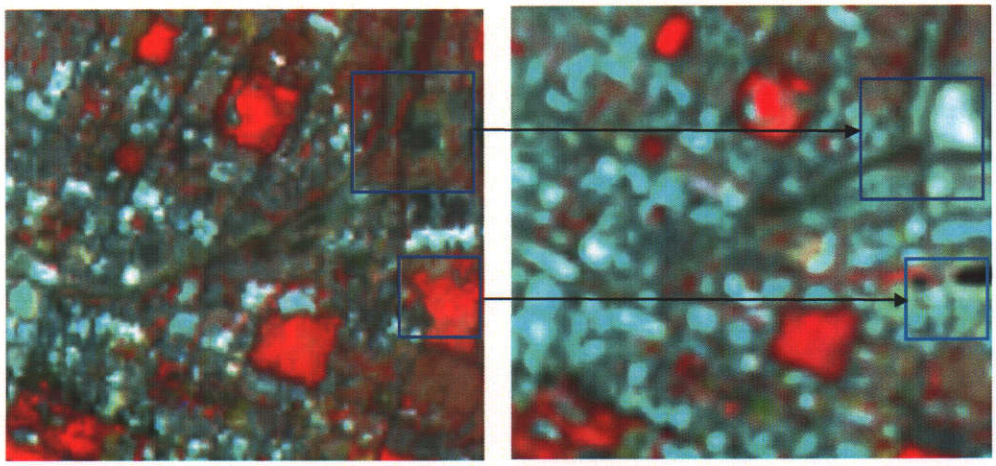

False Color Composite of SPOT (NIR, Red, Green)

False Color Composite of Landsat- 7 ETM+ (NIR, Red, Green)

Figure 6.3 Changes in land cover compositions from 1991 to 2001 in subset one of the City of Perth

Likewise, the results of the green and red bands of Landsat MSS indicate that the D_{TPSA} and $D_{ISARITHM}$ are relatively higher in subsets one and two, as compared to subset three (Table 6.1). This is to be expected as the land covers of subset three in MSS, which was acquired in December 1980, showed more homogeneous as compared to subsets one and two. The results of the paired *t*-test of the D_{TPSA} and $D_{ISARITHM}$ using a significance level of 0.05 showed that the spatial complexity of subsets one and two, subsets one and three and subsets two and three are not statistically significant, as expressed by D (Table 6.6).

The standard deviation measured as the variation from the mean of all pixels was found to be low, as compared to Landsat-7 ETM+ and SPOT (Table 6.7). This could be due to a lower degree of spectrally heterogeneous land covers in the subsets of Landsat MSS. A similar CV among the subsets indicates that the MSS sensor records the land covers of the subsets as similar in terms of spectral heterogeneity.

Table 6.5 Summary statistics of SPOT of the subsets of the City of Perth

	Band	Minimum	Maximum	Mean	Standard Deviation	Coefficient of Variation
Subset One	Green	57	211	93.02	21.72	0.233
	Red	44	213	89.26	22.22	0.249
	NIR	53	162	90.73	19.93	0.220
Subset Two	Green	57	231	94.11	26.79	0.285
	Red	45	228	90.37	26.98	0.299
	NIR	43	177	93.11	21.57	0.232
Subset Three	Green	51	205	83.47	23.1	0.277
	Red	41	192	78.74	23.75	0.302
	NIR	60	176	94.46	16.91	0.179

Table 6.6 *t*-significance test among the subsets of the City of Perth using the D_{TPSA} and $D_{ISARITHM}$ of Landsat MSS bands

	Subsets	1	2	3
D_{TPSA}	1		$t = 1.7354$, p=0.181073	$t = 1.832$, p=0.1643
	2			$t = 0.0798$, p=0.94136
$D_{ISARITHM}$	1		$t = 2.07193$, p=0.13002	$t = 0.8918$, p=0.15482
	2			$t = 0.91260$, p=0.4287

Table 6.7 Summary statistics of Landsat MSS of the subsets of the City of Perth

	Band	Minimum	Maximum	Mean	Standard Deviation	Coefficient of Variation
Subset One	Green	28	75	59.3	12.11	0.204
	Red	60	142	86.63	18.02	0.208
Subset Two	Green	44	100	61.7	10.41	0.169
	Red	50	199	83.65	21.11	0.252
Subset Three	Green	34	92	56.09	11.31	0.202
	Red	37	159	76.33	18.20	0.238

6.1.2 The City of Melville

The City of Melville represents 'medium urban' and it is mostly comprised of residential areas (see Figure 4.6b-1 and 4.6b-2). Four subsets were selected along the transects of the study area (Figure 6.4) which are characterised by the following land uses:

(a) Subset one is largely comprised of residential areas, surrounded by sparse vegetation and grassland (Figure 6.4b);
(b) The land covers of subset two are characterised by shopping complexes along with major roads, open parks and residential areas (Figure 6.4c);
(c) The land covers of subset three are mostly comprised of residential areas, characterised by houses with different types of roof tiles. In addition, there are major and minor roads, some native vegetation and grassland (Figure 6.4d); and
(d) Subset four is mostly comprised of residential area, surrounded by sparse vegetation, native forest, a golf club and bare ground (Figure 6.4e).

The fractal dimensions of the green, red and NIR bands of SPOT, Landsat-7 ETM+ and Landsat MSS of the subsets of the City of Melville using the TPSA and the isarithm algorithms are presented in Table 6.8. The variations of the D_{TPSA} and $D_{ISARITHM}$ over the subsets regardless of the spectral range of the sensor substantiate the hypothesis that the changes in D are a result of changes in land cover complexity. An examination of the D values shows that the variations of the D_{TPSA} among the subsets is more pronounced than the variations of the $D_{ISARITHM}$. Table 6.8 shows that subsets two and three registered higher D_{TPSA} particularly in the green and red bands as compared to subsets one and four, indicating spatially a more complex land cover pattern. In contrast to the D_{TPSA}, $D_{ISARITHM}$ indicates that the land cover pattern of subsets one and two are spatially more complex than subsets three and four (Table 6.8).

Table 6.9 summarises the t values and corresponding p-values from a series of pair-wise t-test undertaken between the subsets of the City of Melville using the D_{TPSA} and $D_{ISARITHM}$ of Landsat-7 ETM+ bands with a 0.05 significance level. The results show that the differences in spatial complexity measured from the TPSA method between subsets one and two, subsets one and three and subsets one and four are

statistically significant. In contrast, the differences in spatial complexity measured from the isarithm method between subsets one and three are statistically significant.

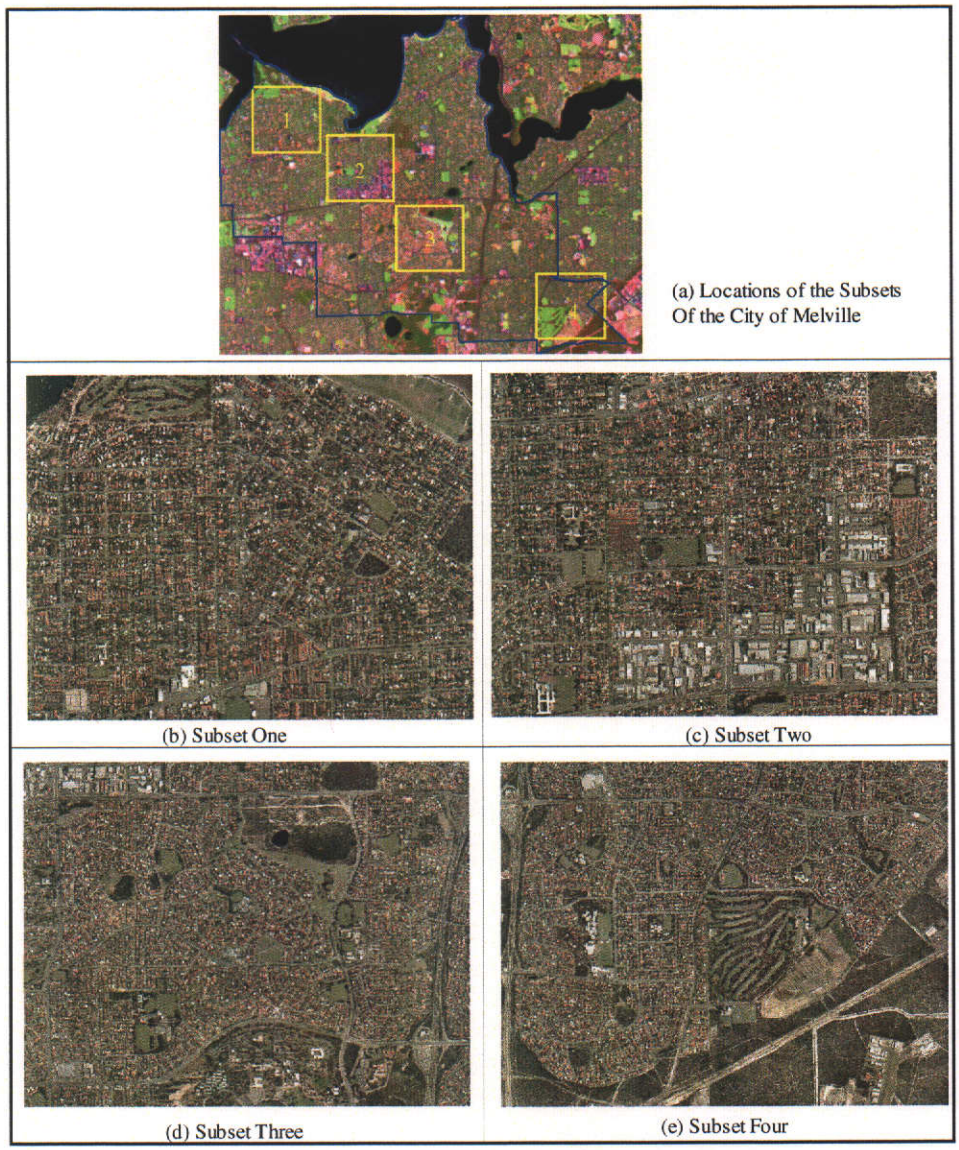

Figure 6.4 Land cover compositions of the subsets of the City of Melville

The variation of the *D* could be attributed to the degree of fragmentation of land covers of the individual subsets. An example of variation of land cover compositions of subsets one and two is shown in Figure 6.4. The land uses of subset one are characterised by residential buildings, internal roads, parks, grassland as compared to shopping complexes, major roads, residential areas and grassland of subset two. This shows that subset two is spatially more complex than subset one.

Table 6.8 Fractal dimension computed from the isarithm and the TPSA algorithm of the City of Melville

		Subset 1		Subset 2		Subset 3		Subset 4	
Sensor	Band	$D_{ISARITHM}$	D_{TPSA}	$D_{ISARITHM}$	D_{TPSA}	$D_{ISARITHM}$	D_{TPSA}	$D_{ISARITHM}$	D_{TPSA}
SPOT (20 m)	Green	3.00	2.85	3.04	2.83	2.87	2.83	2.82	2.77
	Red	2.94	2.84	3.00	2.83	2.85	2.85	2.81	2.73
	NIR	2.99	2.89	2.80	2.85	2.90	2.91	2.90	2.85
Landsat-7 ETM+ (25 m)	Green	2.89	2.68	2.89	2.77	2.80	2.81	2.85	2.75
	Red	2.91	2.74	2.90	2.83	2.81	2.81	2.81	2.76
	NIR	2.79	2.59	2.79	2.68	2.69	2.70	2.89	2.84
Landsat MSS (50 m)	Green	2.77	2.68	2.68	2.74	2.54	2.62	2.71	2.74
	Red	2.77	2.68	2.74	2.80	2.59	2.59	2.60	2.68

Table 6.9 *t*-significance test among the subsets of the City of Melville using the D_{TPSA} and $D_{ISARITHM}$ of Landsat-7 ETM+ bands

	Subsets	1	2	3	4
D_{TPSA}	1		t = -5.54, p=0.0026*	t = -4.06, p=0.0097*	t = -2.66, p=0.0445*
	2			t = 0.478, p=0.6527	t = 0.0079, p=0.993
	3				t = -.0.313, p=0.7668
$D_{ISARITHM}$	1		t = 0.3857, p=0.71556	t = 11.31, p=0.0001*	t = 0.8982, p=0.4802
	2			t = 5.0977, p=0.0038*	t = 0.898, p=0.4802
	3				t = -.2.693, p=0.043*

* Statistically significant

The variation measured by the standard deviation revealed that subset one has the least absolute variation of pixel values centred to its mean, whereas subset two has the highest variation, followed by subset four and subset three (Table 6.10). This result could be attributed to the changing degree of spectral heterogeneity of the land covers of individual subsets. The mean coefficient of variation particularly in the green and red bands was found highest in subset two. The higher fractal dimension and the higher coefficient of variation of subset two is the result of a more fragmented and spatially complex surface, as compared to a more spectral and spatial homogenous pattern of subset one, with a relatively low coefficient of variation and a low *D*.

The variations of the D_{TPSA} computed from the SPOT bands of subsets one, two and three are small indicating a spatially similar pattern of land covers (Table 6.7). In contrast, the D_{TPSA} of subset four were found to be lower indicating spatially less

complex than subsets one, two and three. On the other hand, the $D_{ISARITHM}$ of subset one and two were found higher as compared to subsets three and four.

Table 6.10 Summary statistics of Landsat-7 ETM+ of the subsets of the City of Melville

	Band	Minimum	Maximum	Mean	Standard Deviation	Coefficient of Variation
Subset One	Green	50	255	100.04	15.49	0.155
	Red	43	255	112.92	21.67	0.192
	NIR	29	170	94.59	14.88	0.157
Subset Two	Green	39	255	108.25	25.45	0.235
	Red	25	255	121.45	29.88	0.246
	NIR	10	185	86.38	14.92	0.173
Subset Three	Green	36	187	99.98	16.8	0.168
	Red	22	214	115.12	24.98	0.217
	NIR	10	163	88.79	16.33	0.184
Subset Four	Green	51	195	90.69	15.81	0.174
	Red	39	228	99.67	26.34	0.264
	NIR	49	171	87.88	20.39	0.232

The *t* significance test (Table 6.11) shows that the differences in spatial complexity measured using the TPSA algorithm among subsets are not statistically significant. In contrast, the *t* and corresponding *p*-values as summarised in Table 6.11 indicate that differences in spatial complexity measured using the isarithm method among subsets one and three and subsets one and four are statistically significant. The variations of the results between the D_{TPSA} and $D_{ISARITHM}$ were attributed to the methodological approach as explained in Section 3.3.2.

Table 6.11 *t*-significance test among the subsets of the City of Melville using the D_{TPSA} and $D_{ISARITHM}$ of SPOT bands

	Subsets	1	2	3	4
D_{TPSA}	1		$t = 2.645$, p=0.118	$t = -0.2773$, p=0.807	$t = 3.7811$, p=0.063
	2			$t = -1.511$, p=0.269	$t = 1.835$, p=0.207
	3				$t = 4.0$, p=0.0571
$D_{ISARITHM}$	1		$t = 0.3565$, p=0.7555	$t = 8.877$, p=0.0124*	$t = 5.177$, p=0.0353*
	2			$t = 0.8464$, p=0.4864	$t = 0.0145$, p=0.4171
	3				$t = 0.8814$, p=0.201

* Statistically significant

Likewise, the D (D_{TPSA} and $D_{ISARITHM}$) values of Landsat MSS of subset three were found lower as compared to the D values of subsets one, two and four (Table 6.8). This indicates that the land covers of subset three are spatially less complex. Table 6.12 summarises the results of t significance tests, which shows that the differences in spatial complexity measured using the TPSA algorithm, between subsets two and three and subsets three and four are statistically significant.

Table 6.12 t-significance test among the subsets of the City of Melville using the D_{TPSA} and $D_{ISARITHM}$ of Landsat MSS bands

	Subsets	1	2	3	4
D_{TPSA}	1		t = -2.10, p=0.1268	t = 0.367, p=0.2651	t = -1.529, p=0.2236
	2			t = 8.058, p=0.0039*	t = -0.2779, p=0.799
	3				t = -3.458, p=0.0406*
$D_{ISARITHM}$	1		t = 0.5111, p=0.6445	t = 1.267, p=0.2942	t = 2.8989, p=0.0625
	2			t = 2.83, p=0.0659	t = 1.894, p=0.1544
	3				t = 0.0639, p=0.9530

* Statistically significant

6.1.3 The City of Armadale

The City of Armadale represents a typical 'urban fringe', mostly comprised of residential and forested areas (Figure 4.6c-1 and 4.6c-2). The major land uses of the subsets which are selected along the transects (Figure 6.5) are as follows:

(a) Subset one largely comprises built-up areas which include commercial and administrative centres, shopping areas, residential areas surrounded with sparse to dense trees and major road networks.
(b) The land uses of subset two are comprised of bare ground, grassland, a few residential blocks surrounded by sparse to dense trees and forested areas.
(c) Subset three represents forested area which is fairly uniform and includes some bare ground.

The D values (D_{TPSA} and $D_{ISARITHM}$) of the green, red and NIR bands of Landsat-7 ETM+, SPOT and Landsat MSS of the subsets of the City of Armadale are presented in Table 6.13. An examination of the results indicates that subset one recorded the highest D values followed by subsets two and three. This indicates that the land cover pattern of subset one is spatially more complex than the land cover patterns of

subsets two and three. The variations of the D values among the subsets are a result of changes in land cover compositions and spatial pattern.

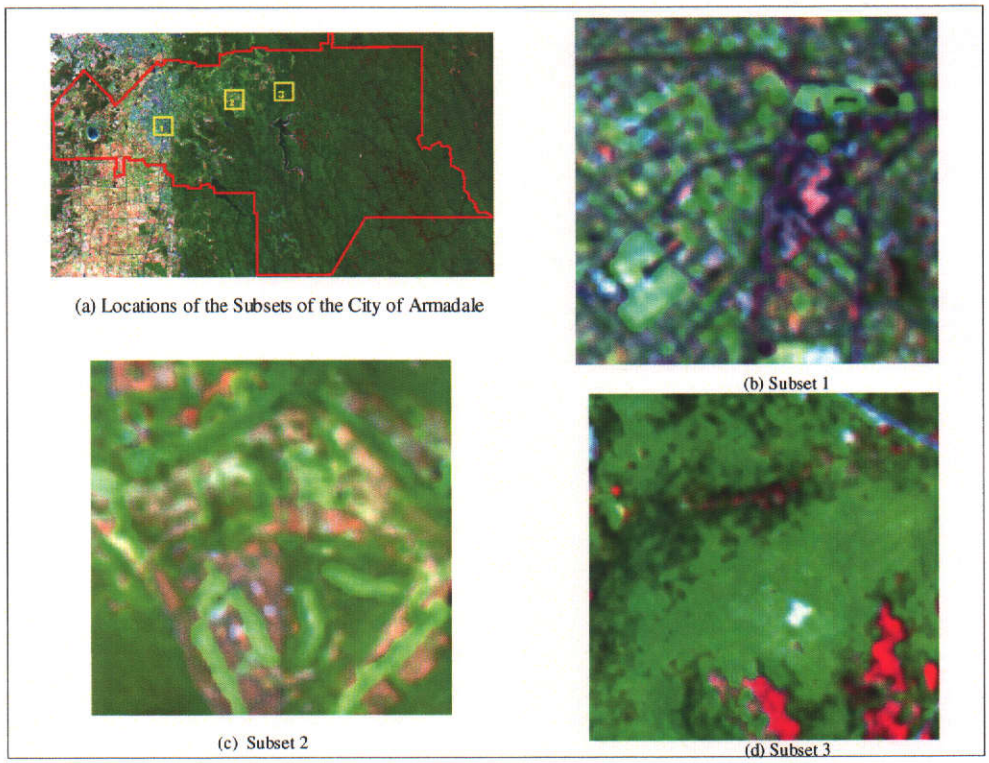

Figure 6.5 Land cover compositions of the subsets of the City of Armadale

Table 6.13 Fractal dimension computed from the isarithm and the TPSA algorithm of the City of Armadale

		Subset 1		Subset 2		Subset 3	
Sensor	Band	$D_{ISARITHM}$	D_{TPSA}	$D_{ISARITHM}$	D_{TPSA}	$D_{ISARITHM}$	D_{TPSA}
SPOT (20 m)	Green	2.94	2.82	2.85	2.67	2.82	2.77
	Red	2.95	2.81	2.85	2.73	2.76	2.75
	NIR	2.92	2.83	2.93	2.82	2.64	2.67
Landsat-7 ETM+ (25 m)	Green	2.86	2.75	2.76	2.70	2.72	2.56
	Red	2.85	2.80	2.74	2.71	2.74	2.56
	NIR	2.86	2.80	2.86	2.78	2.73	2.66
Landsat MSS (50 m)	Green	2.84	2.69	*	*	2.74	2.65
	Red	2.77	2.68	*	*	2.75	2.58

* D values were not computed due to unavailable data

The t-test with a 0.05 significance level using the D_{TPSA} and $D_{ISARITHM}$ of Landsat-7 ETM+ bands among the subsets of the City of Armadale were carried out to examine

whether the spatial complexity of the subsets, as expressed by the D values are significantly different. Table 6.14 summarises the t values and corresponding p values, which reveal that the spatial complexity measured using the TPSA algorithm of subsets one and two, subsets one and three and subsets two and three is significantly different (Table 6.14). Likewise, the differences in spatial complexity measured using the isarithm algorithm of subsets one and two and subsets one and three were found statistically significant (Table 6.14). This is because the land cover compositions of the City of Armadale vary from urban to forested areas. An examination of the land cover compositions of subset one indicates that it is characterised by typical urban features (e.g. major road network, shopping areas, residential areas), as compared to subsets two and three which are characterised by bare ground and forested areas. The land cover compositions of the subsets of the City of Armadale contribute to a significant variation of the city's spatial complexity.

Table 6.14 t-significance test among the subsets of the City of Armadale using the D_{TPSA} and $D_{ISARITHM}$ of the Landsat-7 ETM+ bands

	Subsets 1	2	3
D_{TPSA}	1	$t = 5.14$, p=0.0036*	$t = 7.33$, p=0.00074*
	2		$t = 7.19$, p=0.0008*
$D_{ISARITHM}$	1	$t = 4.0522$, p=0.0098*	$t = 5.4479$, p=0.00283*
	2		$t = 2.54$, p=0.0518

* Statistically significant

The variation measured as standard deviation of Landsat-7 ETM bands reveals that subset three has the least absolute variation whereas subsets one and two showed larger variation (Table 6.15). This indicates that subset three is spectrally more homogeneous due to forested areas as compared to subsets one and two which are more dominated by urban features and bare ground (Figure 6.5). The higher standard deviation of subset two in the red band could be influenced by the high spectral response of the bare ground. The low coefficient of variation of subset three indicates that the land covers are spectrally less heterogeneous. With a low coefficient of variation and a low fractal dimension of subset three, the surface is likely to be spatially and spectrally less complex, as compared to spatially complex land covers of subset one which exhibited to a relatively high D and a moderate CV.

The fractal dimension of SPOT bands of the subsets of the City of Armadale showed higher D values as compared to the D values of subsets two and three. This indicates that the spatial pattern of land covers of subset one is more complex as compared to subsets two and three. The t values and corresponding p values of the pairwise t-significance tests reveal that the differences in spatial complexity measured using the TPSA and the isarithm algorithms, between the subsets are not statistically significant (Table 6.16).

Table 6.15 Summary statistics of Landsat-7 ETM+ of the subsets of the City of Armadale

	Band	Minimum	Maximum	Mean	Standard Deviation	Coefficient of Variation
Subset One	Green	57	204	94.85	16.58	0.17
	Red	54	230	106.06	21.01	0.20
	NIR	47	168	85.72	16.54	0.19
Subset Two	Green	52	138	75.22	16.01	0.21
	Red	42	186	85.53	28.53	0.33
	NIR	63	161	85.12	14.92	0.18
Subset Three	Green	48	78	55.31	4.13	0.07
	Red	40	94	51.97	7.10	0.14
	NIR	50	77	63.96	2.51	0.04

Table 6.16 t-significance test among the subsets of the City of Armadale using the D_{TPSA} and $D_{ISARITHM}$ of the SPOT bands

	Subsets 1	2	3
D_{TPSA}	1	$t = 0.9794$, p=0.1863	$t = 2.563$, p=0.124
	2		$t = 0.1357$, p=0.9045
$D_{ISARITHM}$	1	$t = 1.708$, p=0.229	$t = 4.25$, p=0.052
	2		$t = 1.739$, p=0.224

Likewise, the variation measured as standard deviation of SPOT bands presented in Table 6.17 shows the least absolute variation in subset three whereas subset one has the highest absolute variation. This indicates that subset three is spectrally more homogeneous due to forested areas as compared to subset which is dominated by urban features (Figure 6.5). With a low coefficient of variation and a low fractal dimension of subset three, the surface is likely to be spatially and spectrally less

complex, as compared to spatially more complex land covers of subset one which exhibited a relatively high D and a moderate CV.

The D values of the green and red bands of Landsat MSS vary among the subsets of the City of Armadale indicating the effect of land cover pattern on spatial complexity. An examination of the D values presented in Table 6.13 indicates a similar trend of variation among the subsets as discussed for Landsat-7 ETM+ and SPOT. The t values and corresponding p values of the pairwise t-significance tests reveal that the differences in spatial complexity measured using the TPSA and the isarithm algorithms, between the subsets are not statistically significant (Table 6.18).

Table 6.17 Summary statistics of SPOT of the subsets of the City of the Armadale

	Band	Minimum	Maximum	Mean	Standard Deviation	Coefficient of Variation
Subset One	Green	49	243	75.58	18.32	0.24
	Red	41	237	73.40	19.01	0.26
	NIR	63	235	105.16	19.22	0.18
Subset Two	Green	44	72	54.82	6.55	0.12
	Red	34	81	51.50	10.83	0.21
	NIR	68	135	90.12	11.59	0.13
Subset Three	Green	40	64	46.87	3.07	0.07
	Red	30	65	41.30	3.81	0.09
	NIR	24	89	64.02	9.69	0.15

Table 6.18 t-significance test among the subsets of the City of Armadale using the D_{TPSA} and $D_{ISARITHM}$ of Landsat MSS bands

	Subsets 1	3
D_{TPSA}	1	$t = 0.7336$, p=0.5163
$D_{ISARITHM}$	3	$t = 0.4057$, p=0.712

6. 2 Effect of Spatial Resolution on Fractal Dimension

6.2.1 The City of Perth

The results of the D_{TPSA} of SPOT, Landsat-7 ETM+ and Landsat MSS indicate that on average, the fractal dimension increases with increasing spatial resolution of the

sensor, except for subset one in bands green and red of the SPOT and Landsat-7 ETM+ (Figure 6.6). This suggests an obvious effect of scale on the spatial complexity of urban landscapes. A comparison of average D_{TPSA} between various sensors in the green, red and NIR bands in Figure 6.6 shows that the average D_{TPSA} is the highest in SPOT followed by Landsat-7 ETM+ and Landsat MSS. The higher D values of Landsat-7 ETM+ of subset one could be attributed to the variations in the land cover composition and therefore, heterogeneity over time (e.g. more complexity is expected for Landsat-7 ETM+ as a result of a more complex pattern of built-up areas occurring between ten years of SPOT and Landsat-7 ETM+ acquisition), which was explained in Section 6.1.1.

Similar increase in fractal dimension with increasing spatial resolution was found by Lam (1990). In that study, all bands of Landsat TM including the thermal band with a spatial resolution of 120 m, were resampled to a fixed pixel size of 25 m, and the fractal dimension computed afterwards. The fractal dimension of an urban area was found to vary from 2.21 to 2.73 for the thermal and red bands, respectively. In addition to a lower spectral variability of emitted temperature, as compared to spectral reflectance of earth surfaces, the variation was attributed to the original spatial resolution of the bands.

Likewise, the $D_{ISARITHM}$ computed from all subsets from Landsat-7 ETM+, SPOT and MSS showed a similar trend i.e. the higher the spatial resolution the higher the $D_{ISARITHM}$ (Figure 6.6). The increasing trend of D_{TPSA} and $D_{ISARITHM}$ with increasing spatial resolution could be the result of the loss of mixed pixels composed of varying combinations of digital numbers that correspond to commercial buildings, major and minor roads, residential area and forested area, to more "pure" pixels reflecting a heterogeneous land cover pattern. Figure 6.6 shows that the variation of spatial complexity between Landsat MSS and SPOT is highest in subset three. This is expected as the spatial heterogeneity of the land covers, particularly residential and forested areas of subset three, decrease in a larger pixel (e.g. 50 m) as individual residential blocks and trees are averaged into larger blocks. This signifies that the higher the spatial resolution, the higher the textural information content indicating higher variation, and thus the resolution level at which most processes operate as found by Cao and Lam (1997).

The results in the green, red and NIR bands of SPOT in all subsets revealed higher in the $D_{ISARITHM}$ as compared to D_{TPSA} (Table 6.1). A possible explanation could be that the approach of the isarithm method excludes few random pixels that have abnormally high values and thus, measures the major variation dominating the subsets, thereby yielding a higher D (Qiu *et al.*, 1999).

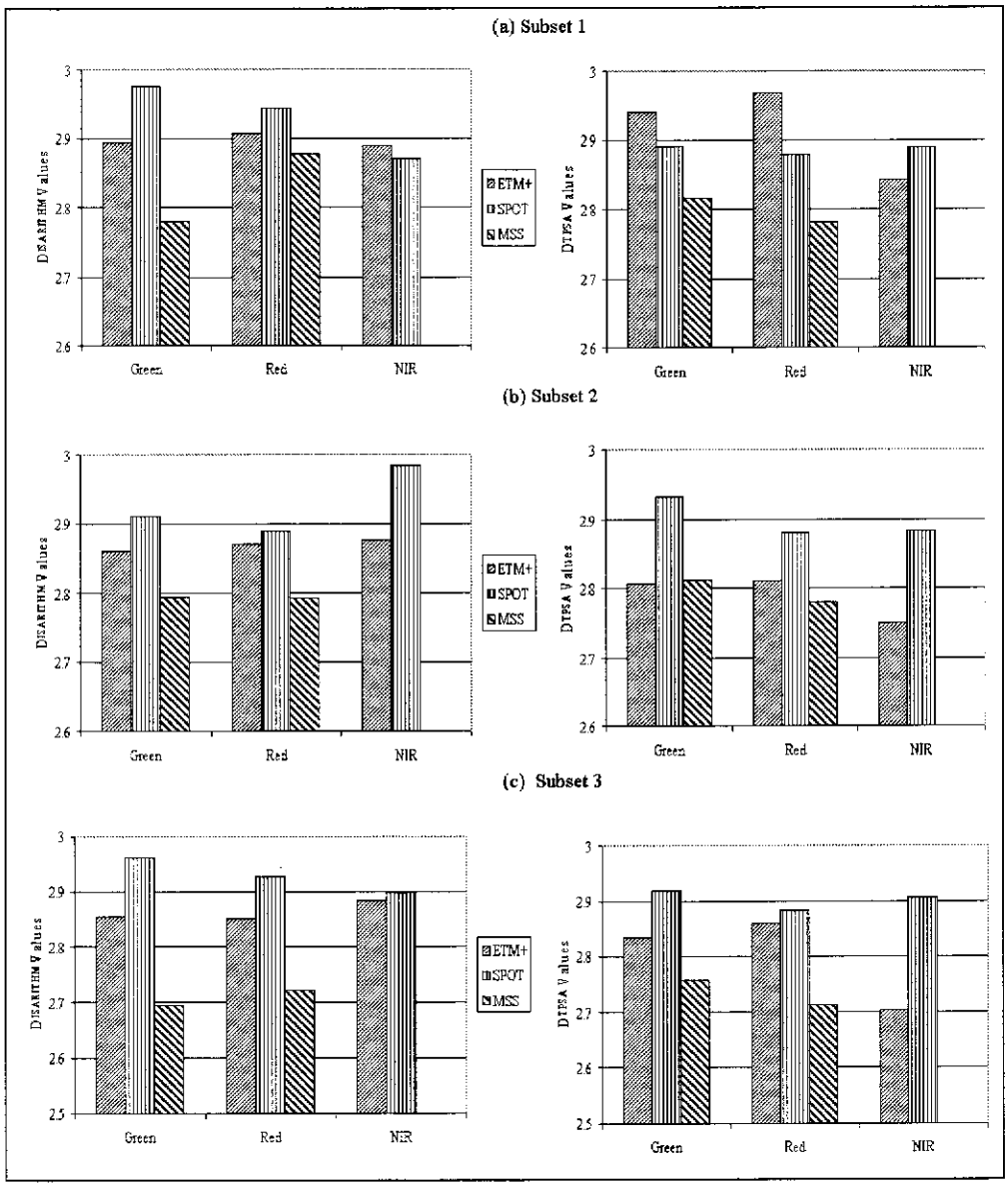

Figure 6.6 The D_{TPSA} and $D_{ISARITHM}$ of the green, red and NIR bands of SPOT, Landsat-7 ETM+ and Landsat MSS of the City of Perth

This is in conformity with the findings of the previous studies by Read and Lam (2002) and Qiu *et al.* (1999), which showed higher $D_{ISARITHM}$ for different land cover types, as compared to D_{TPSA} values. Statistical comparisons between the D_{TPSA} and

the $D_{ISARITHM}$ of SPOT, Landsat-7 ETM and Landsat MSS bands were carried out using the *t*-test with a 0.05 significance level to determine whether the difference is significant. The *t* values and corresponding *p* values presented in Table 6.19 indicate that the differences between the D_{TPSA} and the $D_{ISARITHM}$ in subset two of the City of Perth are statistically significant.

Table 6.19 *t*-significance test between the $D_{ISARITHM}$ and D_{TPSA} computed from SPOT, Landsat-7 ETM+ and Landsat MSS bands of the subsets of the City of Perth

Subsets	1	2	3
SPOT	t = 1.319, p=0.3176	t = 0.832, p=0.4929	t = 1.438, p=0.2873
Landsat-7 ETM+	t = -1.903, p=0.1297	t = 6.779, p=0.0010*	t = 1.217, p=0.2778
Landsat MSS	t = -1.158, p=0.330	t = -0.3017, p=0.782	t = -0.218, p=0.117

Furthermore, there is disagreement in the results of the $D_{ISARITHM}$ of SPOT in the green and red bands of subset one compared to the results obtained from the TPSA method. Figure 6.6 shows that the $D_{ISARITHM}$ of the green and red bands of SPOT in subset one is higher despite the temporal effect on the land cover compositions as explained in Section 6.1.1. The directional pattern of various features present in the subsets (e.g. row or column) could contribute to the disagreement of the results, as the $D_{ISARITHM}$ resulting from the row-column method was considered in the analysis assuming that the row-column method will minimise the directional bias. Another source of discrepancy of the results of the isarithm method could be the selection of the isarithm interval in computing $D_{ISARITHM}$ as the results vary using different isarithm intervals (Lam, 1990).

6.2.2 The City of Melville

The D_{TPSA} and $D_{ISARITHM}$ of the subsets of the City of Melville computed from the green, red and NIR bands of SPOT, Landsat-7 ETM+ and Landsat MSS are presented in Figure 6.7. It shows a similar trend of the D_{TPSA} and $D_{ISARITHM}$ in all spectral band locations like the results of the subsets of the City of Perth i.e. the higher the spatial resolution, the higher the fractal dimension indicating the higher the spatial complexity.

Figure 6.7 shows that the variation of spatial complexity between Landsat MSS and Landsat-7 ETM+ and Landsat MSS and SPOT is higher in the green and red bands of subset three. This could be partially explained to the effect of spatial resolution and the changes of land cover compositions over time. The land covers of subset three comprised of sparse trees and native vegetation as found in Landsat MSS acquired in 1980 have changed to urban area (spatially complex land covers) which was reflected in the SPOT and Landsat–7 ETM+ scenes acquired in 1991 and 2001 respectively, and accordingly, contributed to a higher *D*.

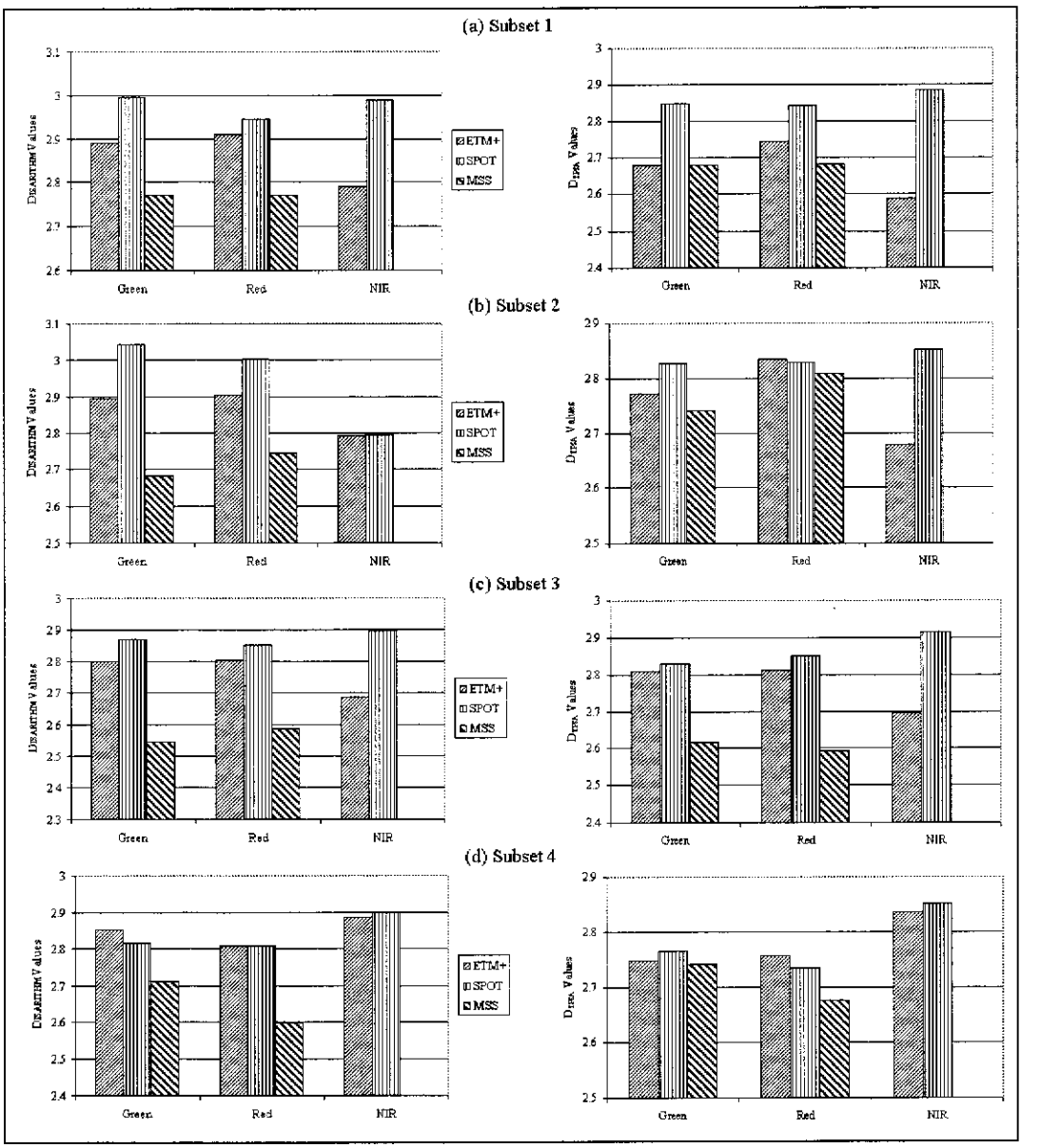

Figure 6.7 The D_{TPSA} and $D_{ISARITHM}$ of the green, red and NIR bands of SPOT, Landsat-7 ETM+ and Landsat MSS of the City of Melville

The results of SPOT and Landsat-7 ETM+ in all the subsets of the City of Melville indicated consistently higher $D_{ISARITHM}$ than the D_{TPSA} (Figure 6.7). A series of *t*-tests with a 0.05 significance level were carried out between the $D_{ISARITHM}$ and D_{TPSA} of SPOT, Landsat-7 ETM+ and Landsat MSS bands in all subsets to examine whether the differences in spatial complexity computed from the isarithm and the TPSA methods are statistically significant. The results presented in Table 6.20 indicate that the difference between the $D_{ISARITHM}$ and D_{TPSA} of subsets one, two and four in Lansat-7 ETM+ and subsets one and four in SPOT are statistically significant.

Table 6.20 *t*-significance test between the $D_{ISARITHM}$ and D_{TPSA} of SPOT, Landsat-7 ETM+, and Landsat MSS of the subsets of the City of Melville

Sensor	1	2	3	4
SPOT	$t = 7.522, p=0.017$*	$t = 1.31, p=0.318$	$t = 0.468, p=0.685$	$t = 7.158, p=0.018$*
Landsat-7 ETM+	$t = 22.85, p=0.000003$*	$t = 11.48, p=0.000008$*	$t = -0.317, p=0.763$	$t = 7.18, p=0.0008$*
Landsat MSS	$t = 1.841, p = 0.1628$	$t = 0.177, p = 0.870$	$t = 1.151, p=0.332$	$t = -2.886, p=0.0632$

* Statistically significant

6.2.3 The City of Armadale

The D_{TPSA} and $D_{ISARITHM}$ of the subsets of the City of Armadale computed from the green, red and NIR bands of SPOT, Landsat-7 ETM+ and Landsat MSS are presented in Figure 6.8. The results in Figure 6.8 show that the D_{TPSA} and $D_{ISARITHM}$ of the green, red and NIR bands is highest in the SPOT data, followed by Landsat-7 ETM+ and Landsat MSS (i.e. the higher the spatial resolution the higher the spatial complexity) in subset one and subset three. In subset two, the green band of Landsat-7 ETM+ recorded a higher D_{TPSA}, as compared to the D_{TPSA} of SPOT (Figure 6.8). This could be the result of the changes in land cover compositions of subset two, which was transformed from a forested area, as recorded in the SPOT image acquired in 1991, to a more spatially heterogeneous land cover dominated by bare ground, residential area and forested area at the time of the Landsat-7 ETM acquisition.

Similar to the results obtained for the City of Perth and the City of Melville, the isarithm method revealed higher fractal dimension ($D_{ISARITHM}$) than the TPSA method in the SPOT and Landsat-7 ETM+ data sets, in all subsets of the City of Armadale.

The t significance test between the $D_{ISARITHM}$ and D_{TPSA} of SPOT, Landsat-7 ETM+ and Landsat MSS bands in Table 6.21 shows that the difference between the $D_{ISARITHM}$ and the D_{TPSA} methods is significant only in subsets one and two of the SPOT data set.

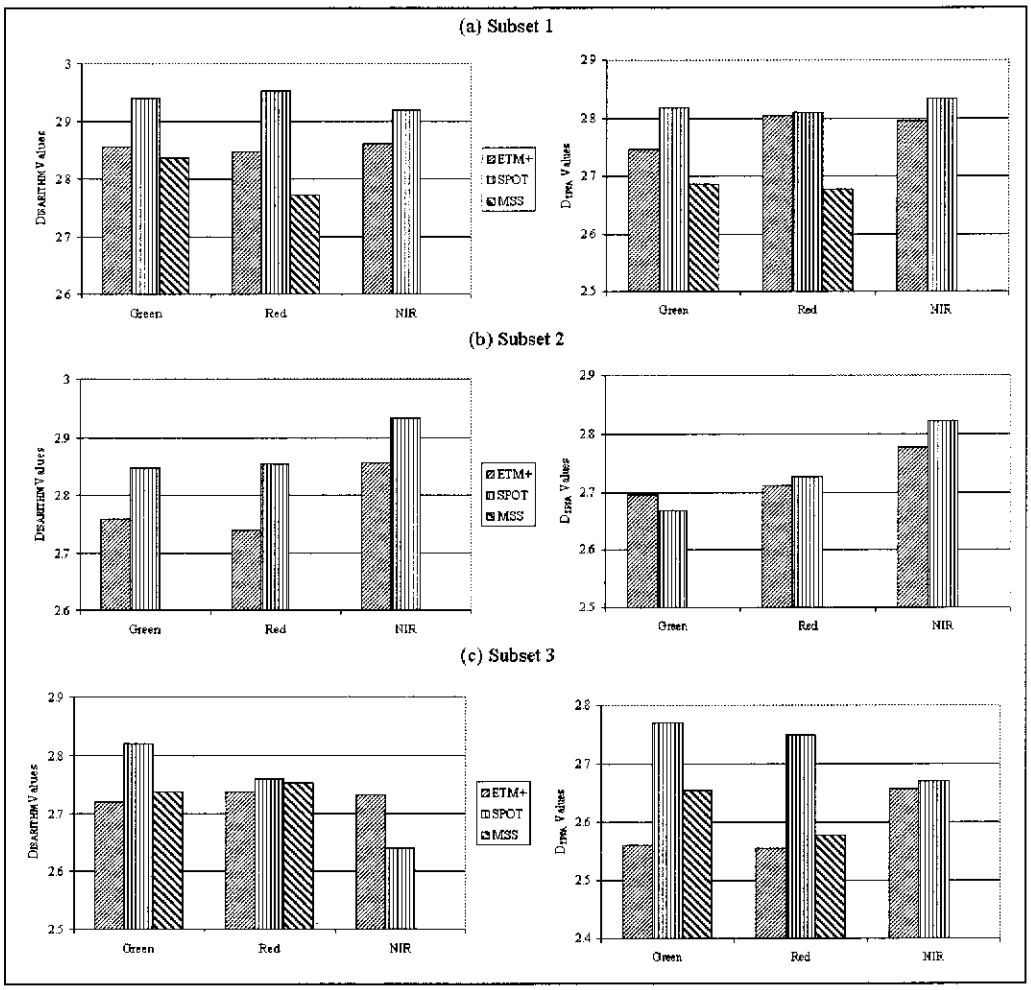

Figure 6.8 The D_{TPSA} and $D_{ISARITHM}$ of the green, red and NIR bands of SPOT, Landsat-7 ETM+ and Landsat MSS of the City of Armadale

Table 6.21 t-significance test between the D_{TPSA} and $D_{ISARITHM}$ of Landsat-7 ETM+, SPOT and Landsat MSS of the subsets of the City of Armadale

Sensor	1	2	3
SPOT	t = 8.029, p=0.01515*	t = 6.252, p=0.0246*	t = 0.433, p=0.7072
Landsat-7 ETM+	t = 3.95, p=0.0584	t = 3.900, p=0.0598	t = 4.039, p=0.0561
Landsat MSS	t = 4.0, p=0.1559	-	t = 3.25, p=0.190

* Statistically significant

The increasing fractal dimension with increasing spatial resolution indicates that the spatial complexity of urban landscapes can be better characterised in the higher spatial resolution satellite data. This also means that at higher spatial resolution, the textural information content is higher. It appeared that the lower fractal dimension resulting from a coarser spatial resolution data (e.g. Landsat MSS) underestimates the spatial complexity of urban land uses. This implies a loss of detailed information, which asserts the inability to extract small and linear landscape features from a coarser resolution data (e.g. Landsat MSS). Thus, data of a higher spatial resolution (e.g. SPOT) where the spatial complexity of urban land covers is the highest could be the most appropriate for analysing heterogeneous land uses.

6. 3 Effect of Spectral Band Location on Fractal Dimension

6.3.1 The City of Perth

The D_{TPSA} and $D_{ISARITHM}$ of the green, red and NIR bands of Landsat-7 ETM+ in Figure 6.6 shows a variation in the D values with changing of the spectral range. In general, the D values of the green and red bands were found higher than the NIR band in all subsets of the City of Perth. The highest D was found in the red band followed by the green and the NIR bands (Table 6.1). Figure 6.2 shows that there are a few areas of grassland along the freeways, major roads, parking lots, commercial buildings, and some residential areas in all subsets. These land uses are mixed. Within these land uses, grassland reflects electromagnetic radiation in green band and absorbs electromagnetic radiation in red band, which results in relatively low digital numbers as compared to the medium to very high reflectance of the built-up areas in that part of the spectrum. This results in spatially more complex pattern of the spectral response in the ETM+ green and red bands than the NIR band and therefore, exhibited larger D values than the NIR band.

On the contrary, the D values of SPOT image computed from the TPSA algorithm reveals a small variation between the visible and the NIR bands. In some instances, the D value of the NIR band was found higher than the visible bands (Figure 6.6a). This could be attributed to the presence of larger amounts of vegetated areas particularly in subset one, along major roads and built-up areas (see Figure 6.3). In the NIR, the high reflectance of grassland and vegetation along with low to medium

electromagnetic radiation of the built-up features in all subsets contributed to spatially more complex spectral characteristics as compared to the visible bands. Likewise, Figure 6.6 shows similar variation of the D among the visible bands of MSS image. In all subsets, the highest D_{TPSA} was found in the green band followed by the red band.

6.3.2 The City of Melville

The variation of the D in the green, red and NIR bands of SPOT, Landsat-7 ETM+ and Landsat MSS of the subsets of the City of Melville is shown in Figure 6.7. An examination of the D computed from the Landsat-7 ETM+ indicates that the red band exhibited the highest D followed by the green and NIR bands in subsets one, two and three (Figure 6.7a to 6.7c). The higher D in the red and green bands could be attributed to the spectral characteristics of land cover compositions of these subsets (see Section 6.1.2), which are spectrally more variable in the visible bands and accordingly, exhibit higher D values than the NIR band. On the other hand, in subset four, the NIR band exhibited higher D values as compared to the visible bands (Figure 6.7d). This could be explained by compositions of subset four, which is characterised by grassland, native vegetation, sparse trees and, to a lesser extent residential area.

Figure 6.7 shows the variation of D among the green, red and NIR bands of SPOT in the subsets of the City of Melville. The results in Figure 6.7 indicate a higher D value in the NIR band as compared to the green and red bands in all subsets except the D of subset two computed from the isarithm algorithm. An examination of the results of the visible bands shows a small variation between the green and red bands. The higher D values in the NIR band of SPOT as compared to the higher D values of the visible bands of Landsat-7 ETM+ in subsets one, two and three could be attributed to the variation of land cover compositions which changed over the years as the SPOT data was acquired in 1991 when the proportion of vegetation was higher than the built-up areas, compared to the acquisition of the Landsat-7 ETM+ scene in 2001, characterised by a higher percentage of built-up areas.

6.3.3 The City of Armadale

The results of Landsat-7 ETM+ of the City of Armadale as shown in Figure 6.8 indicate a higher D value in the NIR band as compared to the visible bands of subsets two and three, while subset one recorded a higher D value in the visible bands than the NIR band. This can be attributed to the different land cover compositions of the subsets of the City of Armadale. The land cover compositions of subset one are characterised by urban features as described in Section 6.1.3 and accordingly, the spectral characteristics of the land cover compositions are more spatially variable in the visible bands which contributes to a higher D. In contrast, the predominant land covers (e.g. forest) of subsets two and three contributed to higher D in the ETM+ NIR band. Similar variation of the D among the green, red and NIR bands of SPOT and Landsat MSS is shown in Figure 6.8. A comparison of the fractal dimension between the TPSA and the isarithm method revealed higher $D_{ISARITHM}$ than D_{TPSA}. This difference in the fractal dimension could be attributed to methodological approach of the isarithm methods as discussed in Section 6.1.2.

The higher fractal dimension in the green and red bands of the subsets that represent urban areas provides an indication of higher textural information present in these bands. This indicates that the measurement of spatial complexity from the visible spectrum is more appropriate for urban areas than other land cover types. In addition, this information could be a useful guideline for selection of bands for display, classification, and analysis as reported by Lam (1990).

6. 4 Spatial Autocorrelation Measure and Fractal Dimension

Moran's I index of spatial autocorrelation is a scale dependent statistic useful for indicating the degree of clustering, randomness or dispersion of a distribution. It (Moran's I) varies from +1 for a perfect positive autocorrelation (e.g. lumped pattern) to –1 for perfect negative correlation (e.g. checkerboard pattern) (Lam *et al.*, 2002). In order to examine whether the degree of clustering, randomness or dispersion of a remotely sensed image could be used to describe the spatial complexity, Moran's I computed from SPOT, Landsat-7 ETM+ and Landsat MSS were compared with the D_{TPSA} and $D_{ISARITHM}$ computed and analysed in the previous section.

The results of Moran's *I* of the subsets of the City of Perth computed from the SPOT, Landsat-7 ETM+ and Landsat MSS are presented in Table 6.22. An examination of the spatial autocorrelation computed from Landsat-7 ETM+ reveals that subset three recorded the highest Moran's *I* followed by subsets one and two (Table 6.22). The relatively high positive Moran's *I* values of subset three indicate a more clumped pattern. The increase in spatial resolution of the SPOT data set evidences a more clustered pattern of subset one as compared to subsets two and three. In Landsat MSS, the variations of Moran's *I* of subsets one and two with subset three are pronounced as compared to the results of SPOT and Landsat-7 ETM+.

Table 6.22 shows that Moran's *I* of the subsets one and two varied between 0.64 to 0.69 among the green and red bands as compared to 0.84 to 0.85 of subset three. This indicates that the land cover patterns of subsets one and three as revealed from a Landsat MSS scene, are less clustered compared to a more clustered distribution of subset three. The variation of Moran's *I* among the subsets could be attributed to land cover compositions and the spatial resolution of the sensor. As described in Section 6.1.1 the land cover compositions of subset three are dominated by residential areas and parkland and accordingly, the representation of similar features among the Landsat MSS pixels are spatially autocorrelated as the features within each pixel remain more or less uniform. On the other hand, the presence of more than one land cover (e.g. buildings, major roads, parking lots, parkland) within Landsat MSS pixels is not correlated, as the features within each pixel are not uniform.

Table 6.22 Moran's *I* of spatial autocorrelation of the City of Perth

		Subset 1	Subset 2	Subset 3
SPOT (20 m)	Green	0.7862	0.7696	0.7479
	Red	0.8078	0.7879	0.793
	NIR	0.8246	0.7772	0.7102
Landsat-7 ETM+ (25 m)	Green	0.7951	0.7893	0.8574
	Red	0.8081	0.789	0.8702
	NIR	0.8344	0.8258	0.8278
Landsat MSS (50 m)	Green	0.6929	0.6503	0.8486
	Red	0.6534	0.6425	0.8419

Correlation analyses between Moran's *I* and the D_{TPSA} and Moran's *I* and the $D_{ISARITHM}$ computed from all bands of Landsat-7 ETM+, SPOT and Landsat MSS are

presented in Table 6.23 and Table 6.24. The results show a negative correlation between Moran's *I* and the *D*, showing an inverse relationship. This indicates that the higher the spatial autocorrelation (e.g. Moran's *I*) indicating a more clustered distribution, the lower the spatial complexity (e.g. *D*) which supports the findings as reported by Read and Lam (2002), Lam *et al.* (2002) and Read (2003). However, the correlation coefficients of Moran's *I* and the *D* of subsets one (Table 6.23) and three (Table 6.24) computed from Landsat MSS and SPOT respectively were found to have positive values. This indicates an increase of the *D* values with increasing the spatial autocorrelation.

Table 6.23 Correlation analysis between Moran's *I* and the D_{TPSA} of the Landsat-7 ETM+, SPOT and Landsat MSS of the subsets of the City of Perth

Sensor	1	2	3
SPOT	-0.17	-0.84	-0.74
Landsat-7 ETM+	-0.75	-0.66	-0.39
Landsat MSS	0.06	-0.21	-0.89

Table 6.24 Correlation analysis between Moran's *I* and the $D_{ISARITHM}$ of the Landsat-7 ETM+, SPOT and Landsat MSS of the subsets of the City of Perth

Sensor	1	2	3
SPOT	-0.96	-0.31	0.35
Landsat-7 ETM+	-0.51	-0.79	-0.99
Landsat MSS	-0.72	-0.22	-0.95

Table 6.25 presents Moran's *I* of the green, red and NIR bands of SPOT, Landsat-7 ETM+ and Landsat MSS of the City of Melville. The higher positive Moran's *I* values particularly in the green and red bands of subset three as shown in Table 6.25 indicate a clustered pattern when analysed using Landsat-7 ETM+. Likewise, the results of SPOT revealed a more clumped distribution in subset three as it recorded the highest Moran's *I* as compared to subsets two, four and one. In Landsat MSS, subset four presents a more clustered distribution followed by subset three, two and one (Table 6.25).

The results of correlation analyses between Moran's *I* and the *D* computed from all bands of SPOT, Landsat-7 ETM+ and Landsat MSS in Tables 6.26 and 6.27 show a moderate to strong negative correlation. An examination of the correlation

coefficients indicates stronger inverse relationships between Moran's *I* and the *D* of Landsat-7 ETM+ as compared to the results of SPOT and Landsat MSS. The results substantiate the idea that Moran's *I* and the *D* are inversely correlated, which is in conformity with the findings of Read and Lam (2002) and Lam *et al.* (2002). However, the correlation coefficients of subset one and subsets two and three as determined from SPOT and Landsat MSS, respectively using the TPSA method reveal positive (Table 6.26 and Table 6.27) which contradicts earlier findings. An examination of the D_{TPSA} of subset three computed from Landsat MSS bands indicates lower *D* values (variations between 2.50 to 2.61), which could be attributed to the positive correlation coefficients.

Table 6.25 Moran's *I* of spatial autocorrelation of the City of Melville

Sensor	Band	Subset 1	Subset 2	Subset 3	Subset 4
SPOT (20 m)	Green	0.6481	0.8086	0.8527	0.7497
	Red	0.7294	0.8281	0.8868	0.816
	NIR	0.7716	0.7858	0.7993	0.7691
Landsat-7 ETM+ (25 m)	Green	0.7125	0.8257	0.8396	0.8271
	Red	0.736	0.8156	0.8887	0.8523
	NIR	0.8516	0.8641	0.8533	0.8757
Landsat MSS	Green	0.6565	0.7903	0.8095	0.893
(50 m)	Red	0.611	0.7907	0.8402	0.8775

Table 6.26 Correlation analysis between Moran's *I* and the D_{TPSA} of the Landsat-7 ETM+, SPOT and Landsat MSS of the subsets of the City of Melville

Sensor	1	2	3	4
SPOT	0.69	-0.86	-0.01	-0.99
Landsat-7 ETM+	-0.84	-0.89	-0.66	-0.52
Landsat MSS	-0.76	0.41	0.59	-0.88

Table 6.27 Correlation analysis between Moran's *I* and the $D_{ISARITHM}$ of the Landsat-7 ETM+, SPOT and Landsat MSS of the subsets of the City of Melville

Sensor	1	2	3	4
SPOT	-0.32	0.81	-0.59	-0.95
Landsat-7 ETM+	-0.96	-0.92	-0.80	-0.79
Landsat MSS	-0.78	-0.95	-0.89	-0.35

Moran's *I* index of subsets of the City of Armadale computed from the Landsat-7 ETM+, SPOT and Landsat MSS is presented in Table 6.28. An examination of the results reveals relatively lower positive Moran's *I* values in subsets one when analysed using SPOT and Landsat-7 ETM+ indicating a less clustered pattern as compared to subsets two and three (Table 6.28). The lower Moran's *I* in subset one is attributed to the land cover composition which was found spatially complex as compared to more homogeneous land covers of subsets two and three (Section 6.1.3). In Landsat MSS, Moran's *I* of subset three particularly in the green band was found lower indicating a less clustered pattern which could be attributed to the spatial resolution and the land cover compositions of the subset.

Table 6.28 Moran's *I* of Spatial Autocorrelation of the City of Armadale

Sensor	Band	Subset 1	Subset 2	Subset 3
SPOT (20 m)	Green	0.7499	0.8468	0.8072
	Red	0.7714	0.9084	0.8252
	NIR	0.7028	0.8530	0.9286
Landsat-7 ETM+ (25 m)	Green	0.7766	0.8515	0.8476
	Red	0.7594	0.8664	0.8618
	NIR	0.8547	0.8274	0.8820
Landsat MSS (50 m)	Green	0.6311		0.5830
	Red	0.6466		0.6386

The correlation analyses between Moran's *I* and the *D* computed from all bands of Landsat-7 ETM+, SPOT and Landsat MSS are presented in Table 6.29 and Table 6.30. Table 6.29 and Table 6.30 indicate a low to moderate negative correlation between Moran's *I* and the *D* computed from Landsat-7 ETM+ and SPOT. In Landsat MSS, a positive correlation was obtained between Moran's *I* and the D_{TPSA} in subset one which could be attributed to the lower *D* values.

Table 6.29 Correlation analysis between Moran's *I* and the D_{TPSA} of the Landsat-7 ETM+, SPOT and Landsat MSS of the subsets of the City of Armadale

Sensor	1	2	3
SPOT	-1.0	-0.05	-1.0
Landsat-7 ETM+	-0.49	-0.25	0.03
Landsat MSS	0.99		0.01

Table 6.30 Correlation analysis between Moran's I and the $D_{ISARITHM}$ of the Landsat-7 ETM+, SPOT and Landsat MSS of the subsets of the City of Armadale

Sensor	1	2	3
SPOT	1.0	-0.35	-0.99
Landsat-7 ETM+	-0.24	-0.67	-0.78
Landsat MSS	0.11		0.21

6.4.1 Spatial Complexity (D) and Non-Spatial Statistics for Characterising the Study Areas

The previous sections discussed the characterisation of the spatial complexity of the study areas computed from the green, red and NIR bands of Landsat-7 ETM+, SPOT and Landsat MSS using the spatial (D and Moran's I) and non-spatial statistical measures (CV and standard deviation). In all study areas, the D computed from the TPSA and the isarithm methods varied among the subsets indicating the effect of changes in land cover compositions on the spatial complexity of the study areas. A comparison of the D among the sensors in each spectral location indicated that the higher the spatial resolution the higher the spatial complexity. The results also showed that D varies as function of the spectral band locations of the sensor.

In order to characterise the spatial pattern of diverse land covers (e.g. buildings, major roads, trees, grassland and open space) of the study areas, the CV and the D of the green, red and NIR bands of Landsat-7 ETM+ are plotted in Figure 6.9. Figure 6.9 shows a high CV and a moderate to very high D in the City of Perth indicating spectrally heterogeneous and spatially complex land covers. This is likely to be due to the complex spatial pattern (e.g. higher level of fragmentation) of the land covers of the City of Perth as explained in Section 6.1.1. On the other hand, the land covers of the City of Melville exhibited a moderate CV with a large variation in D values computed particularly from the isarithm method (Figure 6.9). Likewise, the City of Armadale has the largest range of CV with low to moderate D values indicating that the spectral heterogeneity of the land covers varies from low to very high as compared to low to moderate spatially complex land covers (Figure 6.9). The large variations in CV of the City of Armadale was attributed to the spectral heterogeneity of the land cover compositions which vary from a homogeneous land covers (e.g. forested area) to an area dominated by bare ground and built-up areas.

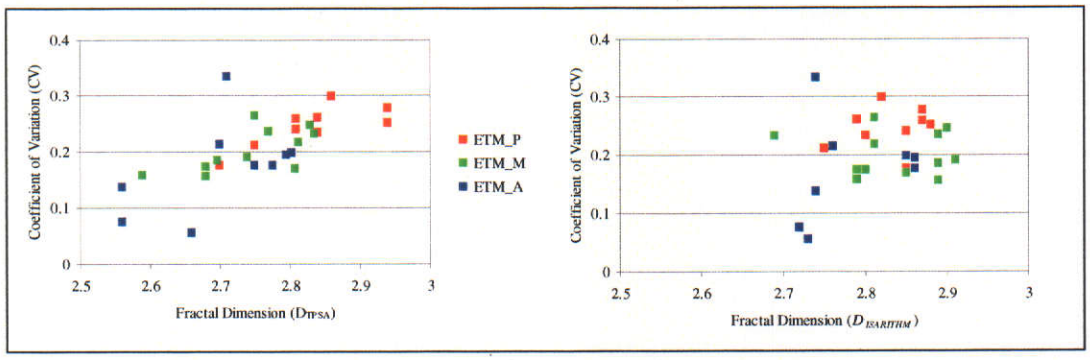

Figure 6.9 Scatter plot of the *D* and the coefficient of variation of Landsat-7 ETM+ on the study areas (ETM_P: Perth; ETM_M: Melville; ETM_A: Armadale)

An examination of the *D* computed from Landsat-7 ETM+ indicates no definite spatial pattern (e.g. cluster of *D*) for characterising the land covers of the study areas (Figure 6.9). Likewise, Figure 6.9 shows no correlation between the CV and the *D* which supports the idea that the CV does not provide any information about spatial patterns of land covers, as reported in previous studies by Lam (1990) and Read and Lam (2002).

The variations of the CV and the *D* computed from the SPOT image of the study areas are plotted in Figure 6.10. It shows a compact cluster of high D_{TPSA} for the City of Perth, an area dominated by spatially complex land covers which decreases as the spatial pattern of land covers change to medium urban and urban fringe. However, the results of the $D_{ISARITHM}$ do not provide a similar pattern to that obtained from the D_{TPSA}, which could be attributed to the methodological approach of the isarithm method as discussed in Section 6.2.1.

The CV and the *D* computed from Landsat MSS areas plotted in Figure 6.11 show no definite spatial pattern as the variations in the *D* are high in all study areas. It appears that the *D* values computed from the TPSA algorithm of SPOT increases as the land cover compositions changes from an urban fringe (e.g. City of Armadale) to medium urban (e.g. City of Melville) to dense urban (e.g. City of Perth). This indicates that the urban land covers could be better characterised in SPOT image as compared to Landsat-7 ETM and Landsat MSS. On the other hand, there was no significant trend found between the CV, an index of spectral variability and *D*, an index of spatial complexity. This demonstrates that although CV and other measures of non-spatial variation (e.g. standard deviation) are good descriptors of an area's

characteristics, they cannot be used as indicators of an areas' spatial complexity as they do not bear a consistent relationship to the measures of spatial complexity (*D* values).

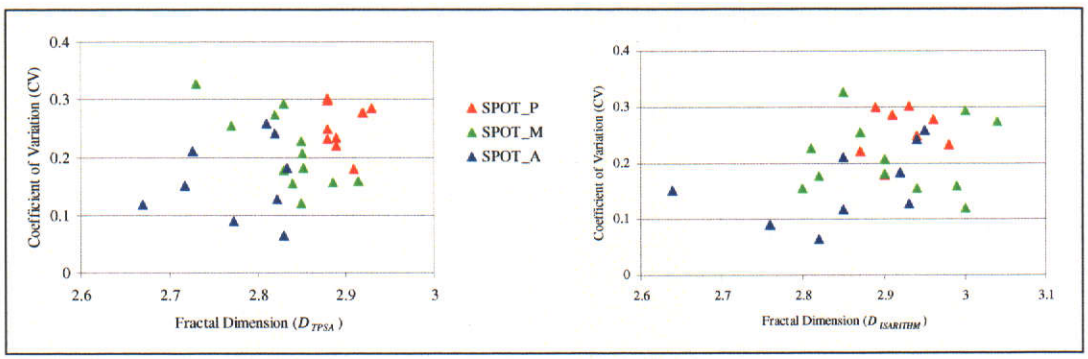

Figure 6.10 Scatter plot of the *D* and the coefficient of variation of SPOT on the study areas (SPOT_P: Perth; SPOT_M: Melville; SPOT_A: Armadale)

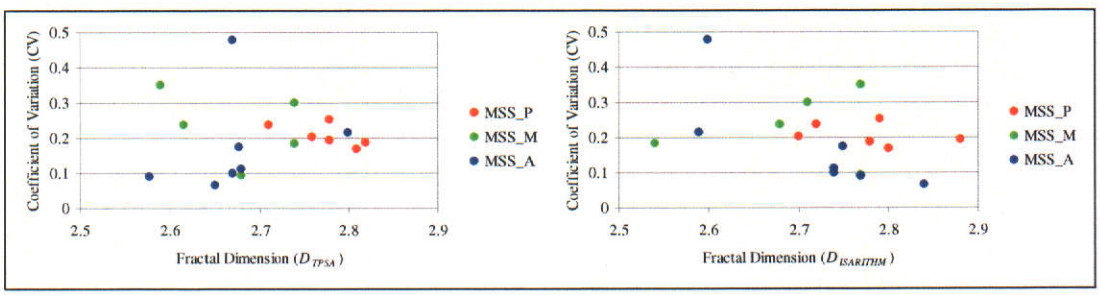

Figure 6.11 Scatter plot of the *D* and the coefficient of variation of Landsat MSS on the study areas (MSS_P: Perth; MSS_M: Melville; MSS_A: Armadale)

6. 5 Summary

This chapter described the analysis of spatial complexity of the study areas computed from the SPOT, Landsat-7 ETM+, and Landsat MSS using fractal measurement algorithms (e.g the TPSA and the isarithm) and Moran's *I* index of spatial autocorrelation measure. The discussions were focussed on the effect of land cover heterogeneity, spatial resolution and spectral location on spatial complexity, computed using the TPSA and isarithm algorithms. The performance of fractal measurement algorithms in measuring the spatial complexity was discussed. Finally, the relevance of statistical measures such as Moran's *I* index of spatial autocorrelation in characterising the spatial complexity of an urban landscape and its relationship with *D* was described.

The fractal dimension computed from the Landsat-7 ETM+, SPOT and Landsat MSS indicated that the City of Perth is spatially more complex than the City of Melville and the City of Armadale. A comparison of the fractal dimension among the study areas showed a cluster of high *D* values in the City of Perth indicating spatially very complex land covers over the study areas. On the contrary, variation of the *D* values (low to high) increases as the land cover compositions change to the City of Melville (e.g. medium urban) and the City of Armadale (e.g. urban fringe) indicating spatially heterogeneous to a more homogeneous pattern of land covers. The non-spatial statistical parameters such as the standard deviation and the coefficient of variation were found useful in describing the spectral variability of the subsets. This in turn could be used as part of the metadata for the images. It is important to note that these indices provided the variation of the pixel values regardless of their locations and thus, they did not bear any relationship to the spatial complexity.

The results of the green, red and NIR infrared bands of the subsets of the study areas showed that the D_{TPSA} and $D_{ISARITHM}$ were highest in SPOT (20m) followed by Landsat-7 ETM+ (25m) and Landsat MSS (50m). According to Cao and Lam (1997), for a non-fractal surface, *D* is expected to be lower as resolution gets coarser and spectral variability is reduced, which supports the findings of this study. Likewise, Emerson *et al.* (1999) found an increase in spatial complexity of urban areas with an increase in spatial resolution from an aggregated imagery (20- by 20 m, 40- by 40 m and 80- by 80 m) generated from a 10- by 10 m imagery. Operating on the assumption that the scale at which the highest fractal dimension is measured may be the scale at which most of the processes operate (Goodchild and Mark, 1987; Lam and Quattrochi, 1992), it could be concluded that the urban areas of the Perth metropolitan area are best represented by SPOT image, with a spatial resolution of 20m. This supports the findings reported by Small (2003), that the urban features are better characterised in a spatial scale (e.g. spatial resolution) which lies between 10 and 20 m.

The D_{TPSA} and $D_{ISARITHM}$ varied in the green, red and NIR bands of Landsat-7 ETM+, SPOT and Landsat MSS in all subsets of the study areas indicating the effect of spectral location on measuring spatial complexity. An examination of the D_{TPSA} and the $D_{ISARITHM}$ of the subsets indicated that the green and the red bands could be better

utilised in characterising the spatial complexity of urban areas, as higher D values were found in the green and the red bands of those subsets that represented urban areas (e.g. buildings and infrastructures). This is in conformity with the findings of many studies, where the fractal dimension of urban areas was found highest in the visible bands of Landsat TM (Quattrochi *et al.*, 2001; Qiu *et al.*, 1999; Quattrochi *et al.*, 1997; Lam, 1990). Likewise, working with hyperspectral images, Qiu *et al.* (1999) found that the largest contrast of fractal dimension between the urban and rural scenes was in the visible wavelength region. The results also demonstrated that the NIR band is better for characterising the spatial complexity of the vegetated areas.

An examination of the D computed from the TPSA and the isarithm method showed higher $D_{ISARITHM}$ values compared to the D_{TPSA}. This was attributed to the approach of the isarithm method which excludes few random pixels that have abnormally high values and thus, measures the major variation dominating the subsets, thereby yielding a higher D (Qiu *et al.*, 1999). The computational method of the isarithm method such as the row, the column and the row-column methods could be another source that contributes to a higher $D_{ISARITHM}$. In this analysis, the $D_{ISARITHM}$ computed from the row-column methods were used for minimising directional bias. This approach could underestimate the results of subsets that are actually aligned either row or column, which is common in an urban environment. In addition, selection of isarithm interval is an important factor as it determines the isarithm values, which affect the resultant $D_{ISARITHM}$ as reported by Clarke (1986) and Lam (1990). Following the suggestions of Lam *et al.* (2002) that the isarithm method is more accurate for D values ranging from 2.3 to 2.5, while for roughen surfaces (D of 2.7-2.9) the TPSA method is the best estimator, it could be concluded that the results of the D_{TPSA} of this study are more relevant as the D values were found higher than 2.5 for all subsets analysed.

Moran's I index of spatial autocorrelation was found positive (> 0.58) in all study areas indicating a clustered distribution. An examination of the results of the study areas showed that the higher the Moran's I, the lesser the fractal dimension, or in other words, the lower the spatial complexity. Thus, an urban landscape with a low Moran's I value, indicative of a random distribution will result in a high D value

indicating high spatial complexity. The correlation analysis between the Moran's *I* and the *D* revealed a strong negative correlation for spatially more complex land cover pattern as compared to a low to moderate correlation coefficient of an area which is spatially less complex. Thus, Moran's *I* could be used to characterise the spatial complexity of an area, which exhibits a higher *D* indicating a spatially more complex land cover pattern.

Chapter 7

LAND COVER HETEROGENEITY AND ITS EFFECT ON THE ACCURACY OF FUZZY CATEGORICAL MAPS

This chapter discusses the accuracy measures determined from the fuzzy error matrix of the fuzzy categorical maps generated by different fuzzy operators as discussed in Chapter 5. In addition to accuracy measures, uncertainty maps were used for assessing the performance of the fuzzy operators for generating fuzzy land cover maps. Furthermore, this chapter discusses the sources of classification error of individual land cover classes of the fuzzy categorical maps derived from the best fuzzy operator. Finally, the fuzzy categorical maps derived from the best fuzzy operator of the study areas are used to assess the effect of land cover heterogeneity on the accuracy measures.

7. 1 Accuracy Measures of Fuzzy Land Cover Maps of the City of Perth

7.1.1 Performance of Fuzzy Operators in Generating Fuzzy Land Cover Maps

The summary of accuracy measures derived from the fuzzy error matrices described in Section 5.3.3 of fuzzy AND, fuzzy OR, fuzzy algebraic product, fuzzy algebraic sum, and fuzzy gamma operators with γ values ranging from 0.1 to 0.95 of the City of Perth is presented in Table 7.1. A comparison of the accuracy measures reveals that the defuzzified memberships generated by the fuzzy gamma operator with a γ value of 0.95 exhibited the highest overall accuracy. The overall accuracy of the fuzzy gamma operator (γ = 0.95) was up to 52 percent higher than that of fuzzy AND, fuzzy OR, fuzzy algebraic product and fuzzy gamma operators with γ values ranging from 0.1 to 0.8, while 3 percent more accurate than the fuzzy algebraic sum and fuzzy gamma operator of 0.90. It is interesting to note that the producer's accuracy, which represents errors of omission of the defuzzified memberships of fuzzy AND and fuzzy algebraic product for all land cover classes was found low compared to high user's accuracy which is an expression of the errors of commission (Table 7.1).

Table 7.1 Summary of accuracy measures of the fuzzy land cover maps of the City of Perth

	Accuracy Measures	Forest	Grassland	Urban	Dense Urban
Fuzzy AND	Fuzzy Producer's Accuracy (%)	58	40	16	31
	Fuzzy User's Accuracy (%)	86	91	81	68
	Fuzzy Overall Accuracy (%)	40			
Fuzzy OR	Fuzzy Producer's Accuracy (%)	87	81	44	79
	Fuzzy User's Accuracy (%)	56	48	51	51
	Fuzzy Overall Accuracy (%)	74			
Fuzzy Algebraic Product	Fuzzy Producer's Accuracy (%)	54	26	10	20
	Fuzzy User's Accuracy (%)	89	92	81	73
	Fuzzy Overall Accuracy (%)	32			
Fuzzy Algebraic Sum	Fuzzy Producer's Accuracy (%)	90	78	63	84
	Fuzzy User's Accuracy (%)	58	46	73	52
	Fuzzy Overall Accuracy (%)	81			
Fuzzy Gamma Operation ($\gamma = 0.1$)	Fuzzy Producer's Accuracy (%)	56	28	11	22
	Fuzzy User's Accuracy (%)	88	91	81	72
	Fuzzy Overall Accuracy (%)	34			
Fuzzy Gamma Operation ($\gamma = 0.5$)	Fuzzy Producer's Accuracy (%)	66	42	22	40
	Fuzzy User's Accuracy (%)	85	88	86	73
	Fuzzy Overall Accuracy (%)	47			
Fuzzy Gamma Operation ($\gamma = 0.7$)	Fuzzy Producer's Accuracy (%)	74	56	39	57
	Fuzzy User's Accuracy (%)	83	84	81	73
	Fuzzy Overall Accuracy (%)	60			
Fuzzy Gamma Operation ($\gamma = 0.8$)	Fuzzy Producer's Accuracy (%)	81	67	53	70
	Fuzzy User's Accuracy (%)	82	79	78	72
	Fuzzy Overall Accuracy (%)	70			
Fuzzy Gamma Operation ($\gamma = 0.9$)	Fuzzy Producer's Accuracy (%)	88	79	70	84
	Fuzzy User's Accuracy (%)	79	70	70	67
	Fuzzy Overall Accuracy (%)	81			
Fuzzy Gamma Operation ($\gamma = 0.95$)	Fuzzy Producer's Accuracy (%)	91	82	73	86
	Fuzzy User's Accuracy (%)	73	61	61	62
	Fuzzy Overall Accuracy (%)	84			

On the other hand, the defuzzified memberships of fuzzy OR and fuzzy algebraic sum exhibited to a high producer's accuracy for all land cover classes, as compared to a low user's accuracy. For the fuzzy gamma operator, as the γ value increases, there is an increase in producer's accuracy with decreasing user's accuracy. The results in Table 7.1 show that the defuzzified memberships generated by the fuzzy gamma operator ($\gamma = 0.90$) offer the most appropriate balance between producer's

and user's accuracy, as compared to the categorical accuracy measures of the gamma values of 0.1 to 0.8 and 0.95.

An examination of the accuracy measures of the defuzzified land cover maps derived from fuzzy AND reveals that the omission errors related to producer's accuracy are very high. In addition to sources of disagreement discussed later, this can be justified by the fact that fuzzy AND underestimates the memberships as it selects the minimum fuzzy membership value among the fuzzified Landsat-7 ETM+ bands in each location of the fuzzy categorical maps. Tables 7.2 shows that the mean fuzzy membership values of the land cover classes of fuzzy AND are smallest compared to the mean values of the fuzzy memberships of fuzzy OR, fuzzy algebraic product, fuzzy algebraic sum and gamma operators with γ values ranging from 0.1 to 0.95. A comparison between the mean fuzzy membership values generated by the fuzzy AND and the fuzzy reference data showed that the mean fuzzy membership of class forest was 68 percent lower than the fuzzy memberships collected in the field, as described in Section 5.3.1, while the classes grassland, urban and dense urban were found up to 95 percent lower than the ground recorded fuzzy values. The conservative estimation of fuzzy memberships produced high omission errors.

Table 7.2 Mean fuzzy membership values of the fuzzy categorical maps generated by fuzzy operators

	Forest	Grassland	Urban	Dense Urban
	Mean	Mean	Mean	Mean
Fuzzy AND	0.25	0.03	0.07	0.09
Fuzzy OR	0.97	0.95	0.94	0.94
Fuzzy Algebraic Product	0.51	0.08	0.07	0.14
Fuzzy Algebraic Sum	0.99	0.96	0.94	0.94
Fuzzy Gamma Operation ($\gamma = 0.8$)	0.76	0.38	0.45	0.57
Fuzzy Gamma Operation ($\gamma = 0.9$)	0.85	0.59	0.66	0.74
Fuzzy Gamma Operation ($\gamma = 0.95$)	0.91	0.75	0.80	0.85

The uncertainty map generated for each fuzzy operator using the confusion index described in Section 5.3.4 show the existence of a large number of uncertain regions,

indicative of the distribution of misclassification, which could also be attributed to high omission and commission errors (Appendix 17).

On the other hand, fuzzy OR considers the highest membership among the layers being integrated. Table 7.2 shows that the mean fuzzy memberships of all land cover classes considered are larger than the mean fuzzy memberships derived for fuzzy AND. This contributed to a high overall accuracy (74 percent), which was 34 percent higher than the overall accuracy achieved by using fuzzy AND. Among the categorical accuracy measures, the user's accuracy of all land cover classes was found to be low, indicating high commission errors. Likewise, the producer's accuracy of the class urban was found to be low compared to forest, grassland and dense. This could be attributed to the lack of compensation of information among the selected bands since fuzzy OR utilised a single fuzzy value of the selected Landsat-7 ETM+ bands (e.g. the output membership is controlled by the maximum value of the input bands) and accordingly, misclassification occurred.

Likewise, the fuzzy algebraic product tends to produce small values resulting in a conservative estimate of fuzzy memberships (Bonham-Carter, 1994). Accordingly, high omission errors occurred which contributed to a low overall accuracy (32 percent). The uncertainty map generated using the confusion index indicates a substantial uncertain region showing the distribution of misclassification (Appendix 17). The accuracy measures of the fuzzy algebraic sum are encouraging as it exhibited an overall accuracy of 81 percent (Table 7.1). Two reasons can be attributed to this high overall accuracy. Firstly, the compensation of information, as the fuzzy algebraic sum considers all fuzzy memberships of the selected bands and secondly, the tendency of generating 'increasive' membership (Bonham-Carter, 1994). This can be seen in Table 7.2 which reveals that the mean fuzzy memberships of all land cover classes produced from the fuzzy algebraic sum are up to 92 percent larger than the mean fuzzy memberships computed from fuzzy AND and the fuzzy algebraic product. However, the user's accuracy of the land cover classes particularly for forest, grassland and dense urban was found to be low, indicating high commission errors.

The overall accuracy of the defuzzified memberships generated by the fuzzy gamma operator with γ values ranging from 0.1 to 0.95 increases from 34 percent to 84

percent (Table 7.1). This can be seen from the uncertainty maps, produced using gamma operators with γ values of 0.1, 0.5 and 0.8 (Appendix 17e, 17i and 7l), which indicate that the confusion index decreases as the γ value increases. The decreasing trend of the confusion index is assumed to be related to an improvement in classification accuracy. An examination of the uncertainty maps indicates that uncertain regions generated by a fuzzy gamma operator of 0.1 present a confusion index above 0.8, and occupy about 48 percent of the total study area. These uncertain areas decrease to 34 percent for a gamma operator of 0.5, and 25 percent for a gamma operator of 0.8.

In addition to the overall accuracy measures, the results of fuzzy gamma operator with γ values ranging from 0.9 to 0.95 are encouraging as their categorical accuracy measures were found more accurate compared to the results of fuzzy algebraic sum (Table 7.1). Despite a fuzzy gamma value of 0.95 achieving a higher overall accuracy than that of γ value equal to 0.9, the user's accuracy obtained using a γ value of 0.90 was found to be much higher than that produced by a γ value of 0.95, indicating a lowering of the commission errors. This improvement in the categorical accuracy measures can be attributed to an appropriate estimation of fuzzy memberships in all classes by the fuzzy gamma operator ($\gamma = 0.90$). On the contrary, the fuzzy gamma operator ($\gamma = 0.95$) overestimated the fuzzy memberships in all classes, which in turn contributed to increased total membership grades in the classified data and the diagonal of the fuzzy error matrix respectively (Appendix 14k). As the total membership grades of the reference data remain the same for all fuzzy operators, the increased membership grades of the diagonal of the fuzzy error matrix contributed to a higher producer's and overall accuracy as compared to a lower user's accuracy (see Section 3.4.4.4 for details). The lower user's accuracy resulted in high commission errors in all classes as compared to a γ value of 0.90. Therefore, the integrated fuzzy memberships generated by a γ value of 0.90 from the selected Landsat-7 ETM+ bands was considered to be the most appropriate. The fuzzy memberships of the land cover classes of the City of Perth generated from γ value of 0.90 are shown in Figure 7.1.

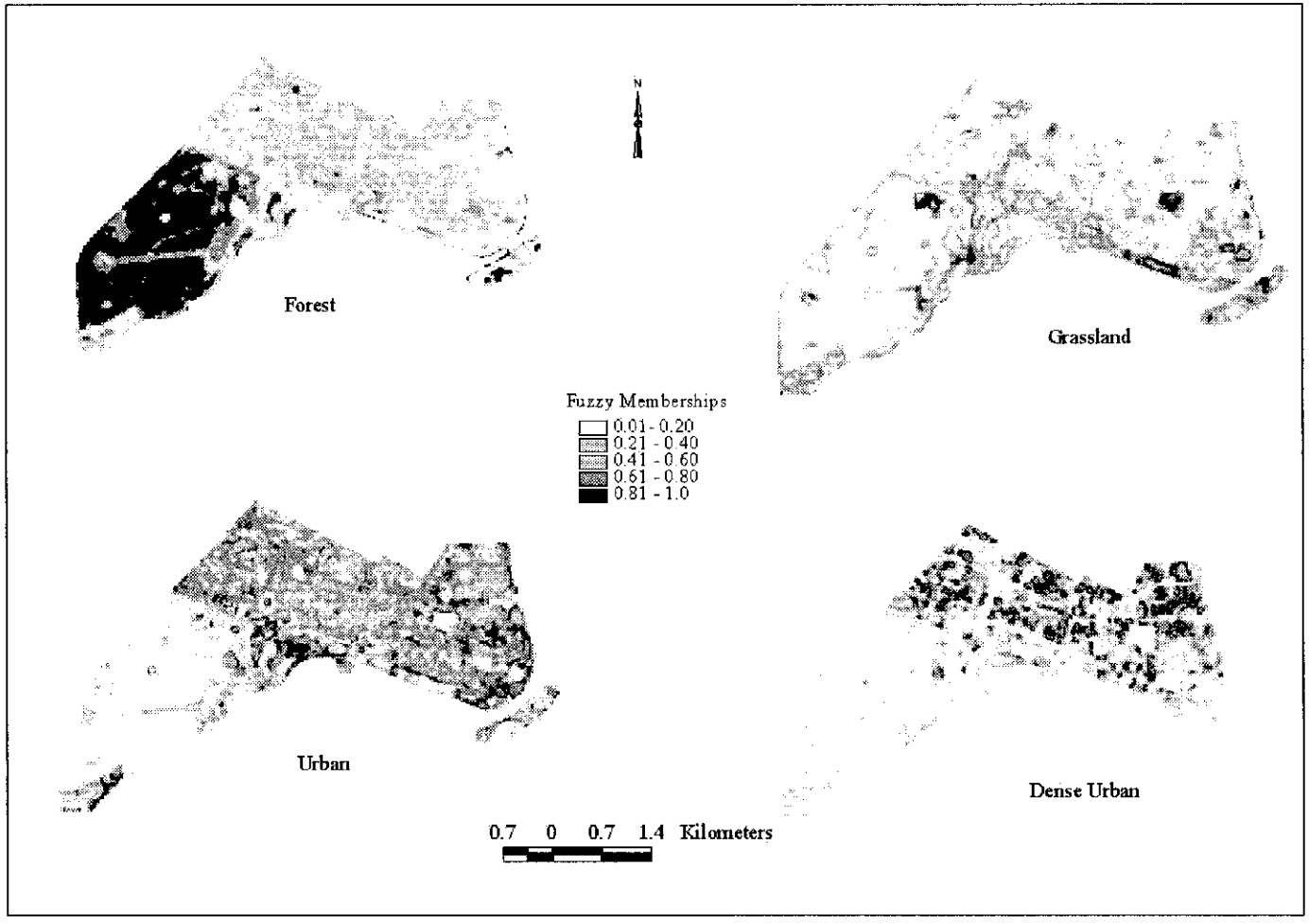

Figure 7.1 Fuzzy membership maps of the land cover classes generated by the fuzzy gamma operator ($\gamma = 0.90$) of the City of Perth

7.1.2 Sources of Classification Errors

The uncertainty map generated using the confusion index derived from the fuzzy memberships of the classes forest, grassland, urban and dense urban of the fuzzy gamma operator ($\gamma = 0.90$) is presented in Figure 7.2. This figure shows a higher uncertainty in the central business district as compared to a low uncertainty in the Kings Park and Botanic Garden area, comprised of forested area. The spatial pattern of the uncertain region determined by the confusion index indicates that the higher uncertainty occurs near boundaries, where transition zones and geographical complexities are encountered (e.g. roads in the forested area, edges between forest and urban area, edges between grassland and urban area) mainly due to the mixture of more than one land cover class within a pixel. Moran's *I* index was computed on the confusion index, resulting in a value of 0.39.

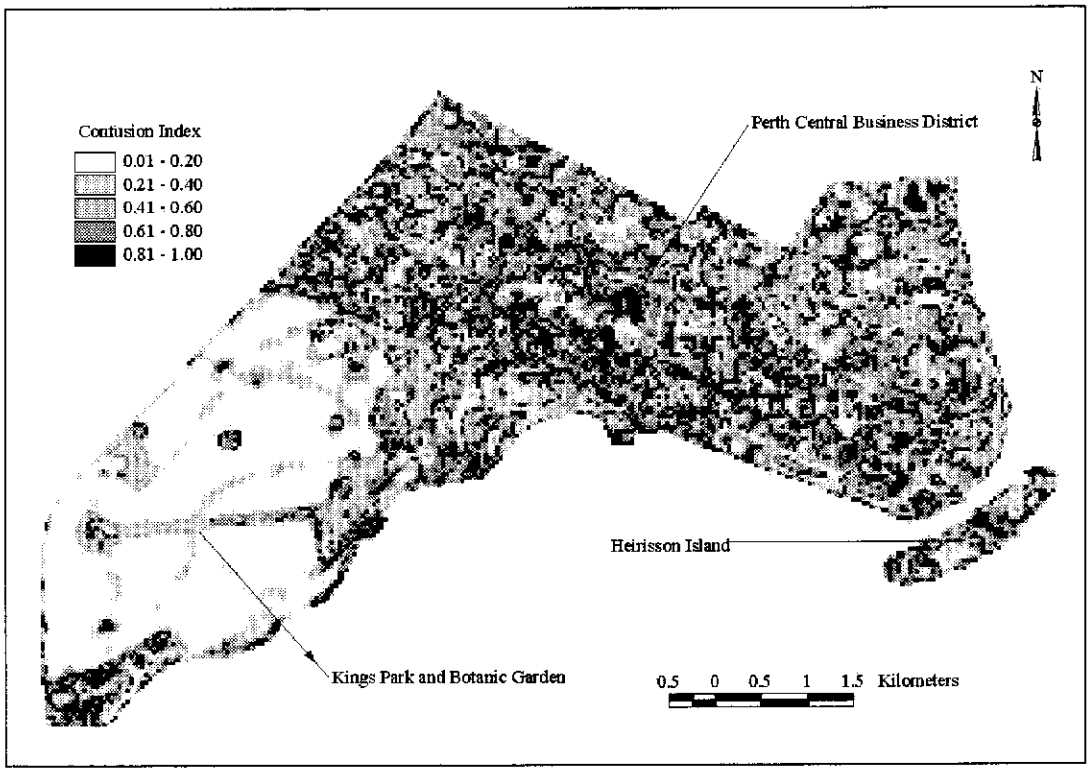

Figure 7.2 Uncertainty map showing the confusion index derived from fuzzy categorical maps of the City of Perth

This value indicates a moderate spatial autocorrelation of the confusion index computed over the entire study area. It indicates that nearby (or connected) pixels tend to present similar values.

An examination of the producer's accuracy of the defuzzified map generated by fuzzy gamma operator with γ value of 0.90 reveals accuracies above 79 percent for forest, grassland and dense urban classes. Among the land cover classes, a relatively high omission error (30 percent) occurred in the class urban which was mostly confused with dense urban and grassland (Appendix 14j). A significant disagreement was found in the user's accuracy between the defuzzified land cover maps and field data for grassland, urban and dense urban classes. The user's accuracy of these classes tended to be between 67 percent and 70 percent indicating a notably high commission error. The commission error of the class grassland (30 percent) could be attributed to wrong allocation of pixels corresponding to the classes forest and urban as grassland. Similar variations of commission error were found for urban and dense urban. The maximum commission error found for the class dense urban (33 percent), mostly corresponded to a wrong inclusion within the class urban.

Several sources of disagreement between the defuzzified map and the reference data were identified. Firstly, a possible source of disagreement between the class grassland and forest may be due to a similar spectral response of native vegetation that composes the forest and grassland classes. As mentioned in Chapter 4, the class grassland of the City of Perth is characterised by a mixture of grass, shrubs and occasional native plants. This is reflected in the fuzzy error matrix corresponding to a γ value of 0.90 in Appendix 14(j), which shows that the omission error of class forest is mostly contributed by a misclassification as grassland, which in turn results in a high commission error for the class grassland. Likewise, the omission errors of class grassland were mostly due to its labelling as forest, which resulted in high commission errors in the class forest.

Secondly, the seasonal effect on the spectral behaviour of the class grassland, as the satellite imagery was acquired during summer, when grassland and some shrubs tend to dry up due to lack of rainfall in the area. This can be seen in Table 4.1 and Figure 4.4, which show that most rainfall occurs in winter, with an average monthly rainfall of 125.62 mm, as compared to 3.49 mm in summer. Accordingly, the spectral responses of the class grassland and sparse forest tend to be similar to soils (e.g. reduction of the characteristic absorption feature of vegetation in the red region of

the spectrum and high reflectance in the NIR) and other man-made features, which may lead to a labelling as urban. For example, the north-east corner of the recreational island (Heirisson island), separated from the City by the Swan River in Figure 7.3 (a) shows higher fuzzy memberships for class urban, as compared to class grassland and forest. However, a randomly selected sample of this area indicates that the land covers are comprised of grass, shrubs and native plants as shown in Figure 7.3 (d). Accordingly, the field-collected fuzzy membership of this randomly selected sample was highest for the class grassland, resulting in a classified image with a high omission error for the class grassland and commission error for class urban. The confusion index of the same sample in the uncertainty map in Figure 7.3 (b) was found to be 0.99, indicating high uncertainty. An examination of the fuzzy categorical maps in Figure 7.1 indicated that the fuzzy membership of class urban is equal to 0.54, as compared to a fuzzy membership of 0.53 of class grassland, which resulted in a confusion index of 0.99 (e.g. high uncertainty).

Similarly, a randomly selected sample of an open space comprised of grassland and shrubs in the north-western part of the study area (Figure 7.4a) was classified in the field as grassland because of this being the dominant land cover (Figure 7.4c). An examination of the fuzzy categorical maps indicated that the highest fuzzy membership for same location corresponded to the class urban followed by dense urban, grassland and forest. It is assumed that the spectral response of dry grass and shrubs was similar to built-up areas, leading to a misclassification as urban. Appendix 14(j) shows that the omission errors of forest and grassland were mostly due to an inclusion of these areas in the class urban.

On the contrary, grasslands that are well managed (e.g. watering system) remain green during summer and their spectral response resembles that of healthy vegetation and accordingly, showed the highest membership degree to that class. For example, the fuzzy memberships of grasslands covering Wellington Square and Langley Park (Chapter 4) were high compared to other land cover classes, which can be seen in Figure 7.5. Furthermore, these two areas show a low confusion index as shown in Figure 7.5(b). Another significant source of disagreement may result from the spectral similarity between urban and dense urban, which led to misclassification.

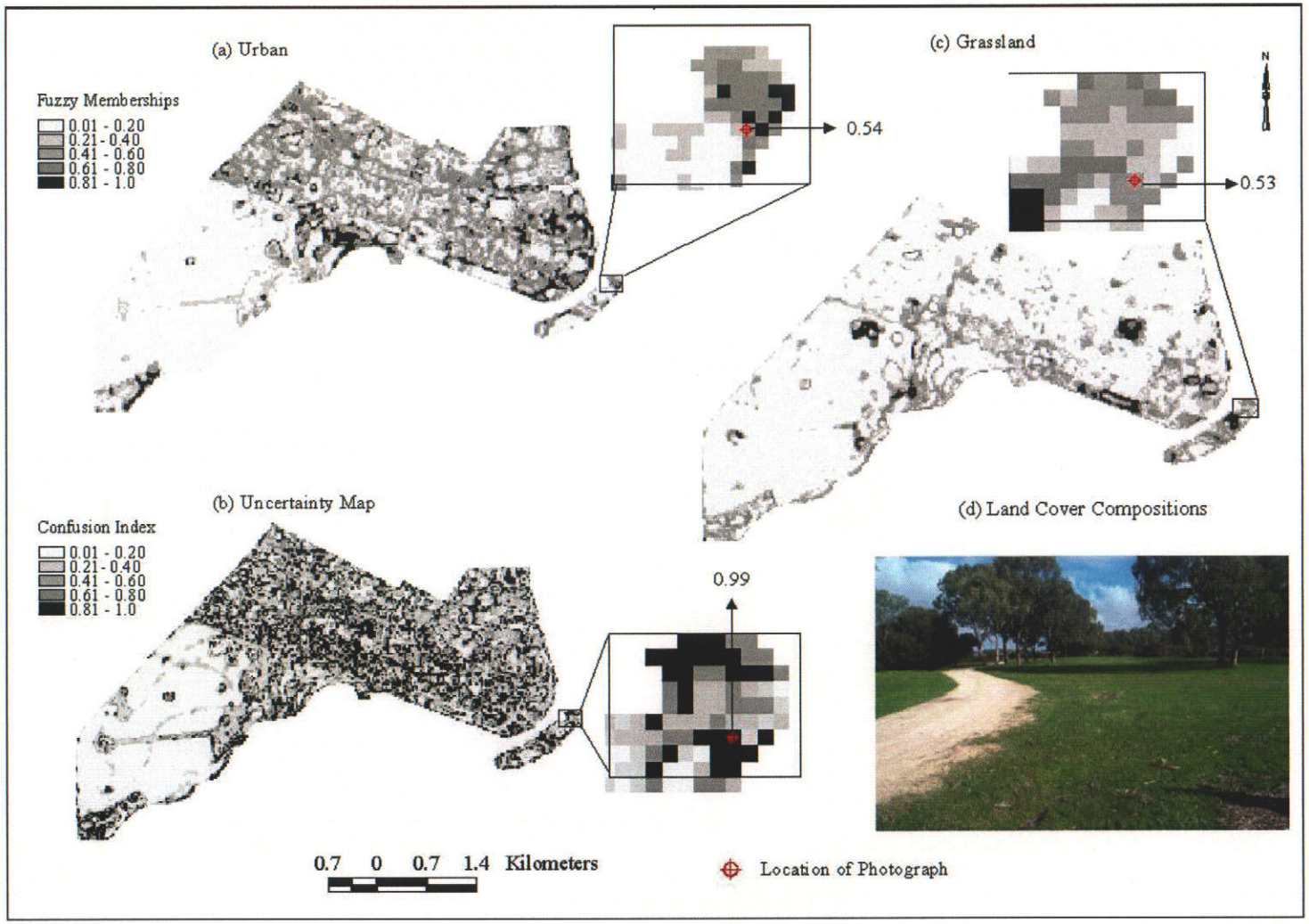

Figure 7.3 Uncertainty map and fuzzy membership maps of a misclassified sample of the class grassland to class urban

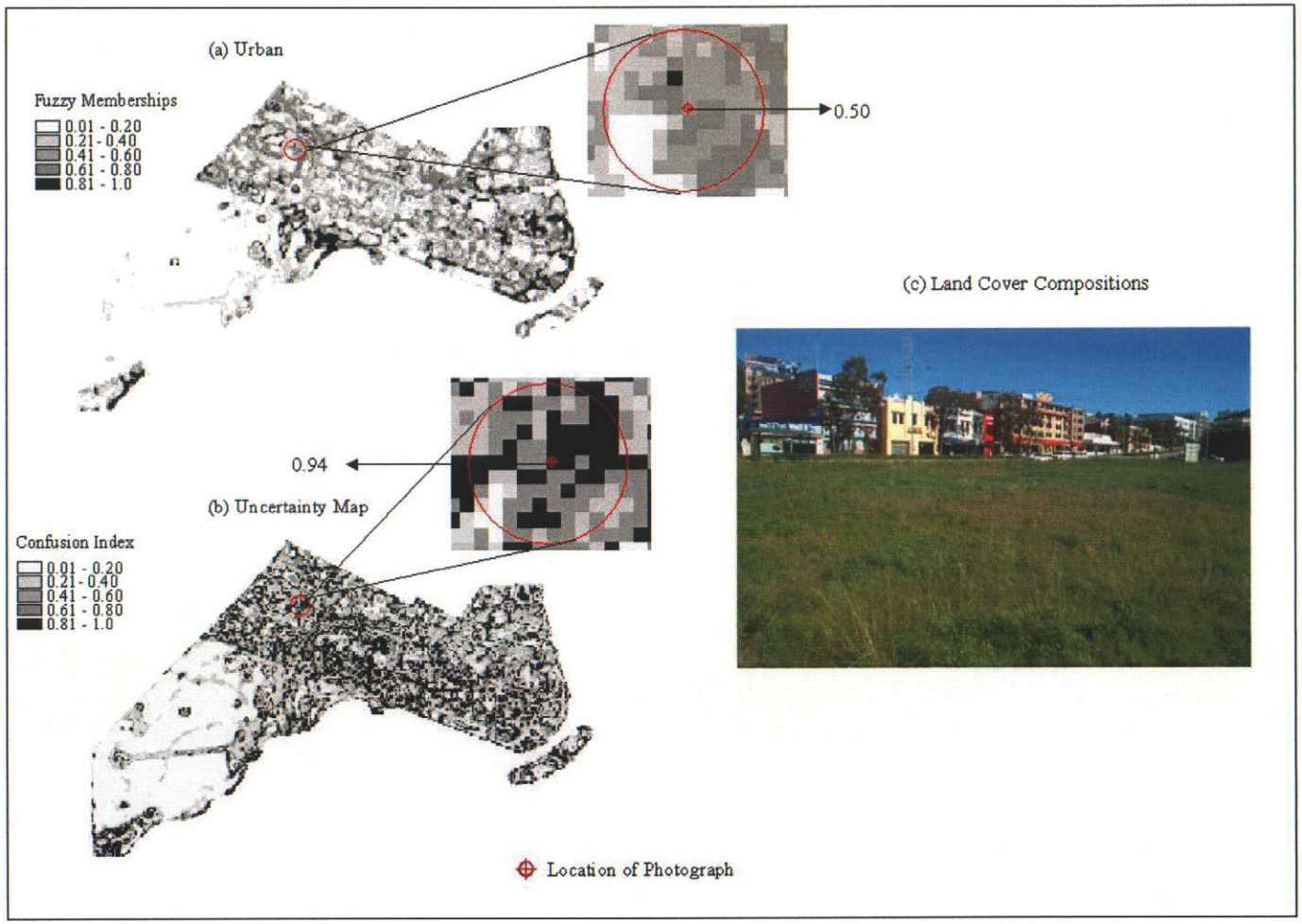

Figure 7.4 Uncertainty map and fuzzy membership maps of a misclassified sample of the class grassland to class urban

This can be seen in Appendix 14(j), which shows that the omission errors of the classes urban and dense urban were mostly due to a misclassification between these classes.

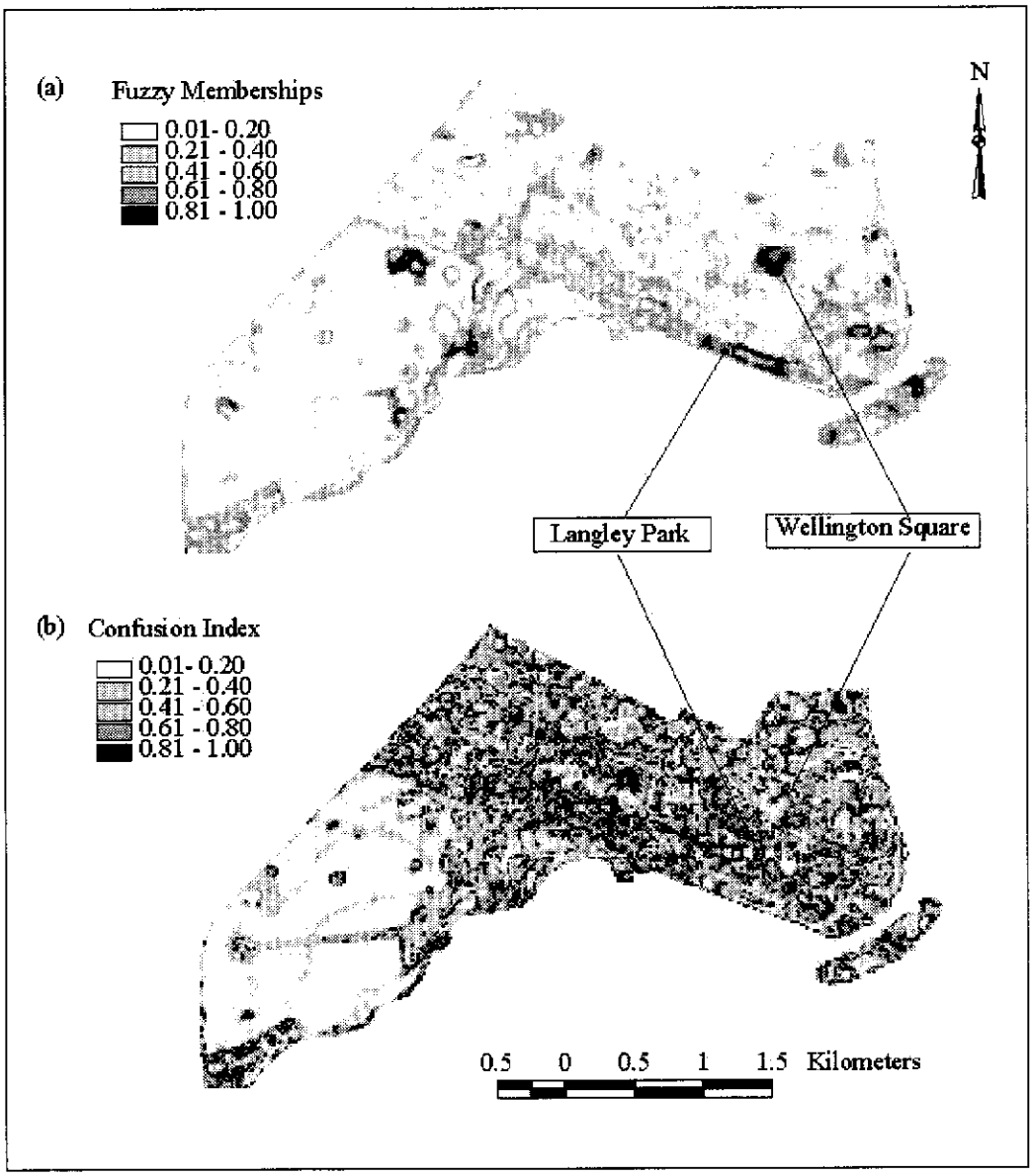

Figure 7.5 Fuzzy memberships map (a) and uncertainty map (b) of the class grassland

7. 2 Accuracy Measures of Fuzzy Land Cover Maps of the City of Melville

7.2.1 Performance of Fuzzy Operators in Generating Fuzzy Land Cover Maps of the City of Melville

The summary of accuracy measures derived from the fuzzy error matrices of different fuzzy operators of the City of Melville is presented in Table 7.3. An examination of the results indicates that a fuzzy gamma operator ($\gamma = 0.95$) exhibited the highest overall accuracy. The overall accuracy of the fuzzy gamma operator ($\gamma = 0.95$) was up to 44 percent higher than the fuzzy algebraic product, fuzzy AND and fuzzy gamma operators with γ values ranging from 0.1 to 0.8, while 2 percent more accurate than the fuzzy algebraic sum and fuzzy gamma operator ($\gamma = 0.90$) and 1 percent more accurate than fuzzy OR (Table 7.3). Similar to the results obtained for the City of Perth, the user's accuracy of fuzzy OR and fuzzy algebraic sum for all land cover classes was found to be low, as compared to a relatively higher producer's accuracy (Table 7.3). On the other hand, the defuzzified memberships resulting from the use of fuzzy AND and fuzzy algebraic product exhibited a high user's accuracy for all land cover classes, as compared to a low producer's accuracy. For the fuzzy gamma operator, as the γ value increased, there was an increase in producer's accuracy with decreasing user's accuracy. Clearly, the results of gamma operators with γ values ranging from 0.1 to 0.95 balance the categorical accuracy measures and accordingly, offers the best fuzzy gamma operator with optimum accuracy measures.

An examination of the results derived from fuzzy AND and fuzzy algebraic product reveals a trend similar to the overall and categorical accuracy measures obtained for the City of Perth. The low producer's accuracy of fuzzy AND and fuzzy algebraic product (see Table 7.3) indicates high omission errors in all categories, along with a low overall accuracy. Although fuzzy algebraic product compensates for the information among the selected bands to be integrated, the underestimation of the fuzzy memberships by this operator results in a low overall and producer's accuracy. On the contrary, the overall accuracy of fuzzy OR and fuzzy algebraic sum was found to be 68 percent and 67 percent respectively. However, the user's accuracies of fuzzy OR for all categories were relatively low indicating high commission errors along with low producer's accuracy for the class dense urban. This could be

attributed to the lack of compensation of information among the selected bands, as this operator is controlled by a single value (i.e. the maximum fuzzy membership) of the selected bands of Landsat-7 ETM+.

Table 7.3 Summary of accuracy measures of the fuzzy land cover maps of the City of Melville

	Fuzzy Accuracy Measures	Forest	Grassland	Urban	Dense Urban
Fuzzy AND	Fuzzy Producer's Accuracy (%)	40	36	34	39
	Fuzzy User's Accuracy (%)	85	76	60	75
	Fuzzy Overall Accuracy (%)	36			
Fuzzy OR	Fuzzy Producer's Accuracy (%)	61	74	70	53
	Fuzzy User's Accuracy (%)	70	52	53	49
	Fuzzy Overall Accuracy (%)	68			
Fuzzy Algebraic Product	Fuzzy Producer's Accuracy (%)	31	21	23	31
	Fuzzy User's Accuracy (%)	90	82	58	74
	Fuzzy Overall Accuracy (%)	25			
Fuzzy Algebraic Sum	Fuzzy Producer's Accuracy (%)	57	72	68	66
	Fuzzy User's Accuracy (%)	55	52	47	51
	Fuzzy Overall Accuracy (%)	67			
Fuzzy Gamma Operation ($\gamma = 0.1$)	Fuzzy Producer's Accuracy (%)	32	24	25	32
	Fuzzy User's Accuracy (%)	89	82	59	74
	Fuzzy Overall Accuracy (%)	27			
Fuzzy Gamma Operation ($\gamma = 0.5$)	Fuzzy Producer's Accuracy (%)	42	41	37	40
	Fuzzy User's Accuracy (%)	84	77	59	73
	Fuzzy Overall Accuracy (%)	40			
Fuzzy Gamma Operation ($\gamma = 0.7$)	Fuzzy Producer's Accuracy (%)	52	53	48	48
	Fuzzy User's Accuracy (%)	82	72	58	73
	Fuzzy Overall Accuracy (%)	51			
Fuzzy Gamma Operation ($\gamma = 0.8$)	Fuzzy Producer's Accuracy (%)	58	60	57	55
	Fuzzy User's Accuracy (%)	80	67	58	73
	Fuzzy Overall Accuracy (%)	58			
Fuzzy Gamma Operation ($\gamma = 0.9$)	Fuzzy Producer's Accuracy (%)	65	68	67	62
	Fuzzy User's Accuracy (%)	76	62	56	70
	Fuzzy Overall Accuracy (%)	67			
Fuzzy Gamma Operation ($\gamma = 0.95$)	Fuzzy Producer's Accuracy (%)	66	71	70	65
	Fuzzy User's Accuracy (%)	70	58	53	67
	Fuzzy Overall Accuracy (%)	69			

Likewise, the user's accuracy for all categories of the defuzzified map of the fuzzy algebraic sum were found low indicating high commission error which could be attributed to overestimation of the fuzzy memberships by the operator.

Tables 7.3 shows that the overall accuracy of the defuzzified maps generated by the fuzzy gamma operator with γ values ranging from 0.1 to 0.95, increases from 27 percent to 69 percent. The increased accuracy was attributed to the compensation of information of the selected bands of the Landsat-7 ETM+ bands along with increased memberships for a distinctive fuzzy set of the classified data. This can be seen on the uncertainty maps of the gamma operators with γ values of 0.1, 0.5 and 0.8 (Appendix 18), which indicate that the uncertain regions decrease as the γ value increases and accordingly, the accuracy increases. The results produced by the fuzzy gamma operator ($\gamma = 0.95$) show the overall and categorical accuracy measures to be higher, as compared to the results of fuzzy algebraic sum and fuzzy OR. Therefore, the integrated fuzzy memberships generated by the fuzzy gamma operator ($\gamma = 0.95$) were considered to be most appropriate for the City of Melville. The fuzzy memberships of fuzzy categorical maps generated by the fuzzy gamma operator ($\gamma = 0.95$) are shown in Figure 7.6.

7.2.2 Sources of Classification Errors

The confusion index derived from the fuzzy categorical maps of the fuzzy gamma operator ($\gamma = 0.95$) of the City of Melville is presented in Figure 7.7. This figure shows that the uncertainty is evenly distributed over the study area indicating a large number of mixed pixels and spectrally similar land cover classes. Moran's *I* index computed on the confusion index was found to be 0.28, indicating a greater dissimilarity between uncertainty values of connected areas (e.g. adjacent pixels), as compared to the result for the City of Perth.

An examination of the categorical accuracy measures of the defuzzified map generated by the fuzzy gamma operator ($\gamma = 0.95$) reveals accuracies above 65 percent for classes forest and dense urban. The omission errors of the class dense urban correspond mostly to an inclusion of these areas within the class urban, while the class forest was mostly confused with grassland and urban areas. Likewise, omission errors occurred in class grassland due to inclusion of these areas within the class urban, while the commission errors of class urban were due to the inclusion of these areas within the class grassland.

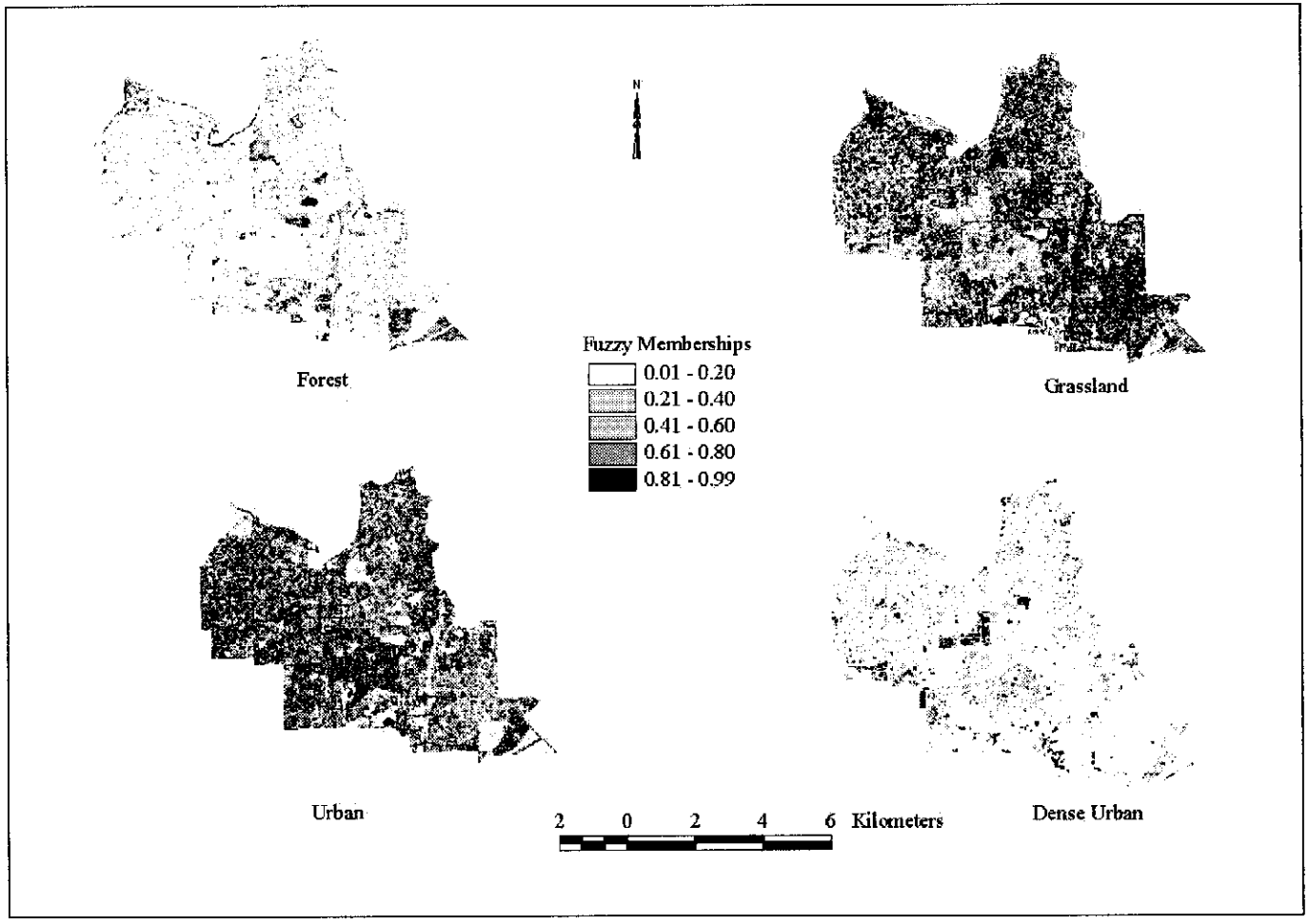

Figure 7.6 Fuzzy membership maps of the land cover classes generated by the fuzzy gamma operator ($\gamma = 0.95$) of the City of Melville

A significant disagreement was found in the user's accuracy between the defuzzified land cover maps and field data for the classes grassland and urban. The user's accuracies of these classes were found to be 58 percent and 53 percent respectively, indicating high commission errors (Table 7.3).

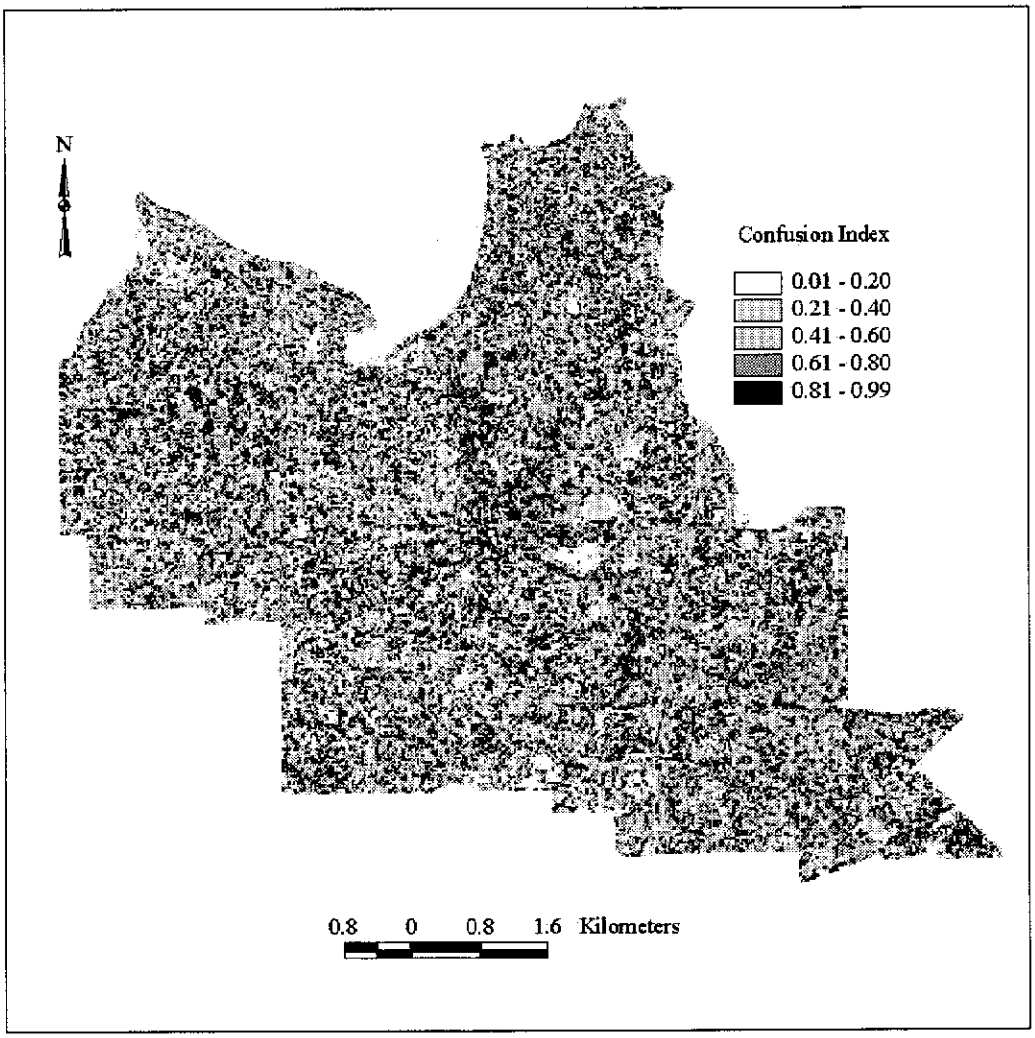

Figure 7.7 Uncertainty map showing the confusion index derived from fuzzy categorical maps of the City of Melville

The fuzzy error matrix (Appendix 15k) shows the commission errors of the class grassland were mainly due to misclassification of urban areas as grassland, while the commission error of the class urban is determined by an inclusion of areas of grassland, forest and dense urban into urban.

Mixed pixels were another source of disagreement between classified and reference data. It is important to note that some major roads (such as freeways and highways) and residential areas are surrounded by sparse trees and grassland, resulting in a

spectral dominance of these land features over urban areas, and consequently an erroneous labelling as grassland or forest. This can be seen in Figure 7.8 (a), which shows a residential block comprised of sparse trees and grassland. According to the dominant land cover, during the field work the highest fuzzy membership was assigned to the class urban. The fuzzy membership of the defuzzified output classification indicates that the same location belongs to the class grassland, thus originating an error of omission. An examination of the fuzzy categorical maps showed a fuzzy membership value of 0.80 for the class grassland (Figure 7.8b), as compared to a fuzzy membership of 0.63 for the class urban. Though the fuzzy classifier correctly identified the two dominant land cover types occurring within the pixel, this resulted in a confusion index of 0.82 indicating high uncertainty between the classes urban and grassland (Figure 7.8c).

Figure 7.9 shows another example of misclassification between urban and grassland given their mixed occurrence within a pixel. An examination of the fuzzy categorical maps showed that the fuzzy memberships of class urban and class grassland were 0.59 and 0.80 respectively, indicating high uncertainty (Figure 7.9b). Based on the dominant land cover, the highest fuzzy membership assigned to the field-collected sample was to class urban, producing an omission error in the class urban and commission error in the class grassland as can be seen in Appendix 15(k). The high level of mixing of the land covers within a pixel and the spectral dominance of one of these land covers causes wrong labelling and accordingly, the occurrence of commission and omission errors. This indicates that the residential areas of the City of Melville are more heterogeneous (e.g. higher mixed components within a pixel) as compared to less heterogeneous areas of the City of Perth, with less mixture of land cover components within a pixel. Thus, the presence of mixed pixels in the City of Melville contributed to a significant misclassification (Appendix 15j), which could be the reason for a lower overall accuracy, as compared to the City of Perth.

Another source of disagreement could be the similar spectral response of native vegetation characterising forest and grassland areas. As mentioned in Chapter 4, the class grassland of the City of Melville is characterised by a mixture of grass, shrubs and occasional native plants.

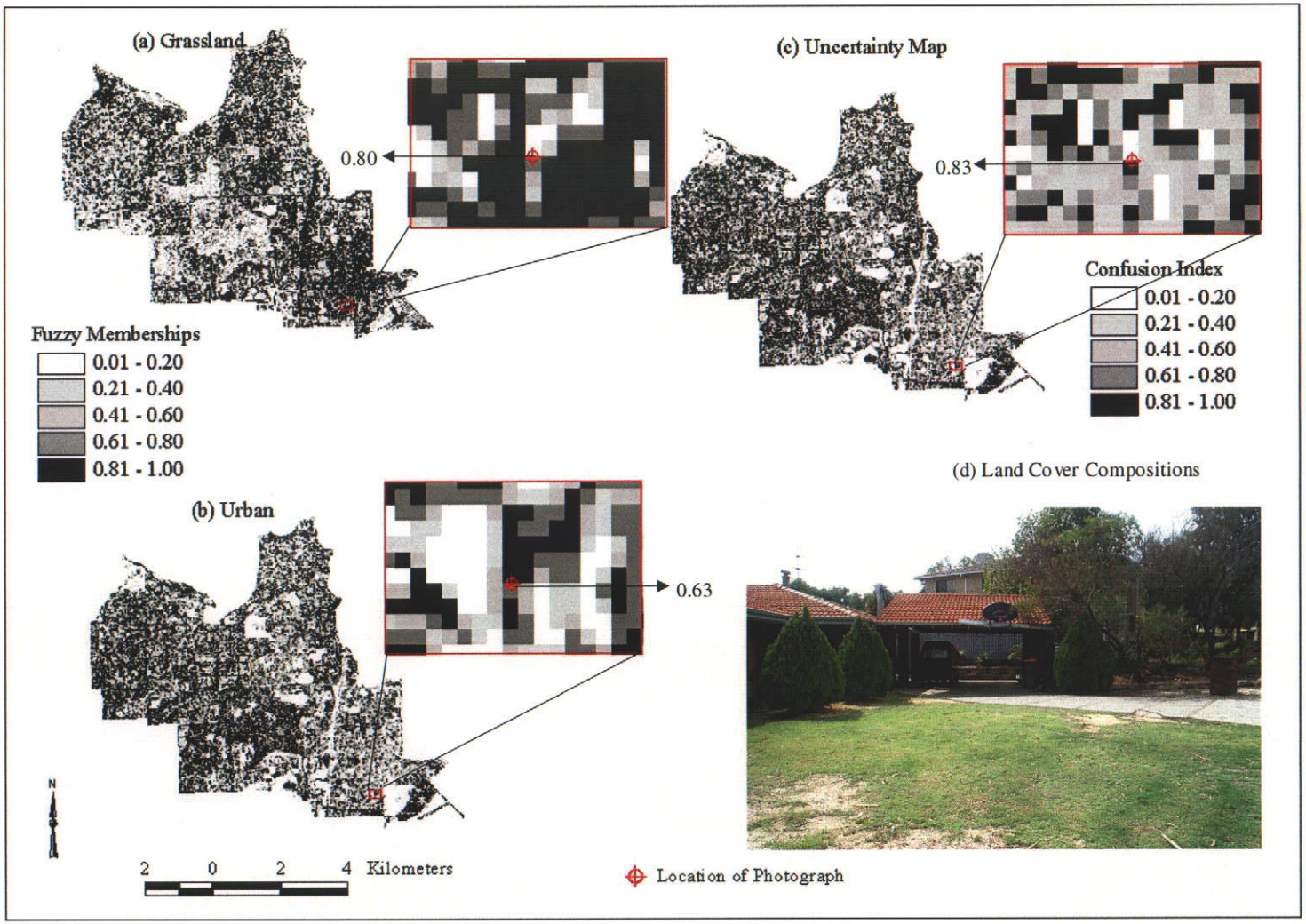

Figure 7.8 Uncertainty map and fuzzy membership maps of a misclassified sample of the class urban to grassland

This could be a source of misclassification of the class grassland as forest. Appendix 15(k) shows that the commission error of the class grassland was mainly due to the misclassification of class forest as grassland.

The seasonal effect on the spectral behaviour of the class grassland could be another source of misclassification. As the satellite imagery was acquired during summer, the spectral response of grassland and some shrubs tend to be similar to soils and other man-made features, which in some areas may lead to their labelling as urban. For example, Figure 7.10 shows an open space comprised of grassland and few trees, which was found during the field visit and accordingly, the highest field derived fuzzy membership was assigned to the class grassland. An examination of the fuzzy categorical maps of the same sample in Figure 7.10 shows this area being labelled as urban because it exhibits the highest fuzzy membership degree to the urban class, followed by the class grassland. The uncertainty map shows a confusion index of 0.66 for this area.

Likewise, Figure 7.10 shows an open space comprised of grassland from a randomly selected sample. The fuzzy classifier assigned the urban label to this sample as it exhibited the highest fuzzy membership to this fuzzy set. Appendix 15(k) shows that the omission errors are mostly due to an inclusion of grassland areas into the class urban. The misclassification of class grassland as urban caused commission errors in class urban (Appendix 15k). Another source of disagreement could be attributed to changes that took place between the acquisition of satellite data, which were acquired in December 2001 and field visits that were undertaken in May 2003. For example, Figure 7.11 shows bare ground as a result of the removal of grassland and trees prior to a residential development and accordingly, the highest fuzzy membership was assigned to class urban. An examination of the fuzzy categorical maps as shown in Figure 7.11 indicates that same location was assigned the highest fuzzy membership to the class grassland, resulting in an error of omission. Lastly, as with the City of Perth, another source of disagreement may result from the spectral similarity between the classes urban and dense urban.

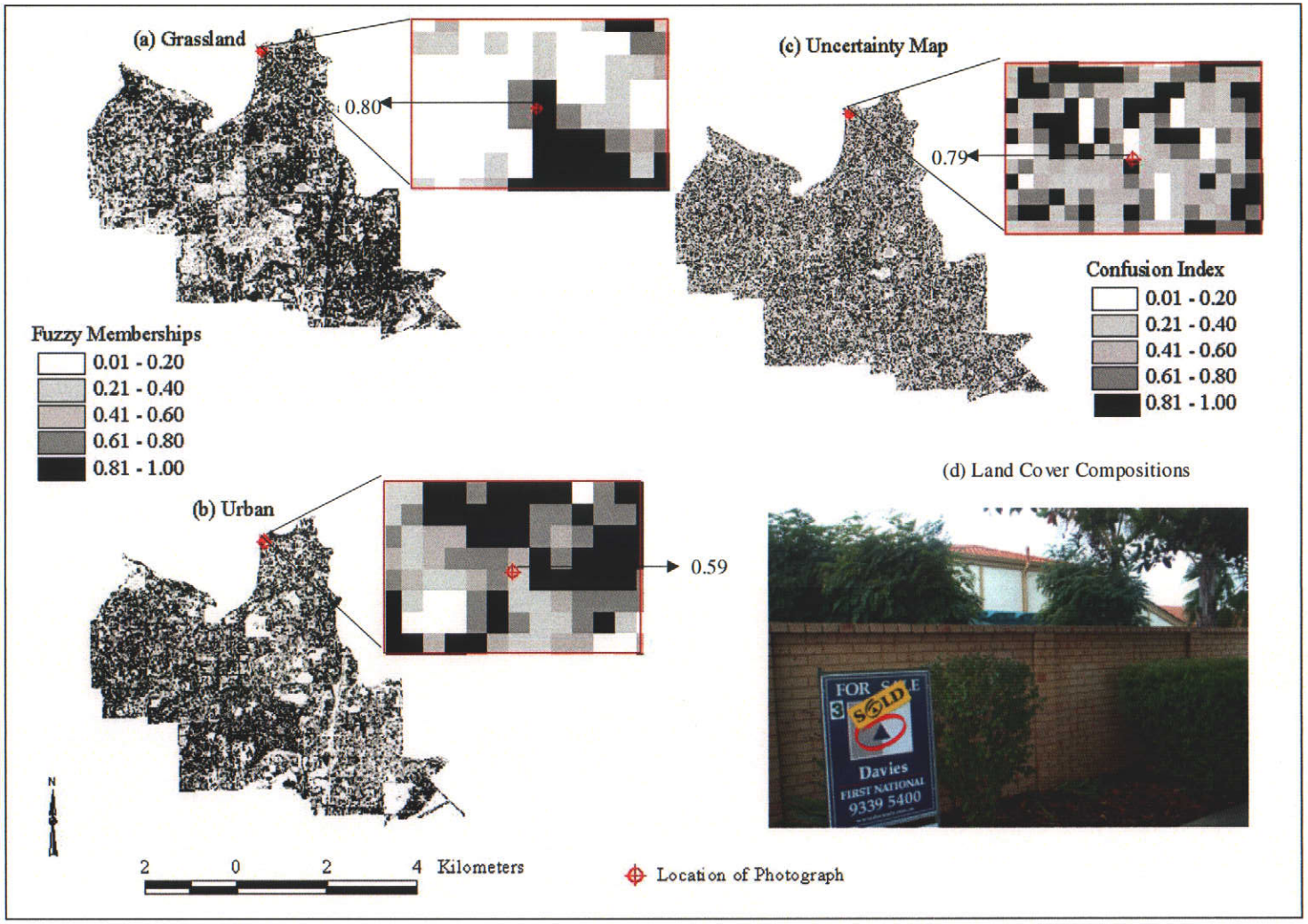

Figure 7.9 Uncertainty map and fuzzy membership maps of a misclassified sample of the class urban to grassland

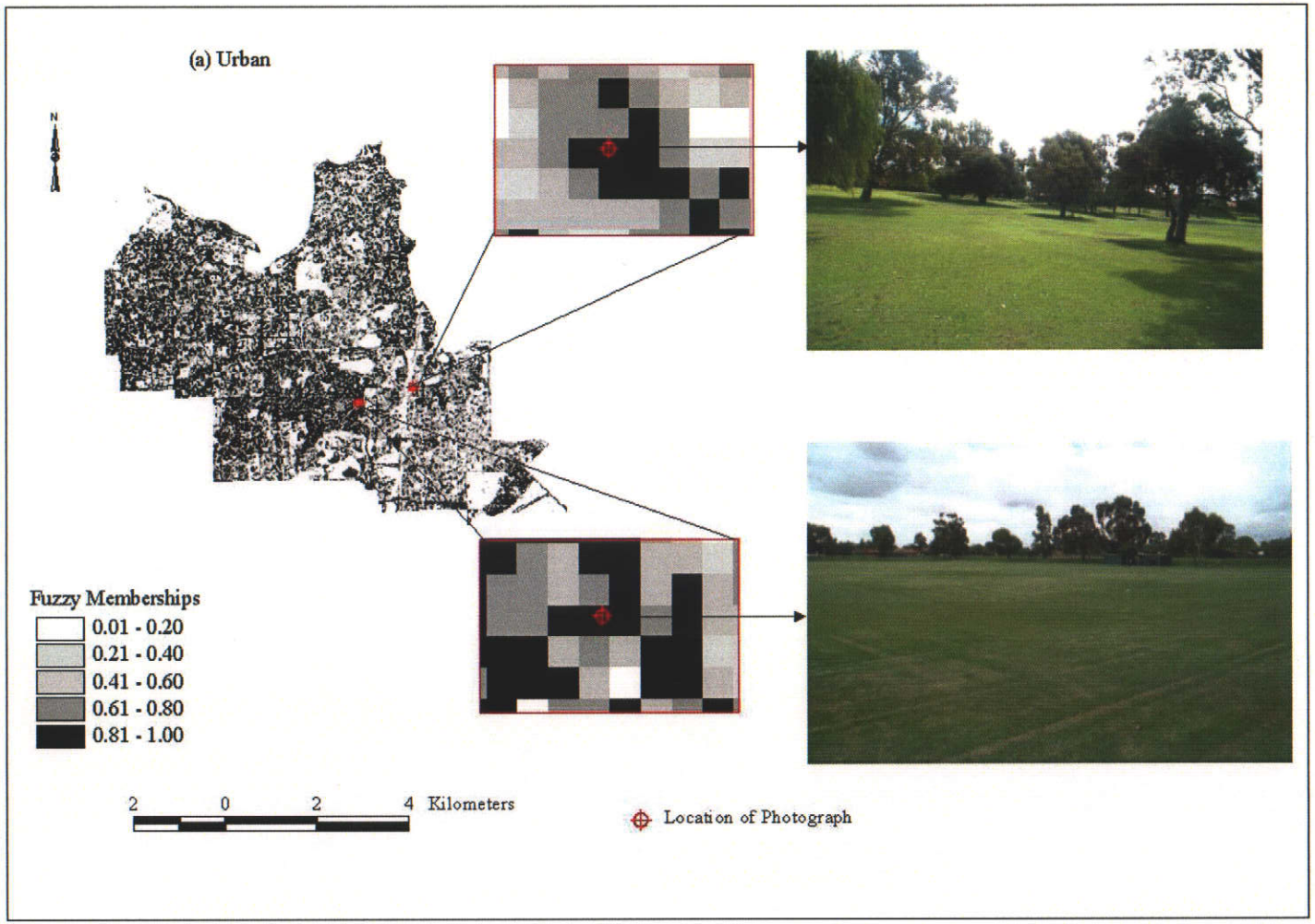

Figure 7.10 Fuzzy membership maps of the class urban showing the samples of the class grassland mislabelled as urban

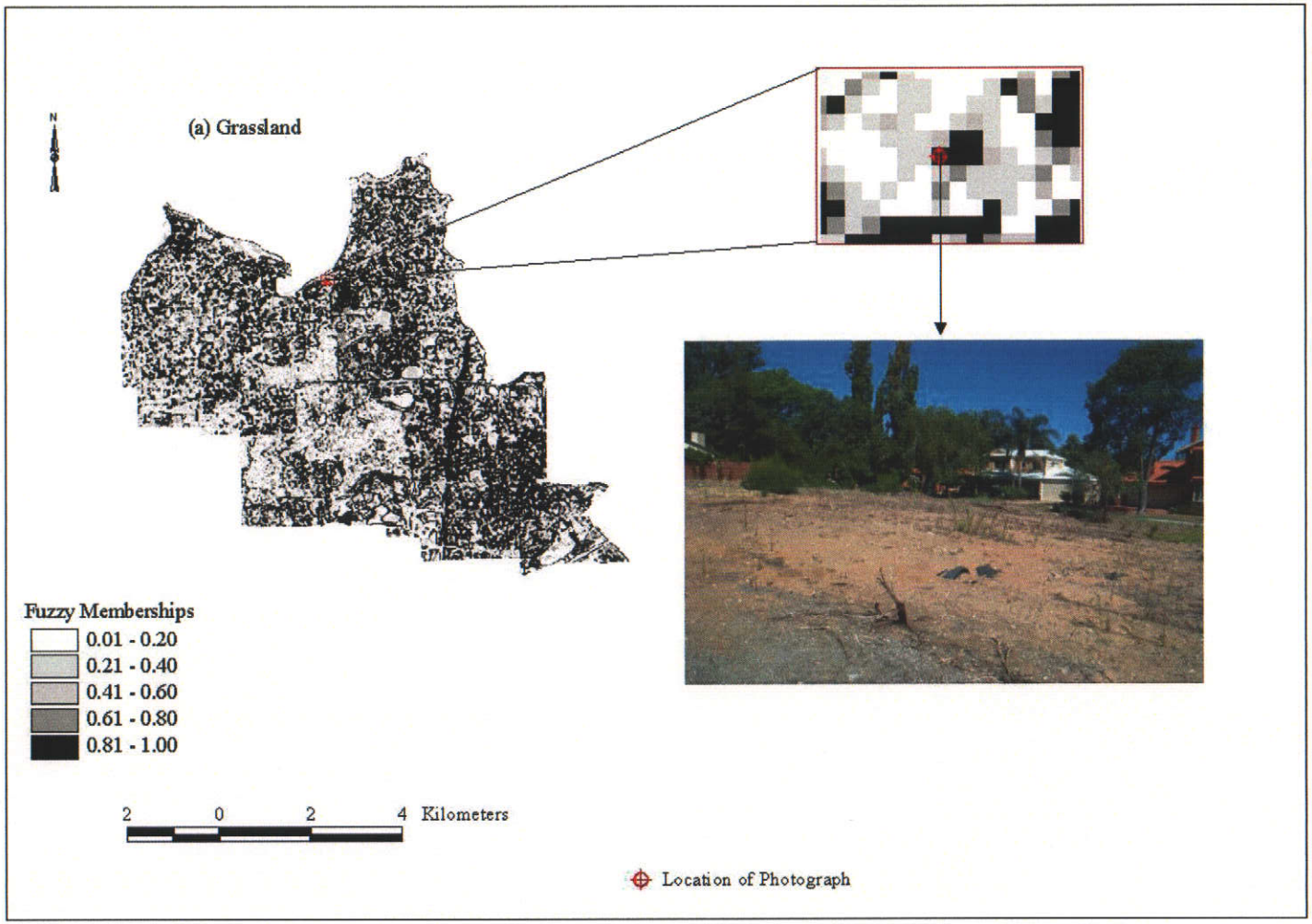

Figure 7.11 Bare ground following clearing of grassland showing in the fuzzy membership maps of the class grassland

7. 3 Accuracy Measures of Fuzzy Land Cover Maps of the City of Armadale

7.3.1 Performance of Fuzzy Operators in Generating Fuzzy Land Cover Maps

A summary of accuracy measures derived from the fuzzy error matrices of different fuzzy operators applied over the City of Armadale is presented in Table 7.4. The overall and categorical accuracy measures of all fuzzy operators indicate that a gamma operator (γ = 0.95) exhibited the highest overall accuracy. The overall accuracy of the fuzzy gamma operator (γ = 0.95) was up to 54 percent higher than that of the fuzzy algebraic product, fuzzy AND and fuzzy gamma operators with γ values ranging from 0.1 to 0.8, while 10 percent more accurate than the fuzzy gamma operator of 0.90, and 7 percent more accurate than the fuzzy OR operator (Table 7.4). Although, the overall accuracy of the fuzzy algebraic sum and γ value of 0.95 was found similar, the fuzzy algebraic sum registered comparatively lower producer's and user's accuracies for class grassland.

Similar to results of the City of Perth and the City of Melville, the categorical accuracy measures of fuzzy AND and fuzzy algebraic product exhibited a high user's accuracy for all land cover classes, as compared to a very low producer's accuracy. On the other hand, the user's accuracy of the fuzzy OR and fuzzy algebraic sum for the class urban and dense urban was found to be low, as compared to a relatively higher producer's accuracy (Table 7.4). For the fuzzy gamma operator, it was found that as the γ value increases, there is an increase in the producer's accuracy with decreasing user's accuracy. Table 7.4 shows that the producer's accuracy of fuzzy AND and fuzzy algebraic product is significantly low, indicating high omission errors in all categories along with a low overall accuracy. This could be attributed to an underestimation of the fuzzy memberships by these operators as fuzzy AND selects the minimum fuzzy membership value recorded for a particular land cover class while the fuzzy memberships of the fuzzy algebraic product tend to be very small due to the effect of multiplying several fuzzy membership values which are less than one.

Tables 7.4 shows that the overall accuracy of the fuzzy gamma operator with γ values ranging from 0.1 to 0.95 increases from 17 percent to 71 percent. The

increased accuracy was attributed to the compensation of information of the selected bands of the Landsat-7 ETM+ bands along with increased memberships of the classified data.

Table 7.4 Summary of accuracy measures of the fuzzy land cover maps of the City of Armadale

	Fuzzy Accuracy Measures	Forest	Grassland	Urban	Dense Urban
Fuzzy AND	Fuzzy Producer's Accuracy (%)	59	3	11	2
	Fuzzy User's Accuracy (%)	97	79	66	13
	Fuzzy Overall Accuracy (%)	29			
Fuzzy OR	Fuzzy Producer's Accuracy (%)	79	56	49	59
	Fuzzy User's Accuracy (%)	81	47	45	18
	Fuzzy Overall Accuracy (%)	64			
Fuzzy Algebraic Product	Fuzzy Producer's Accuracy (%)	44	1	5	2
	Fuzzy User's Accuracy (%)	99	65	89	33
	Fuzzy Overall Accuracy (%)	20			
Fuzzy Algebraic Sum	Fuzzy Producer's Accuracy (%)	80	56	70	78
	Fuzzy User's Accuracy (%)	82	63	51	26
	Fuzzy Overall Accuracy (%)	71			
Fuzzy Gamma Operation ($\gamma = 0.1$)	Fuzzy Producer's Accuracy (%)	35	1	6	1
	Fuzzy User's Accuracy (%)	100	66	87	27
	Fuzzy Overall Accuracy (%)	17			
Fuzzy Gamma Operation ($\gamma = 0.7$)	Fuzzy Producer's Accuracy (%)	68	14	24	14
	Fuzzy User's Accuracy (%)	96	76	67	30
	Fuzzy Overall Accuracy (%)	40			
Fuzzy Gamma Operation ($\gamma = 0.8$)	Fuzzy Producer's Accuracy (%)	74	24	36	21
	Fuzzy User's Accuracy (%)	94	75	65	29
	Fuzzy Overall Accuracy (%)	48			
Fuzzy Gamma Operation ($\gamma = 0.9$)	Fuzzy Producer's Accuracy (%)	78	45	54	43
	Fuzzy User's Accuracy (%)	91	72	63	32
	Fuzzy Overall Accuracy (%)	61			
Fuzzy Gamma Operation ($\gamma = 0.95$)	Fuzzy Producer's Accuracy (%)	80	60	68	67
	Fuzzy User's Accuracy (%)	88	68	63	36
	Fuzzy Overall Accuracy (%)	71			

Table 7.4 shows that the results of fuzzy gamma operator with γ value of 0.95 produced higher overall and categorical accuracy measures as compared to the results of using fuzzy algebraic sum and fuzzy OR. Therefore, the integrated fuzzy memberships generated by a fuzzy gamma operator ($\gamma = 0.95$) from the selected Landsat-7 ETM+ bands was considered to be most appropriate. The fuzzy

membership maps of class forest, grassland, urban and dense urban generated using the fuzzy gamma operator ($\gamma = 0.95$) are shown in Figure 7.12.

On the contrary, the overall accuracy of fuzzy OR was found to be 64 percent, which was comparatively higher than the overall values computed for fuzzy AND and fuzzy algebraic product. However, the user's accuracy and producer's accuracy of the class grassland, urban and dense urban were found to be relatively low, indicating high omission and commission errors. This could be partly attributed to the lack of compensation of information by the operator (fuzzy OR) as it considers single fuzzy membership value from the selected bands of Landsat-7 ETM+. The overall and categorical accuracy measures obtained by using the fuzzy algebraic sum in the process of integrating information from the selected Landsat-7 ETM+ bands were encouraging, as the accuracy measures were found higher as compared to fuzzy OR.

7.3.2 Sources of Classification Errors

The uncertainty map of the City of Armadale using the confusion index derived from the fuzzy categorical maps of the fuzzy gamma operator ($\gamma = 0.95$) in Figure 7.13 shows a lower uncertainty in the forested area that occupies most of the City's area as compared to higher a uncertainty in the urban area. This was likely as the land cover compositions of the urban area are mixed and fragmented, compared to forested area comprised of open forest and woodlands characterised with a variety of trees such as *Eucalyptus calophylla, Eucalyptus wandoo, Banksia attennuata*. An examination of the uncertain region of the City of Armadale indicated that the higher uncertainty occurred near a dry lake, residential areas, edges between grassland and residential area, roads and lakes within the forested area. High levels of uncertainty are mostly due to a mixture of land cover classes within a pixel and spectral similarity among the land cover classes considered in the classification scheme. Moran's *I* index computed on the confusion index was found to be 0.52, indicating that the City of Armadale has the strongest positive spatial autocorrelation of uncertainty values, as compared to the cities of Melville (0.28) and Perth (0.39). This index value also indicates that the City of Armadale presents a more "clustered" spatial distribution of uncertainty.

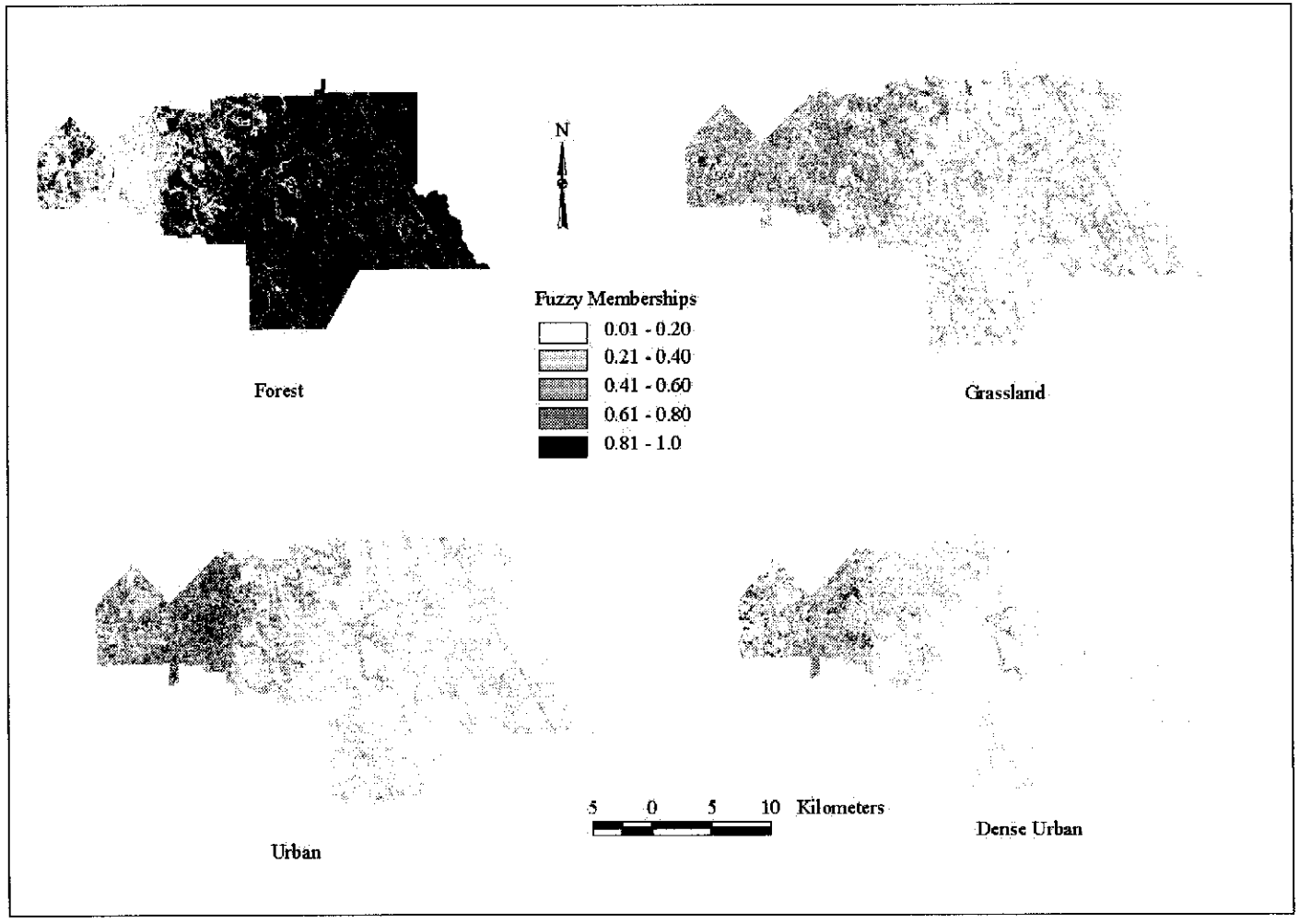

Figure 7.12 Fuzzy membership maps of the land cover classes generated by the fuzzy gamma operator ($\gamma = 0.95$) of the City of Armadale

An examination of the categorical accuracy measures of the defuzzified map generated using fuzzy gamma operator with γ value of 0.95, reveals accuracies above 80 percent for the class forest. A significant disagreement was found in the categorical accuracy measures between the defuzzified land cover maps and the field data for the classes grassland and urban. The user's accuracies of these classes were found to be equal to 68 percent and 63 percent respectively, indicating high commission errors (Table 7.3). Appendix 16(j) shows that the errors of commission of the class urban are mostly due to the inclusion of grassland areas within this class, while the class grassland is mostly confused with the classes forest and urban. Likewise, the producer's accuracy of classes grassland and urban were found to be equal to 60 percent and 68 percent, respectively. The omission errors of the class grassland were mostly due to a misclassification of this class as urban, while the omission errors of the class urban corresponded to a misclassification of this class as class dense urban or grassland (Appendix 16k).

Among the sources of disagreement between classified and reference data, spectral similarity between forest and grassland, urban and dense urban were identified. As mentioned in Chapter 4, the class forest is characterised by native forests, as compared to the class grassland characterised mainly by a mixture of grass, shrubs and occasional native plants, which could in some instances produce a misclassification of the class forest as class grassland. This can be seen in Figure 7.14 (d), which shows a forested area comprised of native plants and shrubs. According to the dominant land cover, the highest fuzzy membership assigned during the field visits corresponded to forest. The fuzzy membership of the defuzzified output indicated that the same location was classified as grassland and accordingly, an error of omission occurred. An examination of the fuzzy categorical maps showed a fuzzy membership value of 0.73 for class grassland (Figure 7.14b) compared to a fuzzy membership of 0.60 for class forest. This resulted in a confusion index of 0.87 indicating a high uncertainty between class grassland and forest (Figure 7.14c).

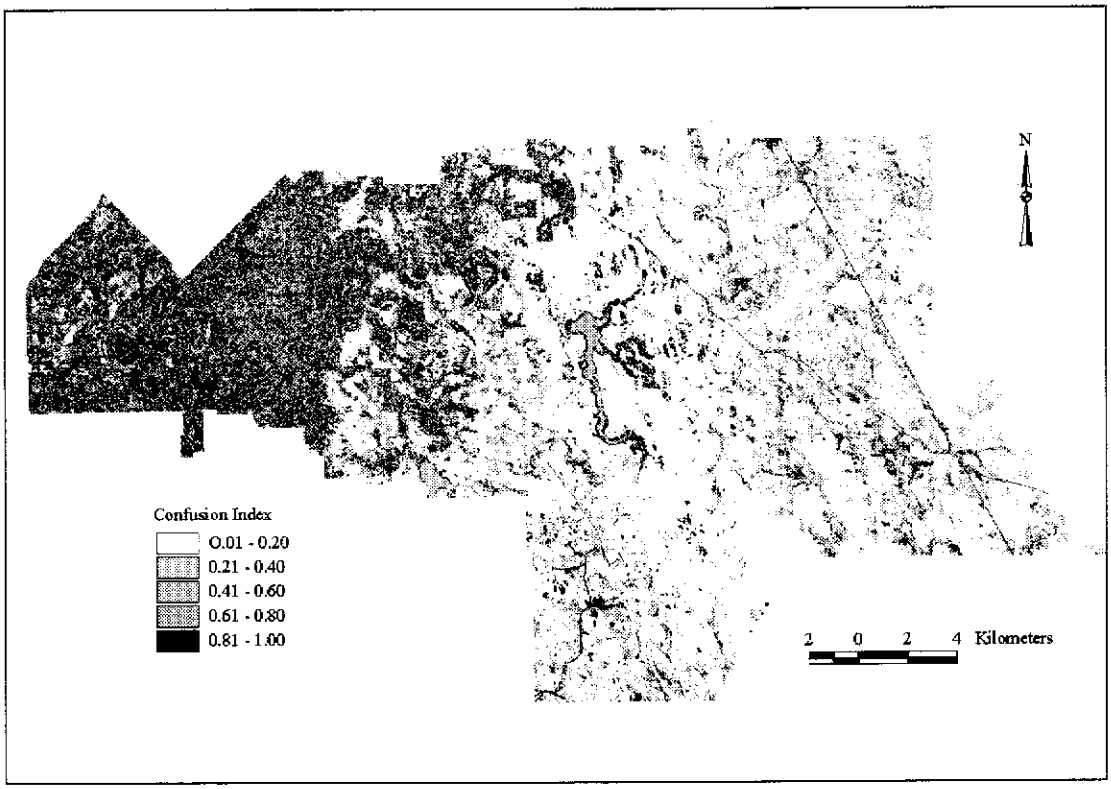

Figure 7.13 Uncertainty map showing the confusion index derived from fuzzy categorical maps of the City of Armadale

The seasonal effect on the spectral behaviour of some land covers (e.g. grassland) as discussed in earlier Sections (e.g. 7.1.2; 7.2.2) could also be a source of misclassification of the class grassland as urban. This is reflected in Appendix 16(j), which shows that the omission error of the class grassland largely results from the labelling of grassland as urban areas. Another major source of disagreement in the City of Armadale could be attributed to the spectral similarity between the classes urban and dense urban. For example, Figure 7.15 (a) shows a residential building and accordingly, the highest fuzzy membership for the field collected data was assigned to the class urban.

The fuzzy classification assigned the label dense urban to this location. An examination of fuzzy categorical maps showed a fuzzy membership value of 0.66 for class dense urban (Figure 7.15b) compared to a fuzzy membership of 0.57 for class urban. This resulted in a confusion index of 0.91 indicating high uncertainty between the classes urban and dense urban (Figure 7.15c). Appendix 16(j) shows that the omission error of class urban was mostly contributed by misclassification to class dense urban. This also resulted in a high commission error for the class dense urban as can be seen in Appendix 16(j).

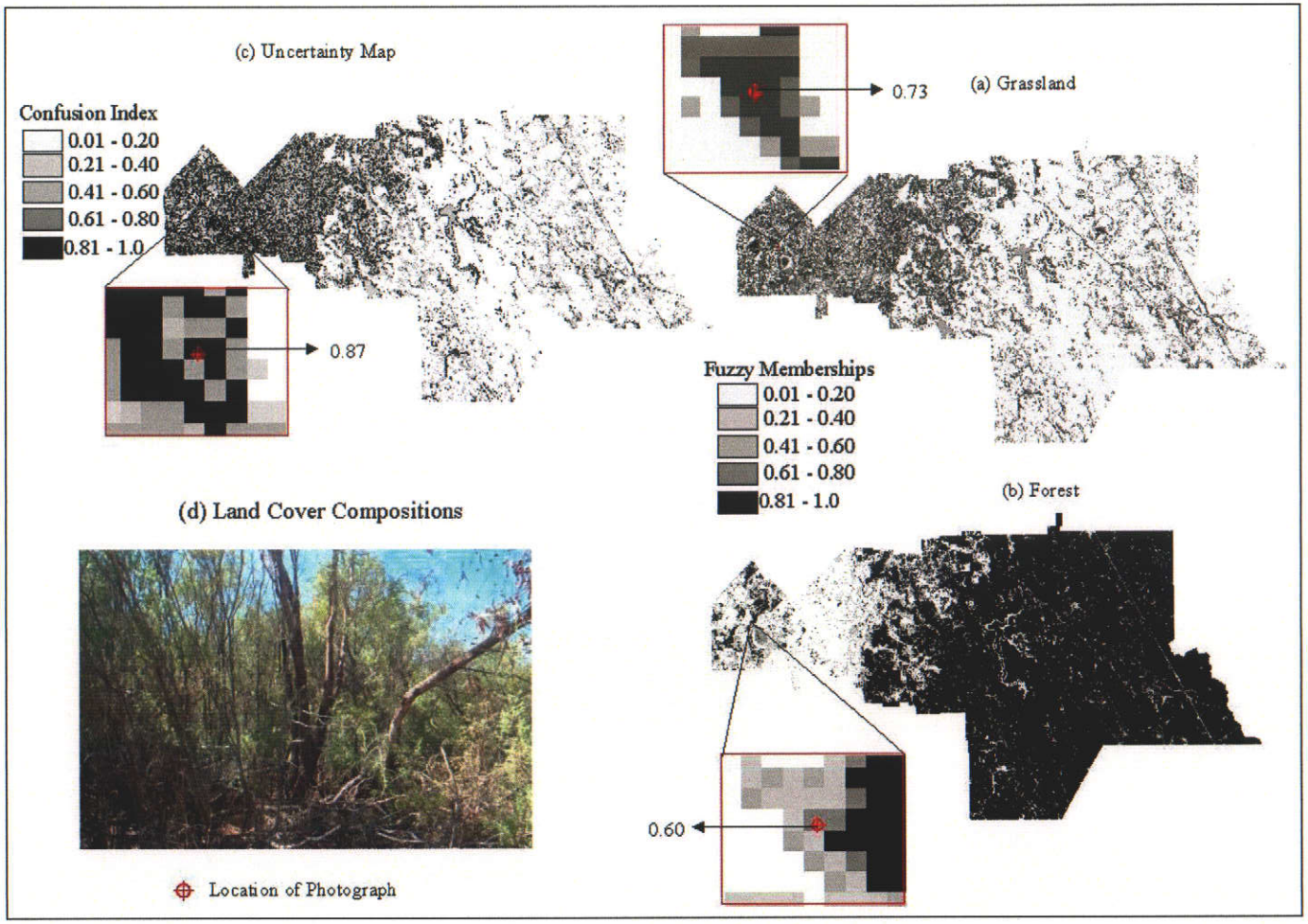

Figure 7.14 Uncertainty map and fuzzy memberships of a misclassified sample of the class forest as class grassland

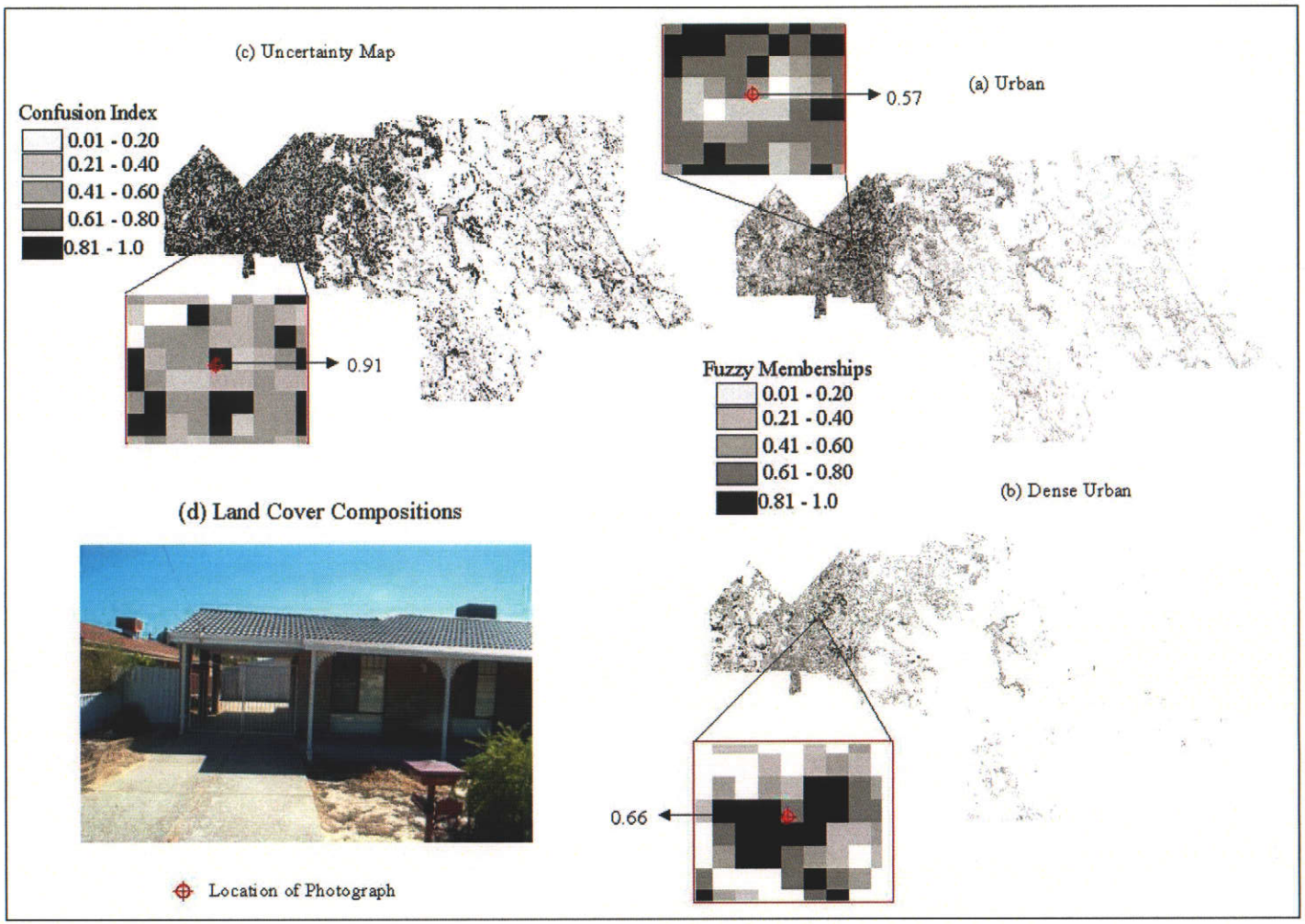

Figure 7.15 Uncertainty map and fuzzy membership maps of a misclassified sample of the class urban to dense urban

7. 4 Factors Affecting the Accuracy of the Fuzzy Land Cover Maps

7.4.1 Land Cover Heterogeneity

The accuracy measures of the study areas derived from the fuzzy error matrix have been discussed in Sections 7.1, 7.2 and 7.3. These analyses considered the overall accuracy, producer's accuracy and user's accuracy along with a confusion index (uncertainty map) measured from the first and second maximum fuzzy memberships of fuzzy categorical maps in each location. Such maps provide a spatial appreciation of the distribution of uncertainty over the classified areas.

The results such as the overall, average producer's and user's accuracy of the study areas presented in Figure 7.16 provide a comparison of the accuracy of interpreting urban land cover classes using the defuzzified maps. Figure 7.16 shows that the overall accuracy of the City of Perth was found up to 13 percent higher than the overall accuracy of the City of Melville and the City of Armadale which was found to be 69 percent and 71 percent, respectively. The main contributing factor to the observed difference of the overall and categorical accuracy measures among the study areas could be attributed to the variation of land cover heterogeneity. It is important to note that the same classification scheme, which is a modification of Anderson's (1976) Level I and Level II was considered in all study areas for generating fuzzy categorical maps.

The results indicated that the classification scheme worked well in generating fuzzy categorical maps of the City of Perth as the overall accuracy of the defuzzified map was found equal to 81 percent (Figure 7.16). The higher overall and categorical accuracy measures of the City of Perth were attributed to (i) the classification scheme properly characterising the land cover types of the area; (ii) the classes tending to be more homogeneous (e.g. less mixing within a pixel) and (iii) pixels being dominated by one land cover type only. An examination of the land cover classes indicated that the class forest was clustered in the western part of the study area, while the classes dense urban and urban were clustered in the remaining of the study area.

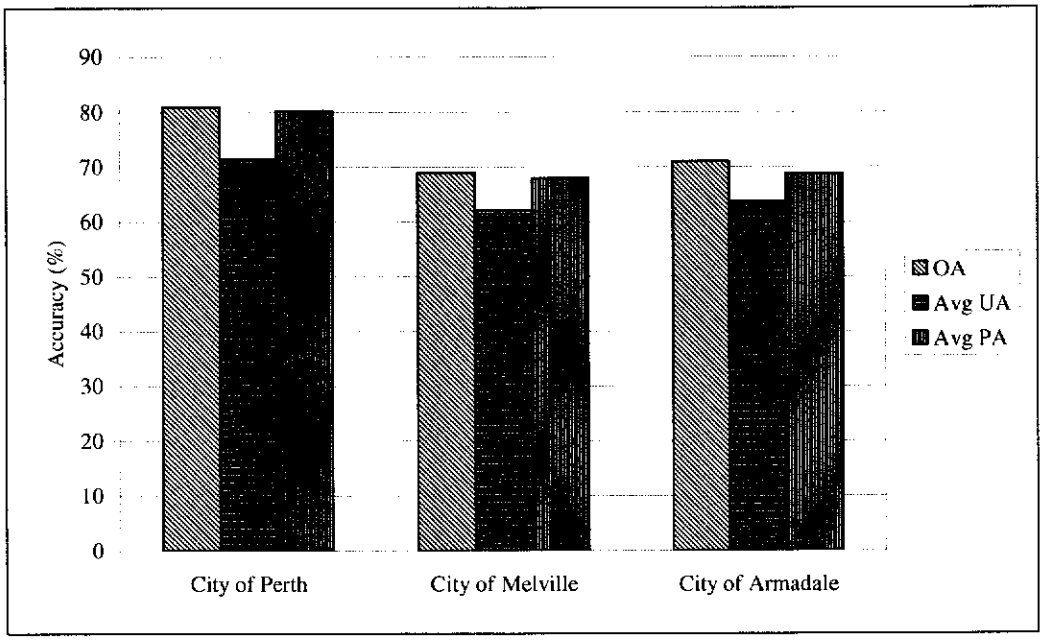

Figure 7.16 The overall (OA), average users (Avg UA) and producers (Avg PA) accuracies for the three study areas

There were distinct parks and playing grounds of a size larger than the spatial resolution of Landsat-7 ETM+ imagery within the study area. The spatial composition of a pixel, i.e. less mixture of land covers within a pixel, and relatively homogeneous land cover classes contributed to high classification accuracy. However, the categorical accuracy measures indicated the occurrence of omission and commission errors, which were attributed to the spectral similarity between class urban and dense urban. Likewise, a seasonal effect was attributed to the spectral similarity between class grassland and urban which contributed to misclassification.

On the other hand, the land covers of the City of Melville were found fragmented and mixed. For example, the class urban largely comprised of residential area, varied from clay on concrete roof tiles surrounding sparse vegetation, steel roof tiles surrounding dense vegetation with tiles, residential areas with concrete roads along with concrete roads, parking lots and major and minor roads. Likewise, the class grassland comprised parks, open space (playing grounds), bare ground with grassland following clearing and prior to construction, and golf clubs comprised of sparse trees and grassland. The class forest was also fragmented and mixed with shrubs and grassland. The heterogeneity of land cover classes (e.g. more mixture of land covers within a pixel) that were considered in the classification scheme contributed to significant misclassification and accordingly, high commission and

omission errors were registered, contributing to a lower overall accuracy, as compared with the City of Perth. This can be seen in the categorical accuracy measures computed from the fuzzy error matrix using the defuzzified maps generated by the fuzzy gamma operator ($\gamma = 0.95$) (Appendix 16k), which showed a significant misclassification of the class urban as class grassland due to their mixed occurrence within a pixel. It is important to note that the class urban in the City of Perth was mostly characterised by construction materials and major roads and accordingly, there was not mixture with the class grassland. This is reflected in a fuzzy error matrix of the City of Perth, which shows that the commission error was mostly due to misclassification of the class urban as dense urban (Appendix 14j).

The categorical accuracy measures of the fuzzy gamma operator ($\gamma = 0.95$) showed a significant misclassification of the class grassland as urban. As the data (Landsat-7 ETM+) were acquired in a dry season (i.e. summer), the similar spectral response of the dried grassland, as compared with class urban contributed to misclassification. It is important to note that parks and reserves of the City of Perth are managed using a watering systems in order to keep the green space intact during summer, which is not so far the dry parks and reserves of the City of Melville. Likewise, misclassification of the class forest as class grassland occurred due to spectral similarity between these classes components and their high level of fragmentation.

In the City of Armadale, the class forest was more clustered, as compared to the fragmented and mixed land covers of the class grassland, urban and dense urban. For this study area, the class grassland was also comprised of irrigated pastures and grazing areas particularly in the eastern part of the study area. The heterogeneity in the composition of this class contributed a significant misclassification to class urban and accordingly, high omission and commission errors occurred for class grassland and urban respectively. Appendix 16(j) shows that 36 percent of the omission errors were mostly due to the misclassification of class grassland as urban.

The spatial composition of the class urban varied largely within the City of Armadale. For example, some areas comprised dense residential building while others varied from single to multiple residential blocks surrounded by sparse or dense vegetation. Likewise, some major roads are surrounded by forested areas while others are surrounded by built-up areas. The heterogeneous land cover

compositions of the class urban (i.e. mixture of land covers within a pixel) contributed to its misclassification as dense urban or grassland. This can be seen in Appendix 16(j), which shows that the omission error (29 percent) was mostly due to a misclassification as either grassland or dense urban. The misclassification of the class urban, particularly roads in the forested area (western part of the study area), as class grassland can be seen in the fuzzy categorical map in Figure 7.17, which shows higher fuzzy memberships in the class grassland. The confusion index of these areas was also found to be high (Figure 7.17c). Likewise, the sand dunes around dams and lakes were classified as dense urban, given their spectral similarity with features comprising urban areas.

The above discussions suggest that the heterogeneity of urban land covers influences significantly the accuracy of information generated from satellite imagery. The accuracy confirms that the classification scheme and technique are suitable to characterise relatively homogeneous areas like the City of Perth. For more spatially mixed areas like the residential areas of the City of Melville, the classification accuracies were relatively low. This could be the attributed to (i) the spatial resolution of the image used in the analysis which is generally not sufficient to discriminate individual features (e.g. buildings, streets, trees) within residential areas which results in mixed pixels; (ii) the classification scheme which fails to characterise the different land cover compositions of the area. Accordingly, more research is needed to evaluate the impact of the remote sensors' spatial resolution on the heterogeneity of highly mixed urban land covers using fuzzy classification techniques.

7.4.2 Classifier's Performance

The levels of heterogeneity of the urban land covers in three study areas were different. It is evident that interpretation of these land covers from remote sensing images, represented in terms of their spectral signature on a pixel by pixel basis, but more importantly in terms of spatial variation, is complex. Fuzzy categorical data offer information on mixed pixel as compared to maximum likelihood classification, which allocates to a single class.

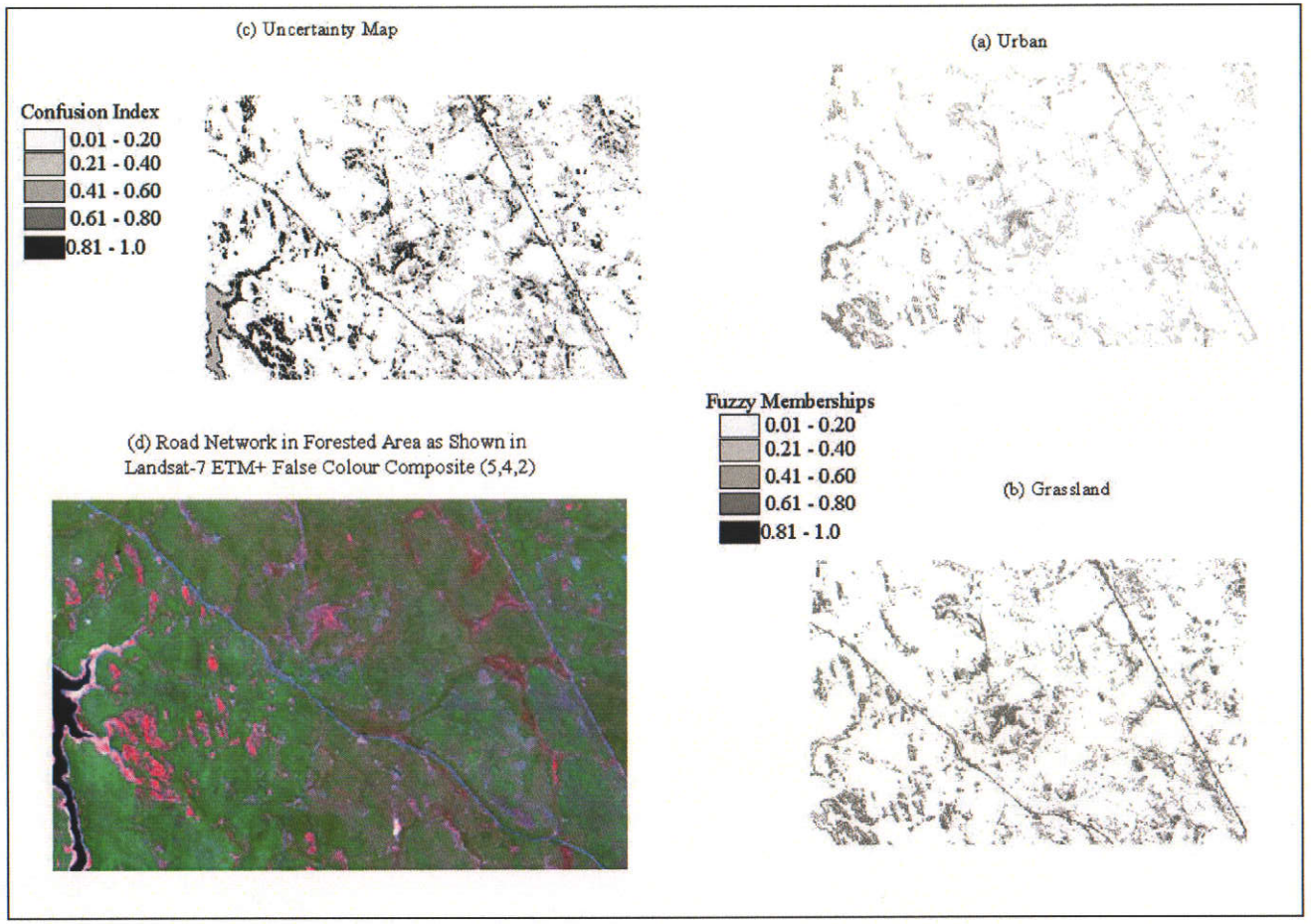

Figure 7.17 Uncertainty map and fuzzy membership maps of a concrete road network misclassified as grassland

A mixed pixel occupies more than one land cover class and displays a composite spectral response. The classification of a mixed pixel by maximum likelihood classifier is to some extent erroneous as the classified output may not be one of its component classes (Zhang and Foody, 1998). Thus, classifying thematic classes of an area using maximum likelihood classifier is problematic particularly from a moderate resolution (30 m) imagery, which is impeded by the abundance of spectrally mixed pixels (Small, 2003). Accordingly, fuzzy classification was applied to compute fuzzy memberships from the selected bands of a Landsat-7 ETM+ scene. The fuzzy memberships were then integrated using different fuzzy operators.

The classifier worked well in generating fuzzy categorical maps particularly for the City of Perth as the overall classification accuracy was found to be 81 percent as compared to the overall classification accuracy of 69 percent and 71 percent for the City of Melville and the City of Armadale, respectively (Figure 7.15). It appeared that accuracy of the defuzzified land cover map of the study areas decreases as land cover heterogeneity increases. One possible reason for decreasing accuracy could be the use of the same classification scheme in all study areas, which has not been able to characterise the more heterogeneous occurrence of the grassland and urban areas that occur in the fringe of the Perth metropolitan area as well as the largely residential areas of the City of Melville. Moreover, it appeared that as the spatial heterogeneity increases, the likelihood of the influence of mixed pixels increases. This can be seen in the residential area of the City of Melville and the City Armadale where the land blocks of residential areas (e.g. 700 – 900 sqm) are composed by green areas (e.g. lawns, backyards, trees) and houses, resulting in misclassifications of what in the ground collected data is labelled urban, as grassland. This is substantiated by the uncertainty maps derived quantitatively by using a confusion index on the fuzzy categorical maps. Likewise, the class grassland was sometimes misclassified as urban due to a seasonal effect on the spectral signatures, which caused similarity between the classes.

A comparison of the results of the present study with available literature indicated that accuracy measures of the City of Perth are encouraging. For example, Melgani *et al.* (2000) applied fuzzy supervised classification in classifying a Landsat-TM scene using four land cover classes (e.g. sandy areas, agricultural land, rangeland and

barren land), reporting an overall and average producer's accuracy of 75.54 percent and 74.71 percent, respectively. These results (e.g. overall and average producer's accuracy) were found up to 6 percent lower than the results of the City of Perth while up to 6 percent higher than the results of the City of Melville and the City of Armadale. The lower accuracy measures of the City of Melville and the City of Armadale were due to the classification scheme, which failed to characterise the different land cover compositions of these areas. In an investigation of fuzzy classification of a suburban land cover, Zhang and Foody (1998) reported an overall classification accuracy of 49.9 percent and 50.2 percent for SPOT HRV and Landsat TM data, respectively using hardened fuzzy classified data and hardened fuzzy ground data derived from indicator kriging. The overall accuracy increased to 74.7 percent and 72.8 percent for SPOT HRV and Landsat TM respectively, when selective hard comparisons were carried out between pure pixels of classified data and pure pixels of the ground data. These accuracy measures were improved further to 92.8 percent and 93.2 percent respectively by taking account of both, the most likely and the second most likely class memberships of the fuzzy classified data and fuzzy ground data derived from indicator kriging. Likewise, Shackelford and Davis (2003) investigated the application of fuzzy logic to improve the classification accuracy of urban and suburban areas using panchromatic and multispectral IKONOS datasets with a spatial resolution of 1 m and 4 m, respectively. Maximum likelihood and fuzzy classification were used to classify urban land cover classes such as road, building, grass, tree, bare soil and water. The results of the fuzzy classification revealed an overall classification accuracy of 92.7 percent and 83.5 percent for panchromatic and multispectral data respectively, which was up to 11 percent higher, as compared to the classification accuracies of a traditional maximum likelihood classifier tested in the same study. The lower overall classification accuracy of the present study could be attributed to the spatial resolution of the sensor used in this research where the presence of mixed pixels is abundant, as shown in the uncertainty maps of the study areas. Furthermore, a large number of 'classes' may have played a role allowing better characterisation of the spatial components of urban landscape.

In addition to the accuracy measures derived from the fuzzy error matrix, the whole process provided a data-driven solution to estimate the source of errors in the

categorical mapping. The fuzzy uncertain maps generated using the confusion index on fuzzy categorical maps indicated the spatial distribution of areas that are more prone to misclassification. This can be seen in the uncertainty maps of the study areas in Figures 7.2, 7.7 and 7.13 which show that the uncertainty of the City of Melville is spread over the study area, indicating the mixture of more than one land cover classe within a pixel or the spectral similarity between the classes which contributed to misclassification and thus, resulted in a low overall accuracy.

7.4.3 Reference Data Issues and Errors of GPS

In generating the elements of the fuzzy error matrix for computing the overall and categorical accuracy measures of defuzzified maps, assigning fuzzy memberships to the field data is an important task. This needs accurate samples along with land cover compositions surrounding the samples. Accordingly, some 200 randomly selected samples from each study area were visited using their known coordinates by means of a GPS. The land cover compositions of the surrounding area were captured using a digital camera (see Section 5.3.1), were analysed and accordingly fuzzy memberships were assigned. There are two issues that are related to field data collection, which warrant further discussion. The area of the land cover classes that were considered in the classification scheme varied among the study areas. Accordingly, the numbers of the randomly field-collected samples of each land cover classes of the study areas also varied. Secondly, the accuracy of GPS was found ± 10 m from a known point coordinate (See Chapter 5). Thus, a 25- by 25 m grid for each sample was considered for generating the elements of the fuzzy error matrix which was assumed to be free from misregistration errors with the defuzzified maps.

7. 5 Summary

This chapter described the overall and categorical accuracy measures of the defuzzified memberships derived from a fuzzy error matrix. As described in Chapter 3, the fuzzy error matrix required defuzzification of the fuzzy layers using maximum membership and accordingly, each location was assigned to a class that represents the highest fuzzy membership. This enabled generating of defuzzified memberships from the fuzzy categorical maps for each fuzzy operator. Similarly, the field data were defuzzified and a fuzzy reference map was generated. Finally, the accuracy of

the fuzzy maps generated by different fuzzy operators was assessed against the field-based fuzzy map using a fuzzy error matrix and the accuracy measures such as, fuzzy overall accuracy, producer's accuracy and user's accuracy were computed, following the procedures described in Section 5.3.3.

The fuzzy accuracy measures of the integrated fuzzy memberships associated with selected Landsat-7 ETM+ bands indicated that the fuzzy minimum operator (e.g. fuzzy AND) was not suitable for generating fuzzy categorical maps. This was attributed to underestimation of class memberships and absence of compensation of information that characterise this operator. Likewise, fuzzy maximum operator (e.g. fuzzy OR) was also not suitable as the class memberships were overestimated and accordingly, high commission errors occurred. On the contrary, fuzzy algebraic product considered the fuzzy memberships of all selected Landsat-7 ETM+ bands but it underestimated the fuzzy memberships, which contributed to a low overall accuracy. However, the results of the fuzzy algebraic sum registered a relatively higher overall accuracy in all study areas. Furthermore, analysis of the fuzzy accuracy measures of the fuzzy gamma operator ($\gamma = 0.95$) showed that the accuracy measures particularly, the categorical accuracy measures outperformed the results obtained by applying fuzzy algebraic sum. Accordingly, fuzzy gamma operator ($\gamma = 0.95$) produced highest overall classification accuracies in all study areas and for all the land cover types considered, being therefore recommended as the optimal fuzzy operators for integrating fuzzy membership values associated with multiple spectral bands in urban landscapes.

Several sources of disagreement between the defuzzified maps and the reference data were identified which varied from one study area to another. In the City of Perth, spectral similarity between forest and grassland, grassland and urban, urban and dense urban contributed to misclassification, which resulted in errors of omission and commission. The uncertainty map generated using the first maximum and second maximum fuzzy memberships of the fuzzy categorical maps substantiated that misclassification was due to equal dominance of some of these classes within a pixel. Likewise, spectral similarity between forest and grassland and grassland and urban, were identified in the City of Melville while spectral similarity between forest and grassland, grassland and urban, urban and dense urban were identified in the City of

Armadale. The uncertainty maps of these study areas substantiated that omission and commission errors resulted from both, the presence of mixed pixels and spectral similarity amongst some classes.

The overall classification accuracy of fuzzy land cover maps derived from a Landsat-7 ETM+ scene of the City of Perth generated by the best fuzzy operator was found to be 81 percent as compared to the overall accuracy of 69 percent and 71 percent for the City of Melville and the City of Armadale, respectively. The results of the City of Perth were found higher than the results of a fuzzy classification of Landsat TM scene reported by Melgani (2000) and Zhang and Foody (1998) in contrast to lower accuracy measure for the City of Melville and the City of Armadale. The lower overall classification accuracy of the City of Melville and the City of Armadale were due to more spatially mixed areas, which resulted in mixed pixels and accordingly, misclassification occurred. Another reason was the classification scheme, which failed to accommodate the different land cover classes of these study areas. The accuracy measures of the study areas were found much lower than the results of a fuzzy classification using IKONOS data sets with a spatial resolution of 1 m and 4 m respectively as reported by Shackelfold and Davis (2003). The higher accuracy of Shackelfold and Davis (2003) was due to the spatial resolution of the image and the utilisation of spectral and spatial methods in the fuzzy classification, which were able to discriminate spectrally similar urban land cover classes.

The accuracy measures of the fuzzy land cover maps indicate that the methodology for deriving fuzzy categorical maps depends on two factors. Firstly, the heterogeneity of the land cover compositions and secondly, the correct representation of the land cover classes in the classification scheme. It appears that the methodology for generating fuzzy categorical maps using fuzzy operators and accuracy assessment from a fuzzy error matrix worked well for a relatively homogenous study area. For mixed land cover classes e.g. residential area of the City of Melville and the City of Armadale, the accuracy could be improved if an additional land cover class (e.g. bare ground for City of Melville and grazing area for City of Armadale) was included in the classification scheme. It is important to note that the classification accuracies were derived from the fuzzy land cover maps based on maximum fuzzy membership in each location and accordingly, the second

maximum membership in each location was not considered. The uncertainty maps derived from the confusion index indicate that the occurrence of mixed pixels was mostly due to confusion between the land cover classes of first and second maximum membership in a pixel location. As demonstrated by Zhang and Foody (1998), the classification accuracies of all study areas could be improved significantly if the second maximum fuzzy membership was considered in the accuracy assessment analysis.

Chapter 8

CONCLUSIONS AND RECOMMENDATIONS

The objectives of this study were twofold. Firstly, to analyse the spatial complexity of a urban landscape as computed from SPOT, Landsat-7 ETM+ and Landsat MSS remotely sensed data for assessing the appropriateness of a scale for urban analysis. Secondly, interpretation of land cover types that characterise highly complex and heterogeneous urban land covers of the Perth metropolitan area using fuzzy set theory for the digital classification of a Landsat-7 ETM+ scene acquired over the area. The research methodology adopted to achieve the objectives is described in Chapter 3 and the implementation of the methods is presented in Chapter 4 and Chapter 5, respectively.

The first expected outcome was related to selecting an appropriate scale (e.g. spatial resolution) for characterising the spatial pattern of urban landscapes based on the fractal dimension computed from SPOT, Landsat-7 ETM+ and Landsat MSS. Associated with this outcome, the effect of spectral resolution and land cover heterogeneity on spatial complexity and the performance of fractal measurement algorithms in computing fractal dimension were identified and discussed in Chapter 6. The second outcome related to the performance of fuzzy operators in generating fuzzy categorical maps along with determining the effect of land cover heterogeneity on fuzzy accuracy measures and identification of sources of classification errors. These outcomes are presented in Chapter 7. The main conclusions based on the findings of this research, and recommendations for further research are presented hereafter.

8. 1 Characterisation of Urban Spatial Complexity using Multiscale and Multisource Remote Sensing Data

The research approach adopted in this study appeared promising in addressing the effect of spatial, spectral and land cover composition on the spatial complexity of urban landscapes using multiscale and multisource remote sensing data. With the increasing availability of commercial satellite remote sensing data, acquired in a

wide range of wavelength varying from visible to microwave, with spatial resolutions varying from sub-meter to a kilometre, the methodology provided an essential means for determining a proper technique for the selection of an appropriate scale for urban analysis. In order to implement the methodology, spatial methods such as the fractal model and Moran's *I* index of spatial autocorrelation were applied to address the issue of scale on the spatial complexity of urban land cover types. Accordingly, fractal measurement algorithms such as the isarithm and the TPSA were applied to SPOT, Landsat-7 ETM+ and Landsat MSS for examining the effect of scale on the spatial complexity. The analysis of the *D* was based on the hypotheses enunciated in Chapter 1 and accordingly, the following results were found.

(a) The fractal dimension computed from the green, red and NIR bands of SPOT, Landsat-7 ETM+ and Landsat MSS using the isarithm and the TPSA algorithms provided insights into the effect of spatial resolution on spatial complexity of the study areas. Fractal dimension was found highest in SPOT followed by Landsat-7 ETM+ and Landsat MSS in all study areas. In addition, the variation of *D* within sample plots selected to characterise the study areas was found highest in SPOT indicating the ability of distinguishing amongst land covers using spatial complexity as an indicator. Decrease in spatial complexity with increasing spatial resolution (e.g. larger pixel size) was attributed to loss of spectrally heterogeneous pixels toward more homogeneous mixed pixels resulting from a mixture of reflectance feature such as buildings, major and minor roads, residential and forested area (e.g. individual features' reflectance averaged over the area covered by a pixel). Theoretically, for a non-fractal surface, fractal dimension is highest at a scale where most of the processes operate (Goodchild and Mark, 1987; Lam and Quattrochi, 1992). With this assumption, the difference of fractal dimensions computed from SPOT, Landsat-7 ETM+ and Landsat MSS in the study areas could be attributed to the differences of the spatial resolution of these sensors. Accordingly, with highest *D* in SPOT image for all study areas, one can conclude that the spatial complexity of the Perth metropolitan is best represented at a resolution of 20 m. The results are in accordance with the

findings of Small (2003) who showed that the spectral response of urban features are better characterised in a scale which varies between 10 and 20 m;

(b) The fractal dimensions of the green, red and NIR bands of each sensor varied indicating the effect of spectral location on spatial complexity of the study areas. Analyses of the spatial complexity indicated that for areas that are predominantly comprised of urban features (e.g. built-up areas), the green and red bands revealed a higher *D*, as compared to the NIR band. For example, the average *D* of the green and red bands of the City of Perth (largely composed of built-up areas) computed from Landsat-7 ETM+ using the TPSA algorithm, varied between 2.86 and 2.88 respectively, compared to 2.77 for the NIR band (see Table 6.1). On the contrary, for areas largely comprised of forest and native vegetation, the *D* of the NIR band was found higher, compared to the green and red bands. For example, the average *D* of the green and red bands of the City of Armadale, representing a typical urban fringe area computed from Landsat-7 ETM+ using the TPSA algorithm, varied between 2.67 to 2.69, as compared to 2.75 for the NIR band (see Table 6.13). The results demonstrated the ability of the fractal model in distinguishing variations in the composition of built-up areas on satellite data in the green and red bands, while forested areas typical of the urban fringes appear better characterised in the NIR band. This is in line with the findings of previous studies, where fractal dimension of urban areas was found highest in the green and red bands of Landsat TM (Quattrochi *et al.*, 2001; Qiu *et al.*, 1999; Quattrochi *et al.*, 1997; Lam, 1990). A higher fractal dimension in the green and red bands could also be an indication of higher textural information content related to built-up areas as compared to the NIR band. This indicates that the green and red spectral ranges can better detect spatial complexity of urban land covers, and therefore would be preferred in urban analysis studies where texture is important, while forested areas appear more spatially complex in the NIR range of the spectrum. Therefore, it can be concluded that the green and red ranges of the spectrum could be used in characterising the spatial complexity of built-up urban areas, while the NIR range could be used to characterise urban fringe areas that appear dominated by natural features like forested areas;

(c) The variation of the *D* among the study areas irrespective of the spectral location of the sensor was attributed to the effect of land cover heterogeneity.

An examination of the land cover types of the study areas indicated that the more complex the spatial pattern, the higher the D indicating higher spatial complexity. For example, the spatial pattern of land cover types of the City of Perth is very complex and accordingly, the City of Perth registered higher D values, compared to the City of Melville and the City of Armadale. It is interesting to note that the land cover patterns of the City of Melville and the City of Armadale varied from spatially complex land cover types to spatially more homogeneous land cover types and accordingly, significant variation of the D was found. An analysis of the spatial complexity, measured as D, particularly for SPOT showed that the complexity of the spatial pattern decreases as the land cover types change from dense urban (e.g. City of Perth) to medium urban (e.g. City of Melville) to urban fringe (e.g. City of Armadale). The results contradict the findings of O'Neill (1988) and Read and Lam (2002) because these studies considered human intervention on natural landscapes, whereas the present study worked mainly on built-up areas. The results of the present study are in conformity with the findings of many studies which revealed higher D for higher degree of human intervention (e.g. urban areas) as compared to lower degree of human intervention (e.g. rural areas) (Lam, 1990; Quattrochi *et at.*, 1997; Quattrochi *et at.*, 2001);

(d) The spatial complexity of the subsets along the transects of the study areas computed using the isarithm and the TPSA indicated a higher $D_{ISARITHM}$ than D_{TPSA}. This was attributed to the approach which uses the isarithms of the image by dividing the range of pixel values into a number of equally spaced intervals for computing the $D_{ISARITHM}$. As a result, it excludes few random pixels that have high values and thus, measures the major variation dominating the subsets, thereby yielding higher dimension (Qiu *et al.*, 1999). Moreover, the orientation of the features of the study areas affect the $D_{ISARITHM}$ as they exhibit different characteristics when measured in different directions i.e. along rows, column and row-column methods. Another source of discrepancy of the results of the isarithm method could be the isarithm values and the isarithm interval as there is no theoretical basis for selecting these parameters. On the contrary, the TPSA calculates the surface area of the prisms formed by the image at varying spatial resolutions and accordingly, computes the D_{TPSA}. The results of the TPSA method were found consistent over the study areas and

considered to be the more robust in measuring the spatial complexity of urban landscapes, which supports the findings of Read and Lam (2002) and Qiu *et al.* (1999);

(e) Moran's *I* of spatial autocorrelation was found useful for characterising the spatial pattern of land covers, while the non-statistical parameters (e.g. the coefficient of variation and standard deviation) were found useful in describing the spectral variability of urban land cover types. The results of the study areas revealed that the higher the Moran's *I*, the less the fractal dimension indicating a lower spatial complexity. A correlation analysis between Moran's *I* and the *D* of the subsets of the study areas computed from SPOT, Landsat-7 ETM+ and Landsat MSS revealed a strong negative correlation. Thus, an urban landscape with a low Moran's *I* value, indicative of a random distribution will result a high *D* value indicating high spatial complexity and vice versa. This implies that Moran's *I* of spatial autocorrelation can be used for characterising land cover patterns of urban area. The results support the findings of Read and Lam (2002) and Lam *et al.* (2002), which showed that these indices (Moran's *I* and *D*) are inversely related. On the other hand, the analysis between the coefficient of variation (CV) and the *D* of the study areas revealed no correlation, supporting the findings of Lam (1990).

8. 2 Fuzzy Land Cover Maps and Fuzzy Accuracy Measures

Urban areas by nature are very complex. Although a human operator can extract information from images of urban areas relatively easily, computer-based automated interpretation using the conventional remote sensing classifiers (e.g. parallelepiped, maximum likelihood, minimum distance from the mean) from a moderate resolution imagery (e.g. 30 m) is impeded by the abundance of mixed pixels (Small, 2003). Accordingly, the conceptual approach developed in this study attempts to incorporate the selection of the best bands of multispectral image, computation of fuzzy memberships of the predefined land cover types from the selected bands, generation of the fuzzy categorical maps by integrating fuzzy memberships of the selected bands using fuzzy operators, creation of a virtual field reference database and derivation of fuzzy memberships of ground data and finally, examining the performance of categorical maps by various fuzzy operators by means of fuzzy accuracy measures, seems effective. To this end, the study has presented a case

study, in which image classification was performed using fuzzy supervised classification of selected bands of Landsat-7 ETM+ acquired over heterogeneous urban land covers of three study areas characterising metropolitan Perth, in Western Australia. A variety of fuzzy operators (e.g. fuzzy minimum, maximum, algebraic product, algebraic sum and fuzzy gamma with γ values ranging from 0.1 to 0.95) were tested for integrating fuzzy membership values of the selected bands for generating fuzzy categorical maps. The accuracy of the fuzzy categorical maps of three study areas was then carried out in a fuzzy error matrix using fuzzy land cover and fuzzy ground-truth data. The uncertainty maps generated using the confusion index determined as 1.0 minus the difference between the first maximum fuzzy membership and the second maximum fuzzy membership were used to substantiate the source of classification errors and possible locations of mixed pixels. Finally, the effect of land cover heterogeneity on the fuzzy accuracy measures was discussed.

The major findings of this study can be summarised as follows:

(a) The transformed divergence analysis, used in traditional crisp classification for establishing a priori the upper bound achievable on classification accuracy for an existing set of spectral classes, as explained in Richards and Jia (1999), provided a sound basis for selecting the most appropriate spectral bands of the Landsat-7 ETM+ that were subsequently fuzzified for the production of fuzzy categorical maps. The highest average separability amongst the land cover classes considered in the classification scheme adopted in this research (e.g. forest, grassland, urban and dense urban) was provided by a combination of Landsat-7 ETM+ bands 1, 3, 4 and 7 for the City of Perth while a combinations of Landsat-7 ETM+ bands of 1, 2, 3, and 7 and 1, 3, 4, 5 and 7 were provided highest separability for the City of Melville and the City of Armadale, respectively;

(b) The approach of assigning a single fuzzy membership in each location (e.g. pixel) using the maximum fuzzy membership value of the class(es) present within a pixel, facilitated the process of defuzzification for accuracy assessment analysis. This approach of defuzzification is based on the approaches discussed by Zadeh (1968) and Zhang and Goodchild (2002);

(c) The accuracy of the fuzzy categorical maps generated by integrating fuzzy membership values associated with multiple spectral bands using various fuzzy

operators reveals that the fuzzy minimum operator (e.g. fuzzy AND) and the fuzzy algebraic product were not suitable for integrating fuzzy class memberships computed from selected Landsat-7 ETM+ bands, as these operators underestimated the class memberships. Accordingly, the lowest overall accuracy measures correspond to the implementation of these fuzzy operators. Likewise, the fuzzy maximum operator (e.g. fuzzy OR) was also not suitable as the class memberships were overestimated and accordingly, high commission errors occurred. It is important to note that fuzzy maximum operator does not offer any compensation of information amongst the bands used in the analysis (e.g. a single value), which contributed to misclassification and accordingly, high omission and commission error occurred. When applying fuzzy operators such as the fuzzy algebraic sum and the fuzzy gamma operators (with varying γ values) all contributing membership values computed in the selected Landsat-7 ETM+ spectral bands have an effect on the result, increasing the accuracy in identification of the fuzzy land cover types. Furthermore, analysis of the accuracy assessment results shows that the fuzzy gamma operator with γ value of 0.90 outperformed the categorical accuracy measures obtained by applying the fuzzy algebraic sum and other fuzzy operators for the City of Perth, while the accuracy measures of γ value of 0.95 were found highest for the City of Melville and the City of Armadale, being therefore recommended as the optimal fuzzy operators for integrating fuzzy membership values associated with multiple spectral bands;

(d) A comparison of the accuracy measures of the fuzzy land cover maps of the study areas indicated that the overall accuracy of the City of Perth was up to 13 percent higher than the overall accuracy of the City of Melville and the City of Armadale which was found 69 percent and 71 percent, respectively (see Figure 7.16). The main factor contributing to the observed difference of the overall and categorical accuracy measures among the study areas could be attributed to the variation of land cover heterogeneity. For example, the land cover classes that were considered in the classification scheme show that the class forest of the City of Perth was clustered in the western part of the study area, while the classes dense urban and urban were clustered in the remaining study areas (See Figure 7.1). An examination of the land cover compositions of the classes forest and

dense urban revealed less mixed and accordingly, misclassification due to the occurrence of more than one land cover type in a pixel was lower. This partly contributed to a higher overall and categorical accuracy as shown in Table 7.1 of Chapter 7. On the contrary, the compositions of the land cover classes considered in the classification scheme of the City of Melville were found highly fragmented and mixed. As discussed in Section 7.2 of Chapter 7 the land cover compositions of class urban, class forest and class grassland were highly mixed and fragmented. This resulted in occurrence of a large number of mixed pixels due to the presence of more than one land cover type (e.g. urban and grassland, urban and trees) as shown in the uncertainty maps (see Figure 7.8 and Figure 7.9). The presence of mixed pixels contributed to a significant misclassification among the classes which partly contributed to low overall and categorical accuracy measures (Table 7.3). Likewise, in the City of Armadale, class forest was found clustered compared to mixed land covers of class grassland, urban and dense urban. For this study area, the class grassland was comprised of irrigated pastures and grazing areas. As the data were acquired in summer, the spectral responses of dried grassland tend to be similar to the class urban. This contributed a significant misclassification to class urban and accordingly, high omission and commission errors occurred for class grassland and urban respectively (Appendix 16k). In addition to the mixed pixels and seasonal variation, spectral similarity between class grassland and forest, urban and dense urban was identified as a source of classification errors. Apart from the sources of classification errors, the lower accuracy of the City of Melville and the City of Armadale compared to the City of Perth may reside in the adoption of the same classification scheme in all study areas. For example, an additional class such as bare ground in the City of Melville and grazing land in the City of Armadale could have improved the accuracy measures. The results suggest that the heterogeneity of urban land covers influences significantly the accuracy of information generated from satellite imagery. The overall and categorical accuracy confirms that the classification scheme and technique are suitable to characterise areas of more homogeneous pixel composition as was the case with the City of Perth. For highly spatially mixed areas like the residential areas of the City of Melville, the classification accuracies were found to be relatively low. This could be attributed to the spatial resolution of the image used in the analysis,

which is generally not sufficient to discriminate individual features (e.g. buildings, streets, trees) within residential areas, resulting in mixed pixels. The spectral similarity among the class forest and grassland, urban and dense urban is a concern, which needs to be addressed in future research.

(e) The overall accuracy of the City of Perth was found up to 6 percent higher than the results reported by Melgani et al. (2000) while up to 31 percent higher than the results reported by Zhang and Food (1998). However, accuracy was found to be lower than the results obtained by Shackelford and Davis (2003) from a high resolution multispectral IKONOS (4 m) and panchromatic data (1 m). The higher accuracy was attributed to the spatial resolution of the data, which can discriminate individual features (e.g. building, street, trees) resulting in the occurrence of low mixed pixels. For mixed land cover classes, e.g. residential area of the City of Melville and the City of Armadale which were impeded by abundance of mixed pixels, the accuracy measures were found slightly lower that the results reported in the literature. An examination of the uncertainty maps of the misclassified samples shows that confusion arises between the most likely and second most likely land cover classes dominating within a pixel. Accordingly, classification accuracies of these study areas could be improved significantly if the second maximum fuzzy membership was considered in the accuracy assessment, as demonstrated by Zhang and Foody (1998).

In addition to sources of classification errors, the uncertainty maps generated from the fuzzy categorical maps allow for locational and quantitative examinations of the misclassification of the classified data. This also provided a basis for identifying the location of mixed pixels. Therefore, the uncertainty information measured as a confusion index could be used as a quality indicator for evaluating fuzzy categorical maps. As reported by Kraak and Ormeling (1996), the uncertainty information could be attached to the fuzzy categorical maps which would facilitate better decision making by the end-user in classifying urban land covers. The findings of this study reinforced the importance of the information richness offered by a fuzzy classification, which enables an improved and integrated handling of remotely sensed data for mapping urban land covers.

8. 3 Recommendations for Future Research

The results generated through this research can be used to analyse multiscale and multisource remote sensing data for assessing the appropriateness of scale selection of any analysis using remotely sensed data. In addition, it demonstrates the usefulness of the fuzzy set theory for deriving fuzzy memberships from the selected bands of multispectral image using fuzzy *c*-means algorithm and integrating fuzzy memberships of the selected bands by the fuzzy operators. The longstanding issue of carrying out the accuracy of fuzzy categorical maps using a fuzzy error matrix considering the fuzzy memberships of the fuzzy categorical maps and the reference data was illustrated. However, some limitations still have to be overcomed. The following recommendations are proposed for future works:

8.3.1 Selecting an Operational Scale for Urban Processes

This research has emphasised the importance of scale when attempting to interpret the spatial complexity using multiscale and multisource remote sensing data for inferring processes occurring on the study areas. With the increasing availability of remotely sensed data at various spatial and spectral resolutions, the findings of this research have generated an understanding of the effects of spatial resolution, spectral resolution and land cover heterogeneity on the characterisation of spatial complexity of urban landscapes using fractal theory. It is important to note that the research has utilised the Landsat-7 ETM+ acquired on 2001 while SPOT and Landsat MSS were acquired in 1991 and 1980 respectively. Accordingly, the results particularly the analysis of spatial resolution using Landsat-7 ETM+, SPOT and Landsat MSS have encountered the temporal effect on the spatial complexity. Thus, it is envisaged that the effect of scale on the spatial complexity would have been more realistic if the data were acquired in the same year eliminating the effect of temporal change. Accordingly, it is recommended to use the same year data for the analysis of the effect of scale on the spatial complexity for selecting an optimal scale at which urban processes are operating. Another avenue could be to acquire a high resolution data set from sensors like QuickBird and IKONOS and "resample" it to different resolutions for assessing the effect of scale on the spatial complexity. In addition, research could be carried out to examine how the spatial complexity of urban landscapes, having a known spatial operational scale are depicted in multiscale

remote sensing images. This would allow testing of the fractal dimension's response to change in resolution.

8.3.2 Fractal Measurement Algorithms

The fractal dimension computed from the isarithm method was found slightly higher than the TPSA method. Although the results of previous studies support the findings of this research, it is recommended to test the performances with the simulated surfaces with known fractal dimension in order to assess the robustness of these algorithms in computing the spatial complexity of urban landscapes.

8.3.3 Classifier's Performance in Generating Fuzzy Land Cover Maps

Although the methodology for generating fuzzy categorical maps, locational and quantitative examination of misclassification using confusion index seems sound, the overall and categorical accuracy measures of the City of Melville and the City of Armadale were not encouraging as compared to the accuracy measures of the City of Perth. The main contributing factors of relatively low accuracy measures of the City of Melville and the City of Armadale were due to (i) spatially mixed areas like the residential areas, resulting in mixed pixels in a Landsat-7 ETM+ scene; and (ii) the spectral similarity between the class grassland and forest, and class urban and dense urban. Accordingly, these issues need to be addressed in future research to improve the classification accuracy. One possible avenue could be the application of the methodology to a high resolution multispectral imagery (e.g. QuickBird, IKONOS) which may enable discrimination of individual features of residential areas that result in mixed pixels. Likewise, spatial measures such as texture could be incorporated with the fuzzy classification to increase the discrimination between spectrally similar classes for the improvement of classification accuracy as attempted by Shackelford and Davis (2003).

REFERENCES

An, P., Moon, W. M. and Rencz, A. (1991) Application of Fuzzy Set Theory for Integration of Geological, Geophysical and Remote Sensing Data, *Canadian Journal of Exploration Geophysics*, Vol. 27, No. 1, pp. 1-11.

Anderson, J. R., Hardy, E. E., Roach, J. T. and Witmer, R. E. (1976) A Land Use and Land Cover Classification System for Use with Remote Sensor Data, USGS Professional Paper 964, Sioux Falls, SD, USA.

ABS (1996) 1996 Census of Population and Housing, Australian Bureau of Statistics, Commonwealth of Australia, Canberra.

ABS (2001) 2001 Census of Population and Housing, Australian Bureau of Statistics, Commonwealth of Australia, Canberra.

Bezdek, J. C. (1975) Mathematics Models for Systematics and Txonomy, in *Proceedings of the Eighth International Conference on Numerical Taxonomy*, G. Estabrook (ed.), Freeman, San Francisco, pp. 143-164.

Bezdek, J. C. (1981) Pattern Recognition with Fuzzy Objective Function Algorithms, Plenum, New York, 256 pp.

Bezdek, J. C., Ehrlich, R. and Full, W. (1984) FCM: The Fuzzy c-Means Clustering Algorithm, *Computers and Geosciences*, Vol. 10, pp. 191-203.

Binaghi, E., Brivio, P. A., Ghezzi, P. and Rampini, A. (1999) A Fuzzy Set-based Accuracy Assessment of Soft Classification, *Pattern Recognition Letters*, Vol. 20, No. 9, pp. 935-948.

Birrell, R. and Tonkin, S. (1992) Constraints and Opportunities for Urban Growth: Sydney and Perth Compared, in Consultants' Reports, *Population Issues and Australia's Future- Environment and Society*, National Population Council, Canberra, pp. 1-47.

Bonham-Carter, G. (1994) *Geographic Information Systems for Geoscientists: Modelling with GIS*, Pergamon Press, New York, 398 pp.

Brown, M., Lewis, H. G. and Gunn, S. R. (2000) Linear Spectral Mixture Models and Support Vector Machines Remote Sensing, *IEEE Transactions on Geoscience and Remote Sensing*, Vol. 38, No. 5, pp. 2346-2360.

Bureau of Meteorology (2001) *Climate Data of Perth Metropolitan Area*, Climate and Consultancy Section of the Western Australian Office of the Bureau of Meteorology, Perth, Western Australia.

Burrough, P. A. (1986) *Principles of Geographical Information Systems for Land Resources Assessment*, Clarendon Press, Oxford, 194 pp.

Burrough, P. A. (1993a) *Principles of Geographical Information Systems for Land Resources Assessment*, Clarendon Press, Oxford, 194 pp.

Burrough, P. A. (1993b) Fractals and Geostatistical Methods in Landscape Studies, in *Fractals in Geography*, N. S.-N. Lam and L. De Cola (Eds.), Prentice Hall, Englewood Cliffs, New Jersey, pp. 87-121.

Burrough, P.A. (1996) Natural Objects with Indeterminate Boundaries, in *Geographic Objects with Indeterminate Boundaries*, P. A. Burrough, and A. U. Frank (Eds.), Taylor & Francis, London, pp. 3-28.

Burrough, P.A. and McDonnell, R. A. (Eds.) (1998) *Principles of Geographical Information Systems*, Oxford Press, New York, 333 pp.

Campbell, J. B. (1987) *Introduction to Remote Sensing*, Second Edition, Guilford Press, New York, 551 pp.

Cannon, R. L., Dave, J. V. and Bezdek, J. C. (1986a) Efficient Implementation of the Fuzzy c-Means Clustering Algorithms, *IEEE Transactions on Pattern Analysis and Machine Intelligence*, Vol. PAMI-8, No. 2, pp. 248-255.

Cannon, R. L., Dave, J. V., Bezdek, J. C. and Trivedi, M. M. (1986b) Segmentation of a Thematic Mapper Image Using Fuzzy c-Means Clustering Algorithm, *IEEE Transactions on Geoscience and Remote Sensing*, Vol. GE-24, No. 3, pp. 400-408.

Cao, C. and Lam, N. S.-N. (1997) Understanding the Scale and Resolution Effects in Remote Sensing and GIS, in *Scale in Remote Sensing and GIS*, Dale A. Quattrochi and Michael F. Goodchild (Eds.), CRC Press, Inc., Boca Raton, Florida, pp. 57-72.

Card, A. (1982) Using Known Map Category Marginal Frequencies to Improve Estimates of Thematic Map Accuracy, *Photogrammetric Engineering and Remote Sensing*, Vol. 48, No. 3, pp. 431-439.

Carr, J. (1990) Surface Roughness Characterisation of Rock Masses Using the Fractal Dimension and the Variogram, *Technical Report No. REMR-GT-14*, US Army Waterways Experimental Station, Vicksburg, MS.

Clarke, K. C. (1986) Computation of the Fractal Dimension of Topographic Surfaces using the Triangular Prism Surface Area Method, *Computers and Geosciences*, Vol. 12, No. 5, pp. 713-722.

Cliff, A. D. and Ord, J. K. (1973) *Spatial Autocorrelation*, Pion, London, 178 pp.

Cochran, W. G. (1977) *Sampling Techniques* (3rd Edition), Wiley, New York, 413 pp.

Congalton, R. G. (1988) A Comparison of Sampling Schemes Used in Generating Error Matrices for Assessing the Accuracy of Maps Generated from Remotely Sensed Data, *Photogrammetric Engineering and Remote Sensing*, Vol. 54, No. 5, pp. 593-600.

Congalton, R. G. (1991) A Review of Assessing the Accuracy of Classifications of Remotely Sensed Data, *Remote Sensing of Environment*, Vol. 37, No. 1, pp. 35-46.

Congalton, R. G. and Green, K. (1999) *Assessing the Accuracy of Remotely Sensed Data: Principles and Practices*, Lewis Publications, Boca Raton, 137 pp.

Curran, P. J. (1988) The Semivariogram in Remote Sensing: An Introduction, *Remote Sensing of Environment,* Vol. 24, No. 3, pp. 493-507.

Curran, P. J. and Williamson, H. D. (1986) Sample Size for Ground and Remotely Sensed Data, *Remote Sensing of Environment*, Vol. 20, No., 1, pp. 31-41.

De Cola, L. (1989) Fractal Analysis of a Classified Scene, *Photogrammetric Engineering and Remote Sensing*, Vol. 55, No. 5, pp. 601-610.

De Cola, L. (1993) Multifractals in Image Processing and Process Imaging, in *Fractals in Geography*, N. S. -N. Lam and L. Dee Cola (Eds.), Prentice Hall, Englewood Cliffs, New Jersey, pp.282-304.

de Jong, S. M. and Burrough, P. A. (1995) A Fractal Approach to the Classification of Mediterranean Vegetation Types in Remotely Sensed Images, *Photogrammetric Engineering and Remote Sensing*, Vol. 61, No. 8, pp. 1041-1053.

Department of Planning and Urban Development (1991) *Household, Dwelling and Labour Force Projections for Western Australia and its Statistical Divisions:1986-2021*, DPUD, Western Australia.

Dombi, J. (1990) Membership function as an Evaluation, *Fuzzy Sets and Systems*, Vol. 35, pp. 1–21.

Dubois, D. and Prade, H. (1985) A Review of Fuzzy Set Aggregation Connectives, *Information Science*, Vol. 36, pp. 85-121.

Dunn, J. C. (1974) A Fuzzy Relative of the Isodata Process and Its Use in Detecting Compact, Well Separated Clusters, *Journal of Cybernetics*, Vol. 3, pp. 22-57.

Dutton, G. H. (1981) Fractal Enhancement of Cartographic Line Detail, *The American Cartographer*, Vol. 8, No. 1, pp. 22-40.

Emerson, C. W., Lam, N. S.-N. and Quattrochi, D. A. (1999) Multi-Scale Fractal Analysis of Image texture and Pattern, *Photogrammetric Engineering and Remote Sensing*, Vol. 65, No. 1, pp. 51-61.

ERDAS (2000) ERDAS Imagine® 8.4.

ESRI (2000) *ARC/INFO ver 8.0.2*, ESRI, Redlands, California.

Falconer, K. (1990) *Fractal Geometry-Mathematical Foundations and Applications*, John Wiley, Chichester, 288 pp.

Finn, J. T. (1993) Use of the Average Mutual Information Index in Evaluating Classification Error and Consistency, *International Journal of Geographical Information Systems*, Vol. 7, pp. 349-366.

Fisher, P. F. (1997) The Pixel: A Snare and a Delusion, *International Journal of Remote Sensing*, Vol. 18, No. 3, pp. 679-685.

Fisher, P. F. and Pathirana, S. (1990) The Evaluation of Fuzzy Membership of Land Cover Classes in the Suburban Zone, *Remote Sensing of Environment*, Vol. 34, pp. 121-132.

Fitzpatrick-Lins, K. (1981) Comparison of Sampling Procedures and Data Analysis for a Land-use and Land-cover Map, *Photogrammetric Engineering and Remote Sensing*, Vol. 47, No. 3, pp. 343-351.

Foody, G. M. (1992) A Fuzzy Sets Approach to the Representation of Vegetation Continua from Remotely Sensed Data: An Example from Lowland Heath, *Photogrammetric Engineering and Remote Sensing*, Vol. 58, No. 2, pp. 221-225.

Foody, G. M. (1995) Cross-entropy for the Evaluation of the Accuracy of a Fuzzy Land Cover Classification with Fuzzy Ground Data, *ISPRS Journal of Photogrammetric Engineering and Remote Sensing*, Vol. 50, No. 5, pp. 2-12.

Foody, G. M. (1996a) Approaches for the Production and Evaluation of Fuzzy Land Cover Classifications from Remotely Sensed Data, *International Journal of Remote Sensing*, Vol. 17, No. 7, pp. 1317-1340.

Foody, G. M. (1996b) Fuzzy Modelling of Vegetation from Remotely Sensed Imagery, *Ecological Modelling*, Vol. 75, pp. 3-12.

Foody, G. M. (2000) Estimation of Sub-Pixel Land Cover Composition in the Presence of Untrained Classes, *Computers and Geosciences*, Vol. 26, No. 4, pp. 469-478.

Foody, G. M. and Arora, M. K. (1996) Incorporating Mixed Pixels in the Training, Allocation and Testing Stages of Supervised Classifications, *Pattern* Recognition Letters, Vol. 17, No. 13, pp.1389-1398.

Foody, G. M. and Cox, D. P. (1994) Sub-pixel Land Cover Composition Estimation Using a Linear Mixture Model and Fuzzy Membership Functions, *International Journal of Remote Sensing*, Vol. 15, No. 3, pp. 619-631.

Foody, G. M. and Curran, P. J. (1994) Scale and Environmental Remote Sensing, in *Environmental Remote Sensing from Regional to Global Scales*, G. M. Foody, and P. J., Curran (Eds.), John Wiley & Sons, New York, pp. 223-232.

Foody, G. M. and Trodd, N. M. (1993) Non-Classificatory Analysis and Representation of Heathland Vegetation from Remotely Sensed Imagery, *GeoJournal*, Vol. 29, No. 4, pp. 343-350.

Foody, G. M., Campbell, N. A., Trodd, N. M. and Wood, T. F. (1992) Derivation and Applications of Probabilistic Measures of Class Membership from the Maximum-Likelihood Classification, *Photogrammetric Engineering and Remote Sensing*, Vol. 58, No. 9, pp. 1335-1341.

Forster, B. C. (1985) An Examination of Some Problems and Solutions in Monitoring Urban Areas from Satellite Platforms, *International Journal of Remote Sensing*, Vol. 6, No. 1, pp. 139-151.

Fournier, A., Fussell, D. and Carpenter, L. C. (1982) Computer Rendering of Stochastic Models, *Communications, ACM*, Vol. 25, No. 6, pp. 371-384.

Goodchild, M. F. (1980) Fractals and the Accuracy of Geographical Measures, *Journal of Mathematical Geology*, Vol. 12, No. 2, pp. 85-98.

Goodchild, M. F. (1994) Integrating GIS and Remote Sensing for Vegetation Analysis and Modelling: Methodological Issues, *Journal of Vegetation Science*, Vol. 5, pp. 615-626.

Goodchild, M. F. and Mark, D. M. (1987) The Fractal Nature of Geographic Phenomena, *Annals of the Association of American Geographers*, Vol. 77, No. 2, pp. 265-278.

Gopal, S., and Woodcock, C. (1994) Theory and Methods for Accuracy Assessment of Thematic Maps using Fuzzy Sets, *Photogrammetric Engineering and Remote Sensing*, Vol. 60, No. 2, pp. 181-188.

Gregotsky, M. E., Jensen, O. and Arkani-Hamed, J. (1991) Fractal Stochastic Modeling of Aeromagnetic Data, *Geophysics*, Vol. 56, pp. 1706-1715.

Hay, A. M. (1979) Sampling Designs to Test Land-use Map Accuracy, *Photogrammetric Engineering and Remote Sensing*, Vol. 45, No. 4, pp. 671-677.

Heddle, E. M., Loneragan, O. W. and Havel, J. J. (1980) Vegetation Complexes of the Darling System, Western Australia, Department of Conservation and the Environment, Perth, Western Australia.

Hord, R. M. and Brooner, W. (1976) Land Use Accuracy Criteria, *Photogrammetric Engineering and Remote Sensing*, Vol. 42, No. 5, pp. 671-677.

Isaaks, E. H. and Srivastava, R. M. (1989) *An Introduction to Applied Geostatistics*, Oxford University Press, New York, 592 pp.

Jager, G. and Benz, U. (2000) Measures of Classification Accuracy Based on Fuzzy Similarity, *IEEE Transactions on Geoscience and Remote Sensing*, Vol. 38, No. 3, pp. 1462-1467.

Jaggi, S., Quattrochi, D. A. and Lam, N. S. -N. (1993) Implementation and Operation of Three Fractal Measurement Algorithms for Analysis of Remote Sensing Data, *Computers and Geosciences*, Vol. 19, No. 6., pp. 745-767.

Janssen, L. L. F. and van der Wel, F. J. M (1994) Accuracy Assessment of Satellite Derived Land Cover Data: A Review, *Photogrammetric Engineering and Remote Sensing*, Vol. 60, No. 4, pp. 419-426.

Jensen, J. R. (1996) Introductory Digital Image Processing: A Remote Sensing Perspective, Prentice Hall, New York, 225 p.

Joria, P. E. and Jorgenson, J. C. (1996) Comparison of Three Methods for Mapping Tundra with Landsat Digital Data, *Photogrammetric Engineering and Remote Sensing*, Vol. 62, No. 2, pp. 163-169.

Jupp, D. L. B., Strahler, A. H. and Woodcock, C. E. (1988) Theory of Autocovariance and Regularization in Digital Images, *IEEE Transactions on Geoscience and Remote Sensing,* Vol. 26, No. 4, pp. 463-473.

Kennedy, M. (2002) *The Global Positioning System and GIS*, Taylor and Francis Inc, New York, 336 pp.

Kent, J. T. and Mardia, K. V. (1988) Spatial Classification Using Fuzzy Membership Models, *IEEE Transactions on Pattern Analysis and Machine Intelligence*, Vol. 10, No. 5, pp. 659-671.

Key, J. R., Maslanik, J. A. and Barry, R. G. (1989) Cloud Classification from Satellite Data Using a Fuzzy Sets Algorithm: A Polar Example, *International Journal of Remote Sensing*, Vol. 10, No. 12, pp. 1823-1842.

Klinkenberg, B. (1992) Fractals and Morphometric Measures: Is Their a Relationship?, *Geomorphology*, Vol. 5, pp. 5-20.

Klinkenberg, B. and Goodchild, M. F. (1992) The Fractal Properties of Topography: A Comparison of Methods, *Earth Surface Processes and Landforms*, Vol. 17, pp. 217-234.

Klir, G. J. and Folger, T. A. (1988) *Fuzzy Sets, Uncertainty and Information*, Prentice Hall, Englewood Cliff, New Jersey, 355 pp.

Klir, G. J. and Yuan, B. (1995) *Fuzzy Sets and Fuzzy Logic: Theory and Applications,* Prentice Hall, New Jersey, 592 pp.

Kolibal, J. and Monde, J. (1998) Fractal Image Error Analysis, *Computers and Geosciences*, Vol. 24, No. 8, pp. 785-795.

Kraak, M. J. and Ormeling, F. J. (Eds.) (1996) *Cartography: Visualisation of Spatial Data*, Longman, Essex, England, 37 p.

Krummel, J. R., Gardner, R. H., Sugihara, G., O'Neill, R. V. and Coleman, P. R. (1987) Landscape Pattern in a Disturbed Environment, *Oikos*, Vol. 48, pp. 321-324.

Kube, P. and Pentland, A. P. (1988) On the Imaging of Fractal Surfaces, IEEE Transactions on Pattern Analysis and Machine Intelligence, Vol. 10, No. 5, pp. 704-707.

Laba, M., Gregory, S. K., Braden, J., Ogurcak, D., Hill, E., Fegraus, E., Fiore, J. and DeGloria, S. D. (2002) Conventional and Fuzzy Accuracy Assessment of the New York Gap Analysis Project Land Cover Map, *Remote Sensing of Environment,* Vol. 81, No, 2-3, pp. 443-455.

LaGro, J., Jr. (1991) Assessing Patch Shape in Landscape Mosaics, *Photogrammetric Engineering and Remote Sensing*, Vol. 57, No. 3, pp. 258-293.

Lam, N. S.-N. (1990) Description and Measurement of Landsat TM Images Using Fractals, *Photogrammetric Engineering and Remote Sensing*, Vol. 56, No. 2, pp. 187-195.

Lam, N. S.-N. and De Cola, L. (1993) Fractal Measurement, in *Fractals in Geography*, N. S. -N. Lam and L. Dee Cola (Eds.), Prentice Hall, Englewood Cliffs, New Jersey, pp. 23-55.

Lam, N. S.-N. and Quattrochi, D. A. (1992) On the Issues of Scale, Resolution, and Fractal Analysis in the Mapping Sciences, *The Professional Geographers*, Vol. 44, No. 1, pp. 88-98.

Lam, N. S.-N., Qiu, H. and Quattrochi, D. A. (1997) An Evaluation of Fractal Surface Measurement Methods using ICAMS (Image Characterisation and Modelling System), *Technical Papers, ACSM/ASPRS Annual Convention, Vol. 5. Auto-Carto 13* (ASPRS and ACSM, Bethesda, Maryland), pp. 377-386.

Lam, N. S.-N., Qiu, H., Quattrochi, D. A. and Emerson, C. W. (2002) An Evaluation of Fractal Methods for Characterising Image Complexity, *Cartography and Geographic Information Science*, Vol. 29, No. 1, pp. 25-36.

Li, H. and Reynolds, J. F. (1993) A New Contagion Index to Quantify Spatial Patterns of Landscapes, *Landscape Ecology*, Vol. 8, pp. 155-162.

Longley, P. A., Goodchild, M. F., Maguire, D. J. and Rhind, D. W. (2001) *Geographic Information Systems and Science*, Wiley, Chichester, 100 p.

Lowell, K. E. (1994) An Uncertainty-based Spatial Representation of Natural Resources Phenomena, Advances in GIS Research, *Proceedings of the 6th International Symposium on Spatial Data Handling*, Taylor and Francis, London, pp. 933-944.

Lunetta, R. S., Iiames, J., Knight, J., Congalton, R. G. and Mace, T. H. (2001) An Assessment of Reference Data Variability Using a "Virtual Field Reference Database", *Photogrammetric Engineering and Remote Sensing*, Vol. 63, No. 6, pp. 707-715.

Mandelbrot, B. B. (1977) *Fractals: Form, Chance and Dimension,* Freeman, San Francisco, California.

Mark, D. M. and Aronson, P. B. (1984) Scale-Dependent Fractal Dimensions of Topographic Surfaces: An Empirical Investigation with Applications in Geomorphology and Computer Mapping, *Mathematical Geology,* Vol. 16, No. 7, pp. 671-683.

Maselli, F., Conese, C. and Petkov, L. (1994) Use of Probability Entropy for the Estimation and Graphical Representation of the Accuracy of Maximum Likelihood Classifications, *ISPRS Journal of Photogrammetry and Remote Sensing,* Vol. 49, No. 2, pp. 13-20.

McBratney, A. B. and Moore, A. W. (1985) Application of Fuzzy Sets to Climatic Classification, *Agricultural and Forest Meteorology,* Vol. 35, pp. 165-185.

McBratney, A. B. and Webster, R. (1981) Spatial Dependence and Classification of the Soil along a Transect in Northwest Scotland, *Geoderma,* Vol. 26, pp. 63-82.

McGarigal, K. and Marks, B. J. (1995) FRAGSTATS: Spatial Pattern Analysis Program for Quantifying Landscape Structure, U.S. Department of Agriculture, Forest Service, Pacific Northwest Research Station, Portland, OR, USA, pp. 122.

Meentemeyer, V. and Box, E. O. (1987) Scale Effects in Landscape Studies, in *Landscape Heterogeneity and Disturbance*, M. G., Turner (Ed.), Springer-Verlag, New York, pp. 15-34.

Melgani, F., Al Hashemy, B. A. R. and Taha, S. M. R. (2000) An Explicit Fuzzy Supervised Classification Method for Multispectral Remote Sensing Images, *IEEE Transactions on Geoscience and Remote Sensing*, Vol. 38, No.1, pp. 287-295.

Meney, K. A. (1999) *Mt Eliza Escarpment Restoration Plan/WMC Resources Ltd. Centre for Urban Bushland Management*, Kings Park and Botanic Garden, Western Australia.

Metternicht, G. (1996) Detecting and Monitoring Land Degradation and Processes in the Cochabamba Valleys, Bolivia, a Synergistic Approach, *Publication No. 36, ITC*, Enschede, The Netherlands.

Metternicht, G. (1998) Fuzzy Classification of JERS-1 SAR Data: An Evaluation of its Performance for Soil Salinity Mapping, *Ecological Modelling* Vol. 111, No. 1, pp. 61-74.

Metternicht, G. (1999) Change Detection Assessment Using Fuzzy Sets and Remotely Sensed Data: An Application of Topographic Map Revision, *ISPRS Journal of Photogrammetry and Remote Sensing,* Vol. 54, No. 4, pp. 221-233.

Metternicht, G. and Zinck, J. A. (1997) Spatial Discrimination of Salt- and Sodium-Affected Soil Surfaces, *International Journal of Remote Sensing,* Vol. 18, No. 12, pp. 2571-2586.

Metternicht, G. and Zinck, J. A. (1998) Evaluating the Information Content of JERS-1 SAR and Landsat TM Data for Discrimination of Soil Erosion Features, *ISPRS Journal of Photogrammetry and Remote Sensing,* Vol. 53, No. 3, pp. 143-153.

Milne, B. T. (1991) Lessons From Applying Fractal Models to Landscape Patterns, in *Quantitative Methods in Landscape Ecology*, M. G. Turner and R. H. Gardner (Eds.), Springer-Verlag, pp. 199-235.

Mohan, B. K., Madhavan, B. B. and Gupta, U. M. D. (2000) Integration of IRS-1A L2 Data by Fuzzy Logic Approaches for Landuse Classification, *International Journal of Remote Sensing*, Vol. 21, No. 8, pp. 1709-1723.

Moon, W. M., Chung, C. F. and An, P. (1991) Representing and Integration of Geological, Geophysical and Remote Sensing Data, *Geoinformatics,* Vol. 2, pp. 177-182.

Muller, S. V., Walker, D. A., Nelson, F. E., Auerbach, N. A., Bockheim, J. G., Guyer, S. and Sherba, D. (1998) Accuracy Assessment of a Land Cover Map of the Kuparuk River Basin, Alaska: Considerations for Remote Regions, *Photogrammetric Engineering and Remote Sensing*, Vol. 64, No. 6, pp. 619-628.

Olsen, E. R., Ramsey, R. D. and Winn, D. S. (1993) A Modified Fractal Dimension as a Measure of Landscape Diversity, *Photogrammetric Engineering and Remote Sensing*, Vol. 59, No. 10, pp. 1517-1520.

O'Neill, R. V., Krummel, J. R., Gardner, R. H., Sugihara, G., Jackson, B., DeAngelis, D. L., Milne, B. T., Turner, M. G., Zygmunt, B., Christensen, S. W., Dale, V. H. and Graham, R. L. (1988) Indices of Landscape Pattern, *Landscape Ecology*, Vol. 1, No. 3, pp. 153-162.

Pachepsky, Y. A., Ritchie, J. C., and Gimenez, D., (1997). Fractal Modelling of Airborne Laser Altimetry Data, *Remote Sensing of Environment*, Vol. 61, No. 1, pp. 150-161.

Pal, S. K., Ghosh, A. and Shankar, B. U. (2000) Segmentation of Remotely Sensed Images with Fuzzy Thresholding, and Quantitative Evaluation, *International Journal of Remote Sensing*, Vol. 21, No. 11, pp. 2269-2300.

Pathirana, S. (1999) Distribution of Errors in a Classified Map of Satellite Data, *Geocarto International*, Vol. 14, No. 4, pp. 70-81.

Pentland, A. P. (1984) Fractal-Based Description of Natural Scenes, IEEE Transactions on Pattern Analysis and Machine Intelligence, Vol. 6, No. 6, pp. 661-674.

Qiu, H.-L., Lam, N. S.-N., Quattrochi, D. A. and Gamon, J. A. (1999) Fractal Characterisation of Hyperspectral Imagery, *Photogrammetric Engineering and Remote Sensing*, Vol. 65, No. 1, pp. 63-71.

Quattrochi, D. A., Emerson, C. W., Lam, N. S.-N. and Qiu, H.-L. (2001) Fractal Characterisation of Multitemporal Remote Sensing Data, in *Scale in Remote Sensing and GIS*, Nicholas J. Tate and Peter M. Atkinson (Eds.), John Wiley & Sons, Ltd., West Sussex, England, pp. 13-34.

Quattrochi, D. A., Lam, N. S.-N., Qiu, H.-L. and Zhao, W. (1997) Image Characterization and Modelling Systems (ICAMS): A Geographic Information System for the Characterisation and Modeling of Multiscale Remote Sensing Data, in *Scale in Remote Sensing and GIS*, Dale A. Quattrochi and Michael F. Goodchild (Eds.), Cambridge University Press, Cambridge, pp. 295-307.

Read, J. M. (2003) Spatial Analyses of Logging Impacts in Amazonia Using Remotely Sensed Data, *Photogrammetric Engineering and Remote Sensing*, Vol. 69, No. 3, pp. 275-282.

Read, J. M. and Lam, N. S-.N. (2002) Spatial Methods for Characterising Land Cover and Detecting Land-Cover Changes for the Tropics, *International Journal of Remote Sensing,* Vol. 23, No., 12, pp. 2457-2474.

Rees, W. G. (1992) Measurement of the Fractal Dimension of Ice-Sheet Surfaces Using Landsat Data, *International Journal of Remote Sensing,* Vol. 13, No. 4, pp. 663-671.

Richards, J. A. (1993) *Remote Sensing Digital Image Analysis: An Introduction*, Second Edition, Springer, Berlin, 340 pp.

Richards, J. A. and Jia, X. (1999) *Remote Sensing Digital Image Analysis: An Introduction*, Third Edition, Springer, Berlin, 363 pp.

Ricotta, C. and Avena, G. C. (1998) Fractal Modelling of the Remotely Sensed Two-Dimensional Net Primary Production Pattern with Annual Cumulative AVHRR NDVI data, *International Journal of Remote Sensing,* Vol. 19, No. 12, pp. 2413-2418.

Ricotta, C., Avena, G. C., Olsen, E. R., Ramsey, R. D. and Winn, D. S. (1998) Monitoring the Landscape Stability of Mediterranean Vegetation in Relation to Fire with a Fractal Algorithm, *International Journal of Remote Sensing,* Vol. 19, No. 5, pp. 871-881.

Robinson, V. B. (1988) Some Implications of Fuzzy Set Theory Applied to Geographic Database, *Computers, Environment and Urban System*, Vol. 12, No. 1, pp. 89-97.

Rosenfield, G. H. and Fitzpatrick-Lins, K. (1986) A coefficient of agreement as a measure of thematic classification accuracy, *Photogrammetric Engineering and Remote Sensing*, Vol. 52, No. 2, pp. 223-227.

Rosenfield, G. H., Fitzpatrick-Lins, K. and Ling, H. (1982) Sampling for Thematic Map Accuracy Testing, *Photogrammetric Engineering and Remote Sensing*, Vol. 48, No. 1, pp. 131-137.

Ruspini, E. H. (1969) A New Approach to Clustering, *Information and Control*, Vol. 15, No.1, pp. 22-32.

Settle, J. J. and Drake, N. A. (1993) Linear Mixing and the Estimation of Ground Cover Proportions, *International Journal of Remote Sensing,* Vol. 14, No. 6, pp. 1159-1177.

Shackelford, A. K. and Davis, C. H. (2003) A Hierarchical Fuzzy Classification Approach for High-Resolution Multispectral Data over Urban Areas, *IEEE Transactions on Geoscience and Remote Sensing*, Vol. 41, No. 9, pp. 1920-1932.

Shelberg, M. C., Lam, N. S.-N. and Moellering, H. (1983) Measuring the Fractal Dimensions of Surfaces, *Proc. Sixth International Symposium on Automated Cartography (Auto-Carto 6)*, Ontario, Canada, pp. 319-328.

Shelberg, M. C., Moellering, H. and Lam, N. S.-N. (1982) Measuring the Fractal Dimensions of Empirical Cartographic Curves, *Proc. Fifth International Symp. Computer-Assisted Cartography (Auto-Carto 5)*, Washington, D. C., pp. 481-490.

Skidmore, A. K. and Turner, B. J. (1988) Forest Mapping Accuracies are Improved Using Supervised Nonparametric Classifier with SPOT Data, *Photogrammetric Engineering and Remote Sensing*, Vol. 54, No. 10, pp. 1415-1421.

Snow, R. S. and Mayer, L. (Eds.) (1992) Fractals in Geomorphology, *Geomorphology*, Vol. 5, 194 p.

Small, C. (2003) High Spatial Resolution Spectral Mixture Analysis of Urban Reflectance, *Remote Sensing of Environment*, Vol. 88, pp. 170-186.

Stone, K. H. (1972) A Geographer's Strength: The Multiple-Scale Approach, *Journal of Geography*, Vol. 71, No. 6, pp. 354-62.

Story, M. and Congalton, R. G. (1986) Accuracy Assessment: A User's Perspective, *Photogrammetric Engineering and Remote Sensing*, Vol. 52, No. 3, pp. 397-399.

Swain, P. H. and Davis, S. M. (Eds.) (1978) *Remote Sensing: The Quantitative Approach*, McGraw-Hill, New York, 396 pp.

Ten Berge, H. F. M., Stroosnijder, L., Burrough, P. A., Bregt, A. K. and de Heus, M. J. (1983) Spatial Variability of Soil Properties Influencing the Temperature of the Soil Surface, *Agricultural Water Management*, Vol. 6, pp. 213-226.

Tobler, W. R. (1988) Resolution, Resampling, and all That, in *Building Database for Global Science*, H. Mounsey and R. Tomlinson (Eds.), Taylor and Francis, London, pp. 129-137.

Trivedi, M. M. and Bezdek, J. C. (1986) Low-Level Segmentation of Aerial Images with Fuzzy Clustering, *IEEE Transactions on System, Man and Cybernetics*, Vol. SMC-16, No. 4, pp. 589-598.

Turcotte, D. L. (1992) *Fractals and Chaos in Geology and Geophysics,* Cambridge University Press, Cambridge.

Turner, M. G., Dale, V. H. and Gardner, R. H. (1989) Predicting Across Scales: Theory, Development, and Testing, *Landscape Ecology*, Vol. 3, No. 3/4, pp. 245-252.

Unwin, D. (1989) Fractals and the Geosciences: Introduction, *Computers and Geosciences (Special Issue on Fractals and the Geoscience)*, Vol. 15, No. 2, pp. 163-165.

Van Genderen, J. L., Lock, B. F. and Vass, P. A. (1978) Remote Sensing: Statistical Testing of Thematic Map Accuracy, *Remote Sensing of Environment*, Vol. 7, pp. 3-14.

Wang, F. (1990a) Fuzzy Supervised Classification of Remote Sensing Images, *IEEE Transactions on Geoscience and Remote Sensing*, Vol. 28, No. 2, pp. 194-201.

Wang, F. (1990b) Improving Remote Sensing Image Analysis through Fuzzy Information Representation, *Photogrammetric Engineering and Remote Sensing*, Vol. 56, No. 8, pp. 1163-1169.

Webster, R. and Oliver, M. A. (1992) Sample Adequately to Estimate Variograms in Remote Sensing, *Journal of Soil Science,* Vol. 43, pp. 177-192.

Weng, Q. (2002) Land Use Change Analysis in the Zhujiang Delta of China using Satellite Remote Sensing, GIS and Stochastic Modelling, Journal of Environmental Management, Vol. 64, pp. 273-284.

Western Australian Planning Commission (WAPC) (1998) *Perth's Bushplan,* WAPC, Western Australia.

Wilkinson, G. G. (1991) The Processing and Interpretation of Remotely-Sensed Satellite Imagery – A Current View, in *Remote Sensing and Geographical Information Systems for Resource Management in Developing countries*, A. S. Belward and C. R. Valenzuela (Eds.), Kluwer Academic Publishers, Dordrecht, pp. 71-96.

Woodcock, C. E. and Gopal, S. (2000) Fuzzy Set Theory and Thematic Maps: Accuracy Assessment and Area estimation, *International Journal of Geographical Information Science*, Vol. 14, No.2, pp. 153-172.

Woodcock, C. E. and Strahler, A. H. (1987) The Factor of Scale in Remote Sensing, *Remote Sensing of Environment,* Vol. 21, No. 3, pp. 311-332.

Woodcock, C. E., Strahler, A. H. and Jupp, D. L. B. (1988a) The Use of Variograms in Remote Sensing: I. Scene Models and Simulated Images, *Remote Sensing of Environment,* Vol. 25, No. 3, pp. 323-348.

Woodcock, C. E., Strahler, A. H. and Jupp, D. L. B. (1988b) The Use of Variograms in Remote Sensing: II. Real Images, *Remote Sensing of Environment,* Vol. 25, No. 3, pp. 349-379.

Yang, X. and Lo, C. P. (2002) Using a Time Series of Satellite Imagery to Detect Land Use and Land Cover Change in the Atlanta, Georgia Metropolitan Area, *International Journal of Remote Sensing*, Vol. 23, No. 9, pp. 1775-1798.

Zadeh, L. A. (1965) Fuzzy Sets, *Information and Control*, Vol. 8, pp. 338-353.

Zadeh, L. A. (1968) Probability Measures of Fuzzy Events, *Journal of Mathematical Analysis and Applications*, Vol. 23, pp. 421-427.

Zadeh, L. A. (1977) Fuzzy Sets, *Information and Control*, Vol. 8, pp. 338-353.

Zhang, J. X. (1996) A Surface-Based Approach to the Handling of Uncertainties in an Urban Oriented Spatial Database, *PhD Thesis*, The University of Edinburgh, Scotland, UK.

Zhang, J. and Foody, G. M. (1998) A Fuzzy Classification of Sub-urban Land Cover from Remotely Sensed Imagery, *International Journal of Remote Sensing*, Vol. 19, No. 14, pp. 2721-2738.

Zhang, J. and Goodchild, M. F. (2002) Uncertainty in Geographical Information, *Research Monograph*, Taylor & Francis, New York, 266 pp.

Zhang, J. and Kirby, R. P. (1999) Alternative Criteria for Defining Fuzzy Boundaries Based on Fuzzy Classification of Aerial Photographs and Satellite Images, *Photogrammetric Engineering and Remote Sensing*, Vol. 65, No. 12, pp. 1379-1387.

Zimmermann, H. -J. (1985) *Fuzzy Set Theory and its Application*, Kluwer Publication, Boston, 363 pp.

Zimmermann, H. -J. (1991) *Fuzzy Set Theory and its Application*, Kluwer Publication, Boston, 399 pp.

Zonneveld, I. S. (1974) Aerial Photography, Remote Sensing and Ecology, *ITC Journal*, Vol. 4, pp. 553-560.

Appendix 1 Field data collection form[1]

Site _____ _____ _____/_____ _____ _____

Type Membership grade Coordinates Suburb LGA

Date ____/____/____ Sample ID _____ Observer _____

Image _____ Photographs _____/_____

Yes No

Observation Level : 1 2 3 4

% of total area occupied by forest area

C#	Species	%

% of total area occupied by parks/ vegetation/open space

C#	Species/grass/shrub/canopies	%

% of total area occupied by commercial area/densely built-up area

C#	Commercial area/ densely built-up area	%

% of total area occupied by residential area/built-up area

C#	Residential/built-up area	%

Cover Type _____

Current feature delineation Very Poor Poor Good Very Good

Describe delineation

1. 1 C#	Comments

[1] Details of each item are attached

For each site, the following information will be recorded:

1	Site	:	Accuracy assessment of four types of grid/polygon label composed of the following codes: a. Type = A (Fuzzy land cover using Fuzzy C-Means Clustering b. Membership grade = FMV of the sample (e.g., 0.1, 0.2, 0.3, 0.4 to 1.0 c. Coordinates = XY coordinates of the sample d. Suburb = Name of the suburb (e.g., Leeming) e. LGA = Name of the Local Government Authority (e.g., Swan)
2	Date	:	Date of field visits
3	Sample ID	:	Item number of info/ASCII (created using Sample command in GRID Module) file
4	Observer	:	Initial of the field staff
5	Image	:	Name of the classified image used for verification
6	Photographs	:	Picture of the site
8	Observation level	:	1 - Walk through the target position 2 - Viewing from road adjacent to target position 3 - Viewing from afar i.e., road or ridge opposite to target position 4 - Photo interpreted/secondary sources data in the office
9	% of area occupied	:	Approximate % area occupied by the features in the target position
10	Cover type	:	Cover type based on % total area F - Forest P - Parks/vegetation/Open spaces R - Residential/low built-up area C – Commercial/high built-up area
11	Current feature delineation	:	Visual analysis of general accuracy level of existing hard copy map generated from satellite imager as viewed with the site. Very poor – Classified features and features boundary do not follow the target area in the field Poor – Classified features and features boundary shifted away from the actual feature and density Good – Classified feature and features boundary generally follows the target positions in the field. Very good – Classified feature and features boundary exactly matches with that of the field.

Appendix 2 Descriptive class statistics of the training samples of the study areas

(a) City of Perth

		Band 1	Band 2	Band 3	Band 4	Band 5	Band 7
Urban	Minimum	95	81	90	70	105	72
	Maximum	127	117	138	93	174	160
	Mean	113	99.83	109.67	81.58	127.08	97.42
	Median	115	99	108	78	118	95
	Std. Dev.	10.58	11.53	14.57	8.91	22.57	24.11
Dense Urban	Minimum	149	134	146	70	128	108
	Maximum	191	172	191	84	172	157
	Mean	164.43	147.93	162.21	77.43	146.86	133.57
	Median	156	140	160	77	141	134
	Std. Dev.	14.11	13.39	14.71	4.53	14.20	15.78
Grassland	Minimum	89	83	72	107	120	66
	Maximum	115	117	145	147	199	116
	Mean	97.3	92.6	93.6	123.2	153.6	82.5
	Median	94	87	79	121	146	76
	Std. Dev.	9.26	12.30	29.53	12.9	24.68	17.55
Forest	Minimum	79	59	53	62	80	46
	Maximum	85	68	70	73	103	60
	Mean	81.83	62	59.58	66.92	89.08	52
	Median	81	60	56	65	87	51
	Std. Dev.	2.28	3.18	5.89	3.31	7.37	4.76

(b) City of Melville

		Band 1	Band 2	Band 3	Band 4	Band 5	Band 7
Urban	Minimum	82	64	66	68	74	48
	Maximum	119	157	186	116	219	203
	Mean	114.34	104.21	123.19	90.38	151.52	123.33
	Median	113	103	123	91	153	122
	Std. Dev.	13.37	14.59	21.37	8.58	25.64	28.28
Dense Urban	Minimum	65	61	65	49	90	50
	Maximum	255	255	255	142	255	255
	Mean	171.77	157.09	174.22	88.45	177.71	158.67
	Median	166.0	152	170	87.	176	153
	Std. Dev.	38.11	37.60	39.14	14.56	38.11	44.8
Grassland	Minimum	79	66	53	95	99	44
	Maximum	119	131	160	195	197	133
	Mean	94.40	97.83	87.43	153.75	142.59	68.81
	Median	94	97	85	155	140	68
	Std. Dev.	5.22	8.13	15.20	17.61	16.53	12.08
Forest	Minimum	72	42	36	17	9	9
	Maximum	98	84	93	96	115	75
	Mean	81.73	63.31	58.53	67.89	79.06	47.72
	Median	80	62	56	70	82	48
	Std. Dev.	5.86	7.34	12.31	11.92	24.27	16.55

(c) City of Armadale

		Band 1	Band 2	Band 3	Band 4	Band 5	Band 7
Urban	Minimum	89	77	81	75	75	47
	Maximum	130	122	143	98	162	124
	Mean	109.29	98.79	113.36	86.14	126.14	94.79
	Median	108	100	119	84	130	98
	Std. Dev.	12.10	14.39	20.65	7.80	25.14	22.78
Dense Urban	Minimum	116	106	122	72	118	85
	Maximum	186	169	202	99	196	184
	Mean	140.25	129.81	151.38	79.81	152	128.88
	Median	129	125	142	78	143	126
	Std. Dev.	21.81	19.81	23.24	7.00	22.46	27.87
Grassland	Minimum	68	51	36	44	71	32
	Maximum	145	145	159	182	220	135
	Mean	91.19	82.97	84.94	103.44	136.36	78.47
	Median	86	74	71	105	127	76
	Std. Dev.	15.75	23.17	34.33	37.52	37.38	25.62
Forest	Minimum	71	52	46	61	64	29
	Maximum	81	61	57	89	90	54
	Mean	74.73	55.96	51.73	71.32	76.23	40.86
	Median	74	55.0	51	70	74	41
	Std. Dev.	2.58	2.64	3.25	7.24	7.21	6.27

Appendix 3 A typical AML for generating fuzzy memberships of the classes forest, grassland, urban and dense urban

```
/*****************************************************************
/*
/*    Name of the Program      :      fuzzy_b1.aml
/*
/*    This aml generates membership functions of each pixel of major
land cover
/*    Landsat TM image (Band 1) of Central City using a supervised
/*    approach (known mean value)
/*    Mean Values : Forest 81.833, Grassland 97.30, Urban 113.51 and
/*    Dense Urban 164.429
/*
/*****************************************************************
*
/*
/*    March, 2002
/*
/*    Zahurul Islam 2002
/*
&terminal 9999
&sv .dir = e:/cop/01_etm/b1
&sv .t_grid = [getgrid %.dir% ' Select the Image ']
grid
docell
&do i = 73 &to 105 &by 1
if(%.t_grid% == %i%)tm%i% = %i%
&end
end
docell
&do i = 106 &to 145 &by 1
if(%.t_grid% == %i%)tm%i% = %i%
&end
end
docell
&do i = 146 &to 190 &by 1
if(%.t_grid% == %i%)tm%i% = %i%
&end
end
docell
&do i = 191 &to 230 &by 1
if(%.t_grid% == %i%)tm%i% = %i%
&end
end
docell
&do i = 231 &to 251 &by 1
if(%.t_grid% == %i%)tm%i% = %i%
&end
end
/*
/* Creating a membership functions using a known mean value of the
clusters
/*
      &do i = 1 &to 1 &by 1
                  &do j = 73 &to 251 &by 1
                        &do
                              &if %i% = 1 &then
                              &sv a = 81.833
                              &else
                              &if %i% = 2 &then
```

```
                                &sv a = 97.30
                                &else
                                &if %i% = 3 &then
                                &sv a = 113.51
                                &else
                                &if %i% = 4 &then
                                &sv a = 164.429
                                &s b = 0.0
                                a%i%%j% = %b% + sqr(abs (tm%j% - %a%))
                                b%i%%j% = 100000000 / a%i%%j%
                                &s sum1 = b%i%%j%
                          &end
                                &s sum2 = 0.0
                                &s t = 0.0
                          &do k = 1 &to 4 &by 1
                                &do
                                      &if %k% = 1 &then
                                      &sv c = 81.833
                                      &else
                                      &if %k% = 2 &then
                                      &sv c = 97.30
                                      &else
                                      &if %k% = 3 &then
                                      &sv c = 113.51
                                      &else
                                      &if %k% = 4 &then
                                      &sv c = 164.429
                                      sum%i%%k% = %sum2% + sqr(abs
(tm%j% - %c%))
                                      z%i%%k% = 100000 / sum%i%%k%
                                      x%i%%k% = %t% + z%i%%k%
                                      &s t = x%i%%k%
                                &end
                          &end
                          u%i%%j% = %sum1% / %t%
                          kill sum%i%1 all
                          kill sum%i%2 all
                          kill sum%i%3 all
                          kill sum%i%4 all
                          kill z%i%1 all
                          kill z%i%2 all
                          kill z%i%3 all
                          kill z%i%4 all
                          kill x%i%1 all
                          kill x%i%2 all
                          kill x%i%3 all
                          kill x%i%4 all
                          kill a%i%%j% all
                          kill b%i%%j% all
                &end
&end
&do i = 1 &to 1 &by 1
      &do j = 73 &to 251 &by 1
            f%i%%j% = con(isnull (u%i%%j%), 0, u%i%%j%)
            kill u%i%%j% all
      &end
&end
&do i = 1 &to 1 &by 1
      &s m = 0.0
      &do j = 73 &to 251 &by 1
            x%i%%j% = %m% + f%i%%j%
```

```
            &s m = x%i%%j%
            kill f%i%%j% all
      &end
&end
&do i = 1 &to 1 &by 1
      &do j = 73 &to 250 &by 1
            kill x%i%%j% all
      &end
&end
&do i = 2 &to 2 &by 1
                  &do j = 73 &to 251 &by 1
                        &do
                              &if %i% = 1 &then
                              &sv a = 81.833
                              &else
                              &if %i% = 2 &then
                              &sv a = 97.30
                              &else
                              &if %i% = 3 &then
                              &sv a = 113.51
                              &else
                              &if %i% = 4 &then
                              &sv a = 164.429
                              &s b = 0.0
                              a%i%%j% = %b% + sqr(abs (tm%j% - %a%))
                              b%i%%j% = 100000000 / a%i%%j%
                              &s sum1 = b%i%%j%
                        &end
                              &s sum2 = 0.0
                              &s t = 0.0
                        &do k = 1 &to 4 &by 1
                              &do
                                    &if %k% = 1 &then
                                    &sv c = 81.833
                                    &else
                                    &if %k% = 2 &then
                                    &sv c = 97.30
                                    &else
                                    &if %k% = 3 &then
                                    &sv c = 113.51
                                    &else
                                    &if %k% = 4 &then
                                    &sv c = 164.429
                                    sum%i%%k%  =  %sum2%  +  sqr(abs
(tm%j% - %c%))
                                    z%i%%k% = 100000 / sum%i%%k%
                                    x%i%%k% = %t% + z%i%%k%
                                    &s t = x%i%%k%
                              &end
                        &end
                        u%i%%j% = %sum1% / %t%
                        kill sum%i%1 all
                        kill sum%i%2 all
                        kill sum%i%3 all
                        kill sum%i%4 all
                        kill z%i%1 all
                        kill z%i%2 all
                        kill z%i%3 all
                        kill z%i%4 all
                        kill x%i%1 all
                        kill x%i%2 all
```

```
                        kill x%i%3 all
                        kill x%i%4 all
                        kill a%i%%j% all
                        kill b%i%%j% all
                &end
&end
&do i = 2 &to 2 &by 1
      &do j = 73 &to 251 &by 1
            f%i%%j% = con(isnull (u%i%%j%), 0, u%i%%j%)
            kill u%i%%j% all
      &end
&end
&do i = 2 &to 2 &by 1
      &s m = 0.0
      &do j = 73 &to 251 &by 1
            x%i%%j% = %m% + f%i%%j%
            &s m = x%i%%j%
            kill f%i%%j% all
      &end
&end
&do i = 2 &to 2 &by 1
      &do j = 73 &to 250 &by 1
            kill x%i%%j% all
      &end
&end
      &do i = 3 &to 3 &by 1
                  &do j = 73 &to 251 &by 1
                        &do
                              &if %i% = 1 &then
                              &sv a = 81.833
                              &else
                              &if %i% = 2 &then
                              &sv a = 97.30
                              &else
                              &if %i% = 3 &then
                              &sv a = 113.51
                              &else
                              &if %i% = 4 &then
                              &sv a = 164.429
                              &s b = 0.0
                              a%i%%j% = %b% + sqr(abs (tm%j% - %a%))
                              b%i%%j% = 100000000 / a%i%%j%
                              &s sum1 = b%i%%j%
                        &end
                              &s sum2 = 0.0
                              &s t = 0.0
                        &do k = 1 &to 4 &by 1
                              &do
                                    &if %k% = 1 &then
                                    &sv c = 81.833
                                    &else
                                    &if %k% = 2 &then
                                    &sv c = 97.30
                                    &else
                                    &if %k% = 3 &then
                                    &sv c = 113.51
                                    &else
                                    &if %k% = 4 &then
                                    &sv c = 164.429
                                    sum%i%%k%  =  %sum2%  +  sqr(abs
(tm%j% - %c%))
```

```
                                        z%i%%k% = 100000 / sum%i%%k%
                                        x%i%%k% = %t% + z%i%%k%
                                        &s t = x%i%%k%
                                  &end
                            &end
                            u%i%%j% = %sum1% / %t%
                            kill sum%i%1 all
                            kill sum%i%2 all
                            kill sum%i%3 all
                            kill sum%i%4 all
                            kill z%i%1 all
                            kill z%i%2 all
                            kill z%i%3 all
                            kill z%i%4 all
                            kill x%i%1 all
                            kill x%i%2 all
                            kill x%i%3 all
                            kill x%i%4 all
                            kill a%i%%j% all
                            kill b%i%%j% all
                  &end
&end
&do i = 3 &to 3 &by 1
      &do j = 73 &to 251 &by 1
            f%i%%j% = con(isnull (u%i%%j%), 0, u%i%%j%)
            kill u%i%%j% all
      &end
&end
&do i = 3 &to 3 &by 1
      &s m = 0.0
      &do j = 73 &to 251 &by 1
            x%i%%j% = %m% + f%i%%j%
            &s m = x%i%%j%
            kill f%i%%j% all
      &end
&end
&do i = 3 &to 3 &by 1
      &do j = 73 &to 250 &by 1
            kill x%i%%j% all
      &end
&end
&do i = 4 &to 4 &by 1
                  &do j = 73 &to 251 &by 1
                        &do
                              &if %i% = 1 &then
                              &sv a = 81.833
                              &else
                              &if %i% = 2 &then
                              &sv a = 97.30
                              &else
                              &if %i% = 3 &then
                              &sv a = 113.51
                              &else
                              &if %i% = 4 &then
                              &sv a = 164.429
                              &s b = 0.0
                              a%i%%j% = %b% + sqr(abs (tm%j% - %a%))
                              b%i%%j% = 100000000 / a%i%%j%
                              &s sum1 = b%i%%j%
                        &end
                              &s sum2 = 0.0
```

```
                              &s t = 0.0
                        &do k = 1 &to 4 &by 1
                              &do
                                    &if %k% = 1 &then
                                    &sv c = 81.833
                                    &else
                                    &if %k% = 2 &then
                                    &sv c = 97.30
                                    &else
                                    &if %k% = 3 &then
                                    &sv c = 113.51
                                    &else
                                    &if %k% = 4 &then
                                    &sv c = 164.429
                                    sum%i%%k%  =  %sum2%  +  sqr(abs
(tm%j% - %c%))
                                    z%i%%k% = 100000 / sum%i%%k%
                                    x%i%%k% = %t% + z%i%%k%
                                    &s t = x%i%%k%
                              &end
                        &end
                        u%i%%j% = %sum1% / %t%
                        kill sum%i%1 all
                        kill sum%i%2 all
                        kill sum%i%3 all
                        kill sum%i%4 all
                        kill z%i%1 all
                        kill z%i%2 all
                        kill z%i%3 all
                        kill z%i%4 all
                        kill x%i%1 all
                        kill x%i%2 all
                        kill x%i%3 all
                        kill x%i%4 all
                        kill a%i%%j% all
                        kill b%i%%j% all
                  &end
&end
&do i = 4 &to 4 &by 1
      &do j = 73 &to 251 &by 1
            f%i%%j% = con(isnull (u%i%%j%), 0, u%i%%j%)
            kill u%i%%j% all
      &end
&end
&do i = 4 &to 4 &by 1
      &s m = 0.0
      &do j = 73 &to 251 &by 1
            x%i%%j% = %m% + f%i%%j%
            &s m = x%i%%j%
            kill f%i%%j% all
      &end
&end
&do i = 4 &to 4 &by 1
      &do j = 73 &to 250 &by 1
            kill x%i%%j% all
      &end
&end
&do i = 73 &to 251 &by 1
          kill tm%i% all
&end
```

Appendix 4 Fuzzy memberships of the land cover classes of forest, grassland, urban and dense urban from the selected bands of Landsat-7 ETM+ of the City of Perth

(a) ETM+ Band 1

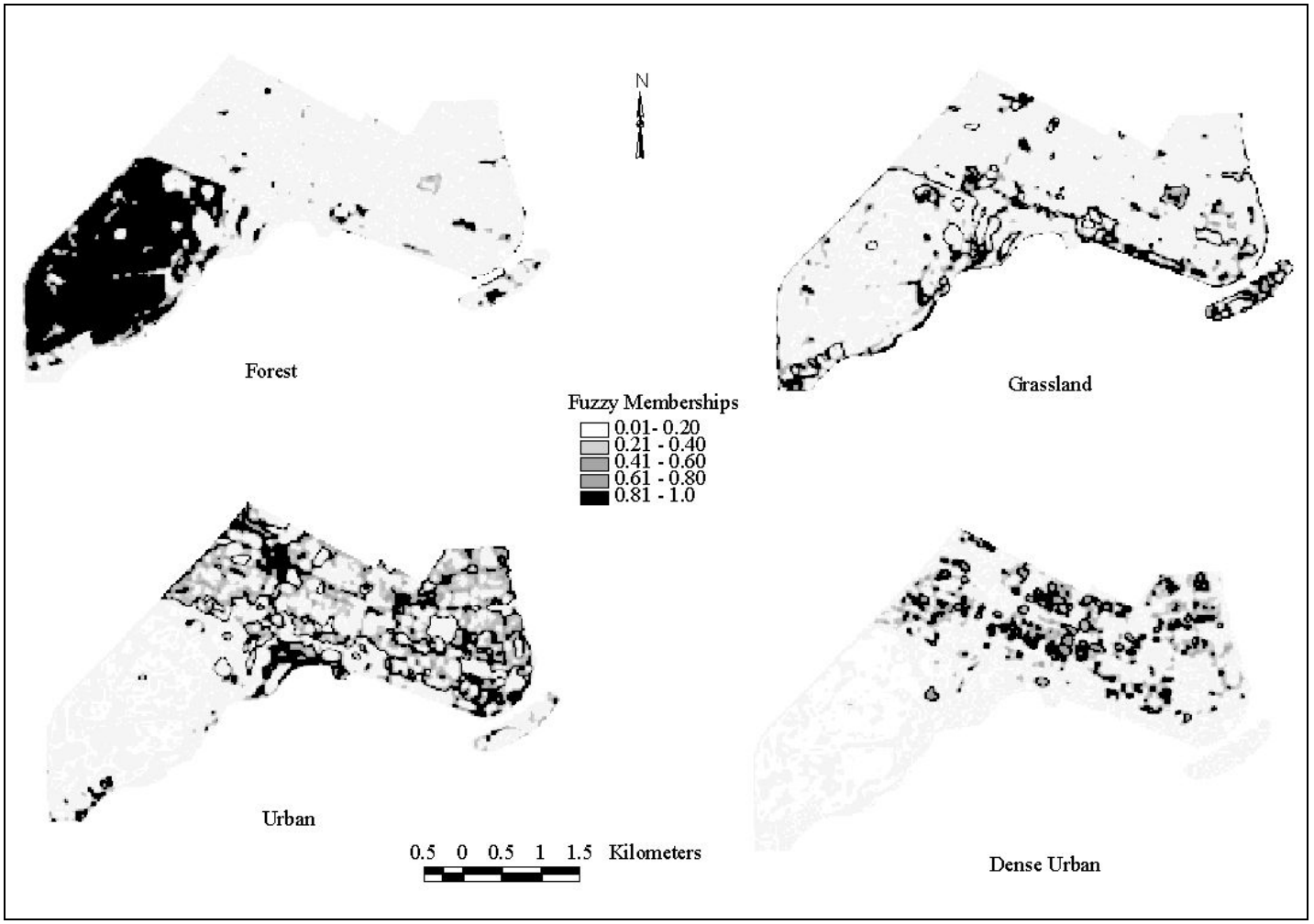

(b) ETM+ Band 3


N
Forest
Grassland
Fuzzy Memberships
0.01- 0.20
0.21 - 0.40
0.41 - 0.60
0.61 - 0.80
0.81 - 1.0
Urban
Dense Urban
0.5 0 0.5 1 1.5 Kilometers

(c) ETM+ Band 4


N
Forest
Grassland
Fuzzy Memberships
0.01- 0.20
0.21 - 0.40
0.41 - 0.60
0.61 - 0.80
0.81 - 1.0
Urban
Dense Urban
0.5 0 0.5 1 1.5 Kilometers

(d) ETM+ Band 7


N
Forest
Grassland
Fuzzy Memberships
0.01- 0.20
0.21 - 0.40
0.41 - 0.60
0.61 - 0.80
0.81 - 1.0
Urban
Dense Urban
0.5 0 0.5 1 1.5 Kilometers

Appendix 5 Fuzzy memberships of the land cover classes of forest, grassland, urban and dense urban from the selected bands of Landsat-7 ETM+ of the City of Melville

(a) ETM+ Band 1

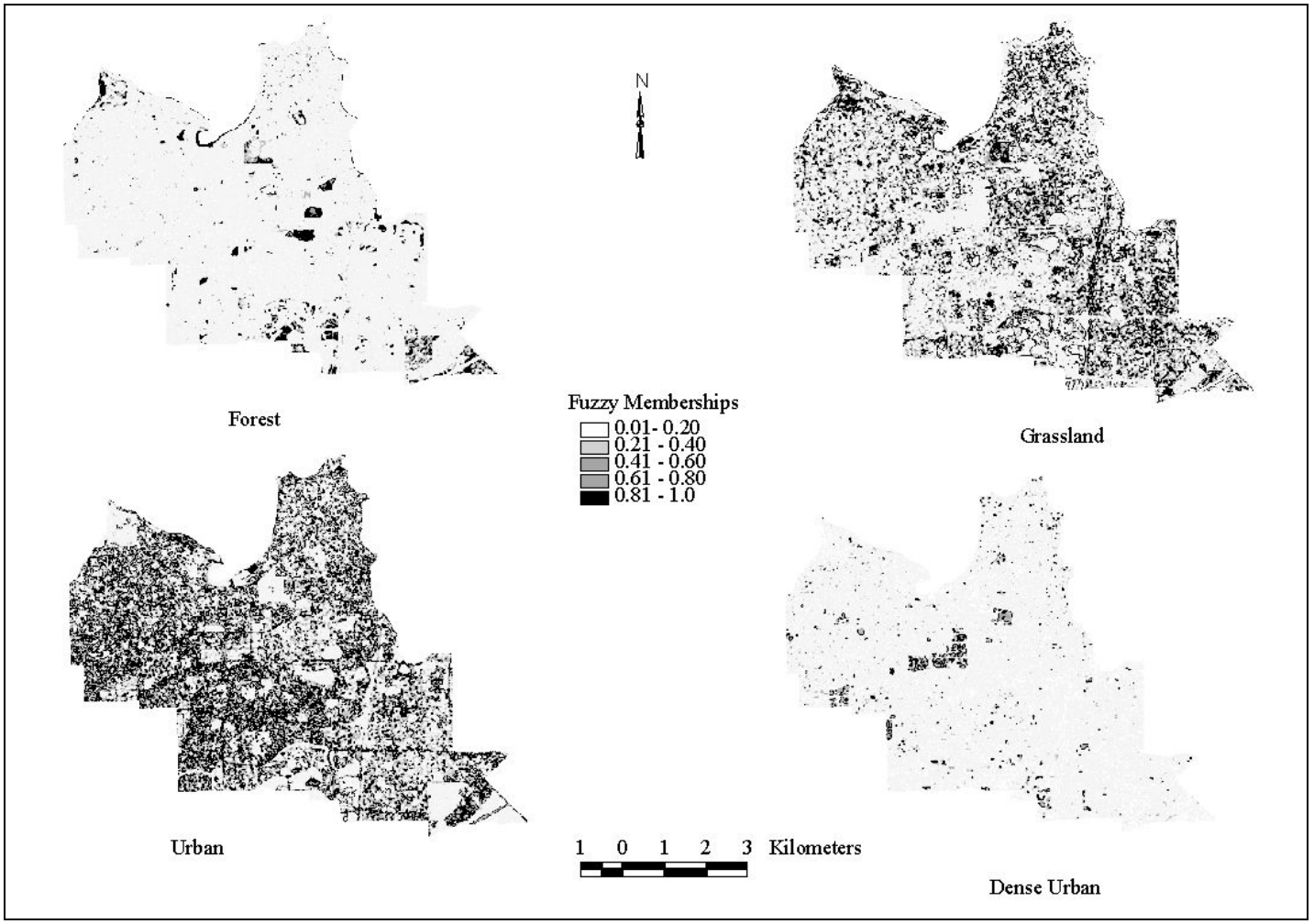

(b) ETM+ Band 2

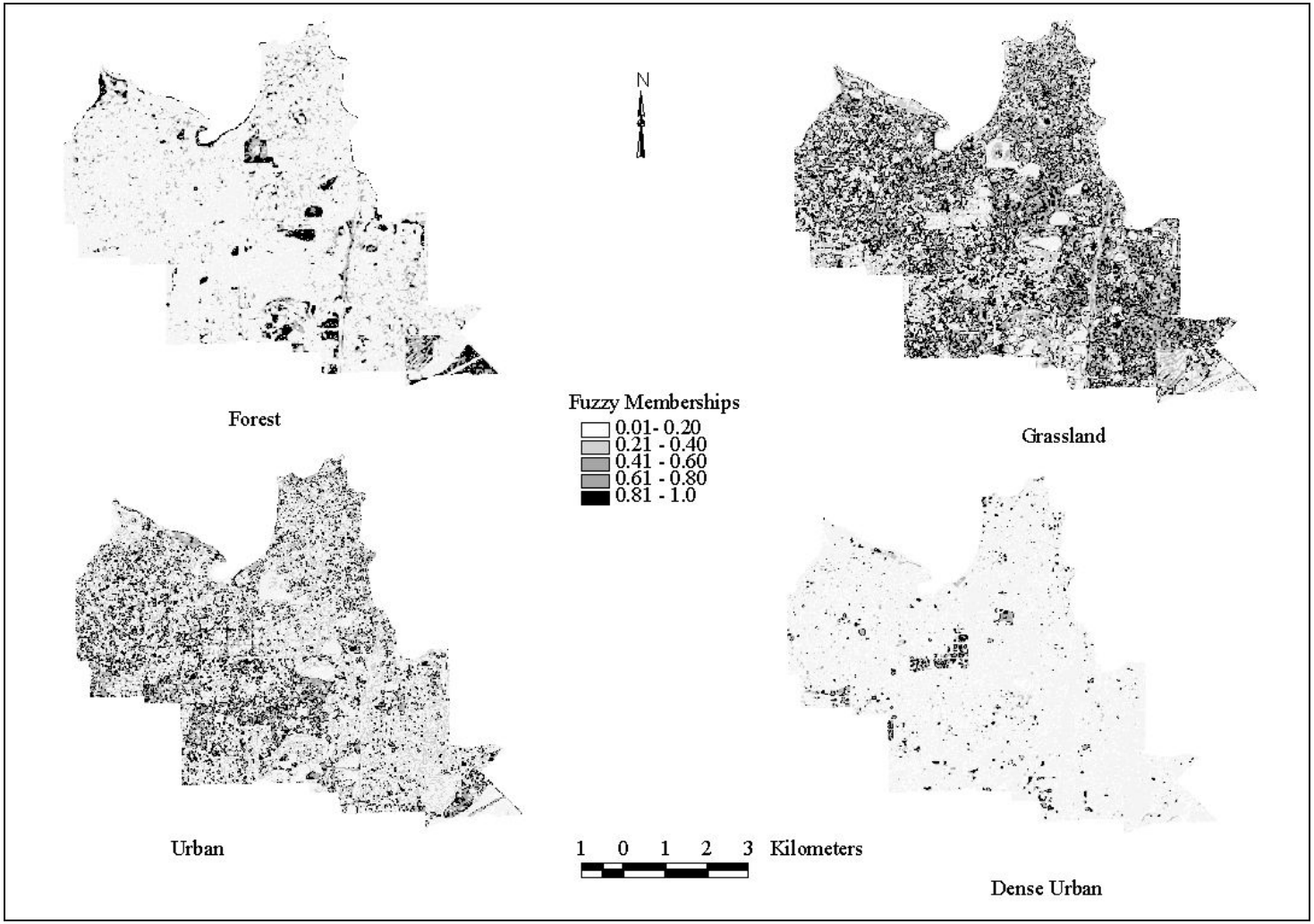
N
Forest
Fuzzy Memberships
0.01- 0.20
0.21 - 0.40
0.41 - 0.60
0.61 - 0.80
0.81 - 1.0
Grassland
Urban
1 0 1 2 3 Kilometers
Dense Urban

(c) ETM+ Band 3

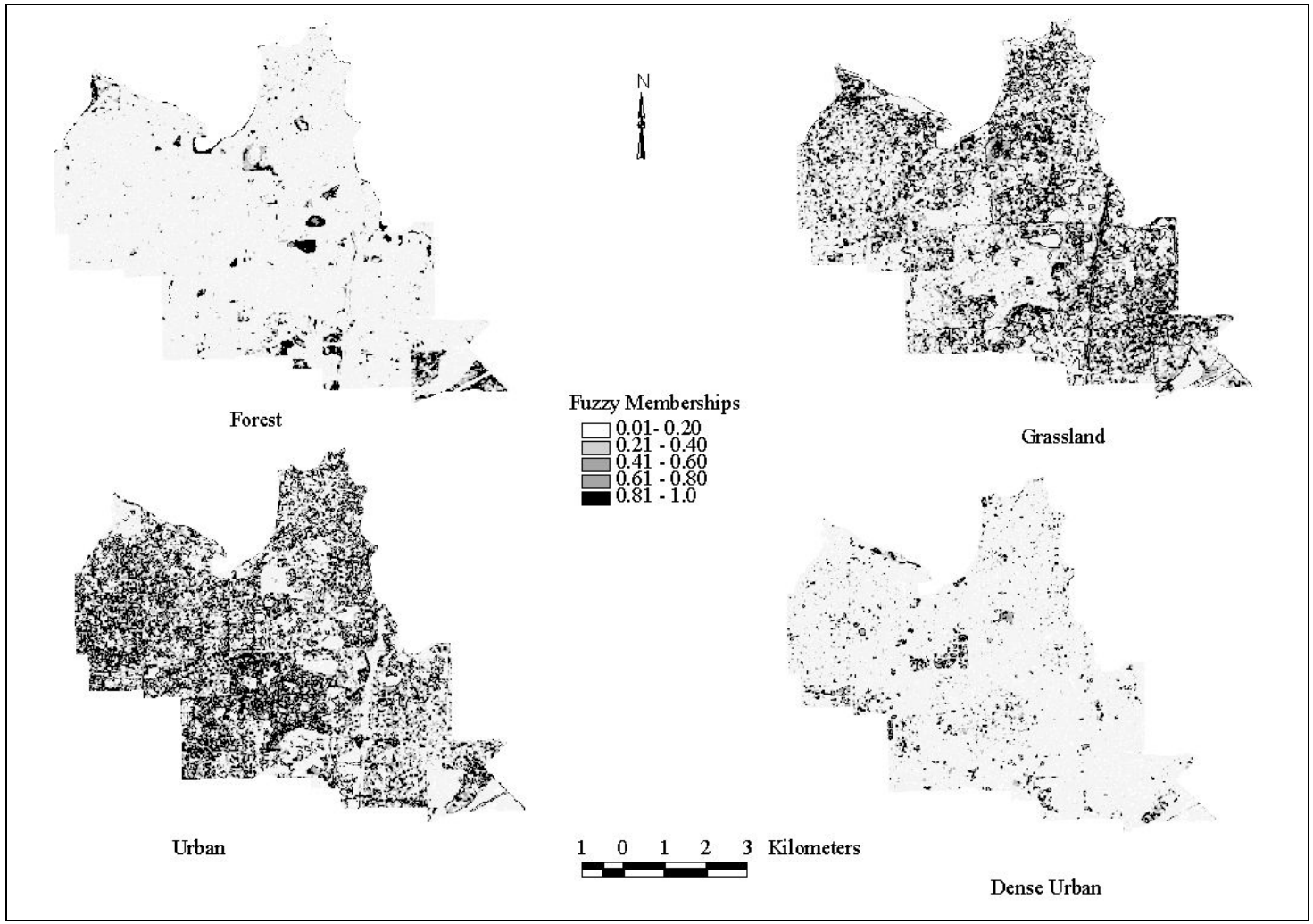
N
Forest
Fuzzy Memberships
0.01- 0.20
0.21 - 0.40
0.41 - 0.60
0.61 - 0.80
0.81 - 1.0
Grassland
Urban
1 0 1 2 3 Kilometers
Dense Urban

(d) ETM+ Band 7

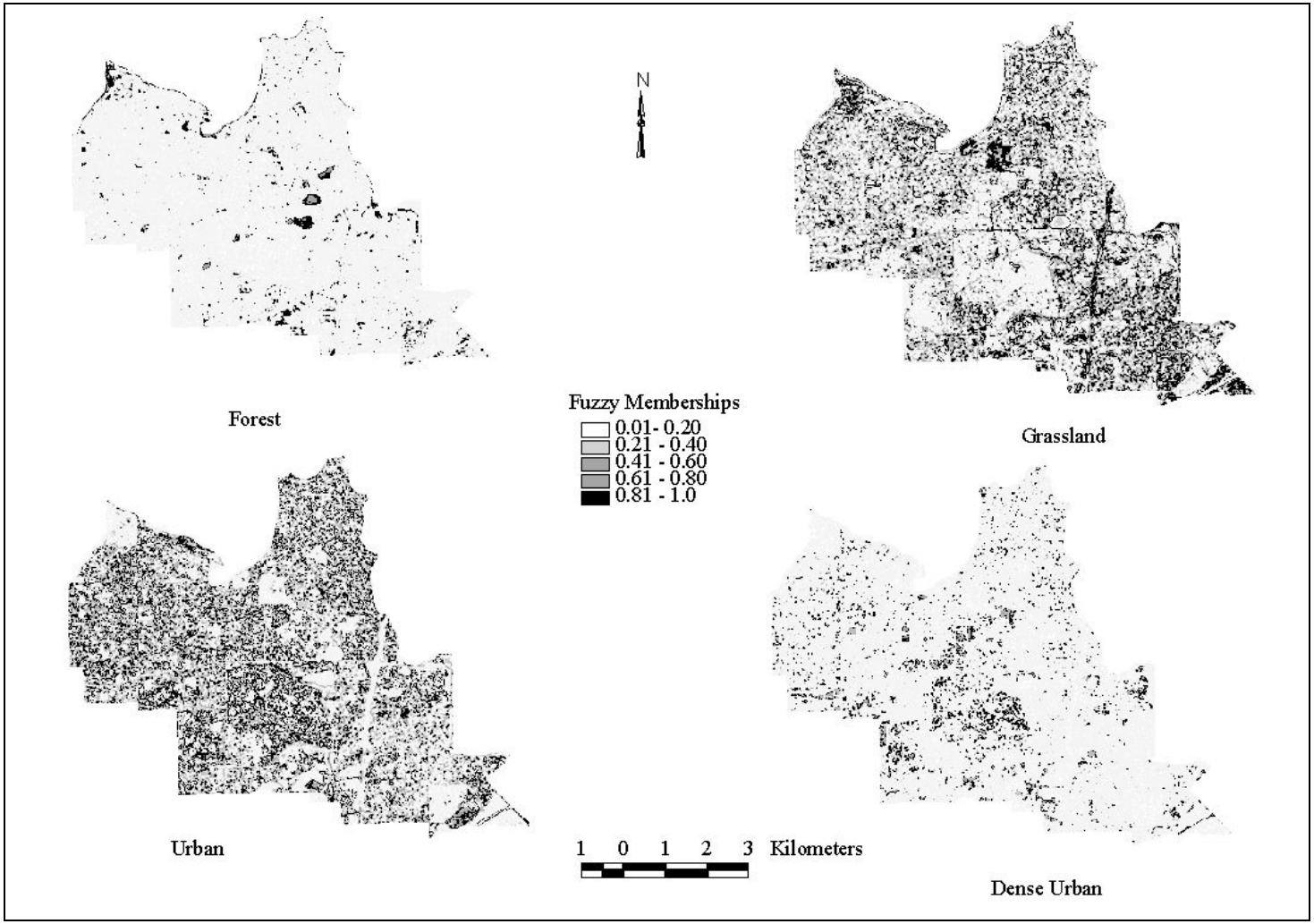
N
Forest
Fuzzy Memberships
0.01- 0.20
0.21 - 0.40
0.41 - 0.60
0.61 - 0.80
0.81 - 1.0
Grassland
Urban
1 0 1 2 3 Kilometers
Dense Urban

Appendix 6 Fuzzy memberships of the land cover classes of forest, grassland, urban and dense urban from the selected bands of Landsat-7 ETM+ of the City of Armadale

(a) ETM+ Band 1

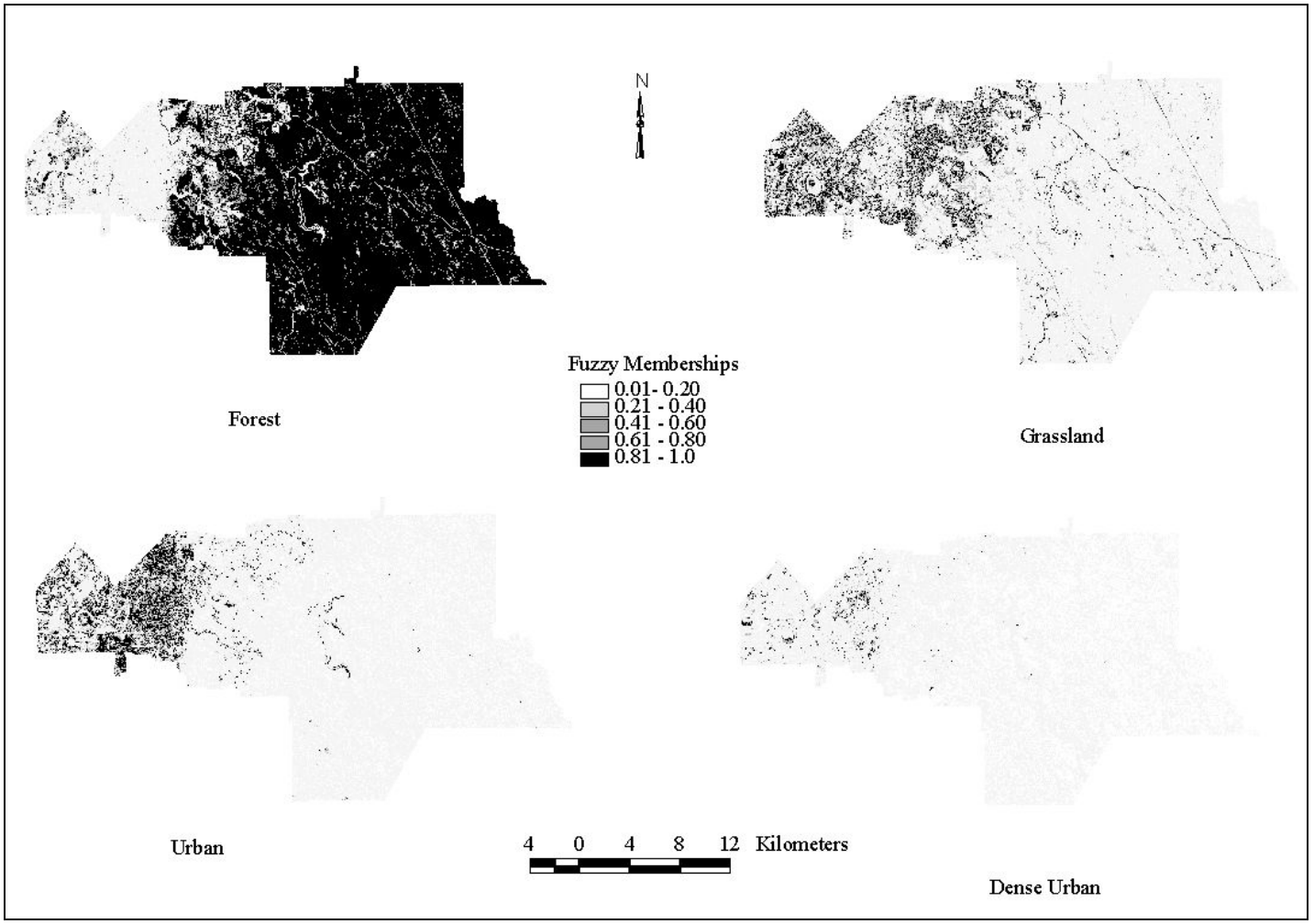

(b) ETM+ Band 3

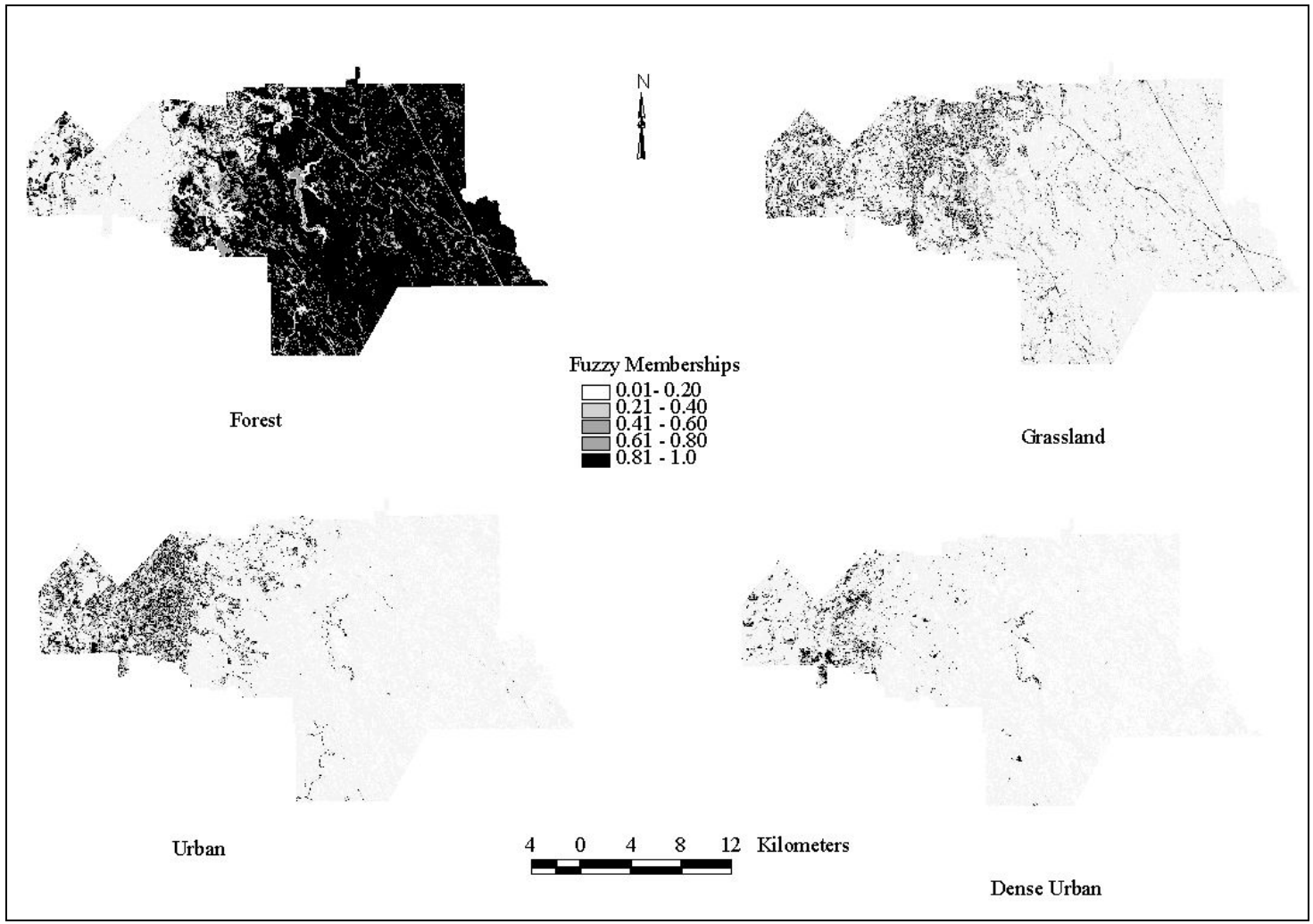
N
Fuzzy Memberships
0.01- 0.20
0.21 - 0.40
0.41 - 0.60
0.61 - 0.80
0.81 - 1.0
Forest
Grassland
Urban
Dense Urban
4 0 4 8 12 Kilometers

(c) ETM+ Band 4

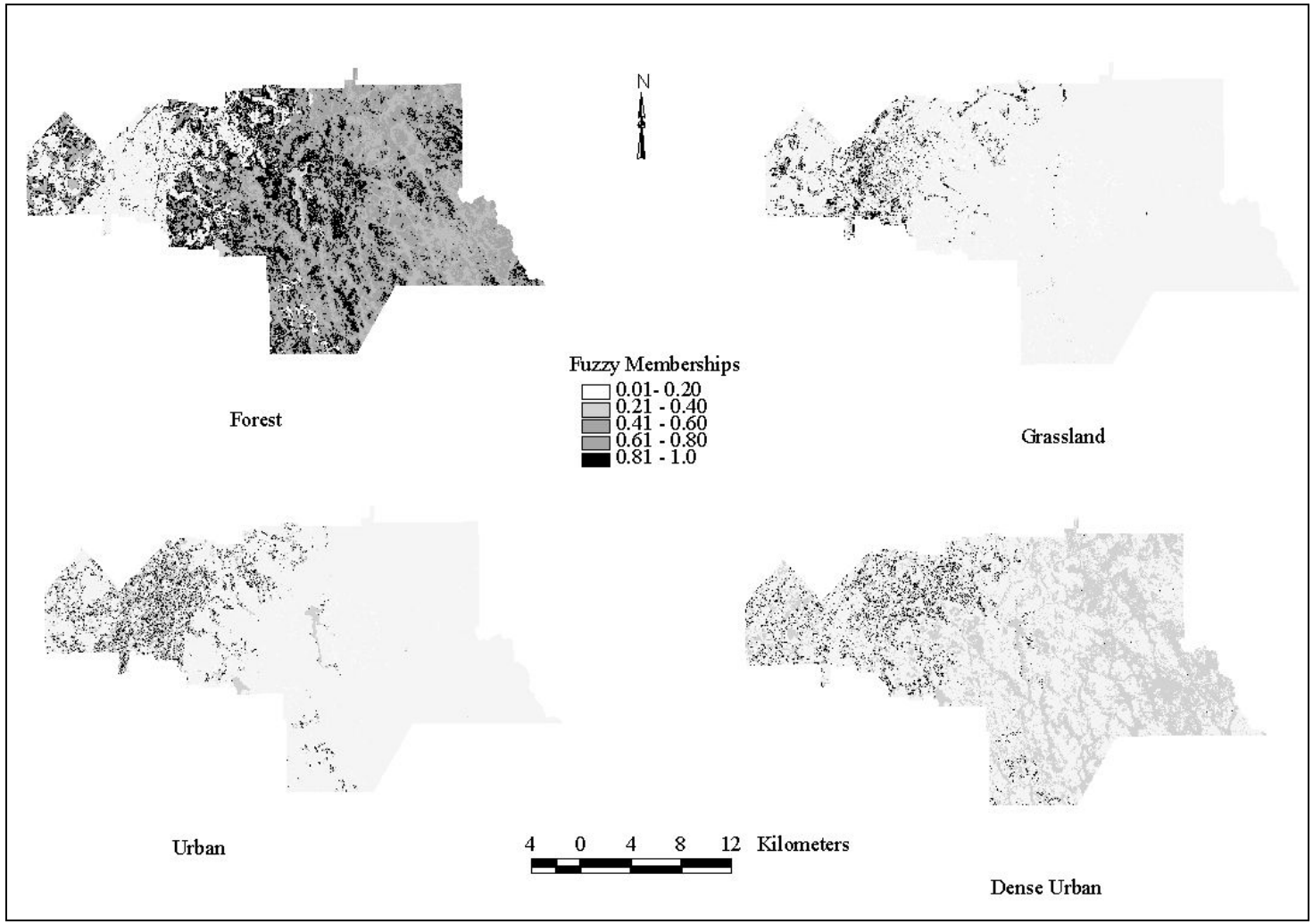
N
Fuzzy Memberships
0.01- 0.20
0.21 - 0.40
0.41 - 0.60
0.61 - 0.80
0.81 - 1.0
Forest
Grassland
Urban
Dense Urban
4 0 4 8 12 Kilometers

(d) ETM+ Band 5

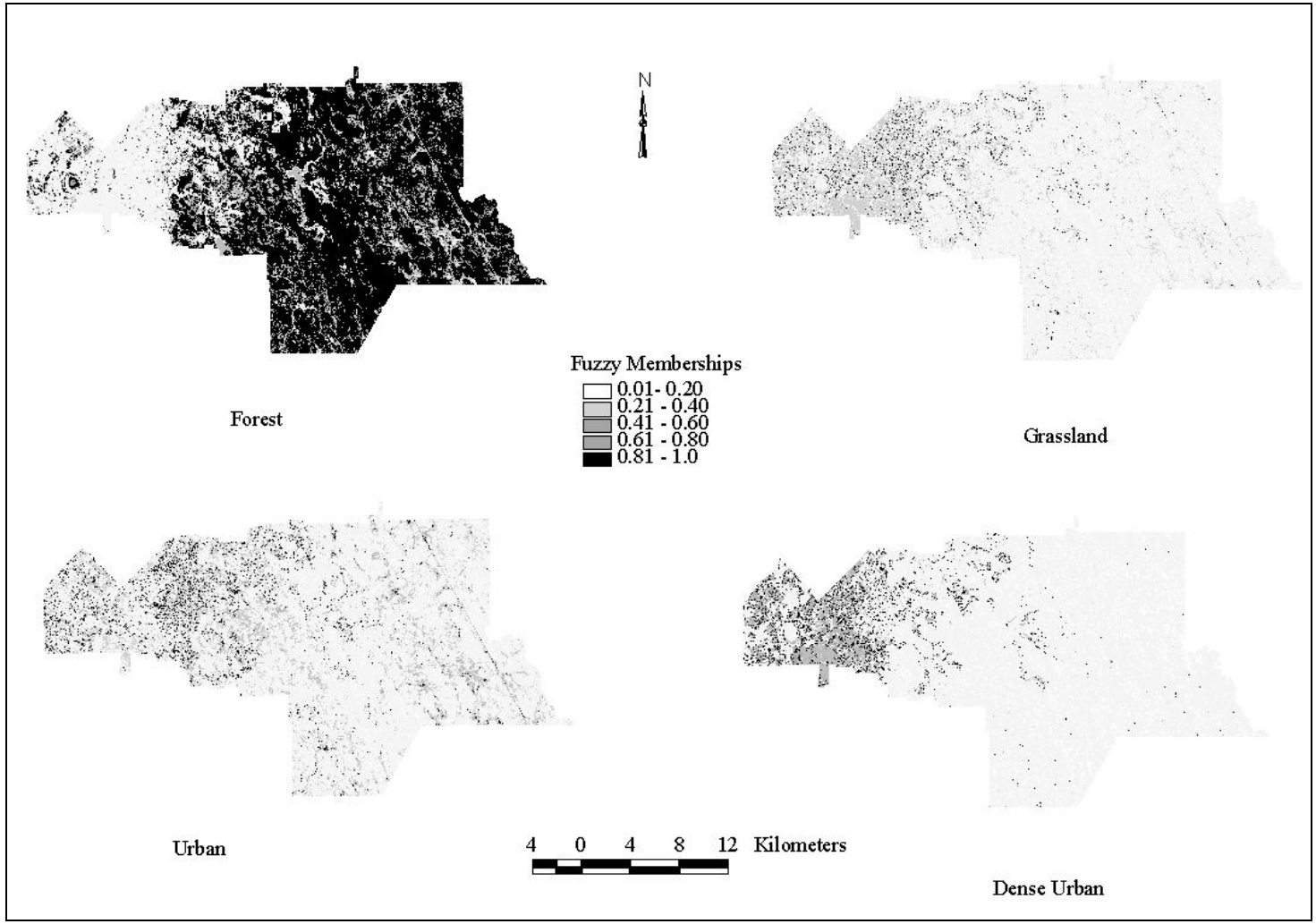
N
Fuzzy Memberships
0.01- 0.20
0.21 - 0.40
0.41 - 0.60
0.61 - 0.80
0.81 - 1.0
Forest
Grassland
Urban
Dense Urban
4 0 4 8 12 Kilometers

(e) ETM+ Band 7

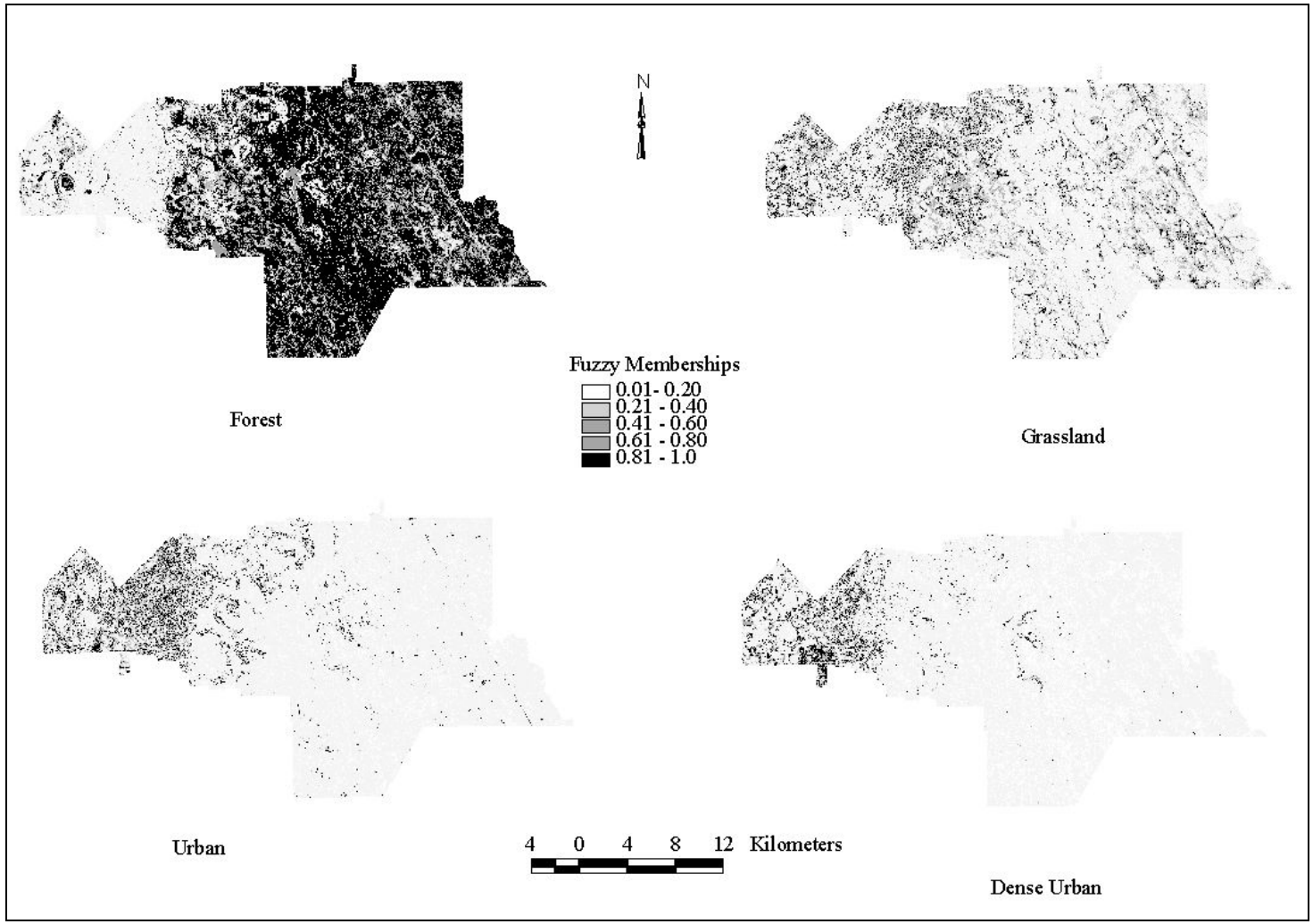
N
Fuzzy Memberships
0.01- 0.20
0.21 - 0.40
0.41 - 0.60
0.61 - 0.80
0.81 - 1.0
Forest
Grassland
Urban
Dense Urban
4 0 4 8 12 Kilometers

Appendix 7 Integrated fuzzy memberships of the land cover classes of forest, grassland, urban and dense urban generated by different fuzzy operators of the City of Perth

(a) AND

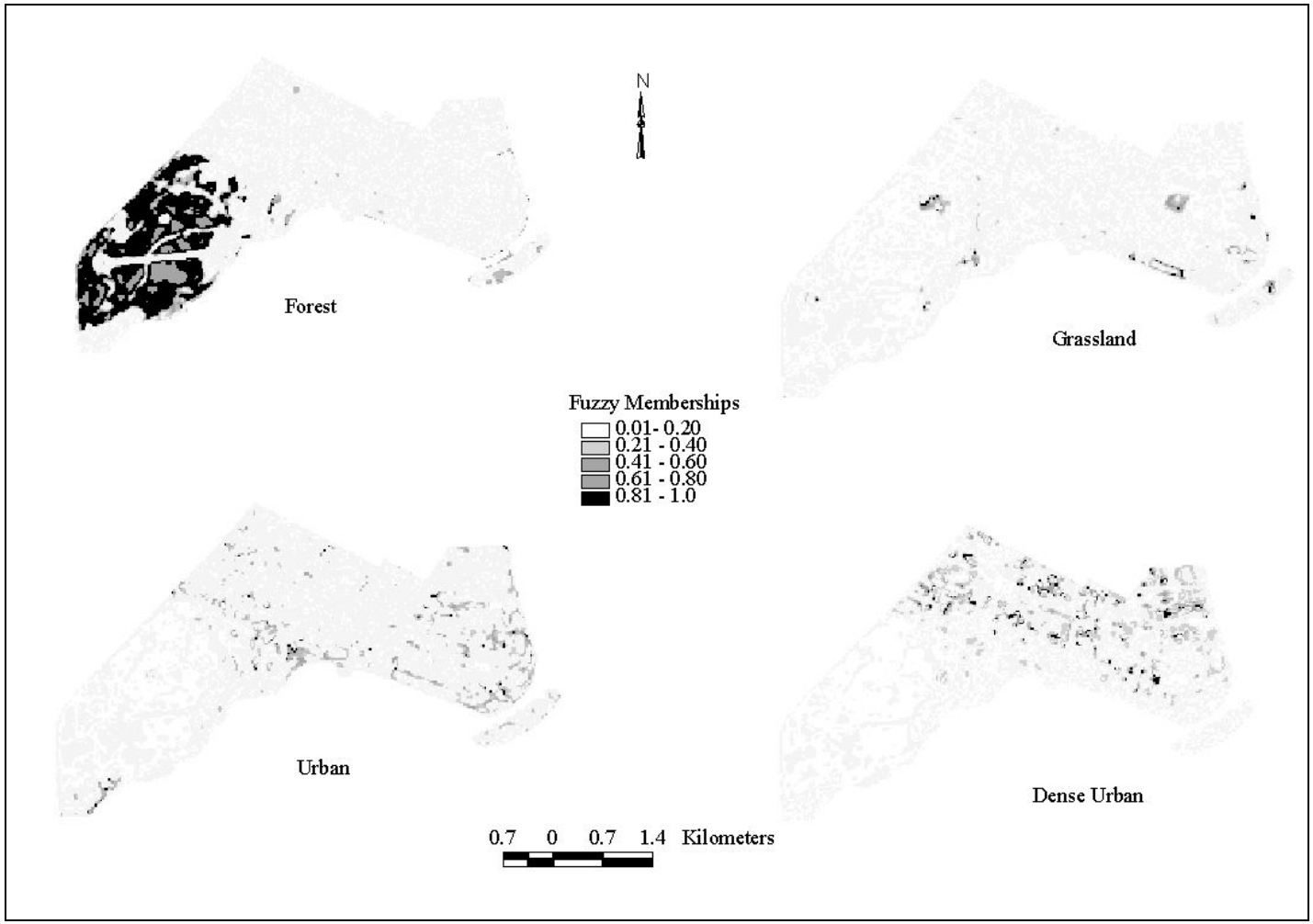

(b) OR

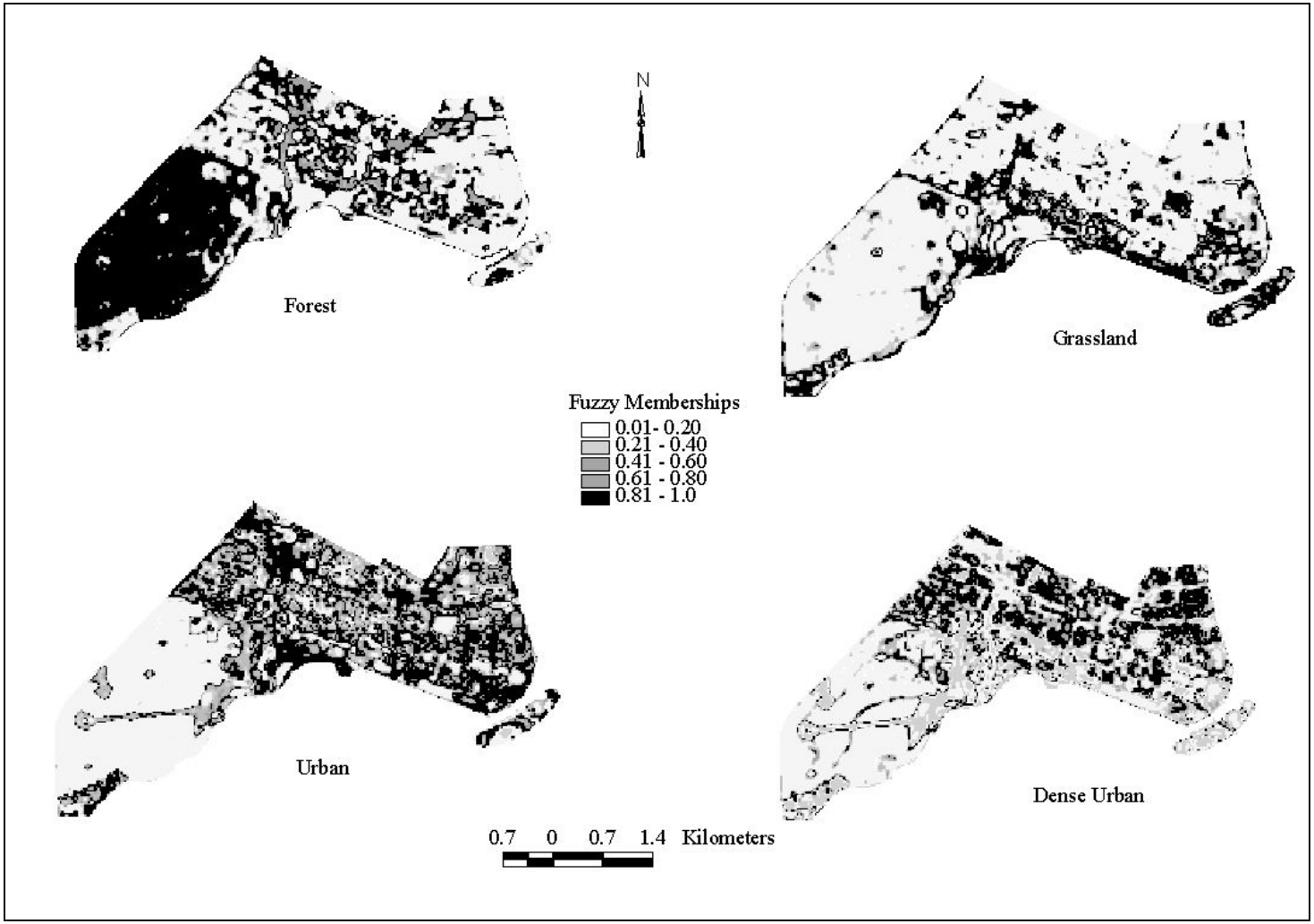
N
Forest
Grassland
Fuzzy Memberships
0.01- 0.20
0.21 - 0.40
0.41 - 0.60
0.61 - 0.80
0.81 - 1.0
Urban
Dense Urban
0.7 0 0.7 1.4 Kilometers

(c) FAP

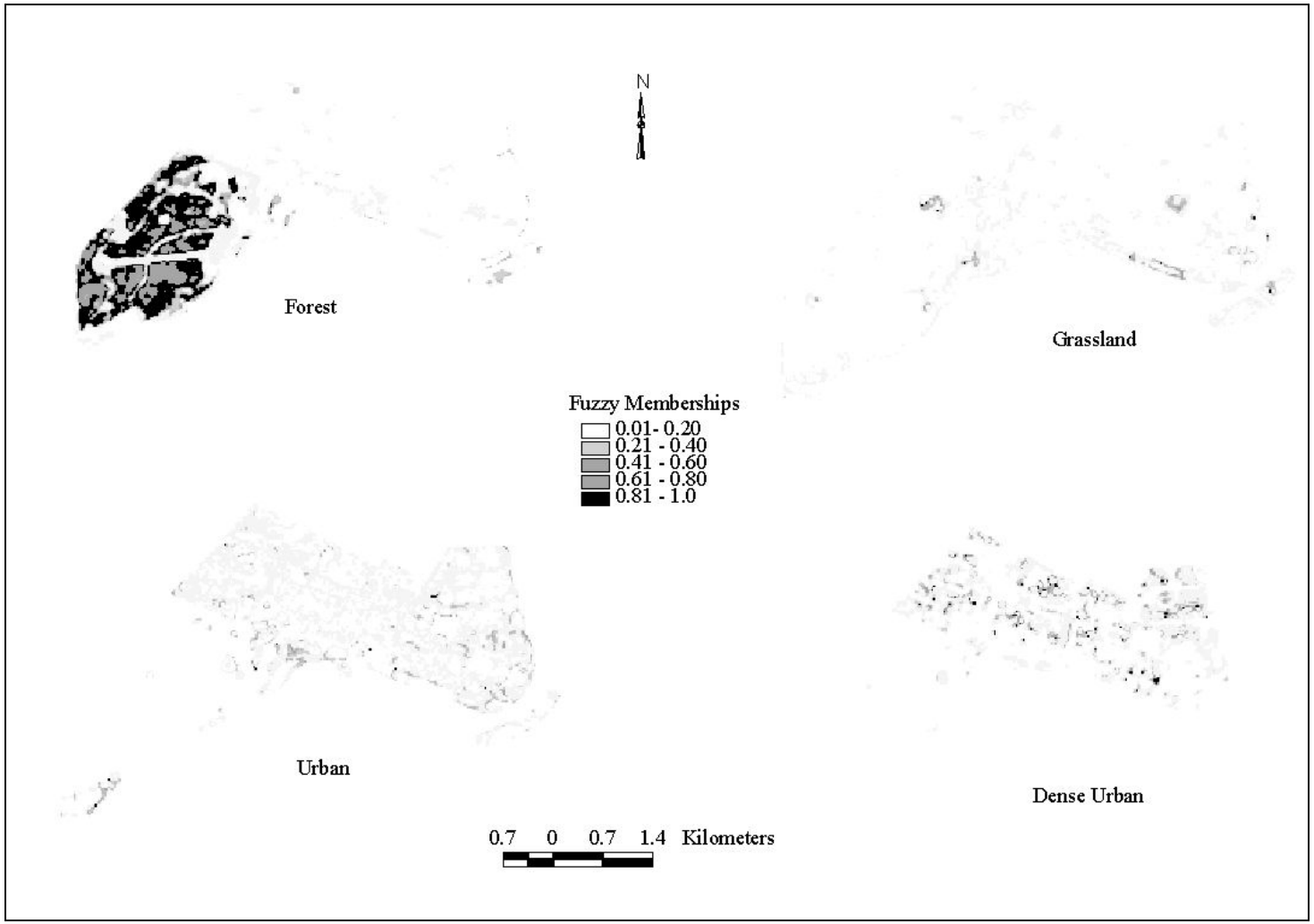
N
Forest
Grassland
Fuzzy Memberships
0.01- 0.20
0.21 - 0.40
0.41 - 0.60
0.61 - 0.80
0.81 - 1.0
Urban
Dense Urban
0.7 0 0.7 1.4 Kilometers

(d) FAS

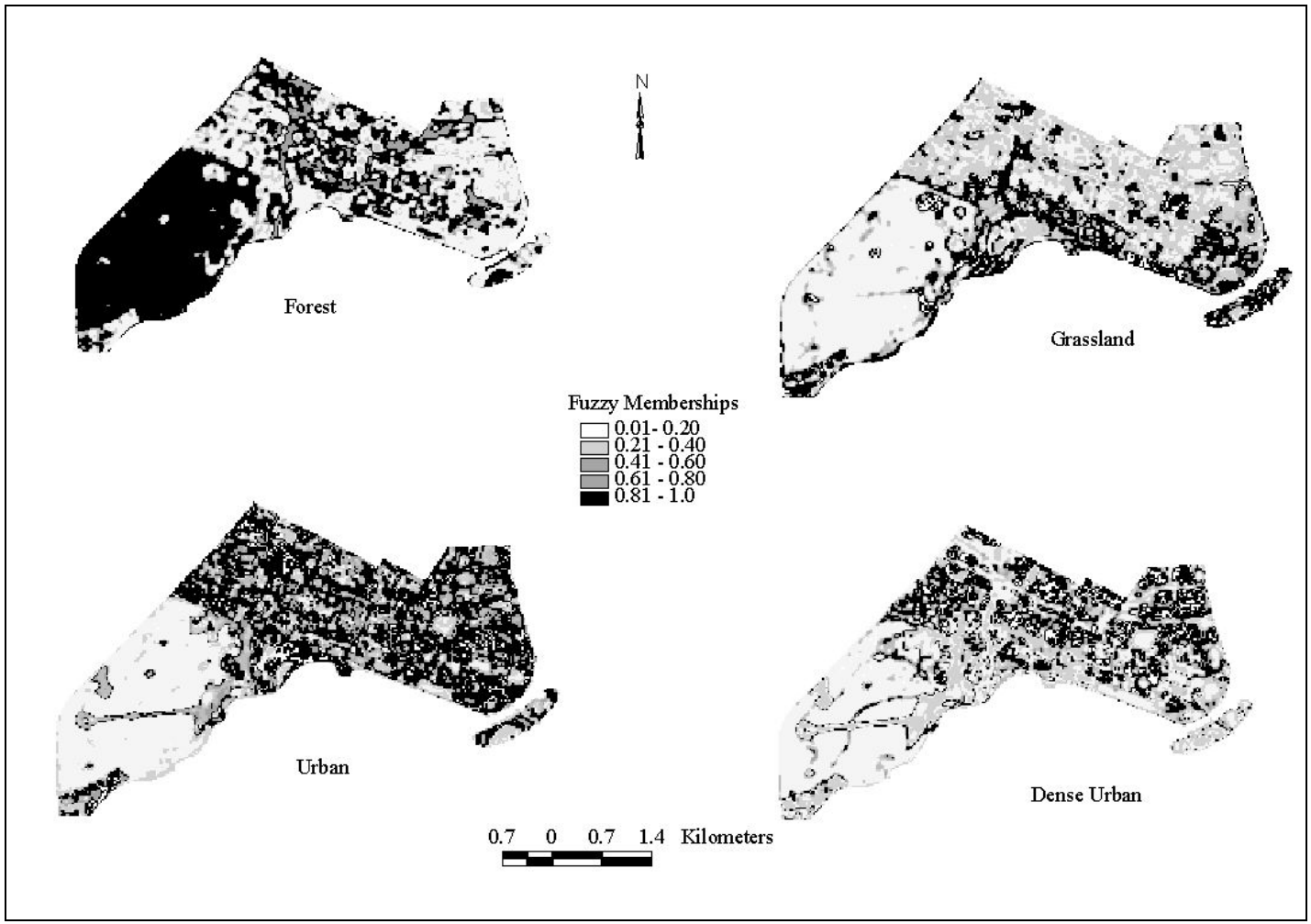
N
Forest
Grassland
Fuzzy Memberships
0.01- 0.20
0.21 - 0.40
0.41 - 0.60
0.61 - 0.80
0.81 - 1.0
Urban
Dense Urban
0.7 0 0.7 1.4 Kilometers

(k) $\gamma = 0.10$

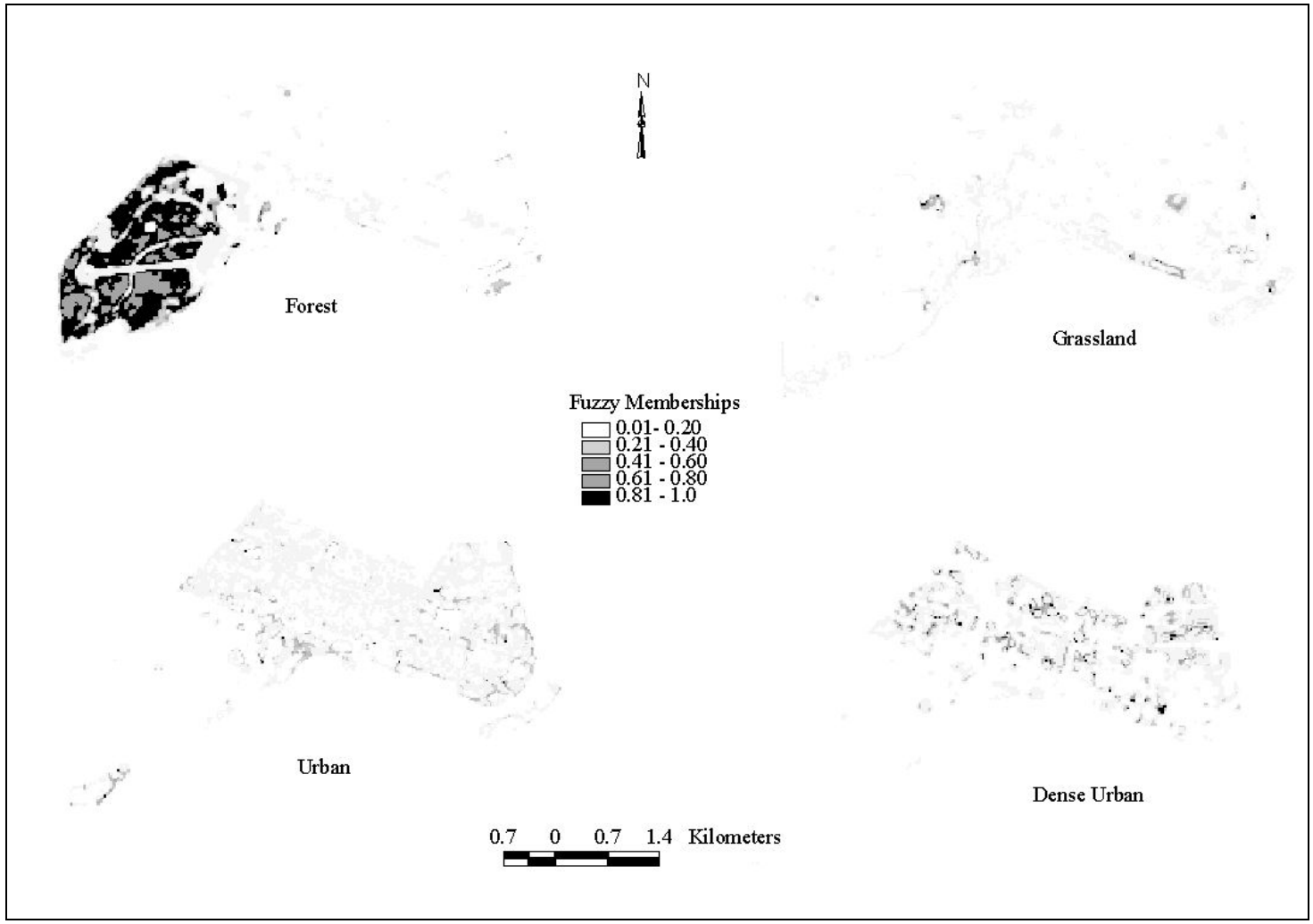
N
Forest
Grassland
Fuzzy Memberships
0.01- 0.20
0.21 - 0.40
0.41 - 0.60
0.61 - 0.80
0.81 - 1.0
Urban
Dense Urban
0.7 0 0.7 1.4 Kilometers

(f) $\gamma = 0.50$

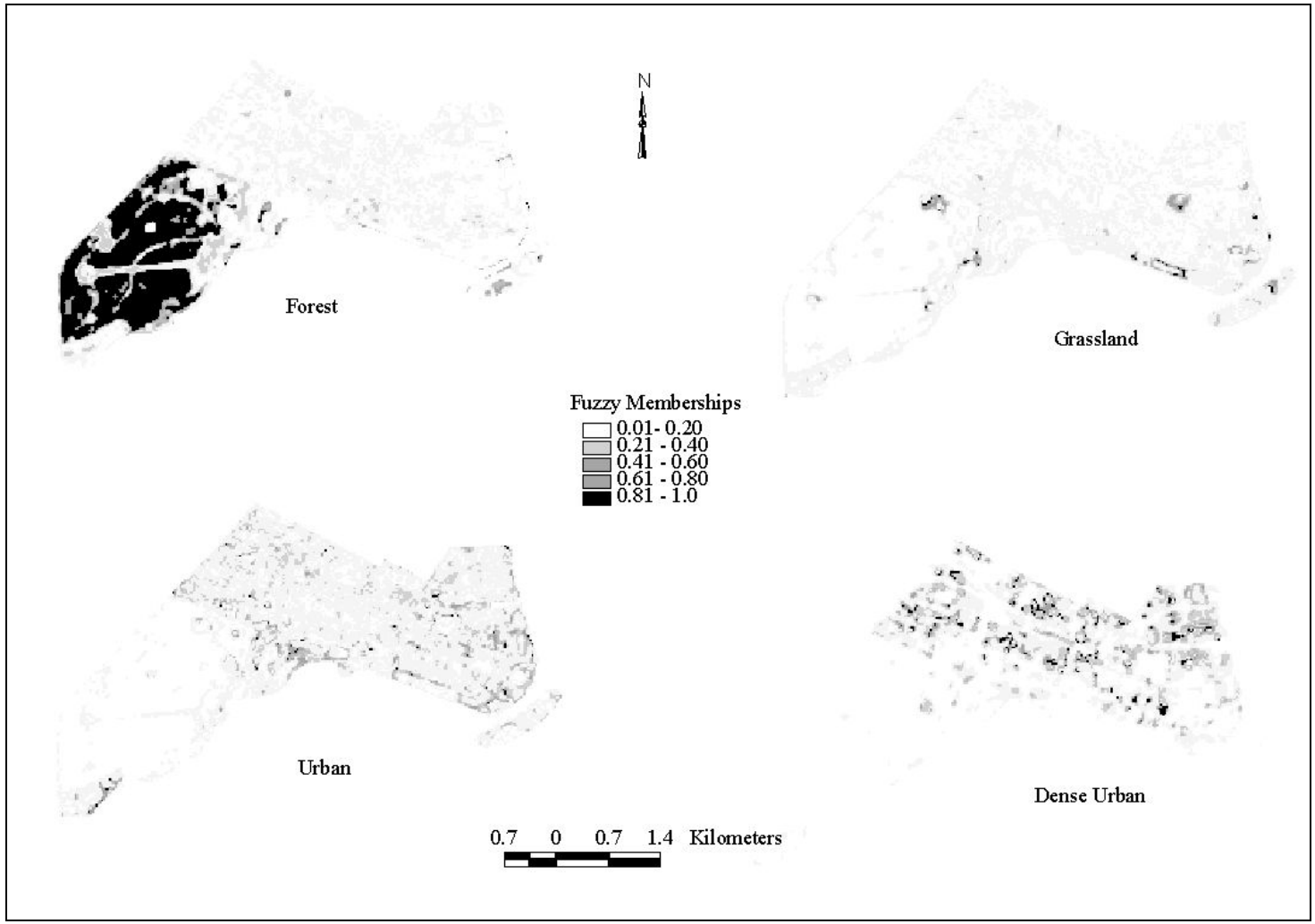
N
Forest
Grassland
Fuzzy Memberships
0.01- 0.20
0.21 - 0.40
0.41 - 0.60
0.61 - 0.80
0.81 - 1.0
Urban
Dense Urban
0.7 0 0.7 1.4 Kilometers

(g) $\gamma = 0.60$


N
Forest
Grassland
Fuzzy Memberships
0.01- 0.20
0.21 - 0.40
0.41 - 0.60
0.61 - 0.80
0.81 - 1.0
Urban
Dense Urban
0.7 0 0.7 1.4 Kilometers

(h) $\gamma = 0.70$

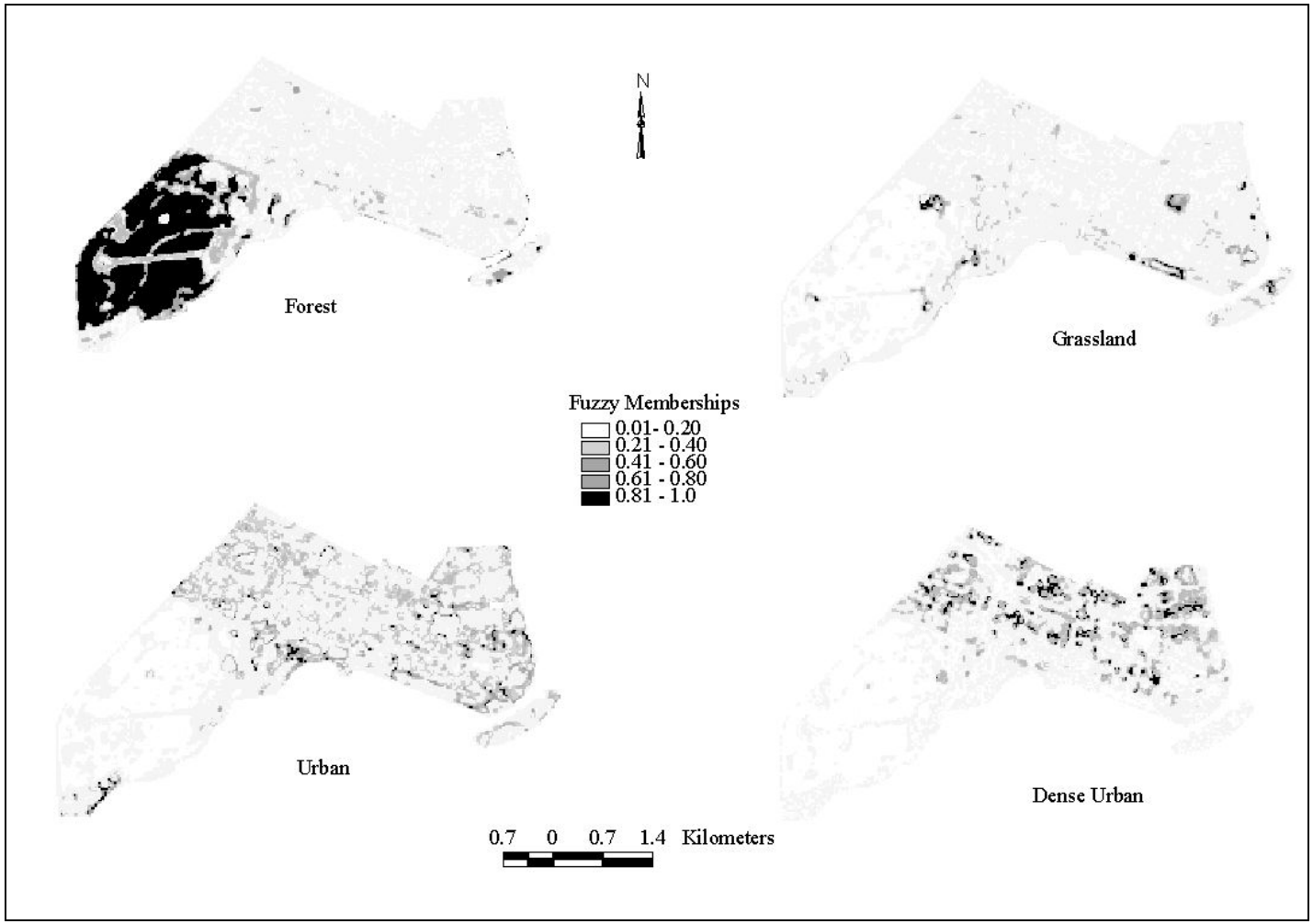
N
Forest
Grassland
Fuzzy Memberships
0.01- 0.20
0.21 - 0.40
0.41 - 0.60
0.61 - 0.80
0.81 - 1.0
Urban
Dense Urban
0.7 0 0.7 1.4 Kilometers

(i) $\gamma = 0.80$

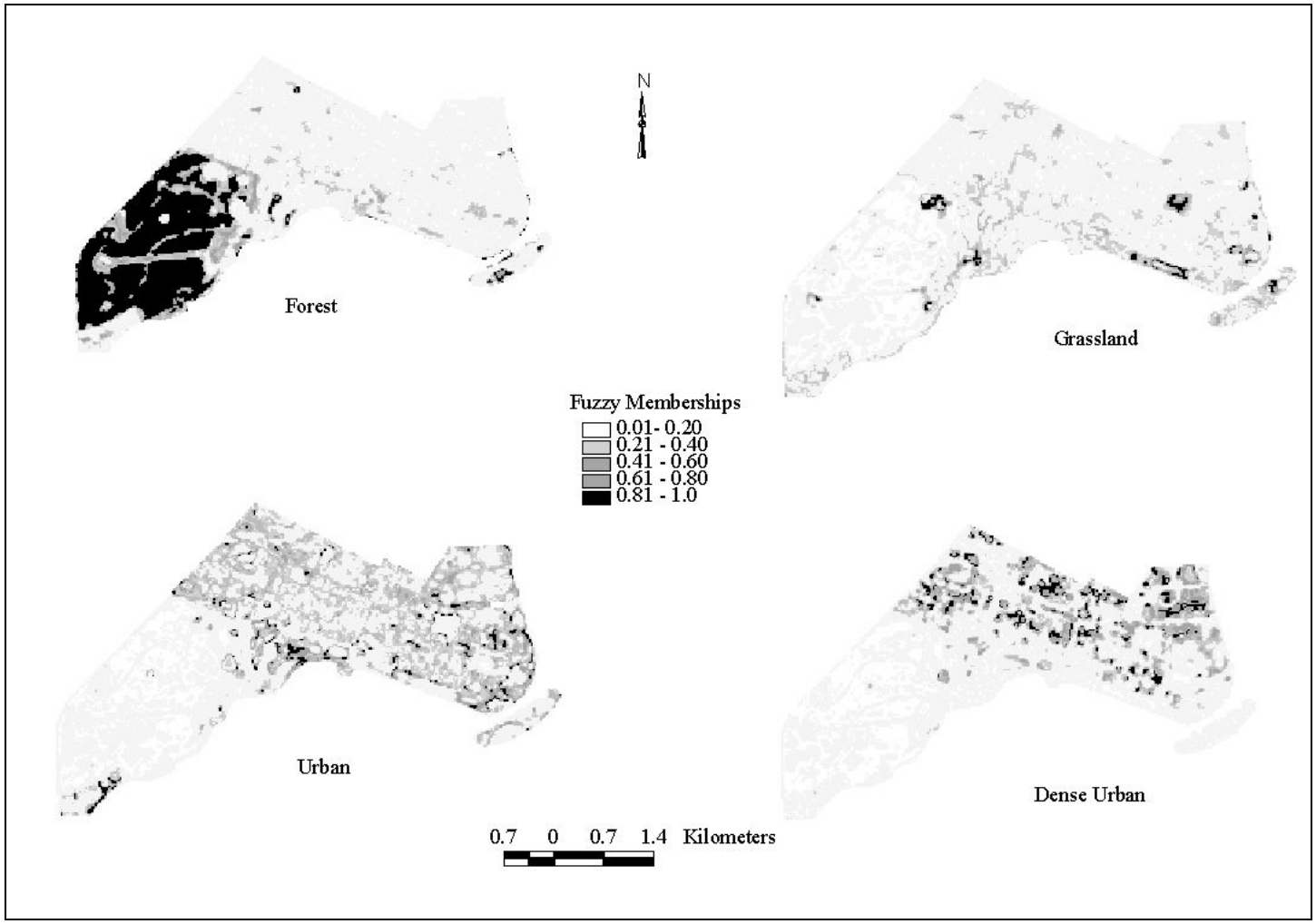
N
Forest
Grassland
Fuzzy Memberships
0.01- 0.20
0.21 - 0.40
0.41 - 0.60
0.61 - 0.80
0.81 - 1.0
Urban
Dense Urban
0.7 0 0.7 1.4 Kilometers

(j) $\gamma = 0.90$

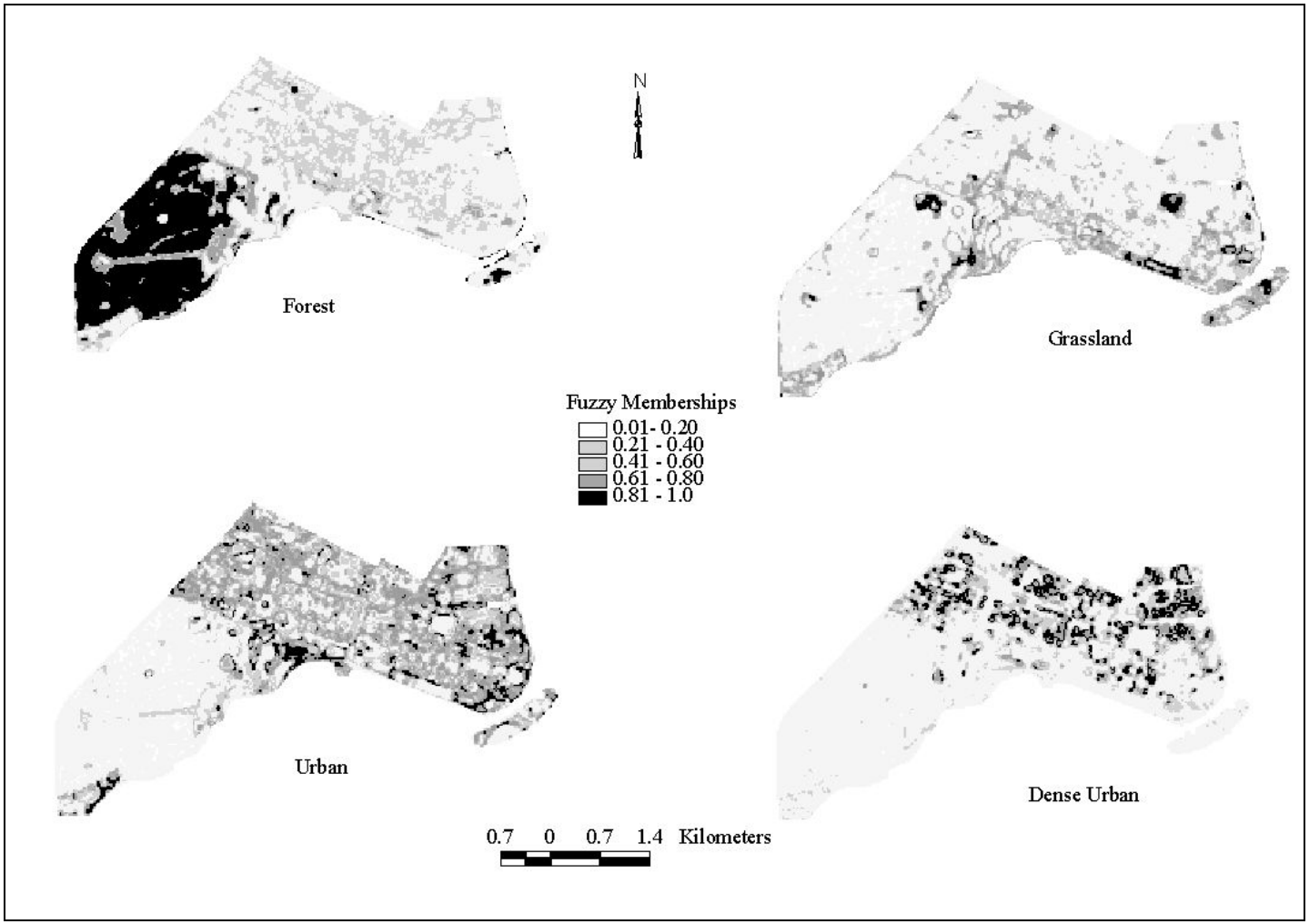
N
Forest
Grassland
Fuzzy Memberships
0.01- 0.20
0.21 - 0.40
0.41 - 0.60
0.61 - 0.80
0.81 - 1.0
Urban
Dense Urban
0.7 0 0.7 1.4 Kilometers

(k) $\gamma = 0.95$


N
Forest
Grassland
Fuzzy Memberships
0.01- 0.20
0.21 - 0.40
0.41 - 0.60
0.61 - 0.80
0.81 - 1.0
Urban
Dense Urban
0.7 0 0.7 1.4 Kilometers

Appendix 8 Integrated fuzzy memberships of the land cover classes of forest, grassland, urban and dense urban generated by different fuzzy operators of the City of Melville

(a) AND

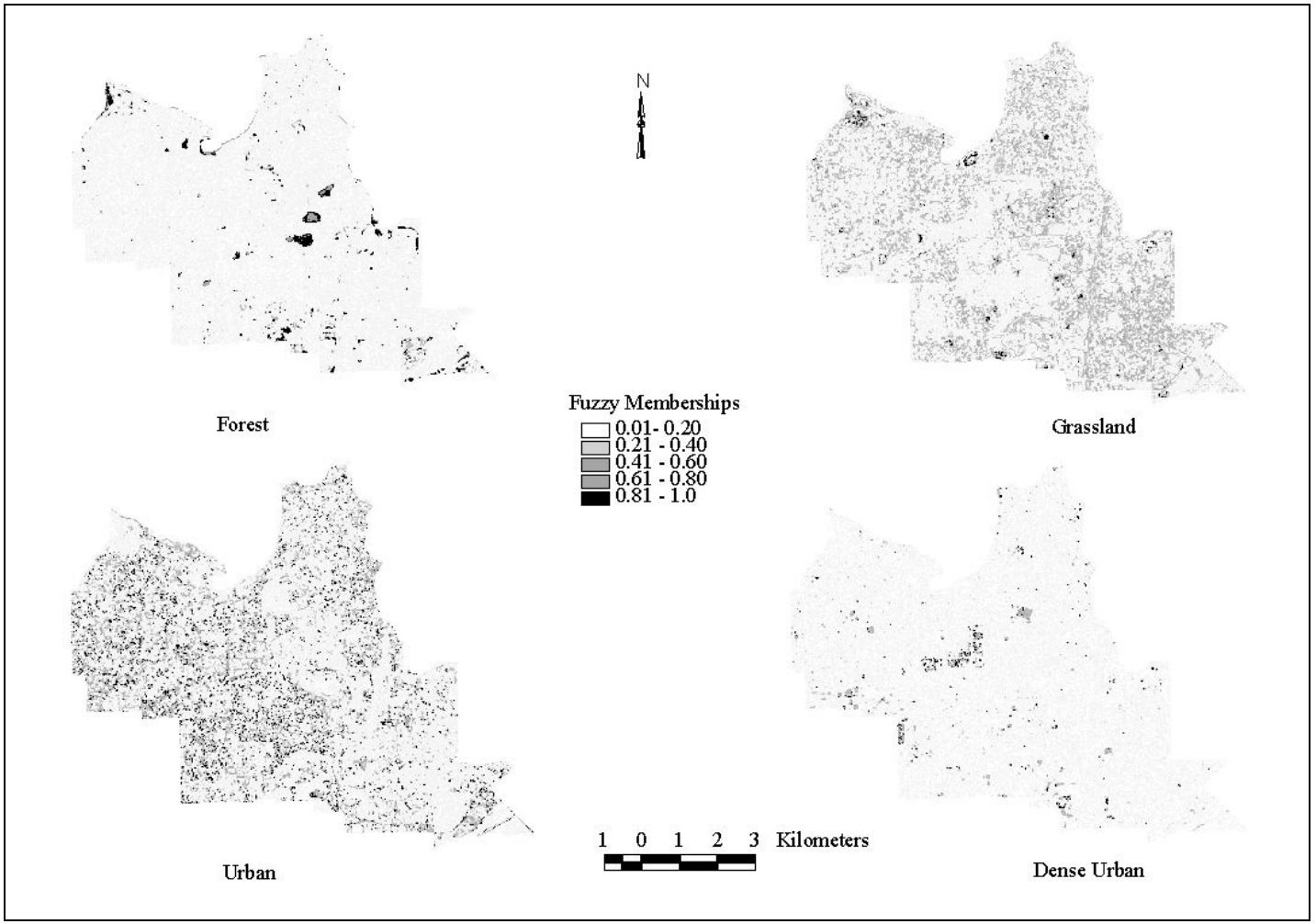

(b) OR

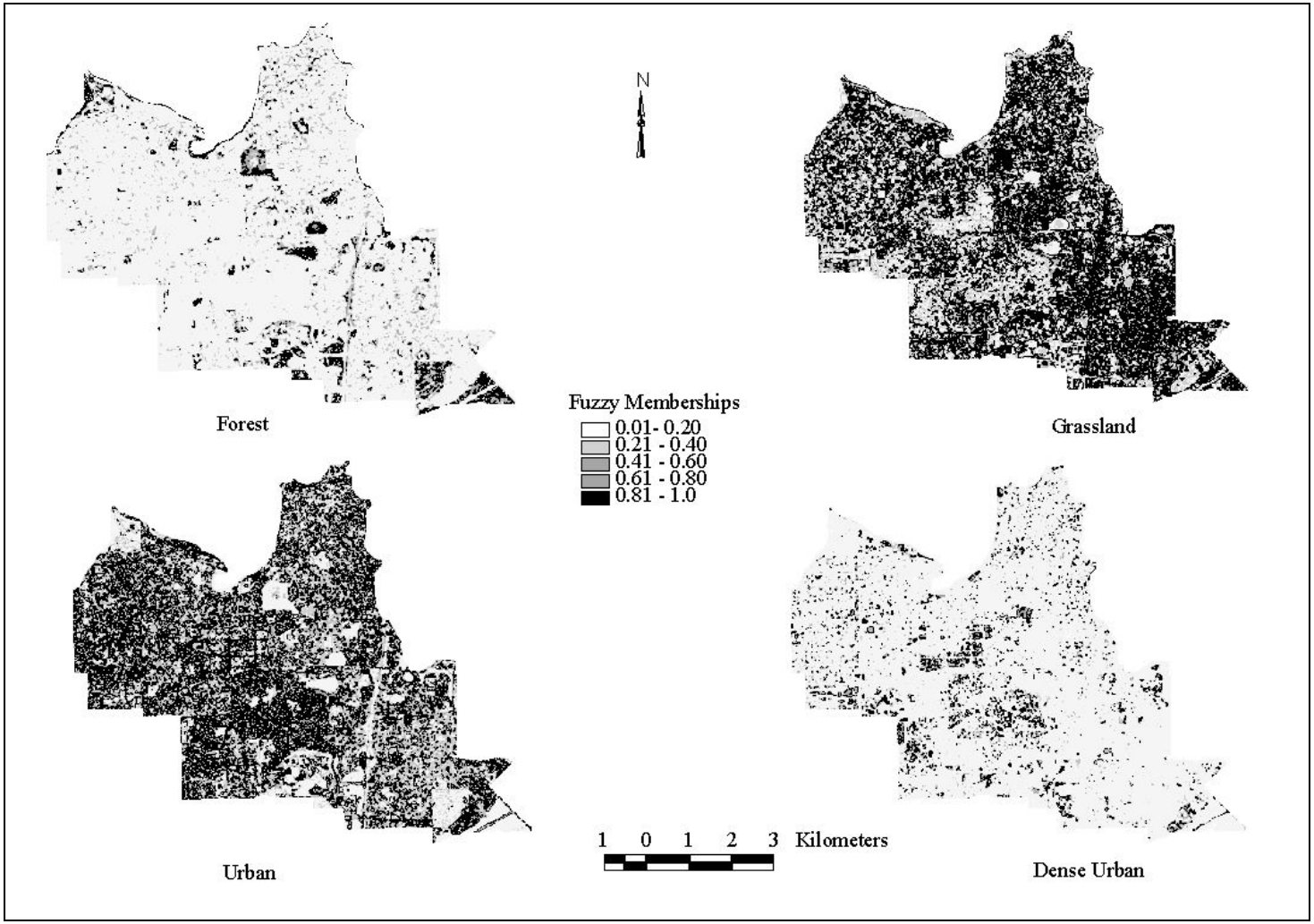
N
Forest
Grassland
Fuzzy Memberships
0.01- 0.20
0.21 - 0.40
0.41 - 0.60
0.61 - 0.80
0.81 - 1.0
Urban
Dense Urban
1 0 1 2 3 Kilometers

(c) FAP


N
Forest
Grassland
Fuzzy Memberships
0.01- 0.20
0.21 - 0.40
0.41 - 0.60
0.61 - 0.80
0.81 - 1.0
Urban
Dense Urban
1 0 1 2 3 Kilometers

(d) FAS

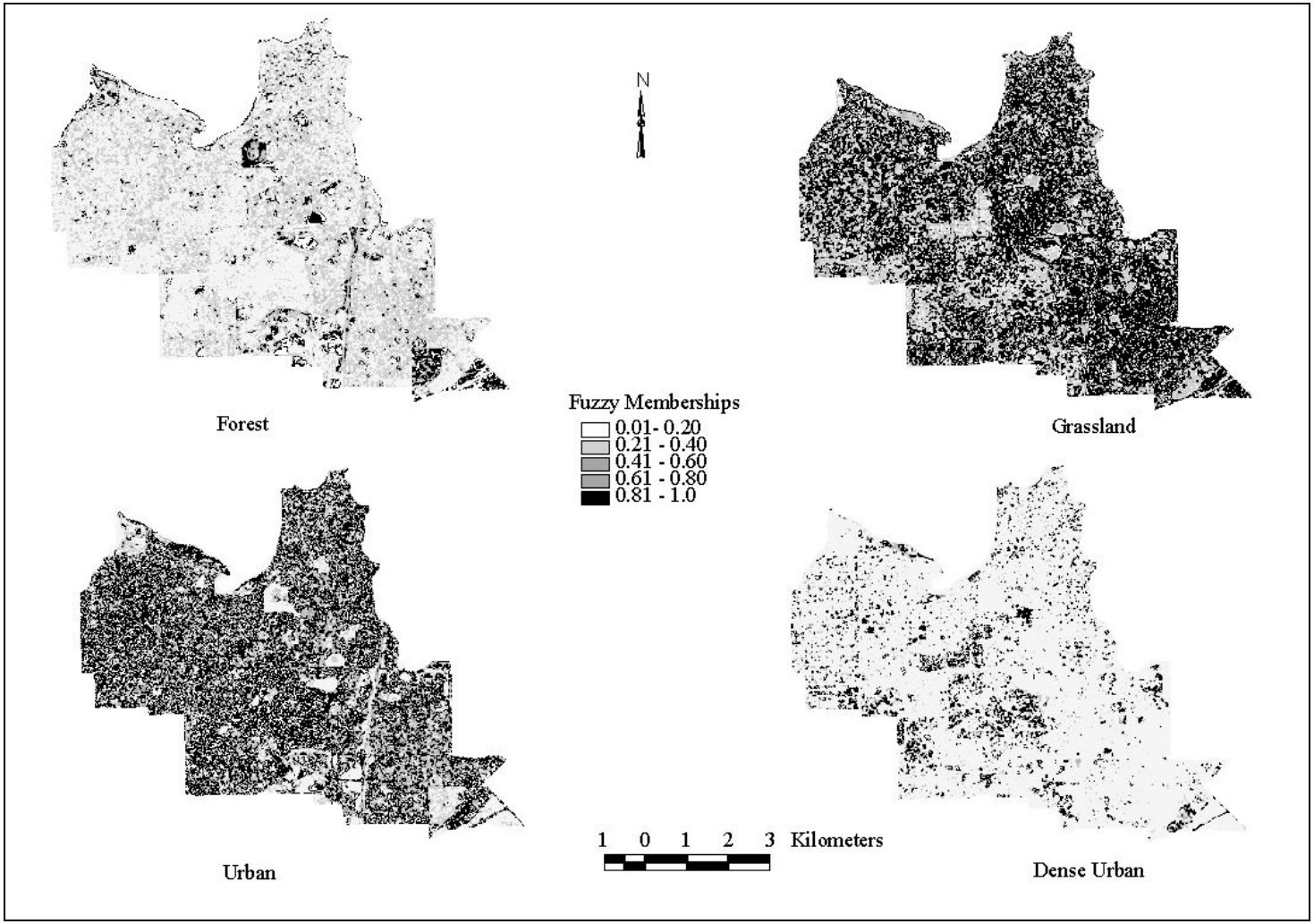
N
Forest
Grassland
Fuzzy Memberships
0.01- 0.20
0.21 - 0.40
0.41 - 0.60
0.61 - 0.80
0.81 - 1.0
Urban
Dense Urban
1 0 1 2 3 Kilometers

(k) $\gamma = 0.10$


N
Forest
Grassland
Fuzzy Memberships
0.01- 0.20
0.21 - 0.40
0.41 - 0.60
0.61 - 0.80
0.81 - 1.0
Urban
Dense Urban
1 0 1 2 3 Kilometers

(f) $\gamma = 0.50$

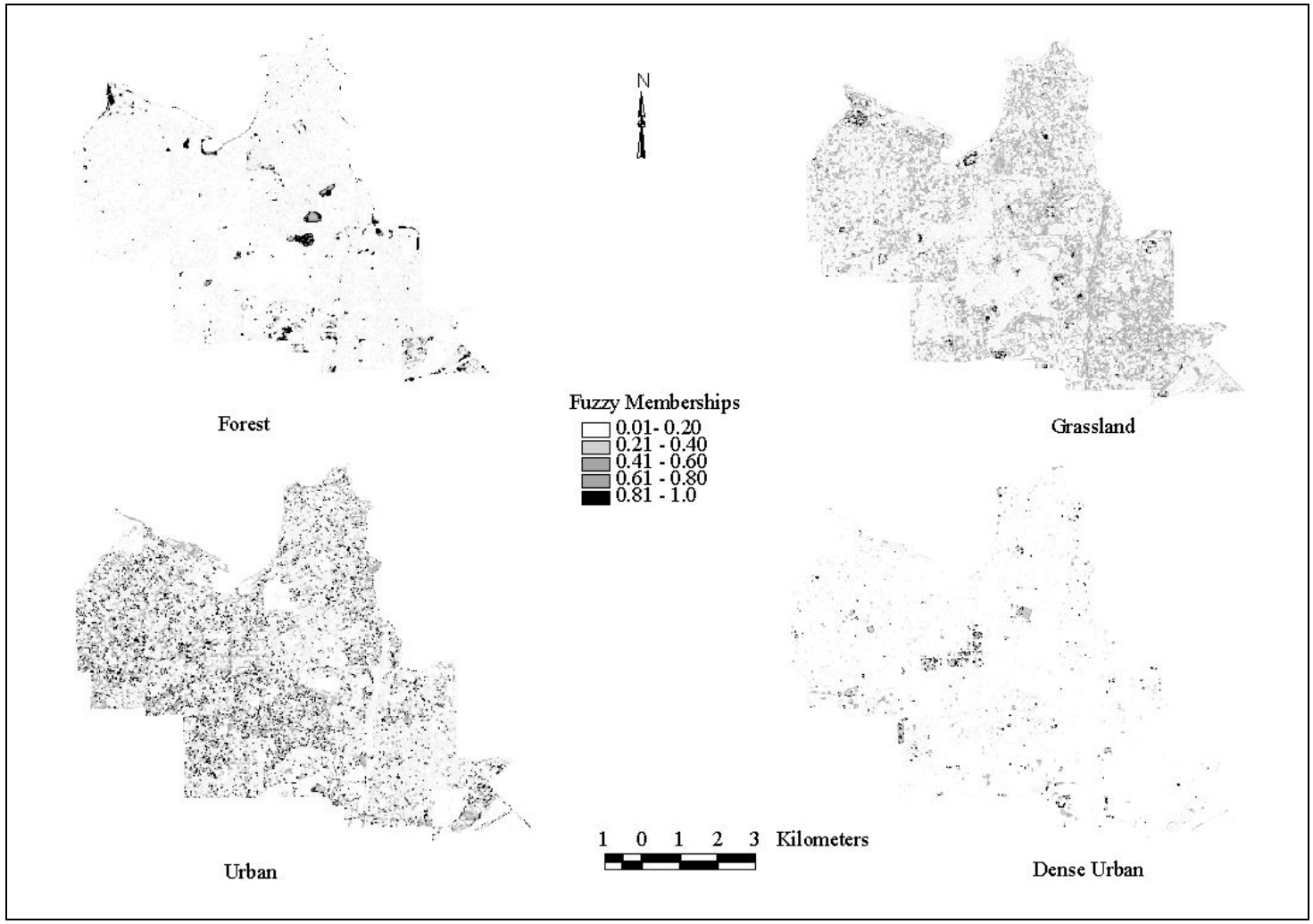
N
Forest
Grassland
Fuzzy Memberships
0.01- 0.20
0.21 - 0.40
0.41 - 0.60
0.61 - 0.80
0.81 - 1.0
Urban
Dense Urban
1 0 1 2 3 Kilometers

(g) $\gamma = 0.60$

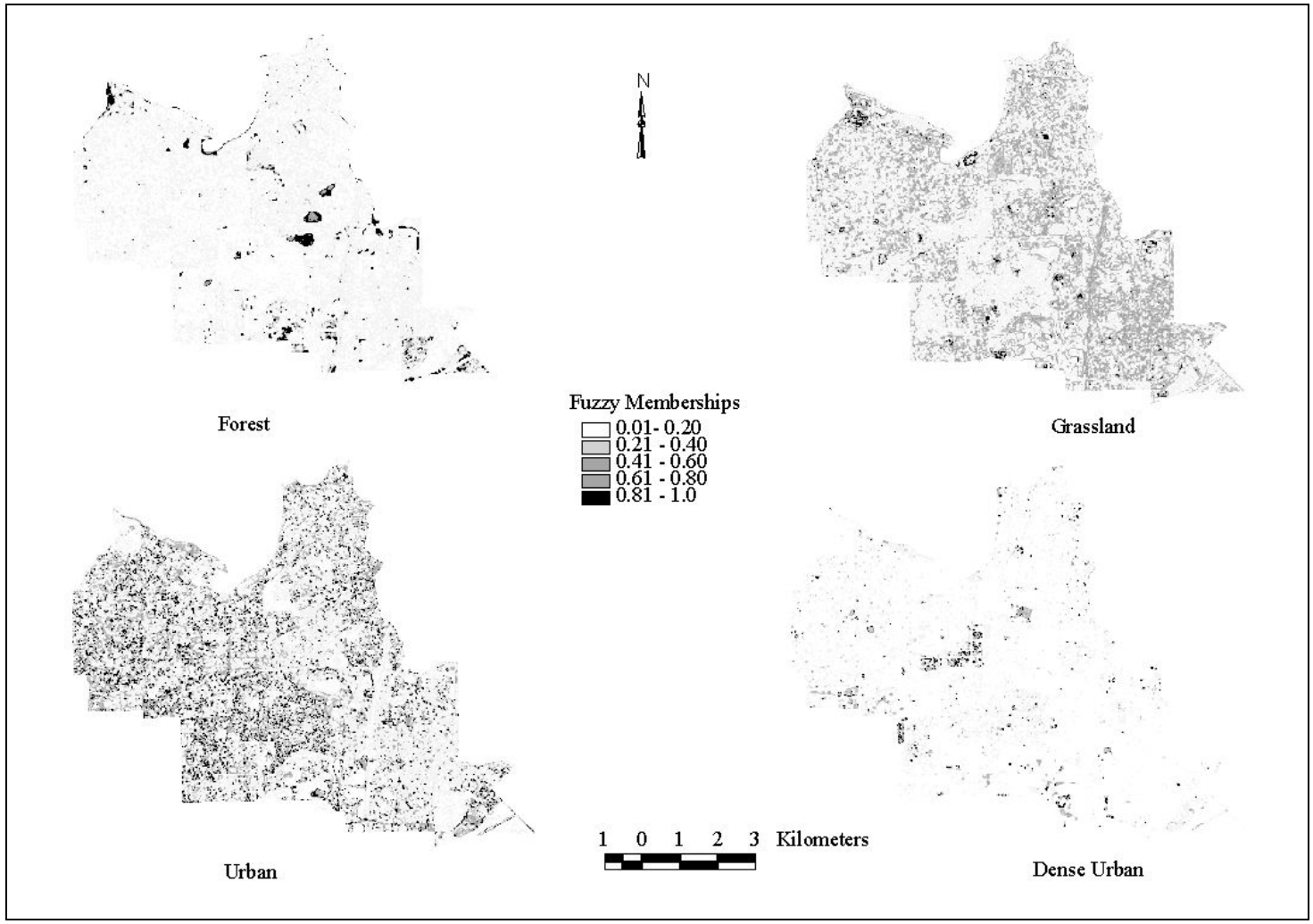
N
Forest
Grassland
Fuzzy Memberships
0.01- 0.20
0.21 - 0.40
0.41 - 0.60
0.61 - 0.80
0.81 - 1.0
Urban
Dense Urban
1 0 1 2 3 Kilometers

(h) $\gamma = 0.70$

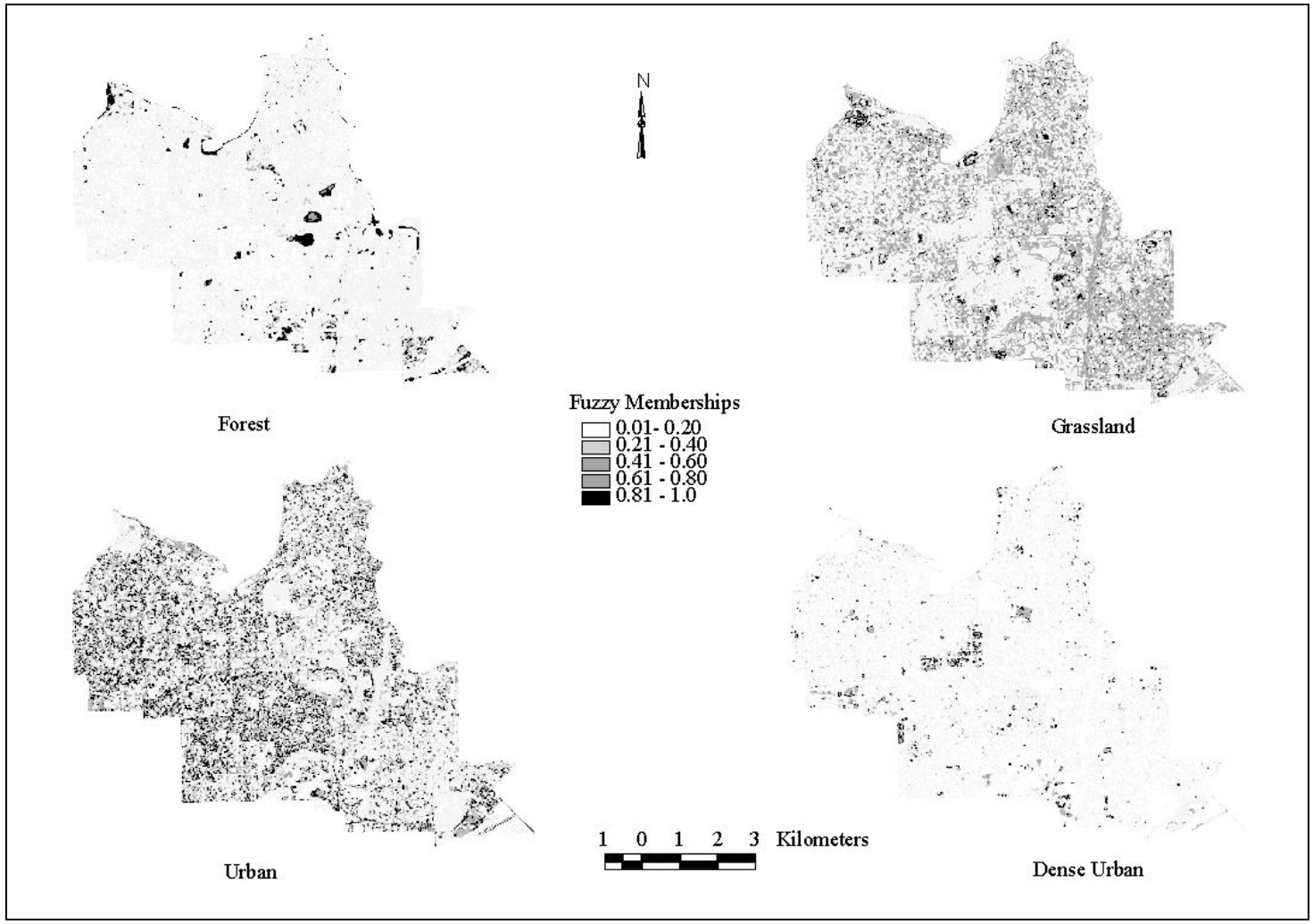
N
Forest
Grassland
Fuzzy Memberships
0.01- 0.20
0.21 - 0.40
0.41 - 0.60
0.61 - 0.80
0.81 - 1.0
Urban
Dense Urban
1 0 1 2 3 Kilometers

(i) $\gamma = 0.80$

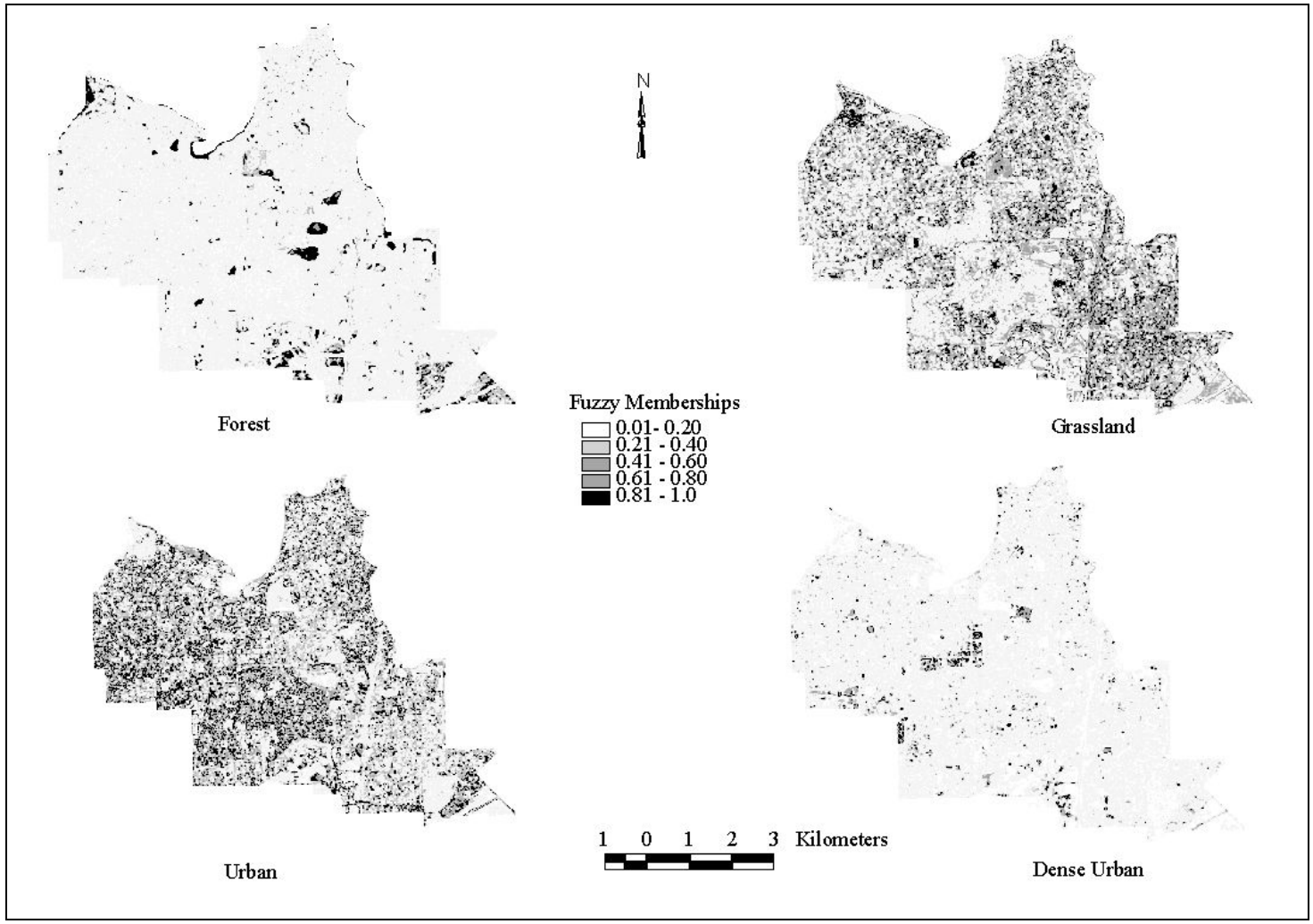
N
Forest
Grassland
Fuzzy Memberships
0.01- 0.20
0.21 - 0.40
0.41 - 0.60
0.61 - 0.80
0.81 - 1.0
Urban
Dense Urban
1 0 1 2 3 Kilometers

(j) $\gamma = 0.90$

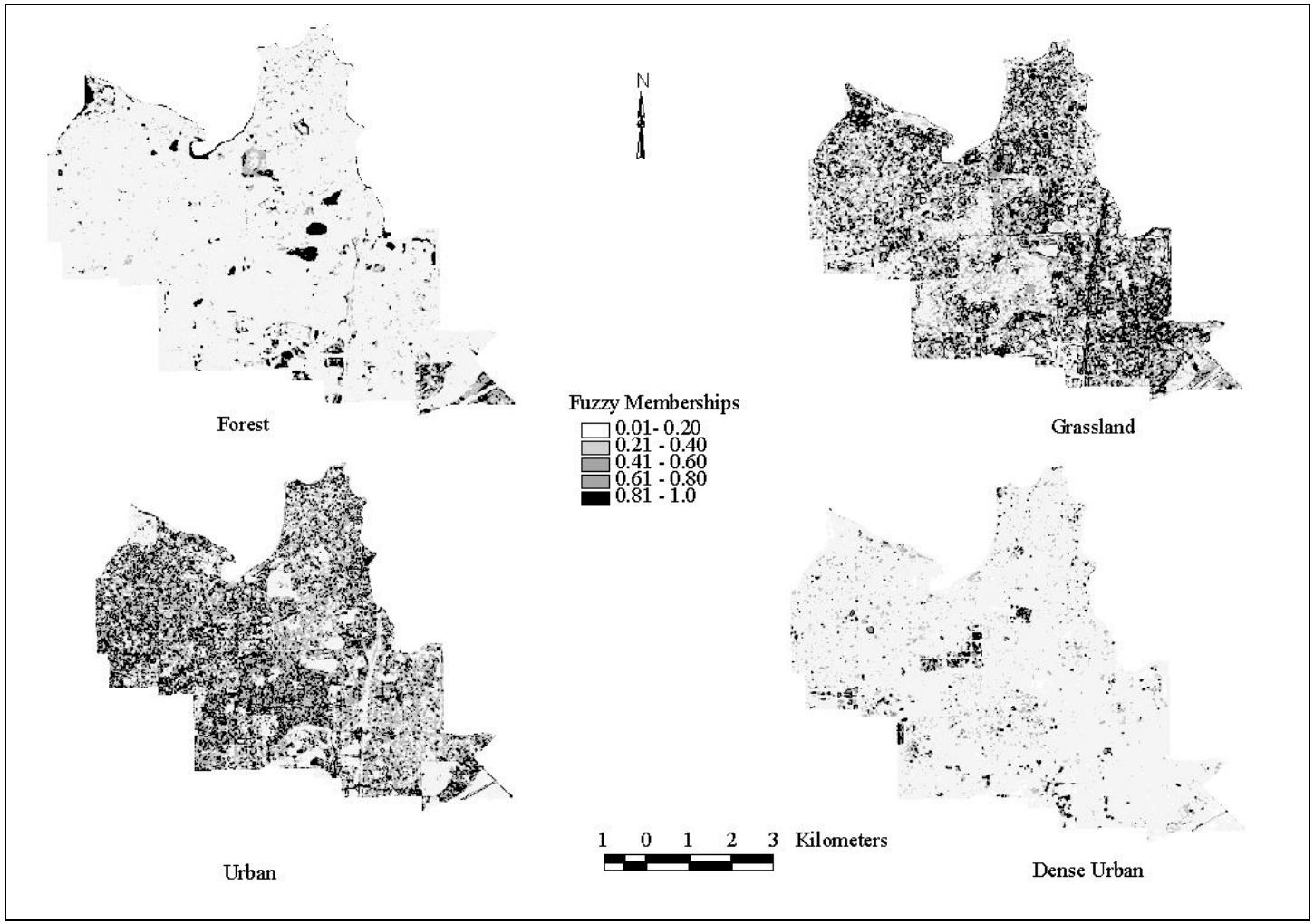
N
Forest
Grassland
Fuzzy Memberships
0.01- 0.20
0.21 - 0.40
0.41 - 0.60
0.61 - 0.80
0.81 - 1.0
Urban
Dense Urban
1 0 1 2 3 Kilometers

(k) $\gamma = 0.95$

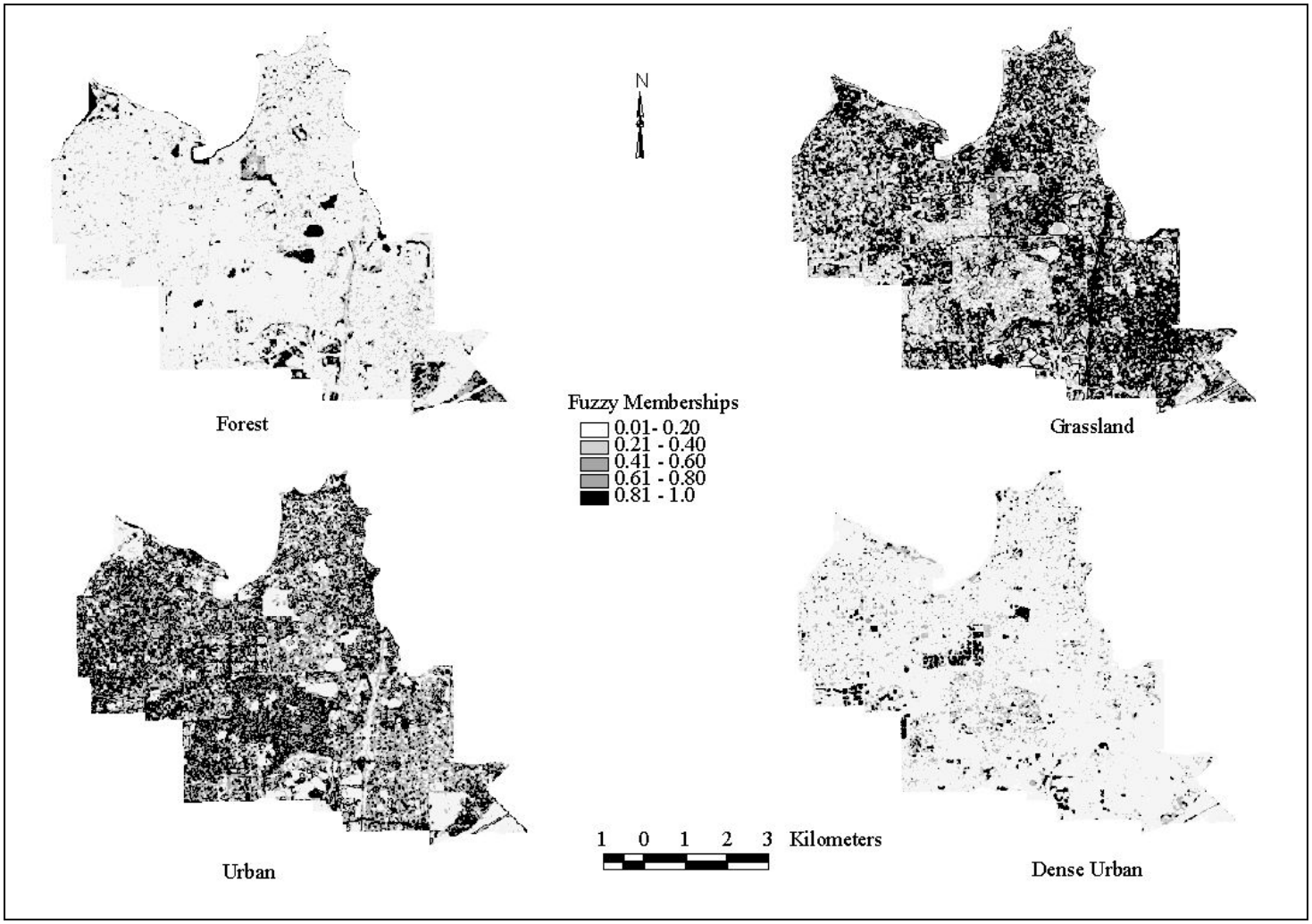
N
Forest
Grassland
Fuzzy Memberships
0.01- 0.20
0.21 - 0.40
0.41 - 0.60
0.61 - 0.80
0.81 - 1.0
Urban
Dense Urban
1 0 1 2 3 Kilometers

Appendix 9 Integrated fuzzy memberships of the land cover classes of forest, grassland, urban and dense urban generated by different fuzzy operators of the City of Armadale

(a) AND

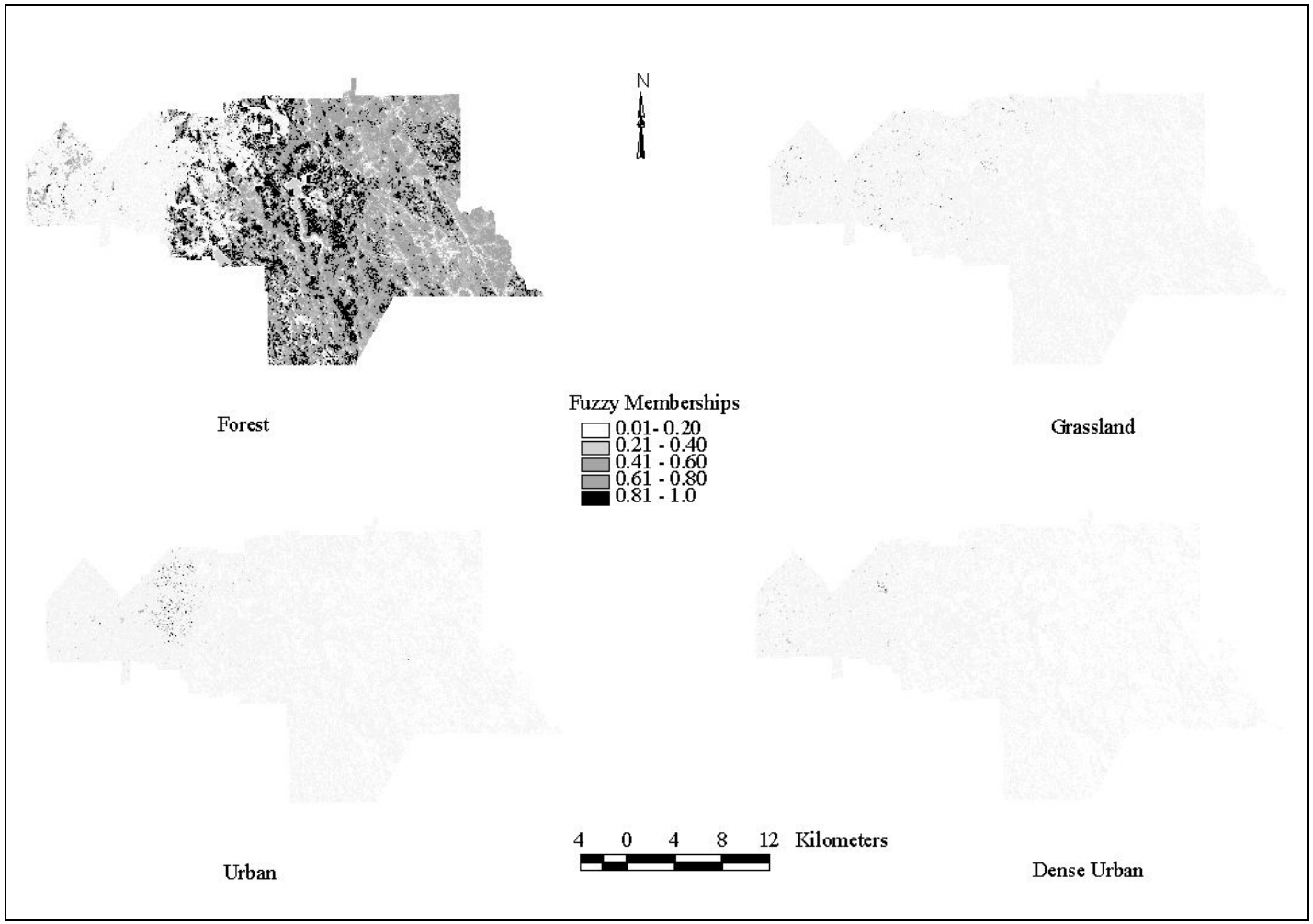

(b) OR

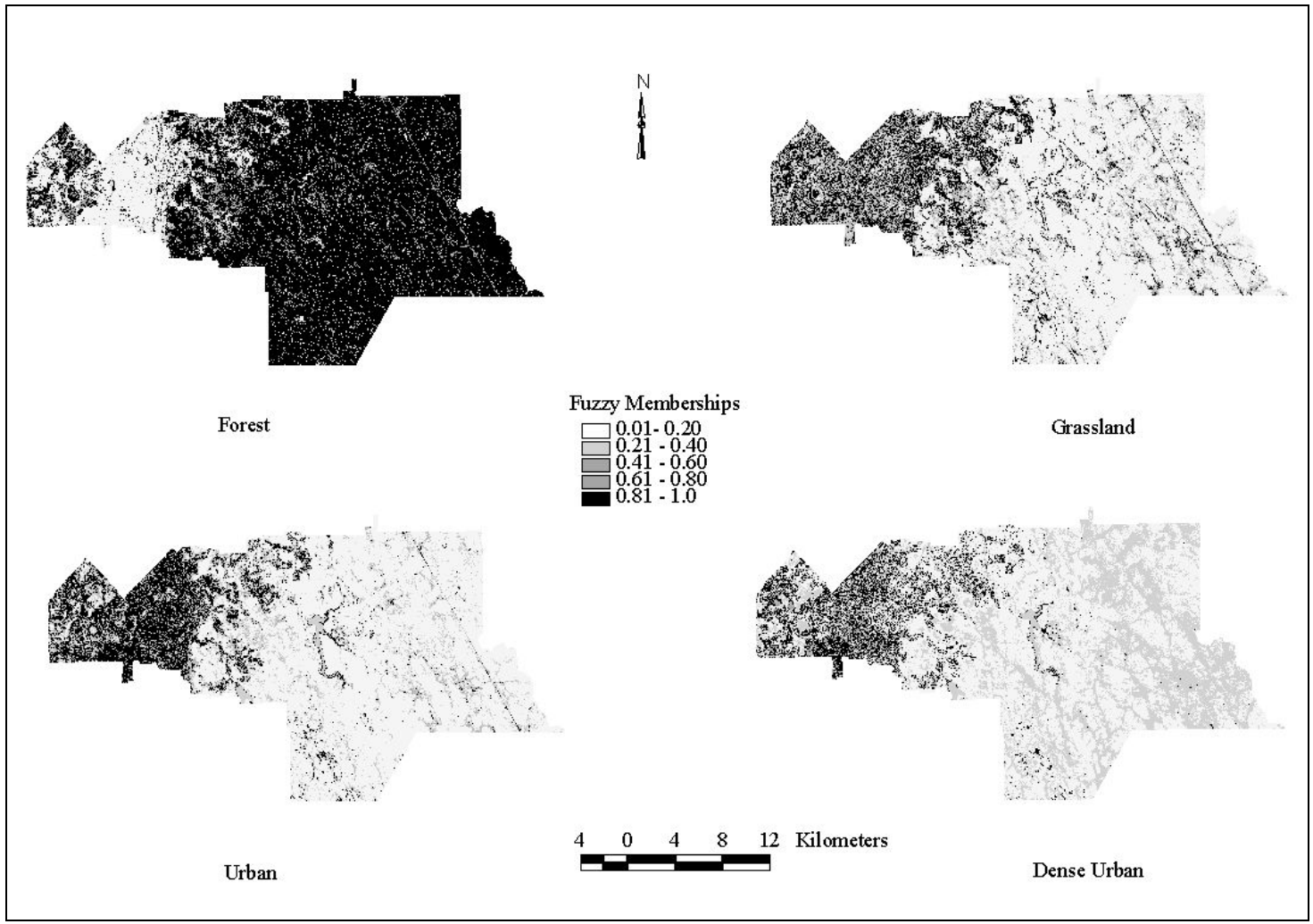
N
Forest
Grassland
Fuzzy Memberships
0.01- 0.20
0.21 - 0.40
0.41 - 0.60
0.61 - 0.80
0.81 - 1.0
Urban
Dense Urban
4 0 4 8 12 Kilometers

(c) FAP

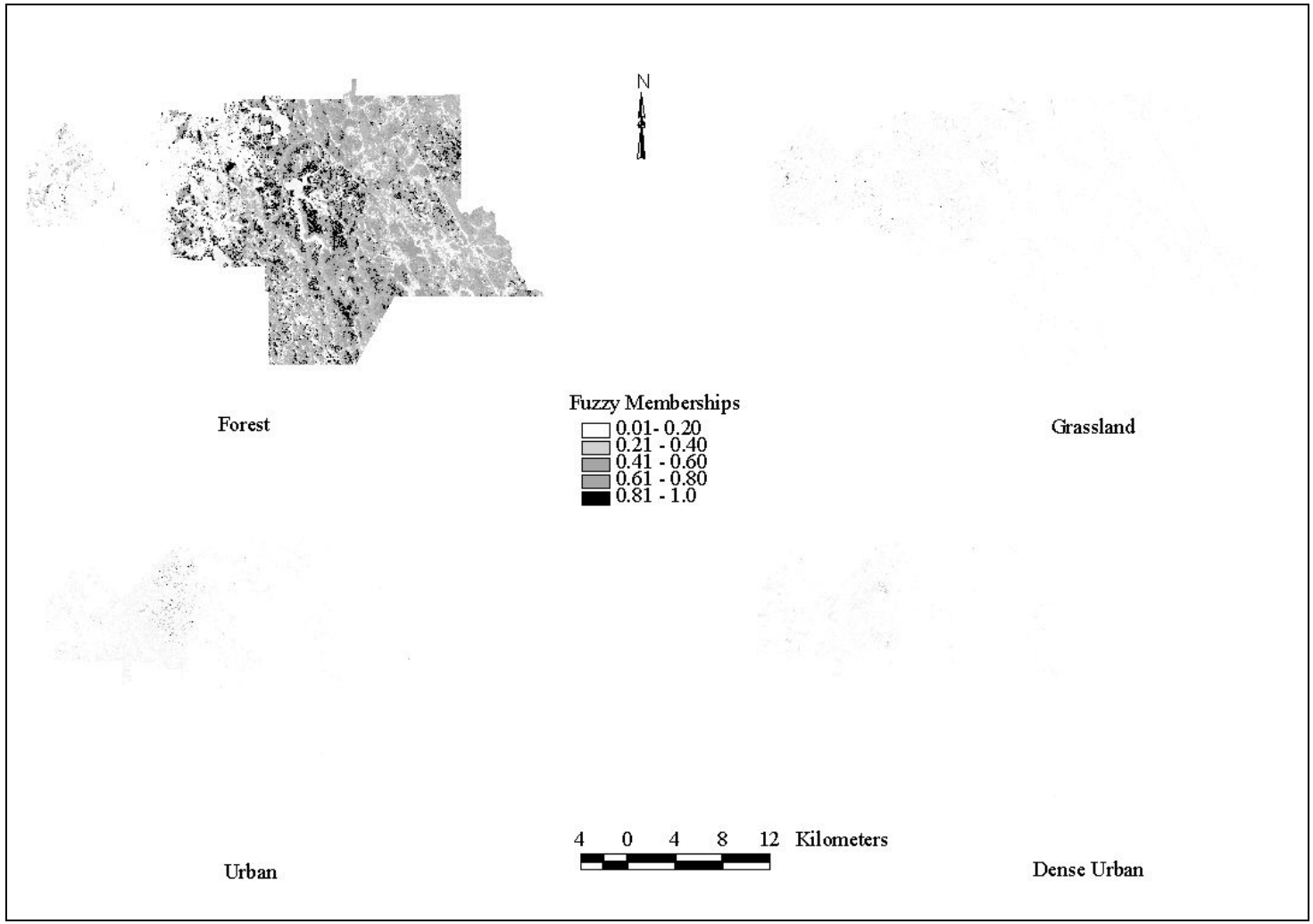
N
Forest
Fuzzy Memberships
0.01- 0.20
0.21 - 0.40
0.41 - 0.60
0.61 - 0.80
0.81 - 1.0
Grassland
Urban
4 0 4 8 12 Kilometers
Dense Urban

(d) FAS

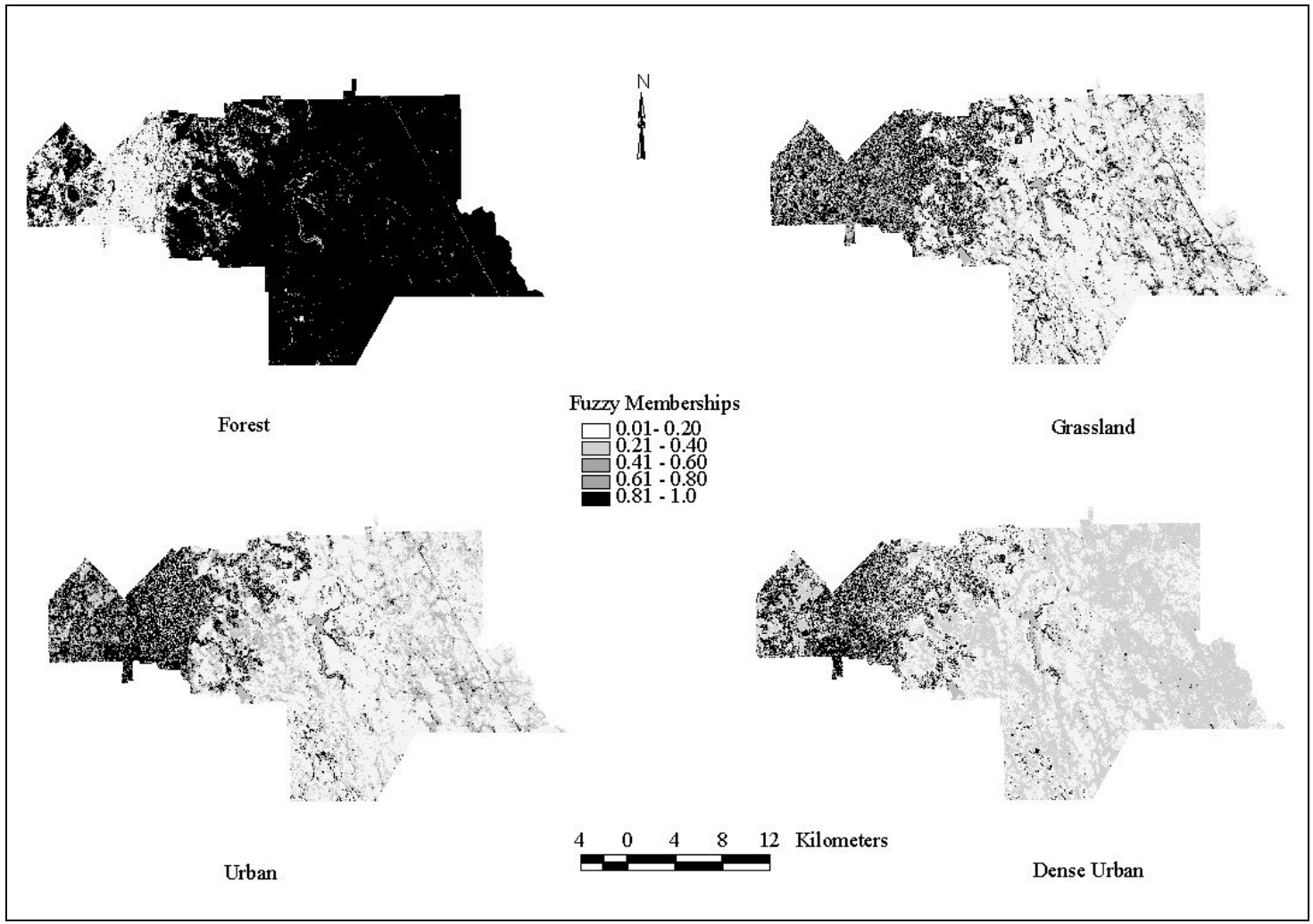
N
Forest
Grassland
Fuzzy Memberships
0.01- 0.20
0.21 - 0.40
0.41 - 0.60
0.61 - 0.80
0.81 - 1.0
Urban
Dense Urban
4 0 4 8 12 Kilometers

(e) $\gamma = 0.10$

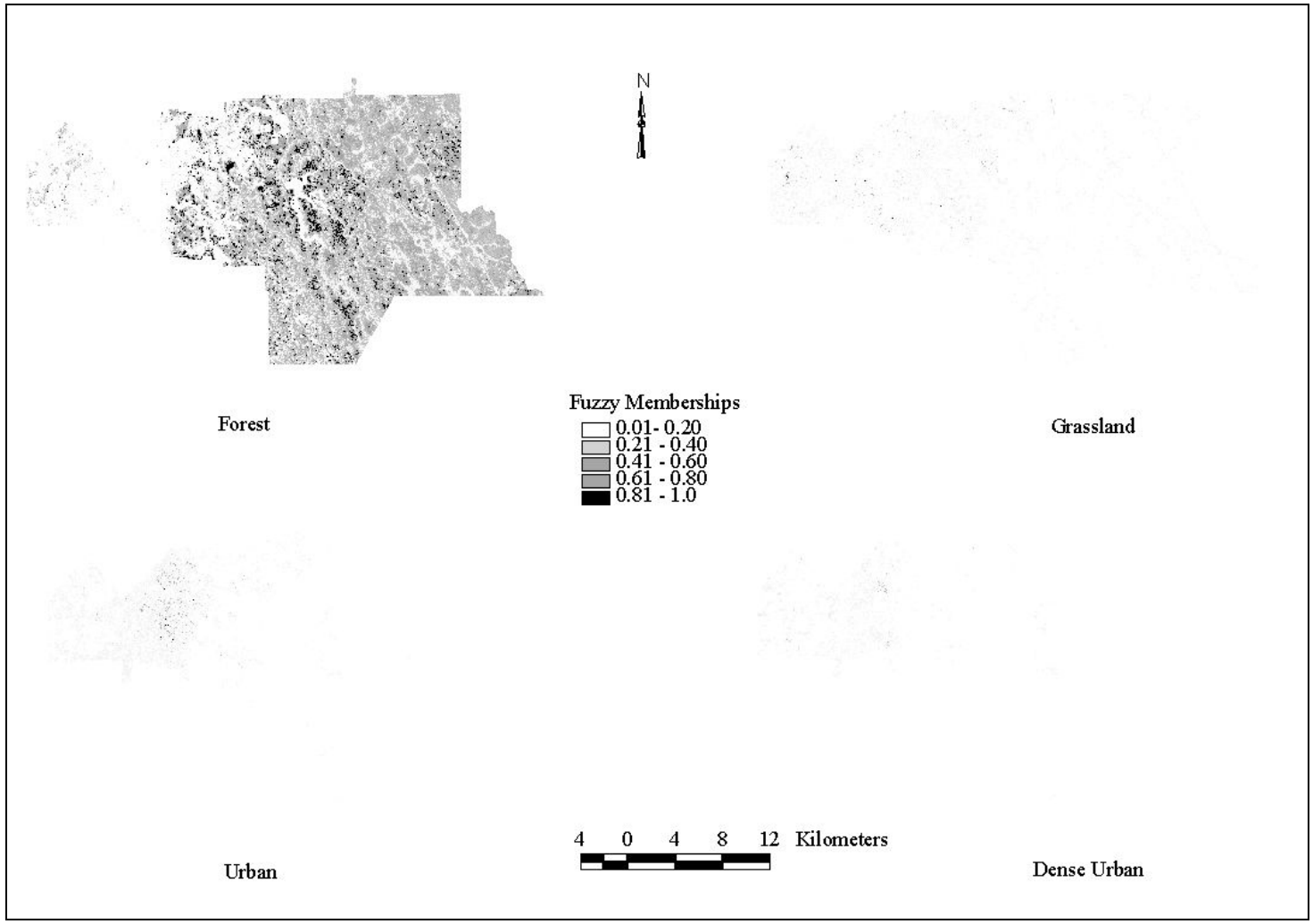

(f) $\gamma = 0.50$


N
Forest
Fuzzy Memberships
0.01- 0.20
0.21 - 0.40
0.41 - 0.60
0.61 - 0.80
0.81 - 1.0
Grassland
Urban
4 0 4 8 12 Kilometers
Dense Urban

(g) $\gamma = 0.60$


N
Forest
Fuzzy Memberships
0.01- 0.20
0.21 - 0.40
0.41 - 0.60
0.61 - 0.80
0.81 - 1.0
Grassland
Urban
4 0 4 8 12 Kilometers
Dense Urban

(h) $\gamma = 0.70$


N
Forest
Fuzzy Memberships
0.01- 0.20
0.21 - 0.40
0.41 - 0.60
0.61 - 0.80
0.81 - 1.0
Grassland
Urban
4 0 4 8 12 Kilometers
Dense Urban

(i) $\gamma = 0.80$


N
Forest
Fuzzy Memberships
0.01- 0.20
0.21 - 0.40
0.41 - 0.60
0.61 - 0.80
0.81 - 1.0
Grassland
Urban
4 0 4 8 12 Kilometers
Dense Urban

(j) $\gamma = 0.90$


N
Forest
Fuzzy Memberships
0.01- 0.20
0.21 - 0.40
0.41 - 0.60
0.61 - 0.80
0.81 - 1.0
Grassland
Urban
4 0 4 8 12 Kilometers
Dense Urban

(k) $\gamma = 0.95$

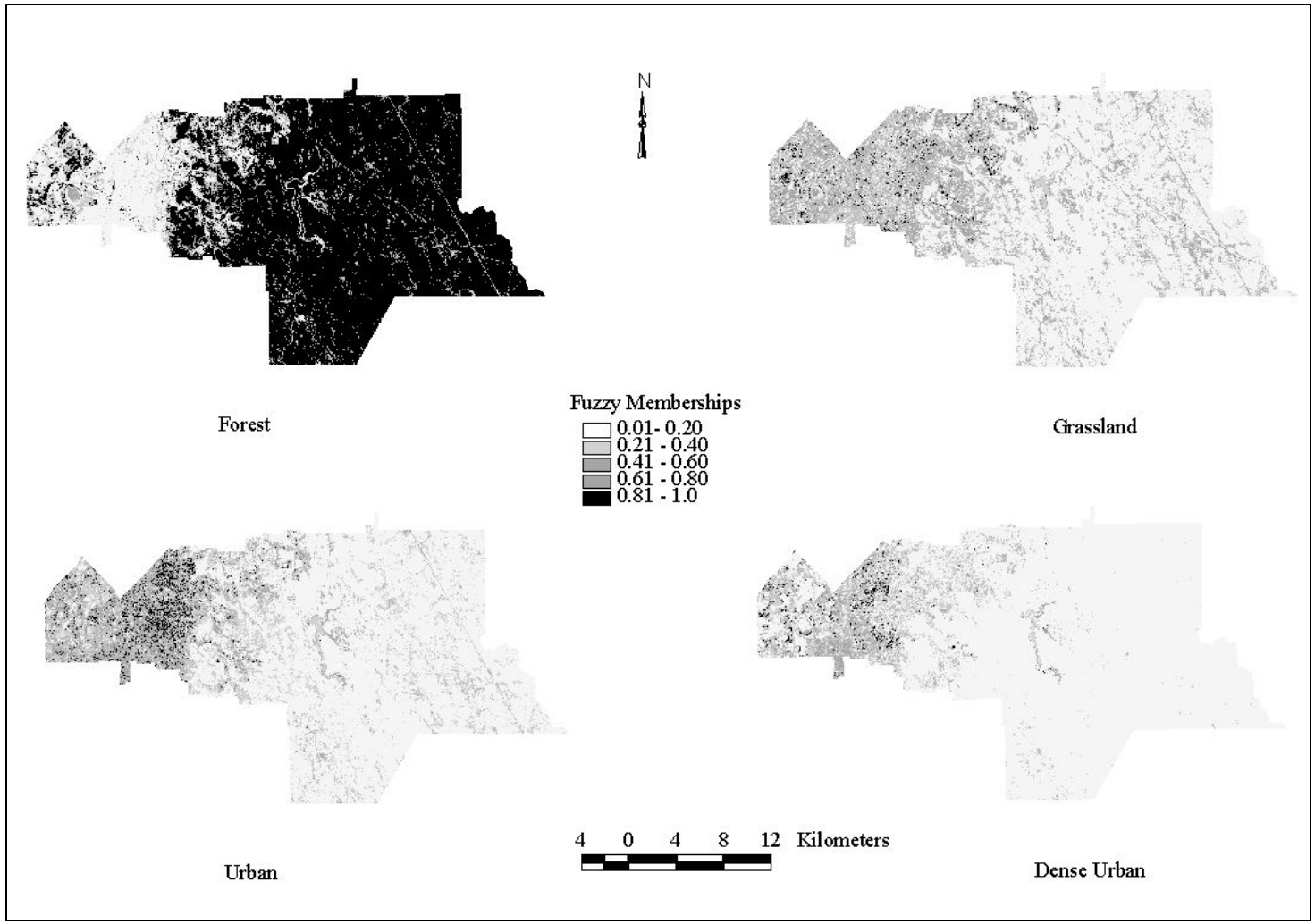
N
Forest
Grassland
Fuzzy Memberships
0.01- 0.20
0.21 - 0.40
0.41 - 0.60
0.61 - 0.80
0.81 - 1.0
Urban
Dense Urban
4 0 4 8 12 Kilometers

Appendix 10 Fuzzy memberships of the field visited sample points

City of Perth				City of Melville				City of Armadale			
Coordinates		Dominant		Coordinates		Dominant		Coordinates		Dominant	
X	Y	Land Cover Class	Fuzzy Membership	X	Y	Land Cover Class	Fuzzy Membership	X	Y	Land Cover Class	Fuzzy Membership
390041	6463121	Forest	0.9	389984	6453544	Forest	0.7	405225	6444544	Forest	0.7
390091	6463171	Forest	0.9	390260	6453422	Forest	0.7	408114	6442658	Forest	0.9
390266	6463271	Forest	0.7	390384	6453444	Forest	0.9	408567	6442617	Forest	0.8
390316	6463396	Forest	0.9	390161	6453421	Forest	0.9	408809	6442542	Forest	0.7
390391	6463246	Forest	0.7	390268	6453197	Forest	0.8	409003	6442370	Forest	0.8
390816	6463221	Forest	0.8	385633	6457245	Forest	0.8	408620	6442647	Forest	0.7
390341	6463546	Forest	0.6	385368	6457292	Forest	0.7	416959	6447405	Forest	0.9
390466	6463971	Forest	0.9	389034	6455720	Forest	0.6	417067	6447284	Forest	0.8
390491	6463721	Forest	0.7	388908	6455394	Forest	0.6	416970	6447136	Forest	0.8
390816	6463846	Forest	0.8	389065	6455311	Forest	0.6	419004	6446937	Forest	0.7
390591	6463771	Forest	0.5	389209	6455795	Forest	0.6	418959	6446864	Forest	0.8
390816	6463596	Forest	0.7	389248	6455913	Forest	0.7	419251	6446784	Forest	0.8
390966	6463846	Forest	0.7	393236	6450815	Forest	0.9	419286	6446675	Forest	0.8
390766	6463921	Forest	0.5	393721	6450785	Forest	0.8	419232	6446566	Forest	0.9
390816	6463996	Forest	0.7	393719	6450684	Forest	0.8	419364	6446479	Forest	0.8
390366	6462946	Forest	0.8	393580	6450412	Forest	0.8	419371	6446263	Forest	0.8
389316	6462071	Forest	0.8	393309	6450394	Forest	0.6	419303	6446343	Forest	0.9
389266	6461996	Forest	0.6	394158	6449966	Forest	0.6	419464	6446742	Forest	0.9
389491	6462121	Forest	0.9	394284	6450194	Forest	0.6	420313	6446081	Forest	0.8
389266	6462621	Forest	0.7	393259	6452767	Forest	0.8	420439	6446082	Forest	0.9
388466	6461921	Forest	0.8	393365	6453030	Forest	0.8	420786	6446317	Forest	0.8
388391	6462196	Forest	0.8	393274	6453393	Forest	0.7	420915	6446436	Forest	0.7
388466	6462096	Forest	0.8	393316	6453543	Forest	0.7	421027	6446600	Forest	0.8
388791	6463046	Forest	0.9	392680	6453526	Forest	0.8	416181	6448080	Forest	0.8
388891	6462996	Forest	0.9	392669	6453331	Forest	0.7	416063	6448145	Forest	0.9
388966	6463046	Forest	0.9	391987	6453014	Forest	0.7	408367	6446201	Forest	0.8
388516	6463096	Forest	0.9	389631	6454492	Forest	0.7	398503	6442046	Forest	0.9
390041	6464221	Forest	0.9	390832	6454048	Forest	0.9	399145	6442772	Forest	0.8
390016	6463571	Forest	0.7	394832	6450417	Forest	0.9	399206	6442899	Forest	0.8
390016	6463046	Forest	0.7	394733	6450051	Forest	0.9	399637	6442390	Forest	0.8
390766	6463671	Forest	0.8	390864	6454087	Forest	0.9	399828	6442348	Forest	0.9
390591	6463721	Forest	0.8	386246	6456983	Forest	0.7	399344	6442357	Forest	0.9
390266	6463171	Forest	0.8	389708	6457269	Forest	0.6	399126	6442185	Forest	0.8
391191	6463271	Forest	0.9	393059	6450119	Forest	0.7	398914	6442283	Forest	0.8
390991	6463571	Forest	0.7	394487	6450175	Forest	0.7	401782	6441733	Forest	0.8
391041	6463671	Forest	0.8	389159	6452519	Dense Urban	0.7	401549	6441394	Forest	0.7
392141	6463571	Forest	0.8	385837	6455251	Dense Urban	0.7	400865	6443085	Forest	0.8
394841	6462996	Forest	0.8	385792	6454990	Dense Urban	0.8	408126	6442669	Forest	0.8
391816	6464546	Forest	0.4	389433	6457914	Dense Urban	0.8	416963	6447426	Forest	0.8
390091	6463771	Forest	0.8	389720	6454819	Dense Urban	0.9	417061	6447286	Forest	0.9
390166	6463346	Forest	0.7	389735	6454907	Dense Urban	0.8	419263	6446786	Forest	0.8
390416	6463696	Forest	0.8	389905	6454997	Dense Urban	0.8	420279	6446073	Forest	0.8
390066	6464071	Forest	0.7	390085	6454994	Dense Urban	0.9	416167	6448088	Forest	0.9

393741	6463571	Forest	0.4	390070	6455172	Dense Urban	0.9	419788	6446479	Forest	0.9
390066	6462296	Forest	0.9	388602	6453893	Dense Urban	0.6	422713	6444629	Forest	0.9
390116	6462396	Forest	0.8	388652	6454035	Dense Urban	0.7	422703	6443929	Forest	0.9
390116	6462546	Forest	0.8	388895	6453992	Dense Urban	0.6	418438	6447604	Forest	0.9
389741	6462596	Forest	0.9	388516	6453968	Dense Urban	0.7	425588	6441879	Forest	0.8
389691	6462546	Forest	0.9	389110	6454635	Dense Urban	0.9	426638	6440804	Forest	0.9
389066	6462896	Forest	0.8	389110	6454194	Dense Urban	0.8	427213	6440239	Forest	0.9
389091	6462721	Forest	0.7	390334	6452394	Urban	0.8	427613	6441254	Forest	0.8
389221	6462546	Forest	0.7	390334	6452344	Urban	0.8	427663	6440929	Forest	0.9
389966	6462621	Forest	0.9	390684	6451769	Urban	0.7	414788	6437704	Forest	0.8
389166	6462571	Forest	0.8	388577	6452790	Urban	0.5	415088	6438004	Forest	0.8
389891	6462496	Forest	0.8	388884	6452094	Urban	0.8	415688	6438004	Forest	0.9
389816	6462396	Forest	0.8	388859	6452419	Urban	0.7	441788	6437879	Forest	0.8
389791	6464146	Forest	0.8	388859	6452619	Urban	0.8	416138	6437804	Forest	0.9
388716	6463276	Forest	0.6	389109	6452669	Urban	0.6	418513	6434529	Forest	0.8
388891	6463271	Forest	0.7	389334	6452894	Urban	0.7	418663	6434354	Forest	0.8
388991	6462221	Forest	0.8	389284	6452994	Urban	0.7	418513	6434529	Forest	0.9
388791	6462171	Forest	0.8	388534	6453569	Urban	0.8	418663	6434354	Forest	0.8
390491.19	6464796	Dense Urban	0.7	388884	6453294	Urban	0.8	419213	6433479	Forest	0.8
390616.19	6464721	Dense Urban	0.4	389684	6453294	Urban	0.5	432263	6437129	Forest	0.9
390441.19	6464646	Dense Urban	0.9	390134	6452969	Urban	0.7	433913	6436329	Forest	0.8
390866.19	6464646	Dense Urban	0.8	390307	6452921	Urban	0.5	434188	6435429	Forest	0.9
390816.19	6464596	Dense Urban	0.8	386534	6456819	Urban	0.6	434213	6436629	Forest	0.8
390866.19	6464571	Dense Urban	0.6	386834	6456744	Urban	0.6	434388	6436404	Forest	0.9
390741.19	6464546	Dense Urban	0.7	386859	6456444	Urban	0.6	420912	6446436	Forest	0.8
390241.19	6464371	Dense Urban	0.4	386683	6456544	Urban	0.8	407137	6446399	Dense Urban	0.8
390891	6463796	Dense Urban	0.8	386359	6456544	Urban	0.6	407036	6446625	Dense Urban	0.6
392016	6464271	Dense Urban	0.5	386292	6456820	Urban	0.5	407497	6442512	Dense Urban	0.6
392241	6464296	Dense Urban	0.6	387213	6455877	Urban	0.5	407575	6442435	Dense Urban	0.8
392366	6464646	Dense Urban	0.7	387209	6455776	Urban	0.6	407440	6442476	Dense Urban	0.6
392591	6464596	Dense Urban	0.5	385184	6455794	Urban	0.7	407281	6442503	Dense Urban	0.8
392591	6464496	Dense Urban	0.5	385554	6455645	Urban	0.8	407305	6442336	Dense Urban	0.6
392916	6463721	Dense Urban	0.5	385484	6455644	Urban	0.8	407136	6442243	Dense Urban	0.7
392191	6463996	Dense Urban	0.7	385858	6455592	Urban	0.8	407115	6442198	Dense Urban	0.8
392166	6463996	Dense Urban	0.7	386865	6454626	Urban	0.7	405608	6444794	Urban	0.8
392341	6464071	Dense Urban	0.8	386084	6454744	Urban	0.6	405044	6444244	Urban	0.7
392641	6464096	Dense Urban	0.6	386509	6454319	Urban	0.8	404966	6443956	Urban	0.7
392391	6464121	Dense Urban	0.8	386409	6453944	Urban	0.8	405380	6443314	Urban	0.8
392566	6464196	Dense Urban	0.7	386459	6453944	Urban	0.7	406538	6444477	Urban	0.8
394416	6463596	Dense Urban	0.8	386156	6455020	Urban	0.7	406518	6444798	Urban	0.5
391391	6464621	Dense Urban	0.8	385943	6454777	Urban	0.8	406489	6445218	Urban	0.6
391641	6464496	Dense Urban	0.5	385334	6453919	Urban	0.8	406773	6445166	Urban	0.6
391641	6464996	Dense Urban	0.8	385809	6453769	Urban	0.7	406408	6446298	Urban	0.7
391516	6464346	Dense Urban	0.7	385969	6453580	Urban	0.8	406201	6442632	Urban	0.7

391341	6464321	Dense Urban	0.8	385584	6454644	Urban	0.8	405710	6442510	Urban	0.9
391891	6464121	Dense Urban	0.7	385482	6454371	Urban	0.8	405654	6441472	Urban	0.7
390791	6464846	Dense Urban	0.8	385859	6454419	Urban	0.8	405972	6441745	Urban	0.9
393766	6464471	Dense Urban	0.7	385559	6454169	Urban	0.8	406626	6442490	Urban	0.9
393216	6463671	Dense Urban	0.6	390885	6458353	Urban	0.6	404710	6442252	Urban	0.8
393166	6463671	Dense Urban	0.6	390721	6458381	Urban	0.5	408519	6444751	Urban	0.8
393891	6464146	Dense Urban	0.5	390509	6458369	Urban	0.5	408696	6444584	Urban	0.7
390816.19	6465496	Urban	0.6	390449	6457935	Urban	0.5	408708	6444725	Urban	0.8
390816.19	6465346	Urban	0.8	390184	6457784	Urban	0.7	408807	6445838	Urban	0.6
390516.19	6465096	Urban	0.7	389909	6457619	Urban	0.7	407536	6446662	Urban	0.8
390591.19	6464846	Urban	0.5	389231	6458158	Urban	0.8	407655	6446827	Urban	0.6
390216.19	6464396	Urban	0.5	389909	6457227	Urban	0.8	407790	6446791	Urban	0.8
390541	6463471	Urban	0.5	389409	6457010	Urban	0.7	407838	6446961	Urban	0.7
391516	6463596	Urban	0.8	389436	6457270	Urban	0.7	407693	6447023	Urban	0.8
391091	6463371	Urban	0.5	388886	6455846	Urban	0.7	407770	6447247	Urban	0.8
391066	6463321	Urban	0.7	392862	6450605	Urban	0.7	407730	6447408	Urban	0.8
390941	6463196	Urban	0.7	393371	6452827	Urban	0.8	408009	6447664	Urban	0.8
391466	6463546	Urban	0.8	392765	6453345	Urban	0.9	408179	6447662	Urban	0.7
391241	6463571	Urban	0.6	393034	6453194	Urban	0.8	408060	6447452	Urban	0.6
391191	6463571	Urban	0.7	392700	6452934	Urban	0.9	408192	6447250	Urban	0.8
391366	6463646	Urban	0.8	392584	6452594	Urban	0.8	408115	6447038	Urban	0.8
391191	6463671	Urban	0.6	392805	6452324	Urban	0.8	407996	6446798	Urban	0.9
392741	6464396	Urban	0.4	393008	6452102	Urban	0.7	408280	6446870	Urban	0.7
392941	6464646	Urban	0.5	392099	6453523	Urban	0.8	408317	6446559	Urban	0.8
392766	6464521	Urban	0.4	391755	6453462	Urban	0.9	407842	6446271	Urban	0.7
392516	6464246	Urban	0.4	391912	6452804	Urban	0.7	407768	6446399	Urban	0.7
392841	6463646	Urban	0.4	389736	6454107	Urban	0.8	404809	6442946	Urban	0.6
392441	6463746	Urban	0.5	390833	6455630	Urban	0.8	404796	6443145	Urban	0.8
392341	6463796	Urban	0.4	390208	6454192	Urban	0.7	405006	6443236	Urban	0.8
392766	6464196	Urban	0.5	388934	6456019	Urban	0.6	404969	6443961	Urban	0.8
393491	6463671	Urban	0.5	387133	6456347	Urban	0.6	405708	6442509	Urban	0.9
393841	6463846	Urban	0.5	389584	6456890	Urban	0.6	408696	6444580	Urban	0.7
393791	6463371	Urban	0.6	393484	6452369	Urban	0.7	407775	6447245	Urban	0.8
393866	6463271	Urban	0.6	390542	6452572	Grassland	0.8	408184	6447657	Urban	0.7
393491	6463221	Urban	0.7	390509	6451944	Grassland	0.8	408270	6446856	Urban	0.8
391691	6464871	Urban	0.5	389148	6453078	Grassland	0.8	407844	6446267	Urban	0.7
391241	6464346	Urban	0.4	389004	6453145	Grassland	0.8	405612	6444814	Urban	0.7
391291	6464071	Urban	0.5	388384	6453394	Grassland	0.8	405356	6444678	Grassland	0.7
391391	6465171	Urban	0.4	390344	6453098	Grassland	0.8	405088	6444681	Grassland	0.8
390191	6464196	Urban	0.4	386377	6456822	Grassland	0.7	404793	6443853	Grassland	0.6
391166	6464621	Urban	0.5	387151	6456691	Grassland	0.7	405182	6443654	Grassland	0.5
390116	6464696	Urban	0.7	387302	6455993	Grassland	0.6	405037	6443535	Grassland	0.6
390316	6464896	Urban	0.6	386901	6455925	Grassland	0.8	404863	6443130	Grassland	0.6
393941	6464721	Urban	0.4	387034	6456241	Grassland	0.7	405603	6443625	Grassland	0.6
393941	6464296	Urban	0.6	385408	6457657	Grassland	0.8	405714	6443970	Grassland	0.7
393216	6464396	Urban	0.6	385534	6456719	Grassland	0.7	405543	6444339	Grassland	0.7
393066	6464396	Urban	0.7	385442	6456797	Grassland	0.8	406734	6445058	Grassland	0.7
393816	6464471	Urban	0.5	385987	6454892	Grassland	0.9	406129	6446125	Grassland	0.5
393266	6463721	Urban	0.7	386214	6453814	Grassland	0.8	406521	6447430	Grassland	0.7
393916	6463971	Urban	0.6	386221	6454453	Grassland	0.8	406458	6447289	Grassland	0.7
389941	6464446	Urban	0.7	385309	6454469	Grassland	0.8	408321	6442581	Grassland	0.8

394841	6463071	Urban	0.5	390959	6458069	Grassland	0.9	408726	6442525	Grassland	0.7
391091	6464821	Urban	0.4	390606	6458567	Grassland	0.7	406836	6442773	Grassland	0.7
393291	6464396	Urban	0.4	390325	6458076	Grassland	0.8	406366	6442821	Grassland	0.7
390016	6462946	Grassland	0.7	390284	6457644	Grassland	0.7	405506	6442360	Grassland	0.7
390216	6464021	Grassland	0.9	389726	6457833	Grassland	0.6	405386	6441516	Grassland	0.6
390166	6463971	Grassland	0.8	389624	6458037	Grassland	0.8	406204	6441838	Grassland	0.7
390391	6464146	Grassland	0.6	389627	6458077	Grassland	0.8	404435	6442562	Grassland	0.7
390416	6464021	Grassland	0.7	389875	6458026	Grassland	0.9	404255	6442503	Grassland	0.7
390341	6463971	Grassland	0.6	390264	6457328	Grassland	0.8	404799	6442083	Grassland	0.8
390141	6464046	Grassland	0.8	389839	6457072	Grassland	0.7	403950	6441995	Grassland	0.7
391166	6463171	Grassland	0.6	388984	6456244	Grassland	0.6	408838	6444452	Grassland	0.7
391141	6463296	Grassland	0.6	388742	6455958	Grassland	0.9	408988	6444408	Grassland	0.7
391191	6463196	Grassland	0.5	388856	6455554	Grassland	0.6	409202	6445898	Grassland	0.7
391141	6463346	Grassland	0.6	389127	6455472	Grassland	0.8	409261	6446056	Grassland	0.6
392266	6463596	Grassland	0.5	393083	6450895	Grassland	0.9	420582	6446160	Grassland	0.6
393616	6463221	Grassland	0.7	393700	6450328	Grassland	0.6	407894	6447651	Grassland	0.7
393916	6463071	Grassland	0.5	393560	6450168	Grassland	0.7	408054	6447750	Grassland	0.7
394616	6462996	Grassland	0.7	393237	6450267	Grassland	0.8	408203	6446101	Grassland	0.8
394191	6462971	Grassland	0.5	393259	6450144	Grassland	0.8	408109	6446156	Grassland	0.7
393916	6462946	Grassland	0.4	394084	6450294	Grassland	0.8	407721	6446572	Grassland	0.7
393382	6463998	Grassland	0.8	394285	6450042	Grassland	0.6	399299	6442623	Grassland	0.6
393473	6464070	Grassland	0.8	392905	6450732	Grassland	0.8	399195	6442525	Grassland	0.7
393492	6464118	Grassland	0.8	393159	6449744	Grassland	0.8	399034	6442525	Grassland	0.8
393364	6464141	Grassland	0.9	393407	6449937	Grassland	0.7	399762	6442358	Grassland	0.7
393791	6464321	Grassland	0.7	393190	6452652	Grassland	0.8	398965	6442195	Grassland	0.6
394166	6463646	Grassland	0.4	393400	6453267	Grassland	0.8	400732	6442577	Grassland	0.7
393516	6463996	Grassland	0.6	392966	6453472	Grassland	0.8	401640	6441775	Grassland	0.6
394216	6464296	Grassland	0.8	392634	6452444	Grassland	0.6	401627	6441737	Grassland	0.7
389191	6462546	Grassland	0.5	392428	6452403	Grassland	0.8	401518	6441558	Grassland	0.6
388766	6462221	Grassland	0.6	392969	6451957	Grassland	0.5	401760	6441484	Grassland	0.7
388666	6462196	Grassland	0.4	393228	6451992	Grassland	0.7	400831	6443136	Grassland	0.7
				393389	6452119	Grassland	0.6	404784	6443402	Grassland	0.8
				392317	6453435	Grassland	0.6	405548	6444275	Grassland	0.7
				391946	6453415	Grassland	0.8	406355	6442816	Grassland	0.7
				391806	6452948	Grassland	0.9	408982	6444413	Grassland	0.7
				392150	6452455	Grassland	0.9	406834	6442775	Grassland	0.7
				389869	6453972	Grassland	0.5	405612	6443030	Grassland	0.7
				389663	6454054	Grassland	0.7				
				389646	6454446	Grassland	0.7				
				389377	6454424	Grassland	0.8				
				390407	6455193	Grassland	0.6				
				390492	6455004	Grassland	0.8				
				390539	6454713	Grassland	0.8				
				390483	6454340	Grassland	0.8				
				390043	6453916	Grassland	0.6				
				388978	6454159	Grassland	0.6				
				390133	6456341	Grassland	0.8				
				390373	64562110	Grassland	0.8				

Appendix 11 Fuzzy land cover maps (defuzzified memberships) generated by different fuzzy operators of the City of Perth

(a)

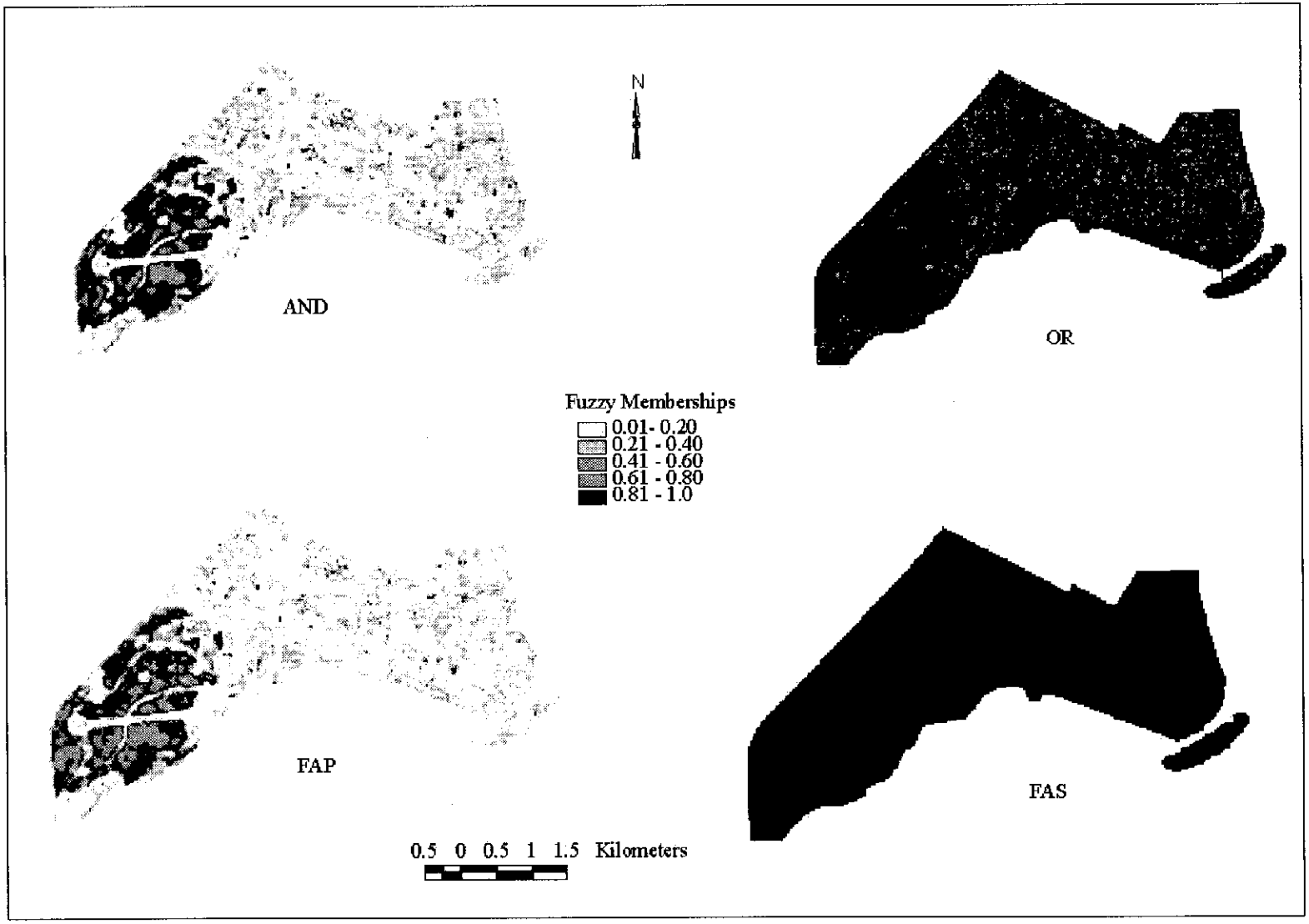

(b)


N
10
50
60
70
Fuzzy Memberships
0.01 - 0.20
0.21 - 0.40
0.41 - 0.60
0.61 - 0.80
0.81 - 1.0
0.5 0 0.5 1 1.5 Kilometers

(c)

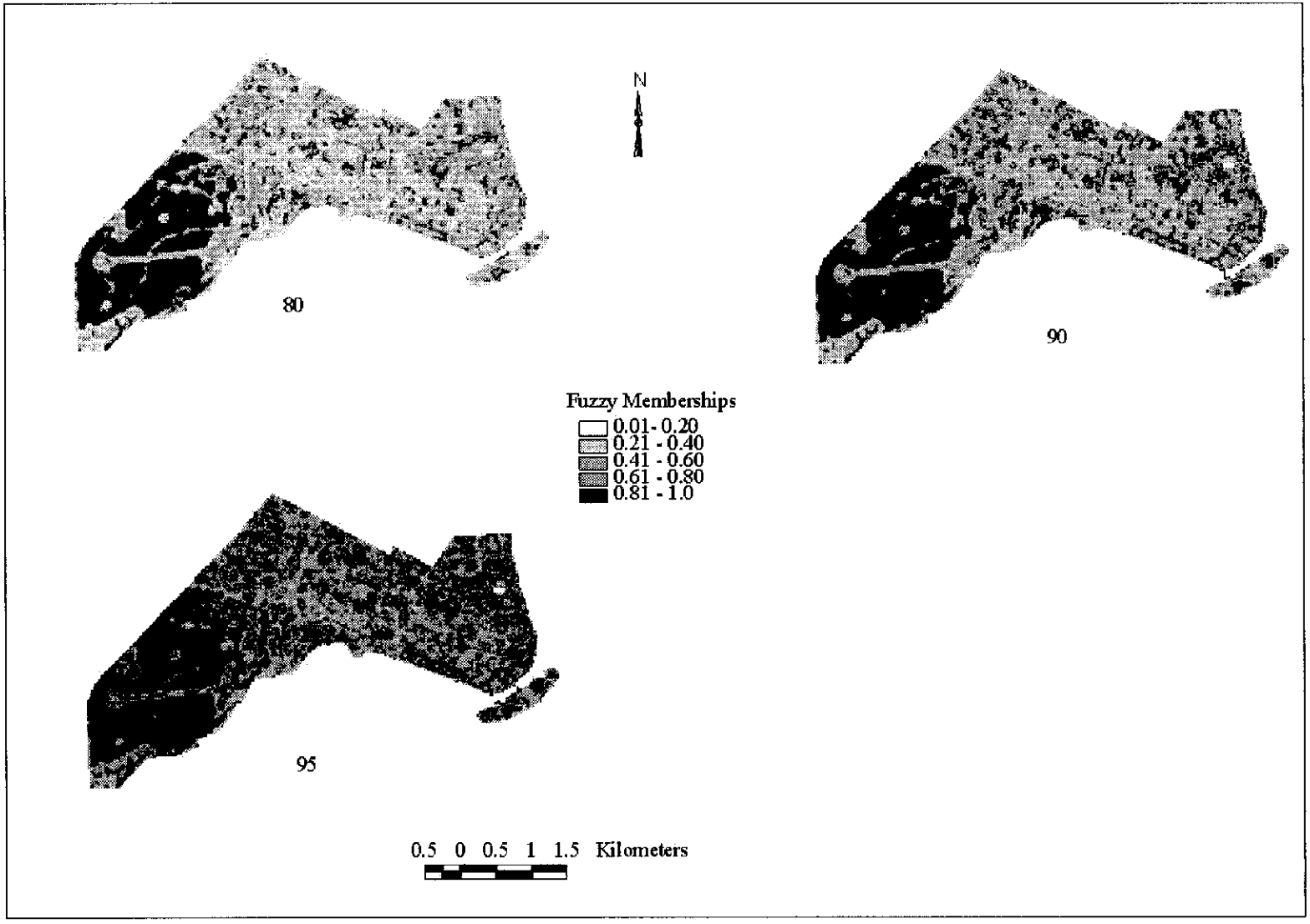
N
80
90
95
Fuzzy Memberships
0.01 - 0.20
0.21 - 0.40
0.41 - 0.60
0.61 - 0.80
0.81 - 1.0
0.5 0 0.5 1 1.5 Kilometers

Appendix 12 Fuzzy land cover maps (defuzzified memberships) generated by different fuzzy operators of the City of Melville

(a)

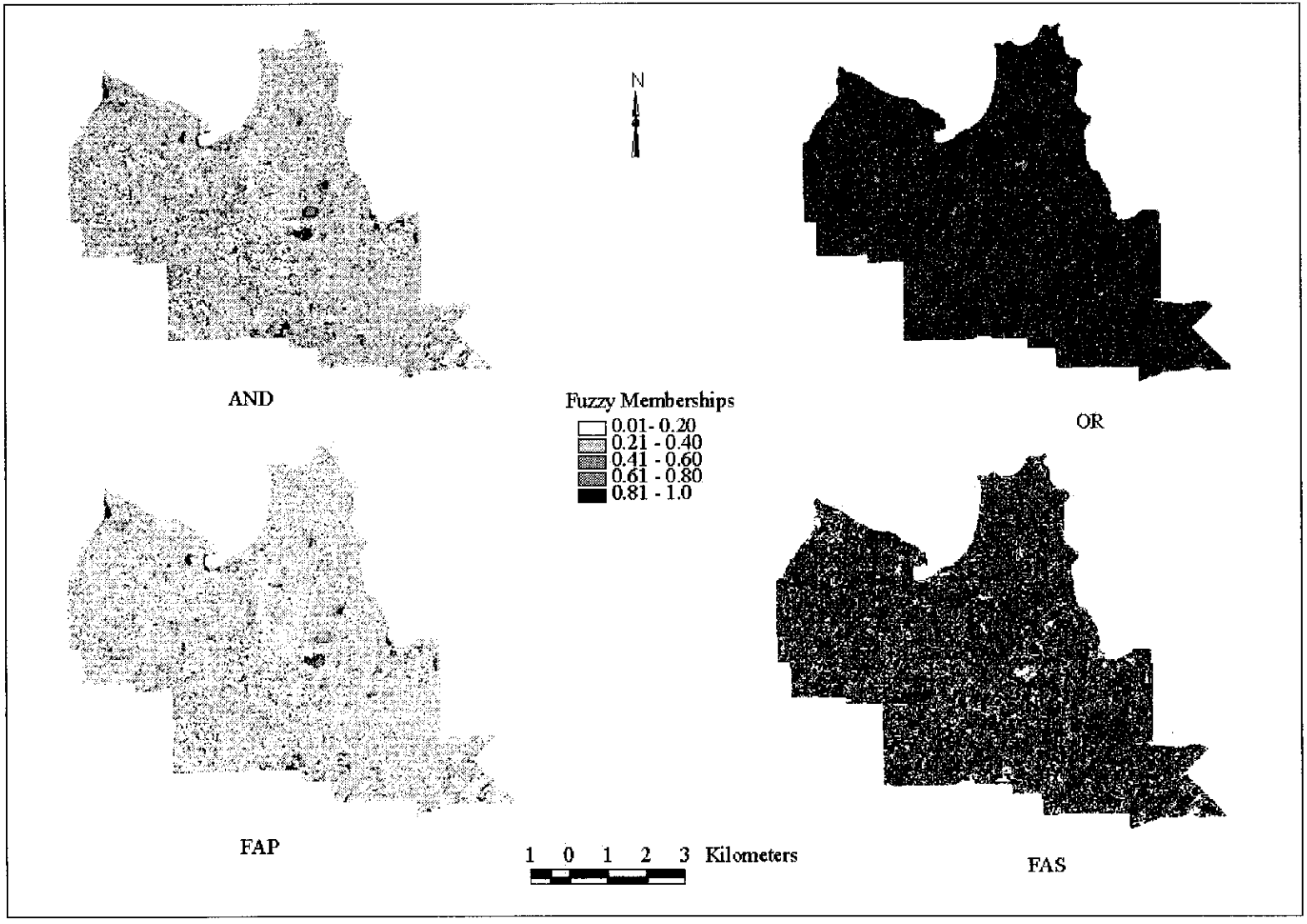

(b)

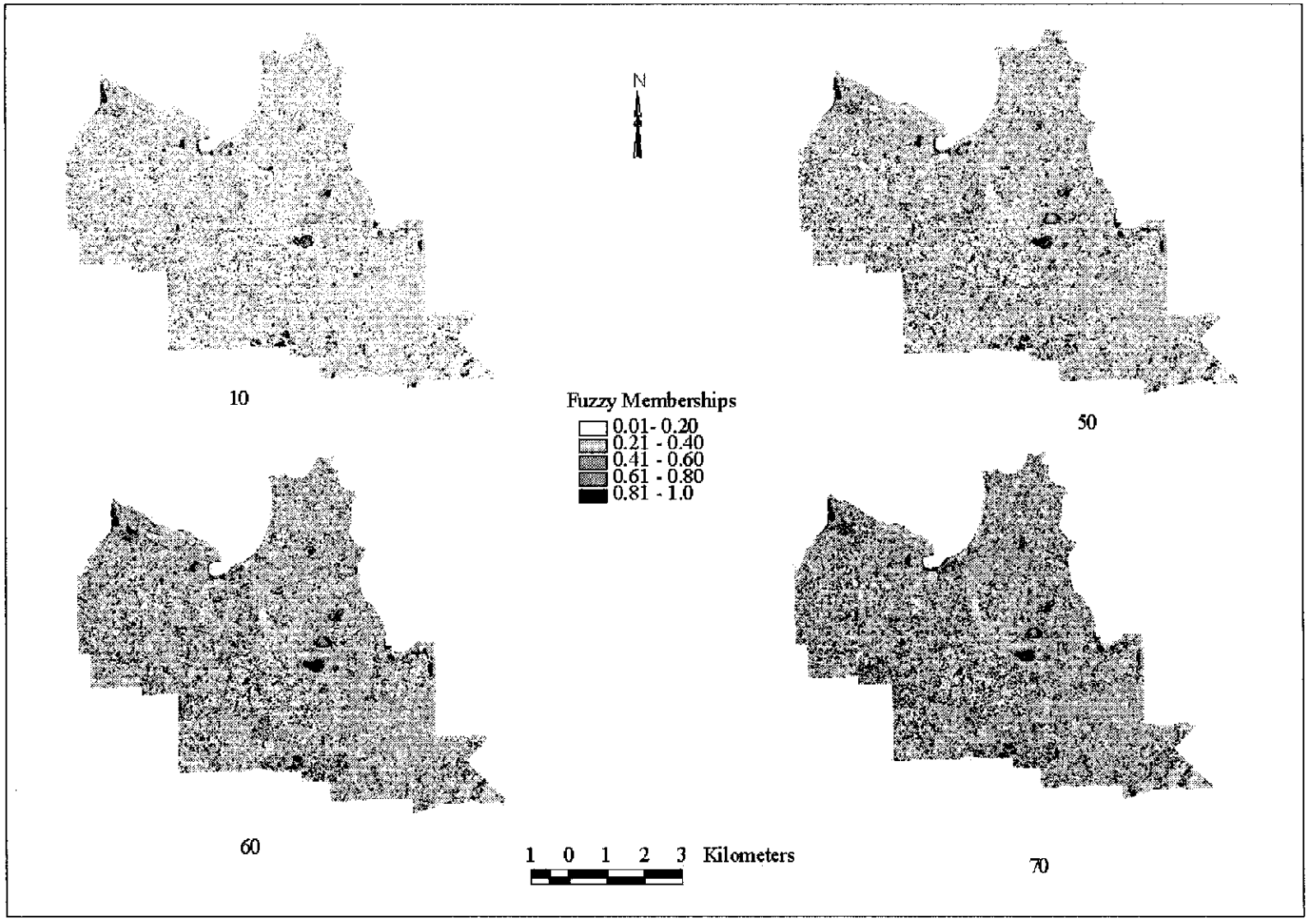
N
10
50
60
70
Fuzzy Memberships
0.01- 0.20
0.21 - 0.40
0.41 - 0.60
0.61 - 0.80
0.81 - 1.0
1 0 1 2 3 Kilometers

(c)

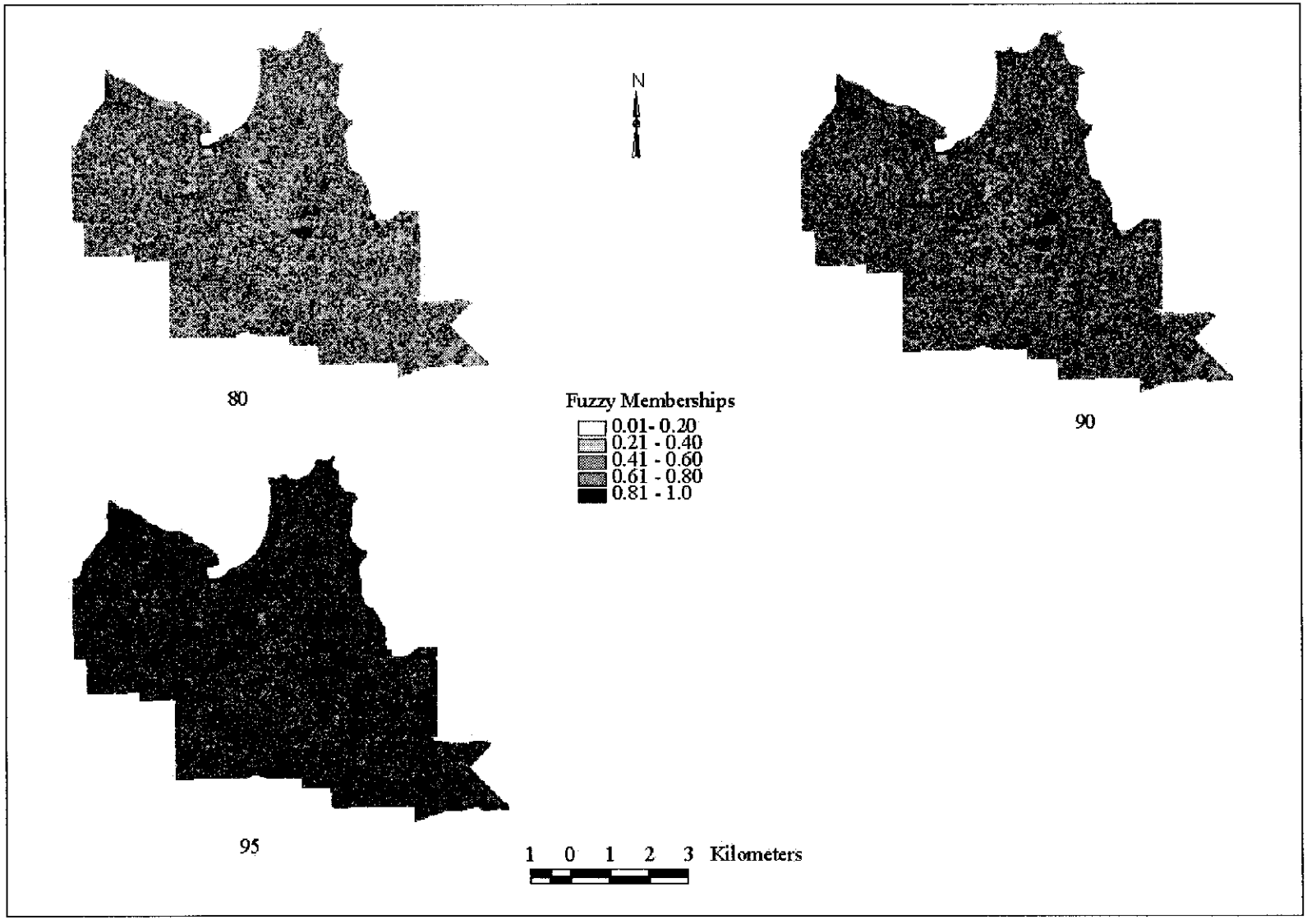
N
80
90
95
Fuzzy Memberships
0.01- 0.20
0.21 - 0.40
0.41 - 0.60
0.61 - 0.80
0.81 - 1.0
1 0 1 2 3 Kilometers

Appendix 13 Fuzzy land cover maps (defuzzified memberships) generated by different fuzzy operators of the City of Armadale

(a)

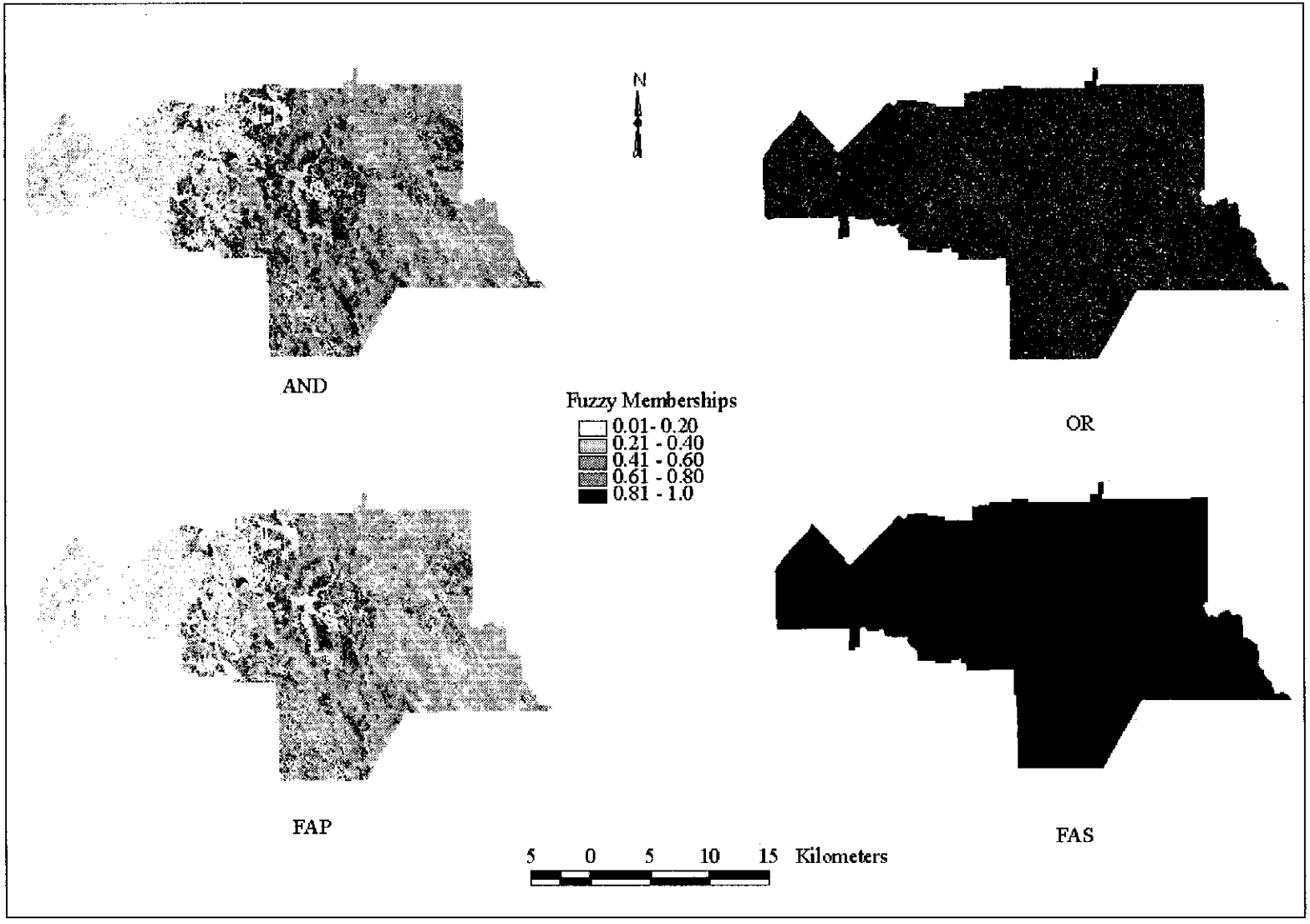

(b)

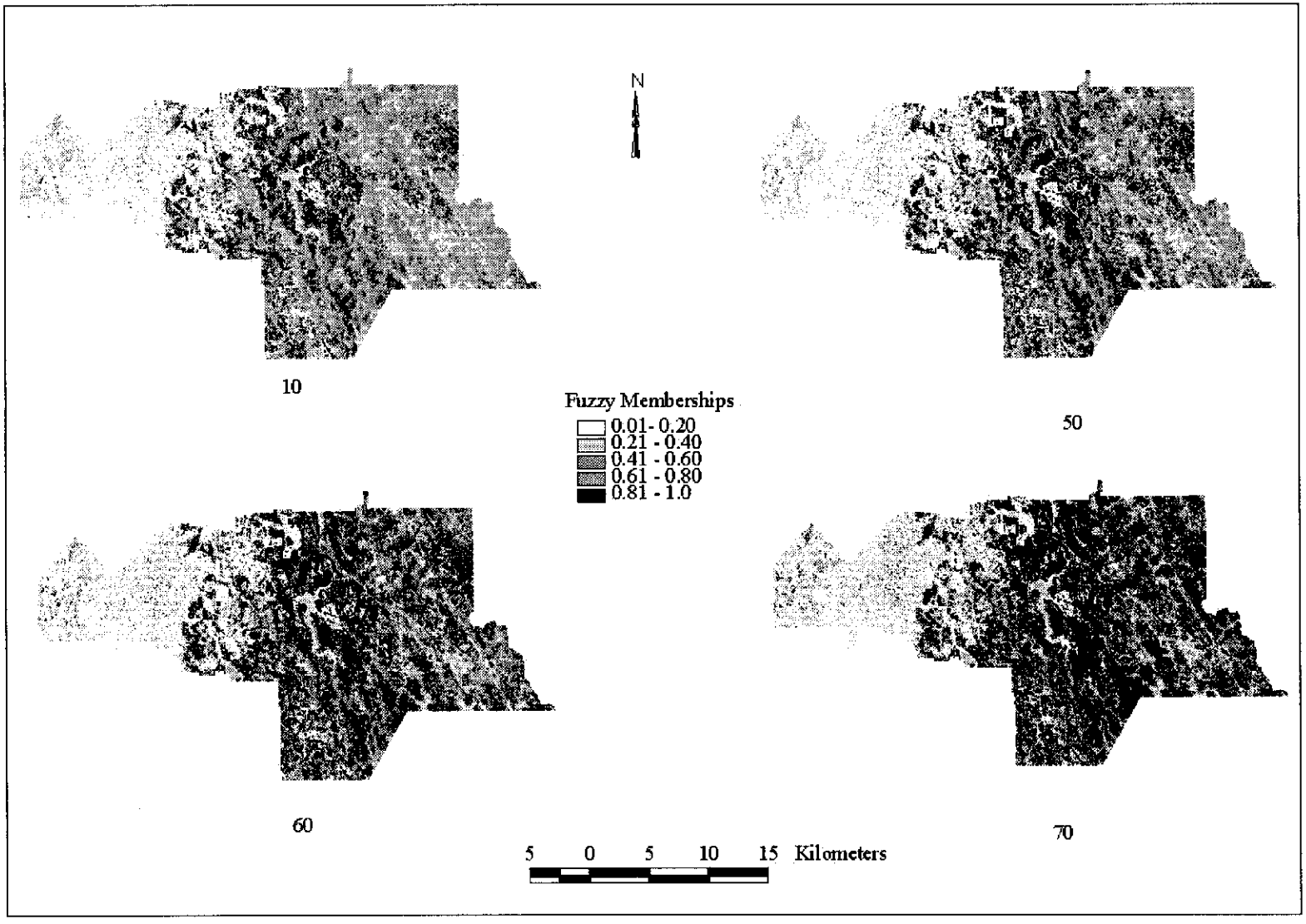
N
10
50
Fuzzy Memberships
0.01 - 0.20
0.21 - 0.40
0.41 - 0.60
0.61 - 0.80
0.81 - 1.0
60
70
5 0 5 10 15 Kilometers

(c)

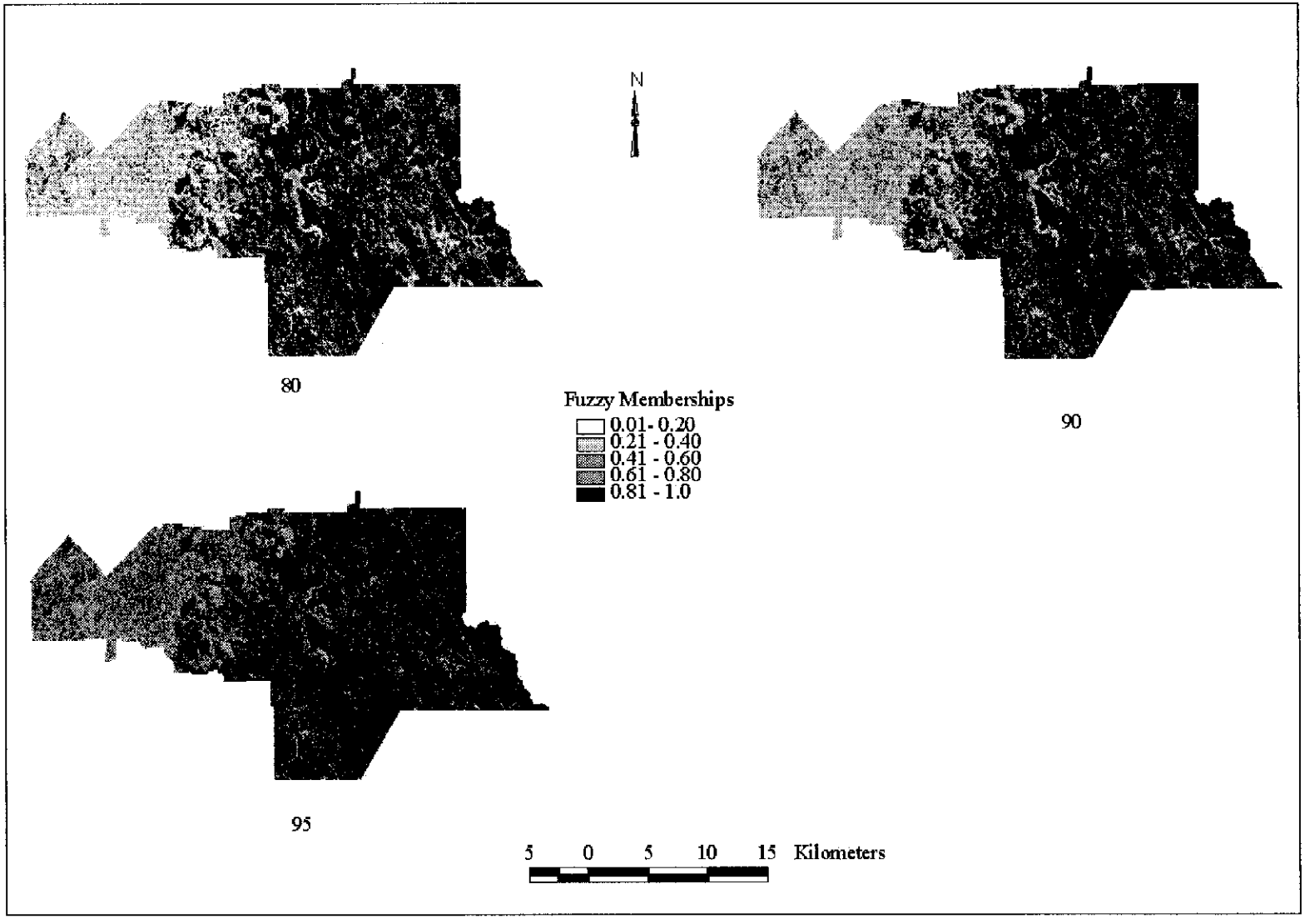
N
80
90
95
Fuzzy Memberships
0.01- 0.20
0.21 - 0.40
0.41 - 0.60
0.61 - 0.80
0.81 - 1.0
5 0 5 10 15 Kilometers

Appendix 14 The accuracy measures of fuzzy land cover maps generated by different fuzzy operators of the City of Perth

(a) Fuzzy AND

		Reference Data					
		Forest	Grassland	Urban	Dense Urban	Total Grades	User's Accuracy (%)
Classified Data	Forest	**26.84**	1.06	0.52	0.05	31.15	86
	Grassland	0.08	**7.24**	0.17	0	7.96	91
	Urban	0.33	0.22	**4.27**	0.46	5.24	81
	Dense urban	0	0	0.43	**6.88**	10.18	68
	Total Grades	45.9	18	26.2	22	**112.1**	
	Producer's Accuracy (%)	58	40	16	31		
	Overall Accuracy (%)	40					

(b) Fuzzy OR

		Reference Data					
		Forest	Grassland	Urban	Dense Urban	Total Grades	User's Accuracy (%)
Classified Data	Forest	**39.96**	2.9	6.7	1.26	71.43	56
	Grassland	3.6	**14.6**	2.25	0.4	30.59	48
	Urban	0.8	0.5	**11.4**	1.9	22.37	51
	Dense urban	1.5	0	5.85	**17.32**	33.89	51
	Total Grades	45.9	18	26.2	22	**112.10**	
	Producer's Accuracy (%)	87	81	44	79		
	Overall Accuracy (%)	74					

(c) Fuzzy Algebraic Product

		Reference Data					
		Forest	Grassland	Urban	Dense Urban	Total Grades	User's Accuracy (%)
Classified data	Forest	**24.81**	0.98	0.29	0	27.91	89
	Grassland	0.02	**4.6**	0.01	0	5.02	92
	Urban	0.01	0	**2.5**	0	3.08	81
	Dense urban	0	0	1.26	**4.35**	5.99	73
	Total Grades	45.9	18	26.2	22	**112.10**	
	Producer's Accuracy (%)	54	26	10	20		
	Overall Accuracy (%)	32					

(d) Fuzzy Algebraic Sum

Reference Data

Classified data	Forest	Grassland	Urban	Dense Urban	Total Grades	User's Accuracy (%)
Forest	**41.5**	2.3	0.9	0.5	71.43	58
Grassland	3.6	**14.1**	2.95	0.4	30.58	46
Urban	0.8	1.6	**16.4**	2.7	22.37	73
Dense urban	0	0	4.35	**18.4**	35.69	52
Total Grades	45.9	18	26.2	22	**112.1**	
Producer's Accuracy (%)	90	78	63	84		
Overall Accuracy (%)	81					

(e) Fuzzy γ Value of 0.1

Reference Data

Classified Data	Forest	Grassland	Urban	Dense Urban	Total Grades	User's Accuracy (%)
Forest	**25.61**	1.01	0.33	0	28.99	88
Grassland	0.33	**4.99**	0.15	0	5.48	91
Urban	0.14	0.04	**2.84**	0.06	3.50	81
Dense urban	0	0	1.38	**4.87**	6.75	72
Total Grades	45.9	18	26.2	22	**112.1**	
Producer's Accuracy (%)	56	28	11	22		
Overall Accuracy (%)	34					

(f) Fuzzy γ Value of 0.5

Reference Data

Classified Data	Forest	Grassland	Urban	Dense Urban	Total Grades	User's Accuracy (%)
Forest	**30.08**	0.12	0.43	0	35.29	85
Grassland	0.22	**7.6**	0.38	0	8.64	88
Urban	0.34	0.2	**5.89**	0.37	6.86	86
Dense urban	0	0	2.14	**8.69**	11.95	73
Total Grades	45.9	18	26.2	22	**112.1**	
Producer's Accuracy (%)	66	42	22	40		
Overall Accuracy (%)	47					

(g) Fuzzy γ Value of 0.6

Reference Data

Classified Data	Forest	Grassland	Urban	Dense Urban	Total Grades	User's Accuracy (%)
Forest	**31.87**	1.3	0.46	0	37.76	84
Grassland	0.38	**8.74**	0.51	0	10.09	87
Urban	0.42	0.3	**7.61**	0.59	9.37	81
Dense urban	0	0	2.44	**10.33**	12.78	81
Total Grades	45.9	18	26.2	22	**112.10**	
Producer's Accuracy (%)	69	49	29	47		
Overall Accuracy (%)	52					

(h) Fuzzy γ Value of 0.7

Reference Data

Classified Data	Forest	Grassland	Urban	Dense Urban	Total Grades	User's Accuracy (%)
Forest	**34.15**	1.44	0.54	0	40.92	83
Grassland	0.68	**10.15**	0.71	0	12.15	84
Urban	0.52	0.46	**10.19**	0.97	12.65	81
Dense urban	0	0	2.78	**12.53**	17.17	73
Total Grades	45.9	18	26.2	22	**112.10**	
Producer's Accuracy (%)	74	56	39	57		
Overall Accuracy (%)	60					

(i) Fuzzy γ Value of 0.8

Reference Data

Classified Data	Forest	Grassland	Urban	Dense Urban	Total Grades	User's Accuracy (%)
Forest	**37.06**	1.66	0.74	0	45.17	82
Grassland	1.26	**12.05**	1.05	0	15.29	79
Urban	0.64	0.73	**13.81**	1.55	17.65	78
Dense urban	0	0	3.16	**15.33**	21.17	72
Total Grades	45.9	18	26.2	22	**112.10**	
Producer's Accuracy (%)	81	67	53	70		
Overall Accuracy (%)	70					

(j) Fuzzy γ Value of 0.9

Reference Data

Classified Data	Forest	Grassland	Urban	Dense Urban	Total Grades	User's Accuracy (%)
Forest	**40.26**	2.07	1.15	0	51.25	79
Grassland	2.37	**14.23**	1.58	0	20.44	70
Urban	0.8	0.9	**18.21**	2.42	25.85	70
Dense urban	0	0	4.05	**18.406**	27.31	67
Total Grades	45.9	18	26.2	22	**112.10**	
Producer's Accuracy (%)	88	79	70	84		
Overall Accuracy (%)	81					

(k) Fuzzy γ Value of 0.95

Reference Data

Classified Data	Forest	Grassland	Urban	Dense Urban	Total Grades	User's Accuracy (%)
Forest	**41.58**	2.3	2.1	0	56.65	73
Grassland	2.95	**14.8**	1.8	0	24.33	61
Urban	0.8	0.9	**19.04**	2.92	31.41	61
Dense urban	0	0	3.65	**18.9**	30.41	62
Total Grades	45.9	18	26.2	22	**112.10**	
Producer's Accuracy (%)	91	82	73	86		
Overall Accuracy (%)	84					

Appendix 15 The accuracy measures of fuzzy land cover maps generated by different fuzzy operators of the City of Melville

(a) Fuzzy AND

Classified Data \ Reference Data	Forest	Grassland	Urban	Dense Urban	Total Grades	User's Accuracy (%)
Forest	**10.26**	0.56	0.35	0.35	12.1	85
Grassland	1.62	**17.77**	3.58	0	23.48	76
Urban	1.78	6.44	**16.66**	1.23	27.92	60
Dense Urban	0.7	0.02	0	**4.52**	6.06	75
Total Grades	25.9	49.3	49.7	11.6	**136.5**	
Producer's Accuracy (%)	40	36	34	39		
Overall Accuracy (%)	36					

(b) Fuzzy OR

Classified Data \ Reference Data	Forest	Grassland	Urban	Dense Urban	Total Grades	User's Accuracy (%)
Forest	15.80	0.6	0.8	0.8	22.70	70
Grassland	4.95	36.27	13.3	0.7	69.96	52
Urban	3	11.2	34.77	3.2	65.75	53
Dense Urban	2	1.2	0	6.1	12.45	49
Total Grades	25.9	49.3	49.7	11.6	136.50	
Producer's Accuracy (%)	61	74	70	53		
Overall Accuracy (%)	68					

(c) Fuzzy Algebraic Product

Classified Data \ Reference Data	Forest	Grassland	Urban	Dense Urban	Total Grades	User's Accuracy (%)
Forest	7.98	0.06	0.26	0.26	8.83	90
Grassland	0.86	10.53	1.39	0	12.78	82
Urban	1.52	5.14	11.48	0.7	19.73	58
Dense Urban	0.7	0	0	3.6	4.88	74
Total Grades	25.9	49.3	49.7	11.6	136.50	
Producer's Accuracy (%)	31	21	23	31		
Overall Accuracy (%)	25					

(d) Fuzzy Algebraic Sum

Classified Data \ Reference Data	Forest	Grassland	Urban	Dense Urban	Total Grades	User's Accuracy (%)
Forest	14.7	0.6	1.6	0.8	26.84	55
Grassland	3.1	35.5	13.4	0	68.44	52
Urban	3.7	12	33.9	2.4	71.77	47
Dense Urban	2	1.2		7.6	14.94	51
Total Grades	25.9	49.3	49.7	11.6	136.50	
Producer's Accuracy (%)	57	72	68	66		
Overall Accuracy (%)	67					

(e) Fuzzy γ Value of 0.1

Classified Data \ Reference Data	Forest	Grassland	Urban	Dense Urban	Total Grades	User's Accuracy (%)
Forest	8.37	0.07	0.3	0.3	9.39	89
Grassland	0.98	11.89	1.69	0	14.57	82
Urban	1.58	5.47	12.41	0.77	21.18	59
Dense Urban	0.7	0.03	0	3.74	5.08	74
Total Grades	25.9	49.3	49.7	11.6	136.5	
Producer's Accuracy (%)	32	24	25	32		
Overall Accuracy (%)	27					

(f) Fuzzy γ Value of 0.5

Classified Data \ Reference Data	Forest	Grassland	Urban	Dense Urban	Total Grades	User's Accuracy (%)
Forest	10.91	0.23	0.61	0.51	12.96	84
Grassland	1.74	20.11	4.06	0	25.95	77
Urban	2.06	7.33	18.32	1.21	31.24	59
Dense Urban	0.7	0.13		4.68	6.38	73
Total Grades	25.9	49.3	49.7	11.6	136.5	
Producer's Accuracy (%)	42	41	37	40		
Overall Accuracy (%)	40					

(g) Fuzzy γ Value of 0.6

Reference Data

Classified Data	Forest	Grassland	Urban	Dense Urban	Total Grades	User's Accuracy (%)
Forest	12.00	0.31	0.75	0.59	14.46	83
Grassland	2.03	23.06	5.23	0	30.56	75
Urban	2.31	8.12	20.84	1.37	35.55	59
Dense Urban	0.7	0.2	0	5.09	6.92	74
Total Grades	25.9	49.3	49.7	11.6	136.50	
Producer's Accuracy (%)	46	47	42	44		
Overall Accuracy (%)	45					
KHAT (%)	41					

(h) Fuzzy γ Value of 0.7

Reference Data

Classified Data	Forest	Grassland	Urban	Dense Urban	Total Grades	User's Accuracy (%)
Forest	13.44	0.41	0.93	0.67	16.37	82
Grassland	2.38	26.32	6.8	0	36.39	72
Urban	2.68	9.18	24.10	1.58	41.25	58
Dense Urban	0.71	0.3	0	5.62	7.65	73
Total Grades	25.9	49.3	49.7	11.6	136.50	
Producer's Accuracy (%)	52	53	48	48		
Overall Accuracy (%)	51					

(i) Fuzzy γ Value of 0.8

Reference Data

Classified Data	Forest	Grassland	Urban	Dense Urban	Total Grades	User's Accuracy (%)
Forest	15.05	0.55	1.18	0.76	18.89	80
Grassland	2.79	29.63	9.02	0	43.93	67
Urban	3.24	10.62	28.43	1.88	48.99	58
Dense Urban	0.75	0.45	0	6.34	8.66	73
Total Grades	25.9	49.3	49.7	11.6	136.50	
Producer's Accuracy (%)	58	60	57	55		
Overall Accuracy (%)	58					

(j) Fuzzy γ Value of 0.9

Reference Data

Classified Data	Forest	Grassland	Urban	Dense Urban	Total Grades	User's Accuracy (%)
Forest	16.84	0.6	1.45	0.8	22.26	76
Grassland	3.01	33.57	11.61	0	53.91	62
Urban	4.09	12.45	33.26	2.21	59.86	56
Dense Urban	0.93	0.6	0	7.18	10.21	70
Total Grades	25.9	49.3	49.7	11.6	136.50	
Producer's Accuracy (%)	65	68	67	62		
Overall Accuracy (%)	67					

(k) Fuzzy γ Value of 0.95

Reference Data

Classified Data	Forest	Grassland	Urban	Dense Urban	Total Grades	User's Accuracy (%)
Forest	17.1	0.6	1.6	0.8	24.37	70
Grassland	3.1	35.17	12.54	0	60.84	58
Urban	3.6	12.68	34.58	2.4	65.54	53
Dense Urban	1.18	0.6	0	7.56	11.36	67
Total Grades	25.9	49.3	49.7	11.6	136.50	
Producer's Accuracy (%)	66	71	70	65		
Overall Accuracy (%)	69					

Appendix 16 The accuracy measures of fuzzy land cover maps generated by different fuzzy operators of the City of Armadale

(a) Fuzzy AND

		Reference Data					
		Forest	Grassland	Urban	Dense Urban	Total Grades	User's Accuracy (%)
Classified Data	Forest	**33.12**	0.26	0.01		33.99	97
	Grassland	0.03	**1.19**	0.29		1.51	79
	Urban	0.19	1.49	**3.8**	0.23	5.79	66
	Dense Urban		0.19	0.77	**0.14**	1.1	13
	Total Grades	56.3	34.8	35.1	6.3	**132.50**	
	Producer's Accuracy (%)	59	3	11	2		
	Overall Accuracy (%)	29					

(b) Fuzzy OR

		Reference Data					
		Forest	Grassland	Urban	Dense Urban	Total Grades	User's Accuracy (%)
Classified Data	Forest	44.27	0.6	1.6	0.6	54.43	81
	Grassland	4.09	19.6	6.4	1.2	42.15	47
	Urban	3.16	9.1	17.1	0.8	38.36	45
	Dense Urban		3.4	8.6	3.7	20.64	18
	Total Grades	56.3	34.8	35.1	6.3	132.50	
	Producer's Accuracy (%)	79	56	49	59		
	Overall Accuracy (%)	64					

(c) Fuzzy algebraic product

		Reference Data					
		Forest	Grassland	Urban	Dense Urban	Total Grades	User's Accuracy (%)
Classified Data	Forest	**24.84**				25.06	99
	Grassland	0.001	**0.28**	0.15		0.43	65
	Urban		0.23	**1.85**		2.09	89
	Dense Urban		0.02	0.22	**0.1**	0.3	33
	Total Grades	56.3	34.8	35.1	6.3	**132.50**	
	Producer's Accuracy (%)	44	1	5	2		
	Overall Accuracy (%)	20					

(d) Fuzzy algebraic sum

Reference Data

Classified Data	Forest	Grassland	Urban	Dense Urban	Total Grades	User's Accuracy (%)
Forest	**45.2**	0.7			54.79	82
Grassland	4.1	**19.5**	4.3	1.4	30.94	63
Urban	1.4	9.8	**24.7**		48.80	51
Dense Urban	0.9	2.7	4.7	**4.9**	18.84	26
Total Grades	56.3	34.8	35.1	6.3	**132.50**	
Producer's Accuracy (%)	80	56	70	78		
Overall Accuracy (%)	71					

(e) Fuzzy γ value of 0.1

Reference Data

Classified Data	Forest	Grassland	Urban	Dense Urban	Total Grades	User's Accuracy (%)
Forest	**19.91**	0.001			19.98	100
Grassland	0.005	**0.35**	0.18		0.53	66
Urban		0.32	**2.10**		2.42	87
Dense Urban		0.03	0.32	**0.1**	0.37	27
Total Grades	56.3	34.7	34.8	7.1	**132.90**	
Producer's Accuracy (%)	35	1	6	1		
Overall Accuracy (%)	17					

(f) Fuzzy γ value of 0.6

Reference Data

Classified Data	Forest	Grassland	Urban	Dense Urban	Total Grades	User's Accuracy (%)
Forest	**35.85**	0.06			37.03	97
Grassland	0.19	**2.81**	0.59	0.06	3.67	77
Urban	0.1	2.35	**6.13**	0.09	8.77	70
Dense Urban		0.4	1.04	**0.63**	2.07	30
Total Grades	56.3	34.7	34.8	7.1	**132.90**	
Producer's Accuracy (%)	64	8	18	9		
Overall Accuracy (%)	34					

(g) Fuzzy γ value of 0.7

Reference Data

Classified Data	Forest	Grassland	Urban	Dense Urban	Total Grades	User's Accuracy (%)
Forest	38.54	0.11			40.25	96
Grassland	0.39	4.69	0.93	0.13	6.16	76
Urban	0.23	3.57	8.48	0.2	12.64	67
Dense Urban		0.66	1.46	0.96	3.19	30
Total Grades	56.3	34.7	34.8	7.1	132.90	
Producer's Accuracy (%)	68	14	24	14		
Overall Accuracy (%)	40					

(h) Fuzzy γ value of 0.8

Reference Data

Classified Data	Forest	Grassland	Urban	Dense Urban	Total Grades	User's Accuracy (%)
Forest	**41.60**	0.22			44.17	94
Grassland	0.81	**8.24**	1.48	0.31	10.92	75
Urban	0.53	5.52	**12.39**	0.48	19.13	65
Dense Urban		1.09	2.23	**1.48**	5.02	29
Total Grades	56.3	34.7	34.8	7.1	**132.90**	
Producer's Accuracy (%)	74	24	36	21		
Overall Accuracy (%)	48					

(i) Fuzzy γ value of 0.9

Reference Data

Classified Data	Forest	Grassland	Urban	Dense Urban	Total Grades	User's Accuracy (%)
Forest	**44.04**				48.18	91
Grassland	2.25	**15.55**	2.69	0.77	21.62	72
Urban	1.24	8.36	**19**	0.81	30.20	63
Dense Urban		1.8	3.68	**2.72**	8.54	32
Total Grades	56.3	34.8	35.1	6.3	**132.50**	
Producer's Accuracy (%)	78	45	54	43		
Overall Accuracy (%)	61					

(j) Fuzzy γ value of 0.95

Reference Data

Classified Data	Forest	Grassland	Urban	Dense Urban	Total Grades	User's Accuracy (%)
Forest	**44.81**	0	0	0	50.85	88
Grassland	3.32	**20.81**	3.79	1.16	30.48	68
Urban	1.91	9.17	**23.93**	0.57	38.20	63
Dense Urban	0	2.1	4.47	**4.22**	11.88	36
Total Grades	56.3	34.8	35.1	6.3	**132.50**	
Producer's Accuracy (%)	80	60	68	67		
Overall Accuracy (%)	71					

Appendix 17 Uncertainty maps generated by different fuzzy operators of the City of Perth

(a)

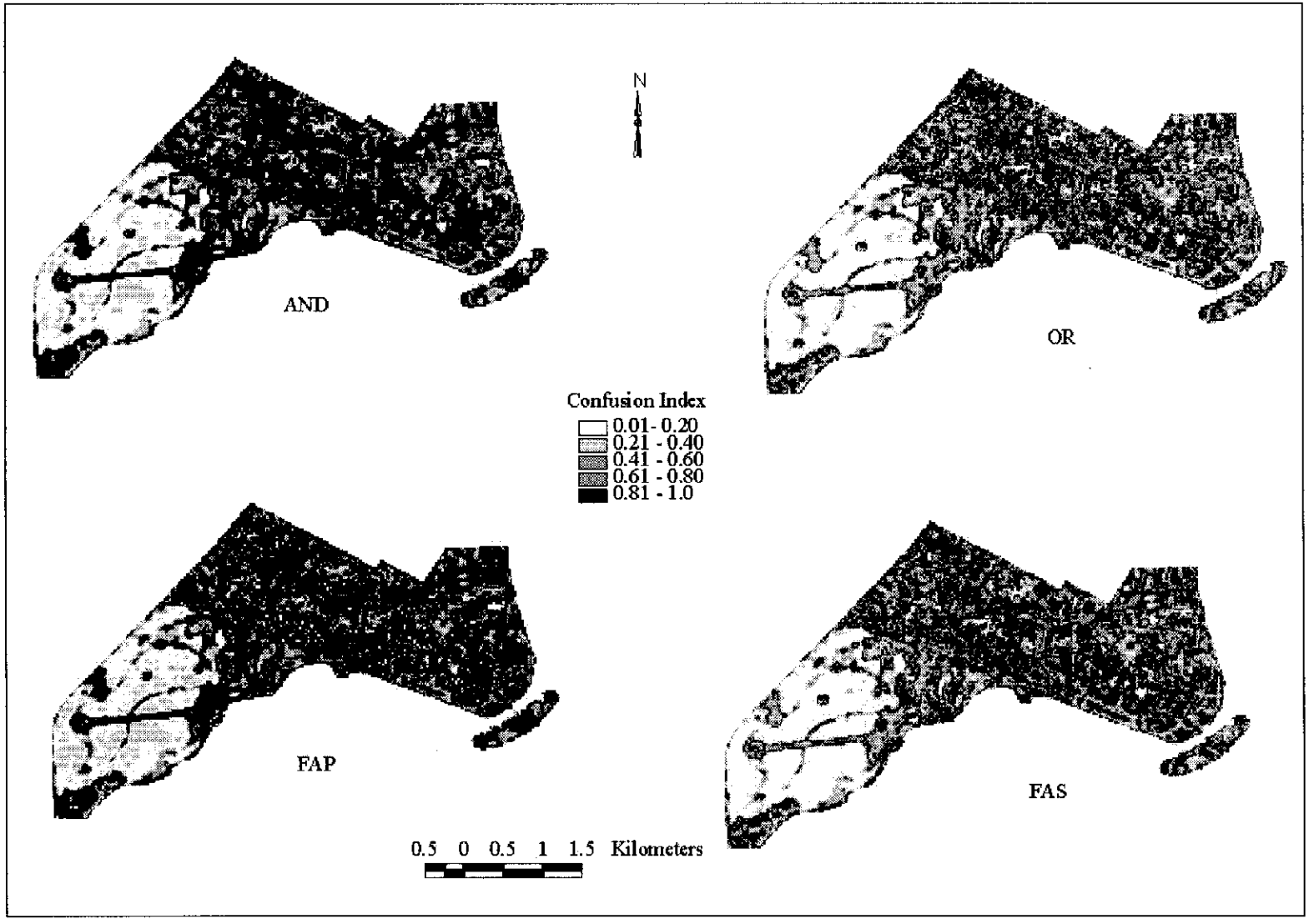

(b)

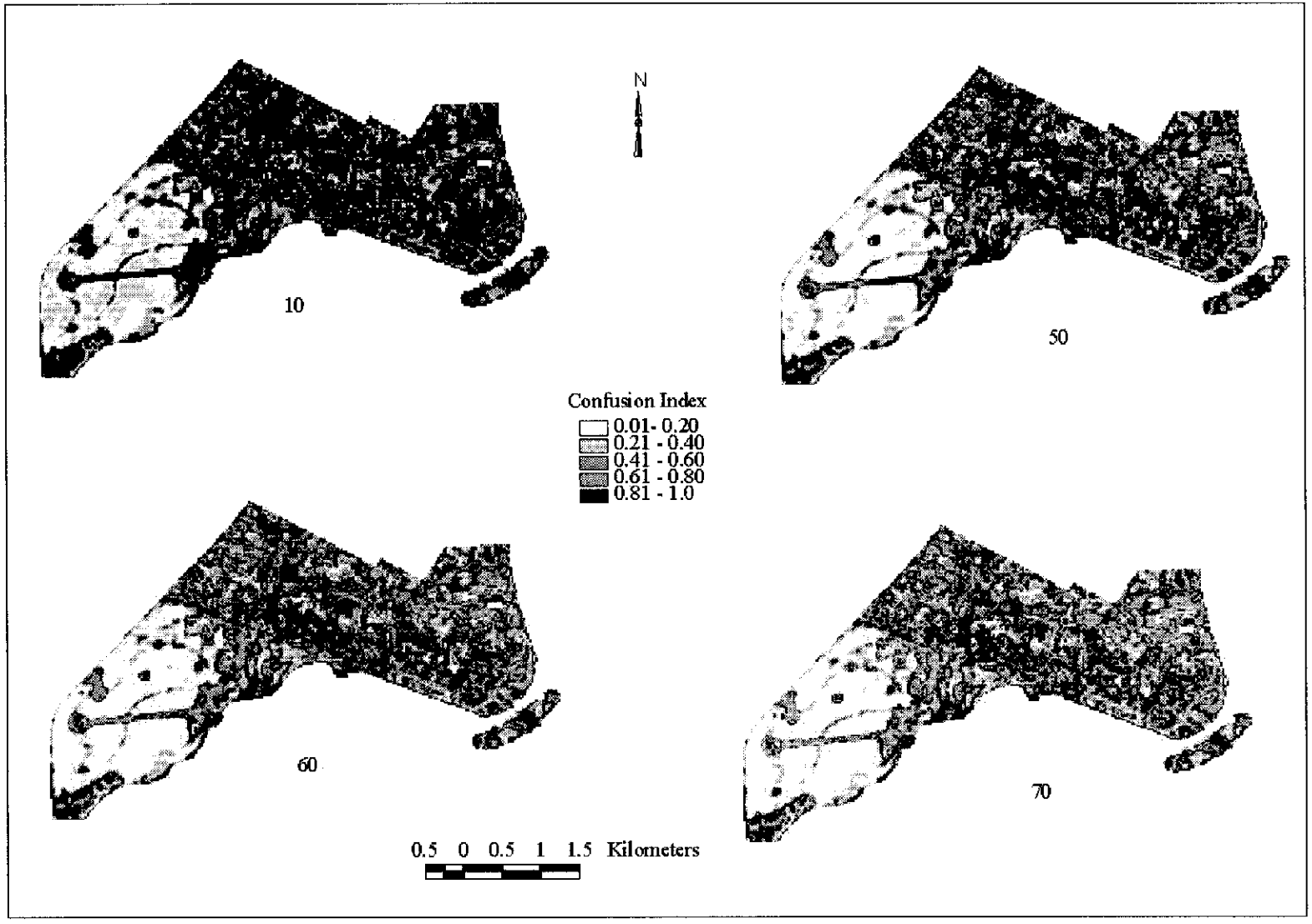
N
10
50
60
70
Confusion Index
0.01- 0.20
0.21 - 0.40
0.41 - 0.60
0.61 - 0.80
0.81 - 1.0
0.5 0 0.5 1 1.5 Kilometers

(c)

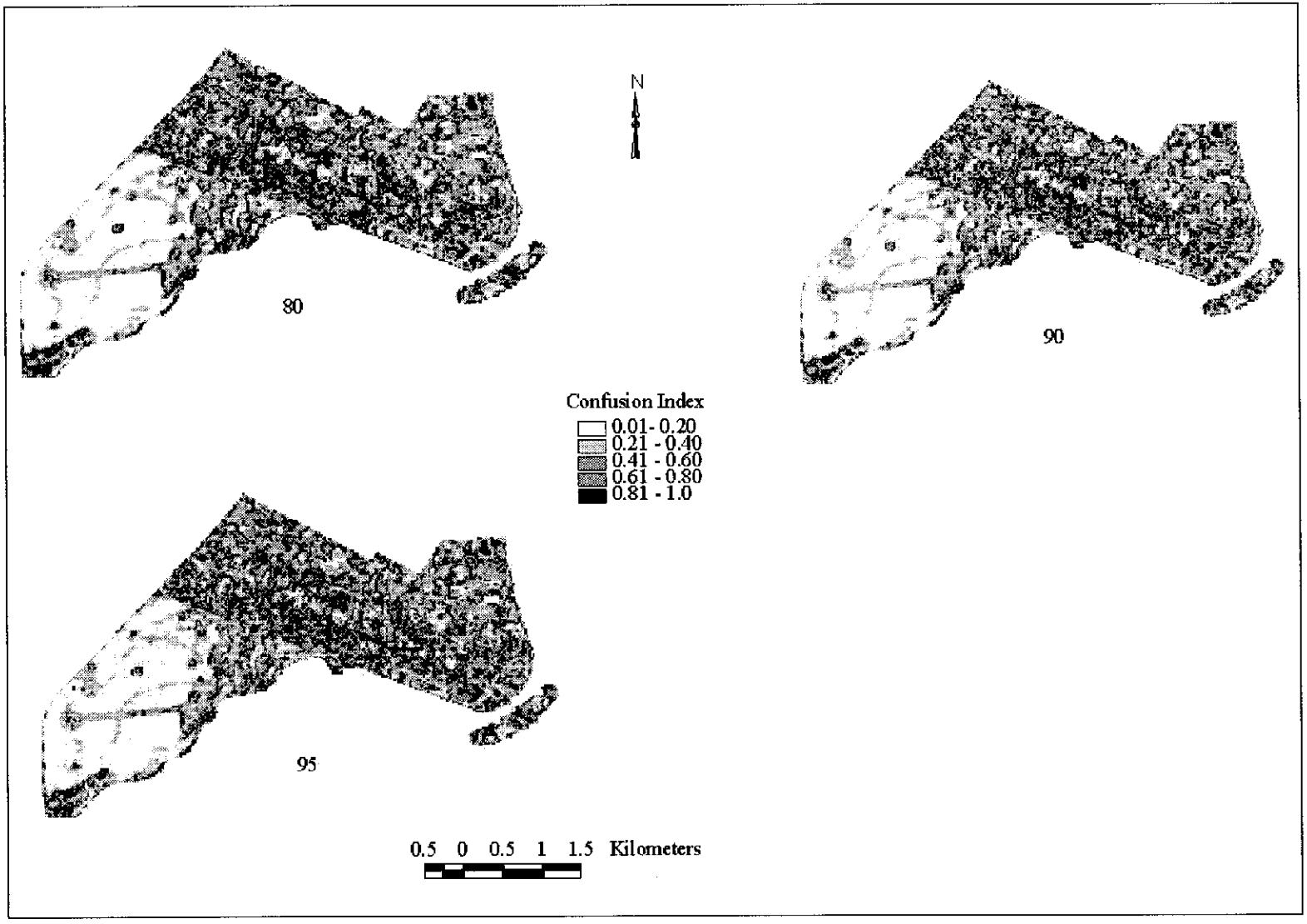
N
80
90
95
Confusion Index
0.01 - 0.20
0.21 - 0.40
0.41 - 0.60
0.61 - 0.80
0.81 - 1.0
0.5 0 0.5 1 1.5 Kilometers

Appendix 18 Uncertainty maps generated by different fuzzy operators of the City of Melville

(a)

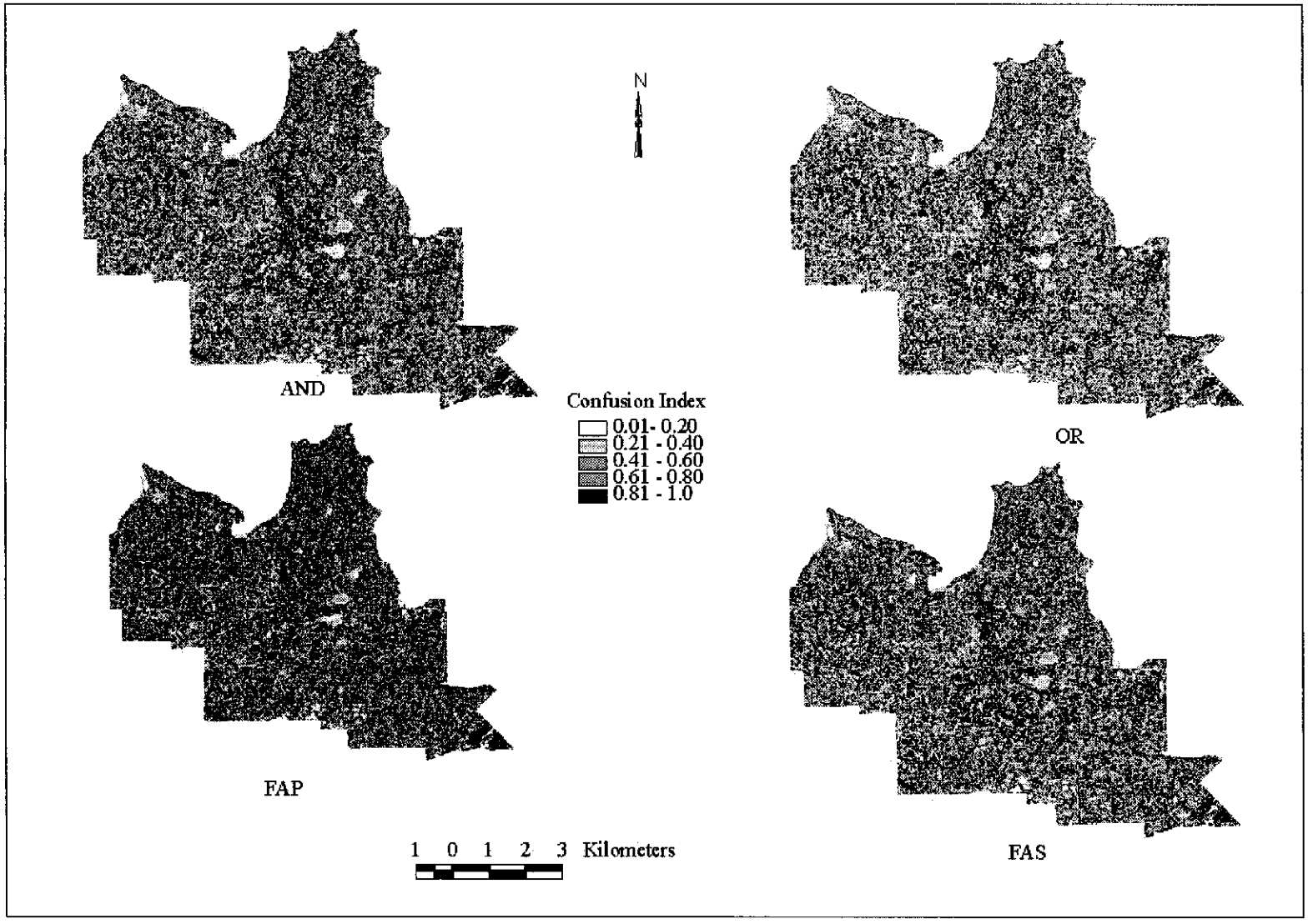

(b)

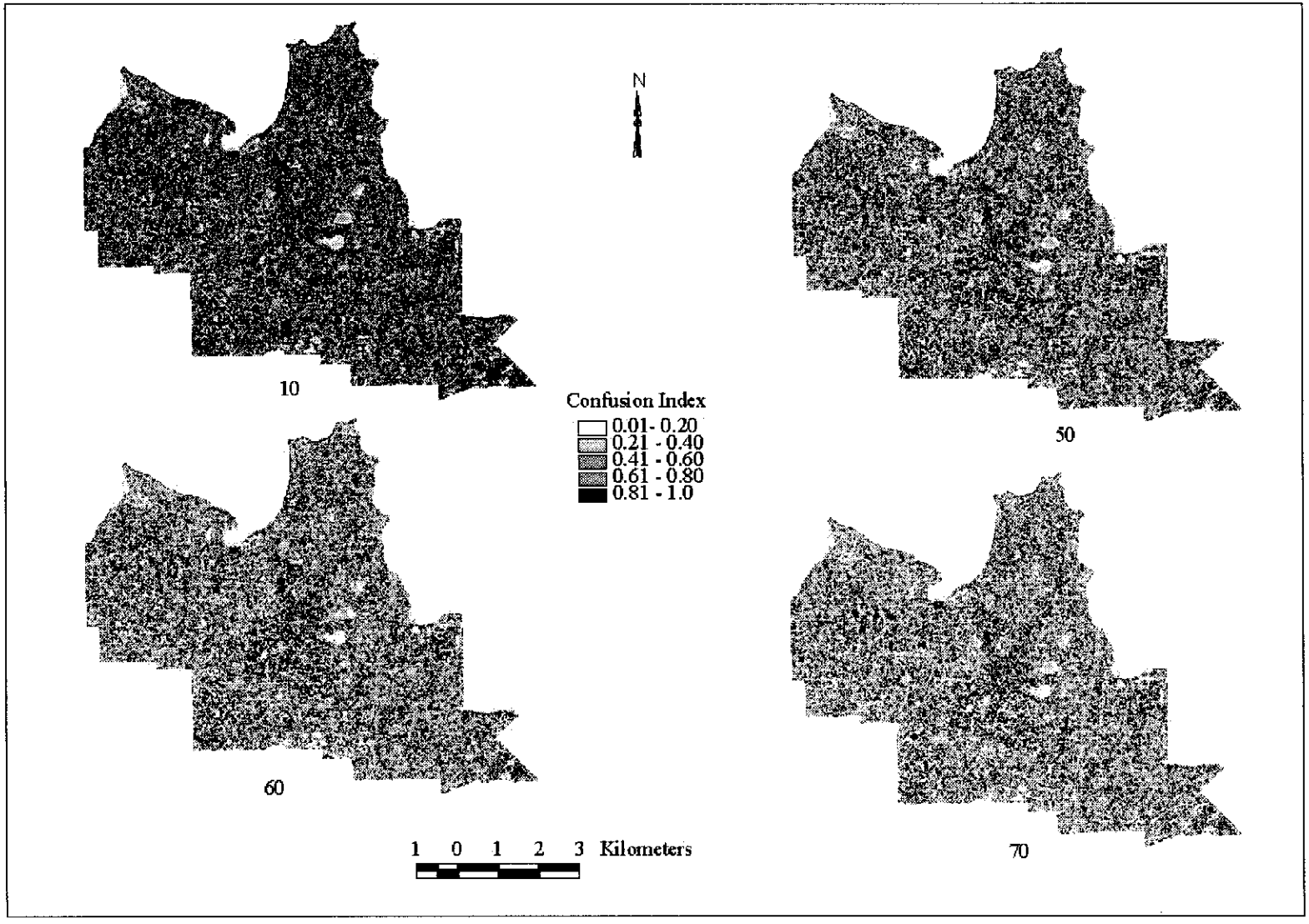
N
10
50
60
70
Confusion Index
0.01- 0.20
0.21 - 0.40
0.41 - 0.60
0.61 - 0.80
0.81 - 1.0
1 0 1 2 3 Kilometers

(c)

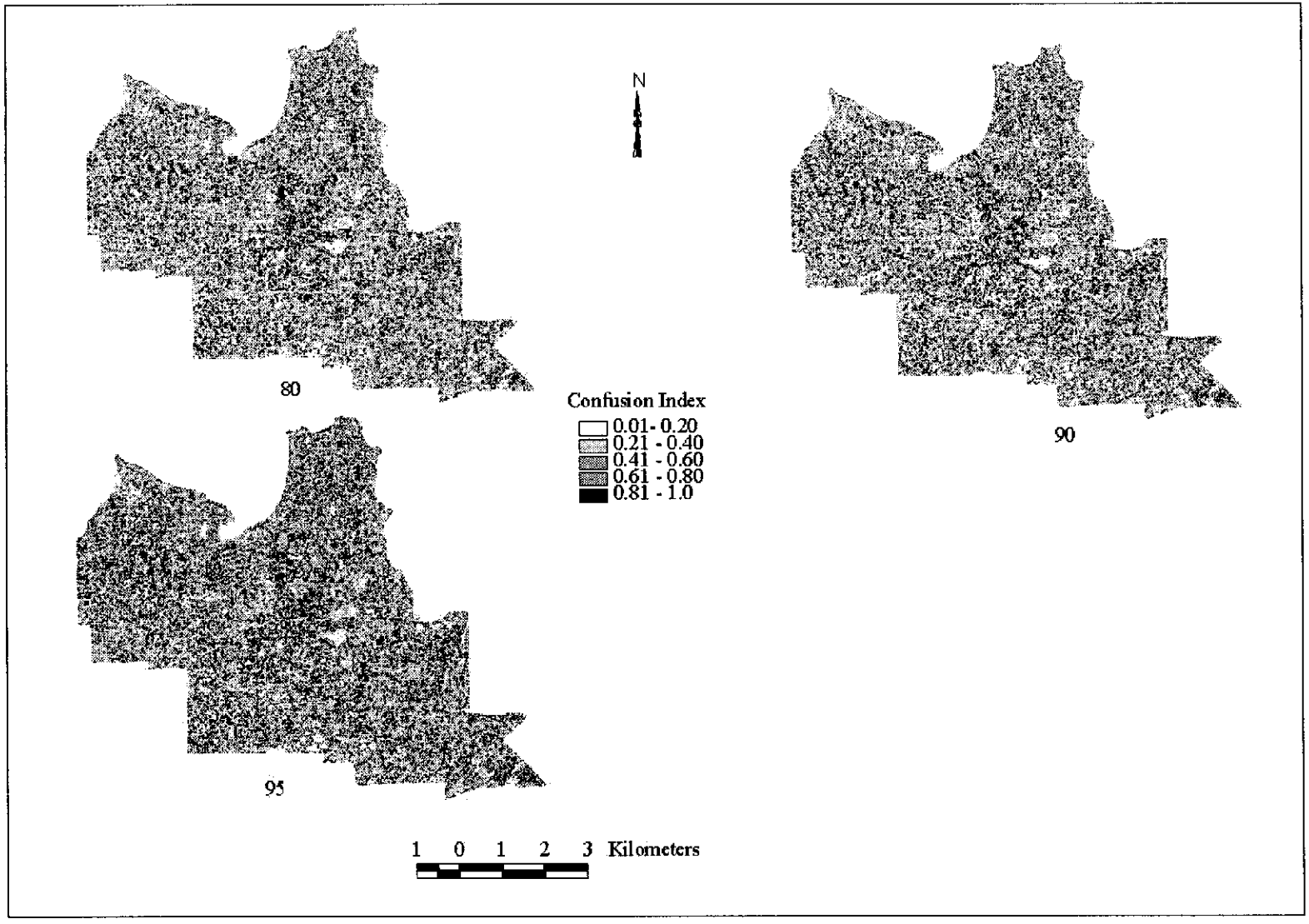
N
80
90
95
Confusion Index
0.01 - 0.20
0.21 - 0.40
0.41 - 0.60
0.61 - 0.80
0.81 - 1.0
1 0 1 2 3 Kilometers

Appendix 19 Uncertainty maps generated by different fuzzy operators of the City of Armadale

(a)

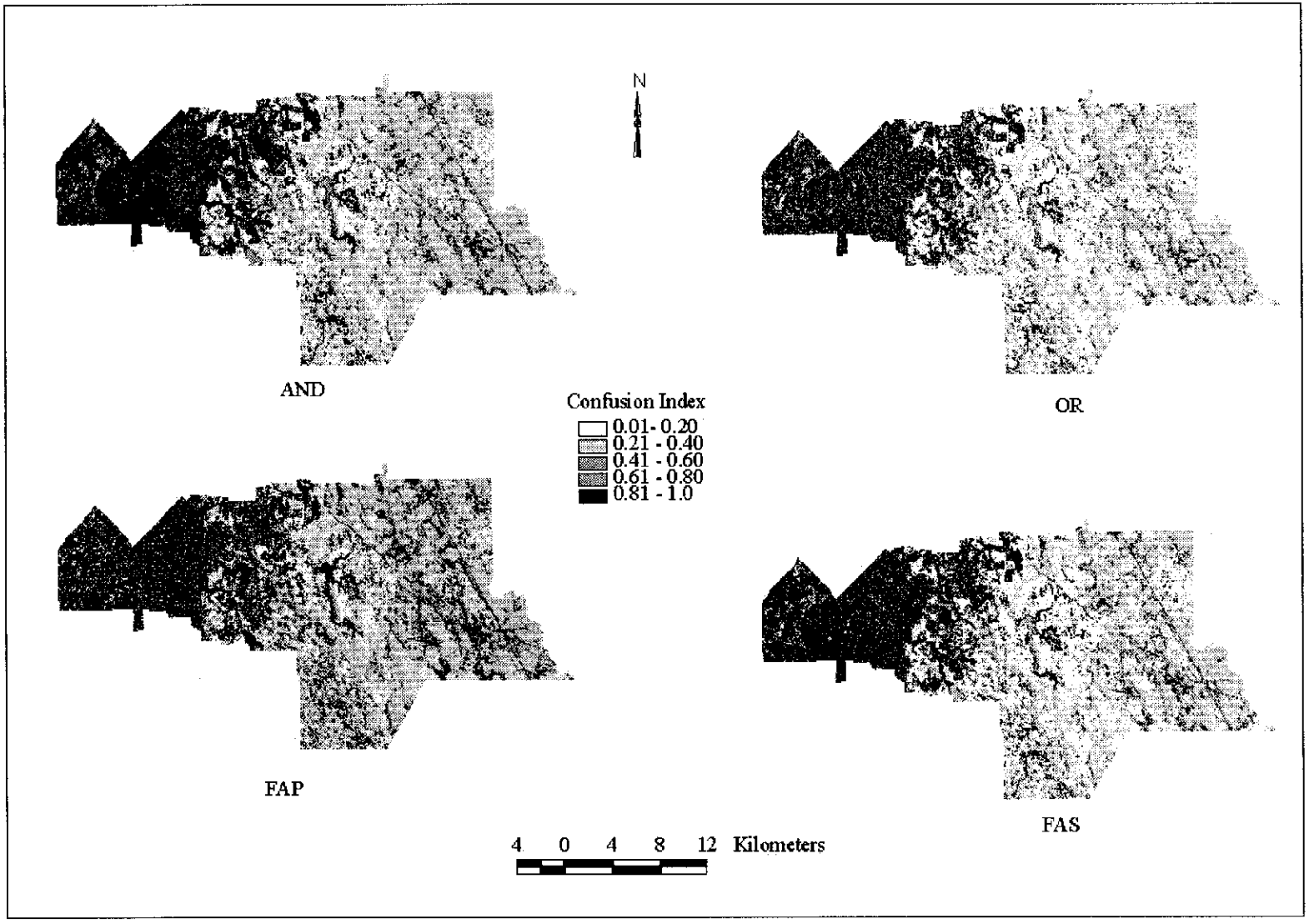

(b)

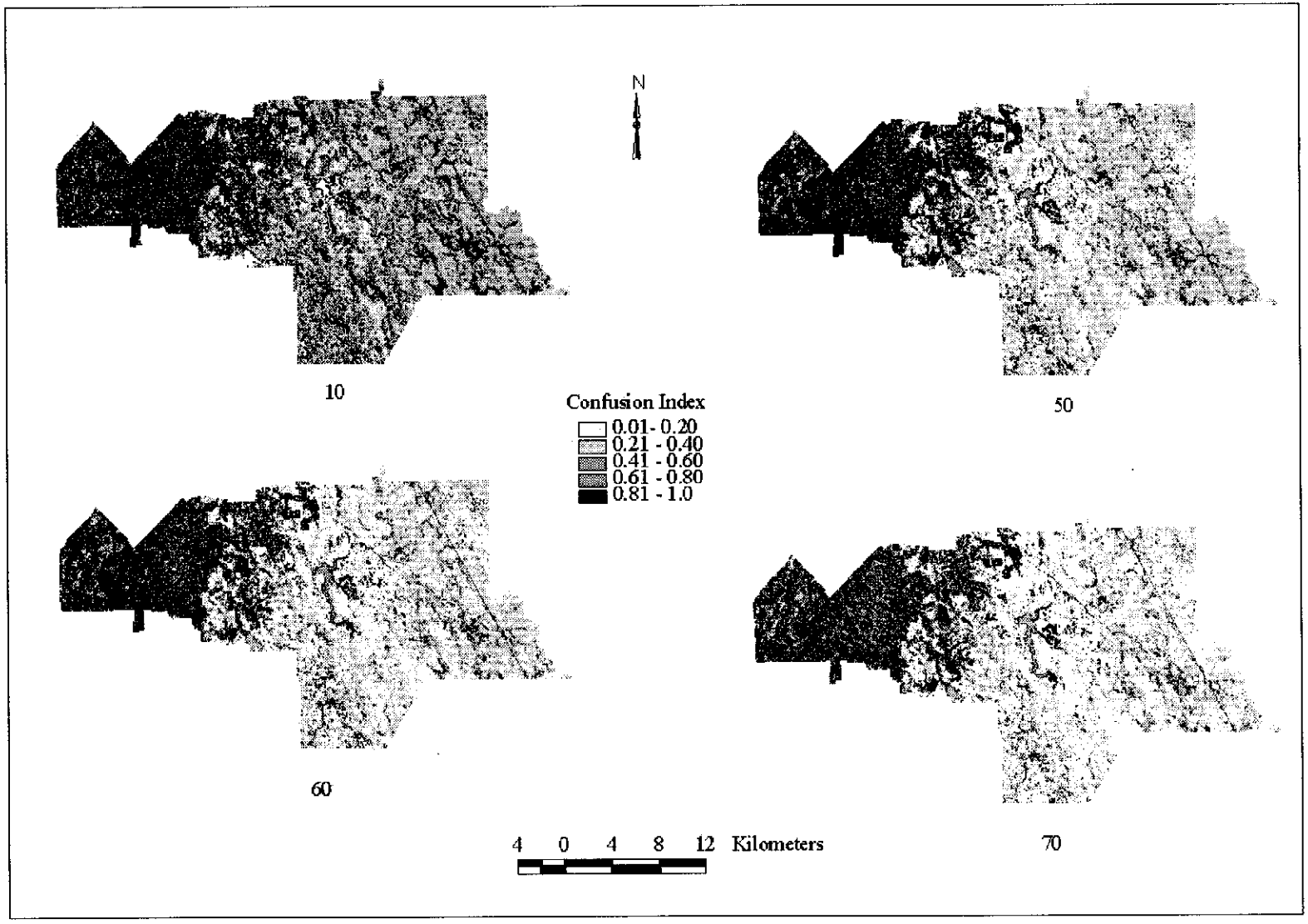
N
10
50
60
70
Confusion Index
0.01 - 0.20
0.21 - 0.40
0.41 - 0.60
0.61 - 0.80
0.81 - 1.0
4 0 4 8 12 Kilometers

(c)

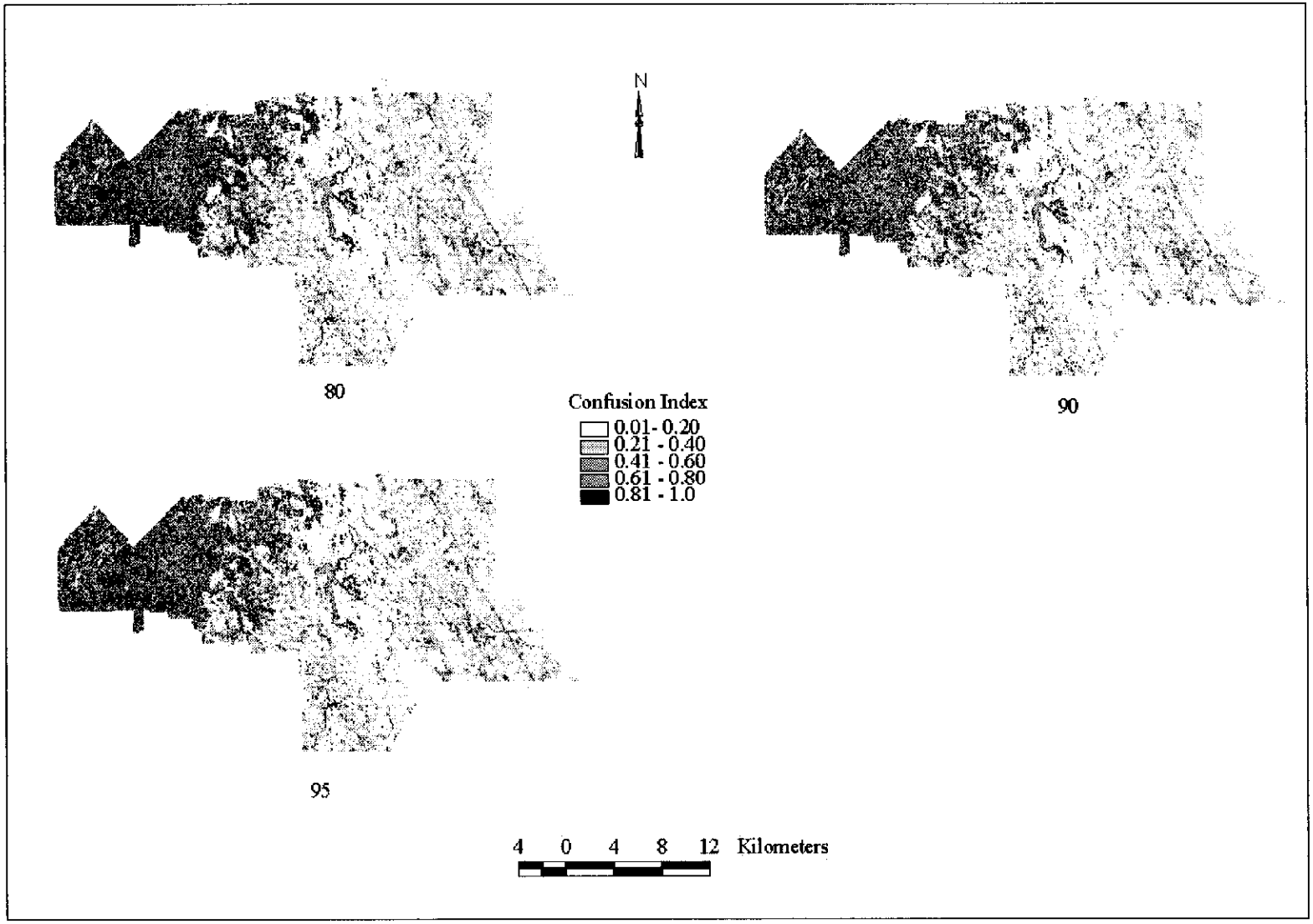
N
80
90
95
Confusion Index
0.01- 0.20
0.21 - 0.40
0.41 - 0.60
0.61 - 0.80
0.81 - 1.0
4 0 4 8 12 Kilometers